Atomically Controlled Surfaces, Interfaces and Nanostructures

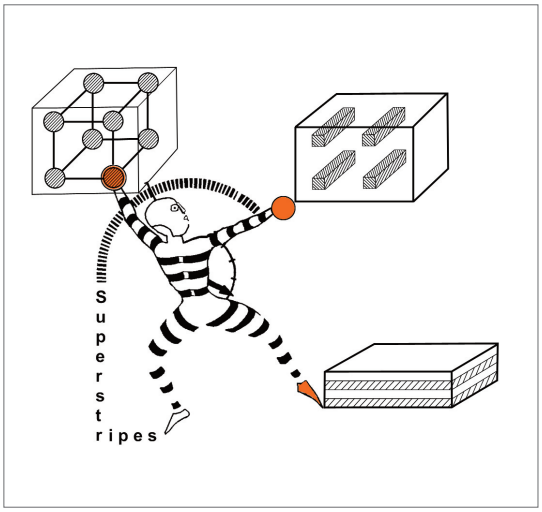

edited by
Antonio Bianconi, Augusto Marcelli

superstripes press
science series

Atomically Controlled Surfaces, Interfaces and Nanostructures

Book of Abstracts of the 13th International Conference on
Atomically Controlled Surfaces, Interfaces and Nanostructures
Frascati Rome, Italy, October 9-15, 2016
ACSIN 2016

edited by
Antonio Bianconi, Augusto Marcelli

superstripes press
science series

Science Series No.9
Title: Atomically Controlled Surfaces, Interfaces and Nanostructures
Published on October 2016
by Superstripes Press, Rome, Italy

http://www.superstripes.net/science/science.htm

Adil Acun, Akira Akaishi, Thierry Angot, Masaaki Araidai, Victor Aristov, Tetsuya Aruga, Mikhail Avdeev, Krzysztof Banas, Agnieszka Banas, Florian Banhart, Friedhelm Bechstedt, Atsushi Beniya, Mrinal Bera, Richard Berndt, Antonio Bianconi, Patrizia Borghetti, Federico Boscherini, Pavel Brunkov, Christian Brylinski, Antoni Bukaluk, Arrigo Calzolari, Giovanni Castorina, Paola Castrucci, Yuliang Chen, Chien Wei Chen, Mingshu Chen, Shirley Chiang, Shohei Chiashi, Deung-Jang Choi, Gianfelice Cinque, Antonio Cricenti, Mario D'Acunto, María E. Dávila, Oscar Rodriguez De La Fuente, Irene Paola De Padova, Okan Deniz, Daniele Di Gioacchino, Yi Du, Katarzyna Dziedzic-Kocurek, Konstantin Eltsov, Paul Evans, Jens Falta, Daniel Farias, Fernando Flores, Dillon Fong, Anna Fontcuberta i Morral, Katharina Franke, Giuseppe Gigli, César González, Laurent Guillemot, Keisuke Hatada, Ayami Hattori, Kersti Hermansson, Zenji Hiroi, Liv Hornekaer, Yudai Hoshi, Qiushi Huang, Toshio Hyodo, Masakazu Ichikawa, Masaki Imamura, Akinori Irizawa, Akira Ishii, Tomonori Ito, Mieczyslaw Jalochowski, Thomas Jarlborg, Boby Joseph, Jun'ichi Kanasaki, Toshio Kawahara, Hanchul Kim, Akio Kimura, Hideki Kishimoto, Katsuyoshi Kobayashi, Pavel Kocan, Jacek Kolodziej, Satoru Konabe, Marek Kopciuszyński, Tomohiro Koyama, Mariusz Krawiec, Carola Kryschi, Osamu Kubo, Wojciech Kwiatek, Guy Le Lay, Geunseop Lee, Bingbing Liu, Bo-Heng Liu, Nicolás Lorente, Karl Ludwig, Stefano Lupi, Salvatore Macis, Augusto Marcelli, Katerina Medjanik, Aleksandr Meilakhs, Ilio Miccoli, Enrique G. Michel, Izumi Mochizuki, Alessandro Molle, Olga Molodtsova, Alberto Morgante, Natalia Mueller, Pingo Mutombo, Tomonobu Nakayama, Masato Oda, Shuichi Ogawa, Toshio Ogino, Enrique Ortega, Woei Wu Larry Pai, Andrea Perali, Daniele Pergolesi, Petar Pervan, Agata Podsiadły-Paszkowska, Fabio Pulizzi, Alessandro Ricci, Mario Rocca, Federico Rosei, Akira Sakai, Kazuyuki Sakamoto, Andrés Santander-Syro, Alexander Saranin, Luis Scalvi, Stefan Schippers, Gerd Schoenhense, Didier Sébilleau, Jalil Shah, Yukichi Shigeta, Tomoko Shimizu, Tomas Skála, Marco Smerieri, Pavel Sobotik, Patrick Soukiassian, Ulrich Starke, Agnieszka Stępniak-Dybala, Rintaro Sugimoto, Gulnar Sugurbekova, Kazutoshi Takahashi, Antonio Tejeda, Masaru Tsukada, Toru Ujihara, Makoto Ushirozako, Michel Van Hove, Alexander Vul, Weimin Wang, Zhiming Wang, Takanobu Watanabe, Joachim Wollschläger, Kehui Wu, Wei Xu, Kazuma Yagyu, Yukiko Yamada-Takamura, Shiro Yamazaki, Hidehiro Yasuda, Dietrich R.T. Zahn, Maria Zamoryanskaya, Agata Zdyb, Ryszard Zdyb, Konstantinos Zekentes, Si Zhou.

These authors presented the scientific reports collected in this book at the ACSIN 2016 conference held in in Frascati, Rome, Italy, Oct 9-15, 2016.

ISBN 978-88-6683-059-7
ISBN-A 10.978.886683/0597

Papers presented at the international conference

ACSIN 2016

Frascati, Rome, Italy October 9-15, 2016

Organized by
Non profit organization for scientific research Superstripes onlus
Rome International Center for Materials Science Superstripes - RICMASS

Conference chair
Antonio Bianconi - RICMASS Rome, Italy

Co-chairs
Augusto Marcelli – INFN-Laboratori Nazionali di Frascati, Italy
Patrick Soukiassian – CEA – Université de Paris-Sud, France

Atomically Controlled Surfaces, Interfaces and Nanostructures

To be cited as: A. Acun et al. “Atomically Controlled Surfaces Interfaces and Nanostructures” edited by A. Bianconi, A. Marcelli (Superstripes Press, Rome 2016) isbn: 9788866830597

Table of Contents

Mo1T session

Multifunctional materials for electronics and photonics

Federico Rosei[1]
[1]*UNESCO Chair in Materials and Technologies for Energy Conversion, Saving and Storage*
Centre for Energy, Materials and Telecommunications, INRS, 1650 Boul. Lionel Boulet, J3X 1S2 Varennes (QC), Canada

Email: *rosei@emt.inrs.ca*
Key words: surfaces and interfaces, nanomaterials, photovoltaic devices, multifunctional materials, bulk photovoltaic effect

The bottom–up approach is considered a potential alternative for low cost manufacturing of nanostructured materials [1]. It is based on the concept of self–assembly of nanostructures on a substrate, and is emerging as an alternative paradigm for traditional top down fabrication used in the semiconductor industry. We demonstrate various strategies to control nanostructure assembly (both organic and inorganic) at the nanoscale. We study, in particular, multifunctional materials, namely materials that exhibit more than one functionality, and structure/property relationships in such systems, including for example: (i) control of size and luminescence properties of semiconductor nanostructures, synthesized by reactive laser ablation [2]; (ii) we developed new experimental tools and comparison with simulations are presented to gain atomic scale insight into the surface processes that govern nucleation and growth [3-5]; (iii) we devised new strategies for synthesizing multifunctional nanoscale materials for electronics and photovoltaics [6-11].

References

1. F. Rosei, *J. Phys. Cond. Matt.* 16, S1373 (2004).
2. D. Riabinina et al., *Phys. Rev. B* 74, 075334 (2006).
3. K. Dunn et al., *Phys. Rev. B* 80, 035330 (2009).
4. F. Ratto et al., *Small* 2, 401 (2006).
5. F. Ratto et al., *Phys. Rev. Lett.* 96, 096193 (2006).
6. C. Yan et al., *Adv. Mater.* 22, 1741 (2010).
7. R. Nechache et al., *Adv. Mater.* 23, 1724 (2011).
8. R. Nechache et al., *Appl. Phys. Lett.* 98, 202902 (2011).
9. T. Dembele et al., *J. Power Sources* 233, 93 (2013).
10. S. Li et al., *Chem. Comm.* 49, 5856 (2013).
11. R. Nechache et al., *Nature Photonics* 9, 61 (2015).

Silicene, the Artificial Graphenelike Silicon

G. Le Lay
Aix-Marseille University, UMR 7345 - Laboratoire PIIM, Campus de Saint-Jérôme, Avenue Escadrille Normandie-Niémen, 13397 Marseille cedex 20

Email*: guy.lelay@univ-amu.fr*

The Hot Research Front “Silicene growth and properties” is ranked 4th among the 10 Top Physics Fronts identified by Thomson Reuters for the years 2011-2014, after “Observation of Higgs boson”, “Globalneutrino data analysis” and “Nonlinear massive gravity” [1].
Silicene, synthesized in 2012 [2], is a novel two-dimensional (2D) honeycomb allotrope of silicon with a significant spin-orbit coupling (SOC). It was artificially created, since, at variance with graphene, which descents from graphite, it has no parent crystal in nature. It appears as an emerging 2D electronic materials and is considered as a promising candidate for ultimate scaling of nanoelectronic devices. Indeed, the recent fabrication of the first silicene field effect transistors operating at room temperature demonstrates its potential [3].
In this invited talk, I will first present the archetype 3×3 silicene phase formed on a silver (111) substrate [2], its sister phases [4], its functionalization with hydrogen, and the growth and properties of multi layer silicene, which hosts Dirac fermions and which is stable in ambient air, protected by its ultra-thin native oxide [5].
I will conclude with the prospects offered by this tantalizing 2D silicon allotrope [6,7], whose synthesis has been quickly followed by those of its close cousins germanene [8,9] and stanene [10,11], just two and three years later, respectively.

References

1. C. Day, Physics Today, 25 September 2015.
2. P. Vogt et al., Phys. Rev. Lett., 108, 155501 (2012).
3. Tao et al., Nature Nanotechnol., 10, 227 (2015)
4. A. Resta et al., Sci. Rep., 3, 2399 (2013).
5. P. De Padova et al., 2D Mater., 1, 021003 (2014).
6. Le Lay G., Nature Nanotechnology, 10, 202 (2015).
7. G. Le Lay, E. Salomon and T. Angot, Europhysics News, 47, 17 (2016).
8. M. E. Dávila, L. Xian, S. Cahangirov, A. Rubio and G. Le Lay, New Journal of Physics, 16, 095002 (2014).
9. M. E. Dávila and G. Le Lay, Sci. Rep., 6, 20714 (2016).
10. Feng-feng Zhu et al., Nature Materials, 14, 1020 (2015).
11. J. Yuhara et al., to be published.

Enhanced Raman Spectroscopy of Semiconductor Nanocrystals

Dietrich R.T. Zahn[1], Volodymyr M. Dzhagan[1], Alexander G. Milekhin[2,3]
[1]*Semiconductor Physics, Technische Universität Chemnitz, D-09107 Chemnitz,*
[2]*Semiconductor Physics, pr. Lavrentjeva, 13, 630090 Novosibirsk, Russia*
[3]*Novosibirsk State University, Pirogov str. 2, 630090 Novosibirsk, Russia*

Email: *zahn@physik.tu-chemnitz.de*
Key words: Enhanced Raman Spectroscopy, Semiconductor Nanocrystals, Metal Nanocluster Arrays, Localized Surface Plasmon Resonance

Semiconductor nanocrystals (NCs) or quantum dots (QDs), *e.g.* colloidal CdSe NCs, are found in numerous applications, in particular as strong luminescent light emitters as their size dependent light emission can cover the entire visible spectral range. While the luminescence can be detected easily even for single QDs, recording the Raman spectrum of a single QD and thus determining its vibrational properties remains a challenge.
Here we use the example of CdSe quantum dots to illustrate several approaches how the Raman response of the QDs can be enhanced and finally quasi-single QD Raman spectra obtained. Beginning with enhancement via resonant excitation and utilizing interference enhanced Raman scattering this contribution will then focus on an investigation of resonant surface-enhanced Raman scattering (SERS) by optical phonons in colloidal CdSe NCs homogeneously deposited on arrays of Au nanoclusters using the Langmuir–Blodgett technology. The thickness of deposited NCs, determined by transmission and scanning electron microscopy, amounts to approximately 1 monolayer. Special attention is paid to the determination of the localized surface plasmon resonance (LSPR) energy in the arrays of Au nanoclusters as a function of the nanocluster size by means of micro-ellipsometry. SERS by optical phonons in CdSe NCs shows a significant enhancement factor with a maximal value of 2×10^3 which depends resonantly on the Au nanocluster size and thus on the LSPR energy. The deposition of CdSe NCs on the arrays of Au nanocluster dimers enabled us to study the polarization dependence of SERS. It was found that a maximal SERS signal is observed for the light polarization along the dimer axis. Finally, SERS by optical phonons was observed for CdSe NCs deposited on structures with a single Au dimer. A difference of the LO phonon energy is observed for CdSe NCs on different single dimers. This effect is explained as the confinement-induced shift which depends on the CdSe nanocrystal size and indicates quasi-single NC Raman spectra being obtained. Finally the application of tip-enhanced Raman scattering (TERS) to single QDs will be discussed.

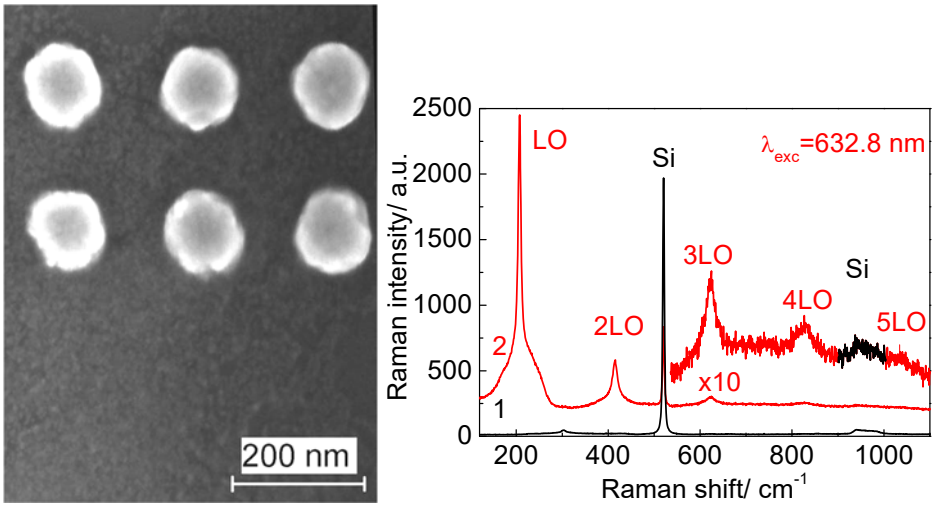

Figure 1: left: Typical SEM image of 1 monolayer of CdSe NCs deposited on a Au nanocluster array. White circular areas with a diameter of about 100 nm refer to Au nanoclusters. right: Raman spectra of CdSe NCs on bare Si (curve 1) and SERS spectra on arrays of Au nanoclusters with diameters of 76 nm (curve 2), measured with λ_{exc}= 632.8 nm.

Publishing nanoscience and nanotechnology at the cutting edge

Fabio Pulizzi
Nature Nanotechnology

Email: *f.pulizzi@nature.com*
Key words: nanotechnology, publishing

Nature Nanotechnology was launched in 2006 and is one of the journals that make up the physical sciences portfolio of the Nature Research Journals (NRJs) section of Springer Nature. During my talk I will introduce the journal and use it as a representative of the NRJs. I shall explain the scope of the journal, the type of papers we look for and the editorial process that we use to decide whether a manuscript belongs to our journal.

Mo2T session

Characterization of exosomes using atomic force microscopy and scanning electron microscopy

Toshio Ogino[1], Kazuki Ito[1], Keiji Yokota[1], Yuta Ogawa[1], Tamiko Minamisawa[2], Sachiko Matsumura[2], Kanako Suga[2], Kiyotaka Shiba[2], Yasuo Kimura[3], Ayumi Hirano-Iwata[4]
[1] *Yokohama National University*
[2] *Japanese Foundation for Cancer Research*
[3] *Tokyo University of Technology*
[4] *Tohoku University*

Email: *ogino-toshio-rx@ynu.ac.jp*
Key words: 23-Nanobiotechnology in biosensors, medicine, 21-Scanning probe and surface microscopy, Exosome, Lipid bilayer, Atomic force microscopy, Cancer cell

Interactions between solid surfaces and biomaterials, such as protein molecules, DNAs, cells and various biomembranes, consist of electrostatic repulsive or attractive force, van der Waals attractive force, hydration repulsive force, and hydrophobic attractive force, and their understanding is the basis of biodevices. We previously demonstrated that protein molecule adsorption to solid surfaces strongly depends both on the molecular structures and solid surface chemistry [1,2]. By utilizing the molecule-solid interactions, novel techniques of biomaterial characterization are expected to establish.
Exosomes are nano-vesicles with 30-150 nm diameters wrapped with a lipid bilayer like cells, and released from whole cells including cancer cells [3,4]. Because exosome membranes and inclusions are originated in the host cell, their characterization attracts much attention toward early diagnosis of cancer and its metastasis control. Exosomes are nanosized vesicles and cannot be observed using optical microscopy. Therefore, their characterization have been performed by transmission electron microscopy assisted by the freeze-drying technique. However, sample preparation of this technique is complex and its data are limited to the exosome sizes and shapes.

In this work, we used atomic force microscopy (AFM). In this method, AFM images are taken after exosome adsorption and the inevitably occuring deformation, and it would be a disadvage to obtain the real shape and size. However, we have found that the deformation caused by the adsorption itself contains much information about exosome membrane properties and that it can be effectively used to identify the host cell.
We used exosomes extracted from three types of cultivated cancer cells; human colorectal cancer (HT-29), fibrosarcoma (HT1080) and pancreatic cancer (MIA PaCa2). Those exosomes were adsorbed to SiO_2/Si substrates and observed in buffer solutions by AFM. The dried samples were observed by scanning electron microscopy to extract the exosome properties.
Figure 1 shows an AFM image of exosomes from HT-29 attached on a SiO_2/Si substrate surface. Based on the size, height and shape of the adsorbates, we can classify them into four adsorption types sketched in Figure 1(a-d). Because the adsorption type reflects the properties of the host cell, this classification can be used to estimate the

host cell type. More exact identification can be done by extracting many parameters, such as average height, maximum height, adsorption area and aspect ratio, from these figures. Those data can be used to prepare a discriminator for unknown exosomes in a multi-dimensional space by plotting whole data from individual exosomes. We have found that probability to assign the unknown AFM image to the correct host cell one is high. Dried samples also can be used to investigate the host cell properties because they reflect host cell membrane properties and amount of inclusions specific to the host cell.

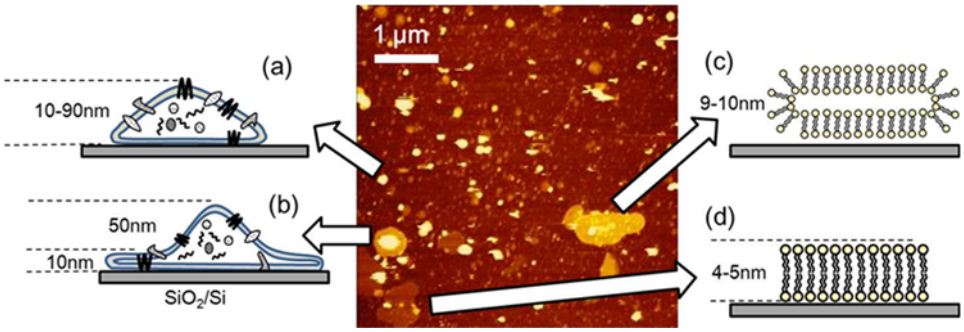

Figure 1: AFM image of exosomes derived from HT-29 cells on a SiO_2/Si substrate and their type classification.

Acknowledgement
This work was partly supported by CREST-JST and Grant-in-Aid for Scientific Research (15K13361) from MEXT.

References

1. K. Yamazaki, T. Ikeda, T. Isono, T. Ogino, Selective adsorption of protein molecules on phase-separated sapphire surfaces, *J. Colloid Interface Sci.*, 361, 64 (2011). http://dx.doi.org/10.1016/j.jcis.2011.05.016.
2. Y. Kamiya, K. Yamazaki, T. Ogino, Protein adsorption to graphene surfaces controlled by chemical modification of the substrate surfaces, *J. Colloid Interface Sci.*, 431, 77 (2014). http://dx.doi.org/10.1016/j.jcis.2014.06.023.
3. S. Mathivanan, H. Ji, R. J. Simpson, Exosomes: Extracellular organelles important in intercellular communication, *J. Proteomics*, 73, 1907 (2010). http://dx.doi.org/10.1016/j.jprot.2010.06.006.
4. A.V. Vlassov S. Magdaleno, R. Setterquist, R. Conrad, Exosomes: Current knowledge of their composition, biological functions, and diagnostic and therapeutic potentials, *Biochim. Biophys. Acta* 1820, 940 (2012).

Multilayer Silicene

Paola De Padova
Consiglio Nazionale delle Ricerche -ISM, via Fosso del Cavaliere 100, 00133 Roma, Italy

Email: *depadova@ism.cnr.it*
Key words: multilayer silicene, surface x-ray diffraction

The discovery of silicene [1- 3], a novel silicon two-dimensional (2D) allotrope, by the first compelling experimental evidence of its synthesis [1], boosted, nowadays, the research on 2D materials [4].
Multilayer silicene grown on the Ag(111) surface exhibits in ARPES features which displays circular horizontal cross-sections in precise positions in momentum space; they can be attributed to π and π cones, which confirms the presence of Dirac fermions with a very high Fermi velocity [5]. These films grow in sequential flat terraces, after the initial formation of 3×3-reconstructed monolayer, which is in a 4×4 coincidence super cell respect to silver (111) unit cell. All terraces have a honeycomb $\sqrt{3}\times\sqrt{3}R(30°)$ surface symmetry, with respect to 1×1 silicene, as showed by STM and LEED and furthermore they present strong resistance towards oxidation [5].

At present there is a debate on the possibility that the multilayer silicene is indeed thin film of bulk-like silicon [6]. Here, we report the AES/LEED, Raman spectroscopy, x-ray diffraction, energy dispersive X-ray reflectivity and grazing incidence in-plane x-ray diffraction, which provides the multilayer silicene physical fingerprints [7]. These measurements rule out that the $\sqrt{3}\times\sqrt{3}$ Multilayer silicene/Ag(111) is due to the $\sqrt{3}\times\sqrt{3}$ reconstruction from silver atoms that act as surfactant in the formation of diamond-like crystalline Si film. Furthermore, these results are of crucial importance for applying silicene in the well-established silicon based widespread electronics, taking into account that the first FET single layer silicene was successfully realized [8].

References

1. P. Vogt, P. De Padova, C. Quaresima, J. Avila, E. Frantzeskakis, M. C. Asensio, A. Resta, B. Ealet, and G. Le Lay, *Phys. Rev. Lett.* 108, 155501 (2012).
2. C.-L. Lin, R. Arafune, K. Kawahara, N. Tsukahara, E. Minamitani, Y. Kim, N. Takagi, and M. Kawai, *Appl. Phys. Exp.*, 5, 045802 (2012).
3. A. Fleurence, R. Friedlein, T. Ozaki, H. Kawai, Y. Wang, and Y. Yamada-Takamura, *Phys. Rev. Lett.* 108, 245501 (2012).
4. M E Dávila *et al*., New Journal of Physics 16,095002 (2014); A. J. Mannix *et al*., Science, 350, 1516, (2015); F. F Zhu et al., 14, 1020 (2015).
5. P. De Padova *et al*., J. Phys.: Condens. Matter, Fast Track Comm. 25, 382202 (2013); P. Vogt *et al*., Appl. Phys. Lett. 104, 021602-1 (2014); E. Salomon *et al*., J. Phys.: Condens. Matter, 7, 185003 (2014); P. De Padova *et al*., Appl. Phys. Lett., 96, 26190, (2010); [8] P. De Padova *et al*., 2D Materials 1, 021003 (2014)

6. L. Tao *et al.,*Nat. Nanotech. 10, 227 (2015); T. Shirai *et al*. Phys. Rev. B 89, 241403-1, 2414035 (R) (2014); J. Chen *et al*., Sci. Rep., DOI: 10.1038/srep13590; J. Mannix *et al.,* ACS Nano, 8, 7538 (2014); Y. Borensztein, A. Curcella, S. Royer and G. Prévot, Phys. Rev. B 92, 155407 (2015); S. K. Mahatha *et al*., Phys. Rev. B, 92, 245127 (2015); K. Kawahara *et al*., Surface Science 651, 70 (2016).
7. P. De Padova *et al.,* paper in preparation.
8. L. Tao *et al.,*Nat. Nanotech. 10, 227 (2015).

Reversible phase transitions on semiconductor surfaces: soft modes and dynamical fluctuations

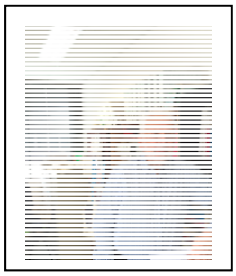

F. Flores[1], A. Tejeda[2], D. Gonzalez-Trabada[1] and J. Ortega[2]
[1] *Departamento de Física Teórica de la Materia Condensada and Condensed Matter Physics Center (IFIMAC). Universidad Autónoma de Madrid, 28049 MADRID. SPAIN*
[2]*Laboratoire de Physique des Solides. Université Paris-Sud. CNRS. UMR 8502. F-91405 ORSAY. FRANCE*

Email: *fernando.flores@uam.es*
Key words: Semiconductor surfaces; phase transitions; electron.phonon interaction; many-body sffects.

The enhancement of quasi-particle interactions in low dimensional systems gives rise to fascinating phase transitions like low-dimensional superconductivity, magnetic ordering or metal-insulator transitions. In particular, metallic overlayers on semiconductor surfaces are prone to creating temperature induced reversible phase-transitions, very often associated with dynamical fluctuations of surface atoms and/or with the many-body properties of the system.
In this talk, first of all a review of those systems will be presented discussing some properties of well-known dynamical fluctuation phase transitions. α-Sn/Ge(111) is a paradigmatic case [1] that changes its symmetry from √3x√3 to 3x3 around 200 K, with a soft-phonon mode [2] identified as the driving mechanism of the transition [3]. However, another competing mechanisms associated with either electron correlation effects or electron-phonon interaction give rise in this system, at very low temperature (≈ 50 K), to a √3x√3- Mott insulating phase [4]. The competing mechanisms of that transition will be discussed, with a detailed emphasis in the electron-phonon interaction. In this context, the properties of another similar system: K/Si(111):B [5] will be discussed.

Finally, experimental and theoretical evidence of a new √3x√3 →2√3x2√3 reversible phase transition for Sn/Si(111):B will be presented [6] (see figure 1). The transition appears at 520 K and the system has 6 Sn-atoms per unit cell (2√3x2√3). LEED and STM-images, as well as photoemission experiments, will be shown. All these results are explained by means of a microscopic diffusive mechanism whereby a Sn-tetramer diffuses on the surface among 24 equivalent ground states, giving rise to the √3x√3 symmetry. This is similar to other dynamical fluctuation phase transitions, but it includes as an essential new ingredient the diffusion of tetramers along the surface. Results for the geometry of this surface and the diffusive Sn-tetramer processes will be shown as calculated using an appropriate DFT-molecular dynamics approach

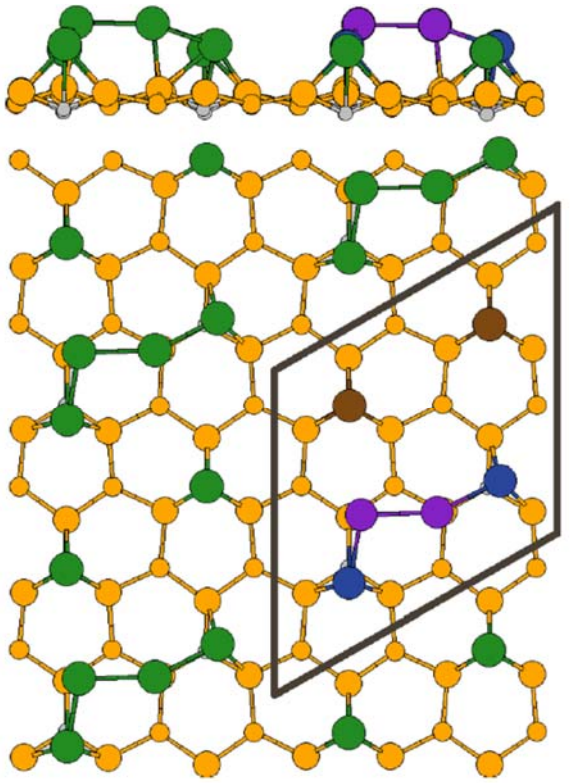

Figure 1: Side and top views for the Sn/Si(111):B-2√3x2√3 atomic structure.

References

1. J.M. Carpinelli et al, Nature (London) 381, 398 (1996)
2. R. Pérez, J. Ortega and F.Flores, Phys Rev Lett.86, 4891 (2001)
3. J. Avila et al, Phys Rev Lett 82, 442 (1999)
4. R. Cortés et al, Phys Rev Lett 96, 126103 (2006)
5. L.A. Cardenas et al, Phys Rev Lett 103, 046804 (1999); HH Weitering et al, Phys Rev Lett 78 1331 (1997)
6. W. Srour et al, Phys Rev Lett (2015) 114, 196101 (2015).

Collective Multi-Atom Diffusion of Ag/Ge(110) and Motion of Liquid Alloy Droplets of Au/Ge(110)

Shirley Chiang,[1] C. H. Mullet,[1] M. C. Tringides,[2] M. van Zijll,[1] B. H. Stenger,[1] E. Huffman,[1] D. Lovinger,[1] A. L. Dorsett,[1] J. H. Miller,[1] E. M. Russell,[1] C. A. Gabris[1]
[1]*Department of Physics, University of California, Davis*
[2] *Dept. of Physics, Iowa State University and Ames Lab-USDOE*

Email: *chiang@physics.ucdavis.edu*
Key words: 19- Frontiers aspects of semiconductor, surfaces and interfaces; 21- Scanning probe and surface microscopy

The growth of Ag deposited on Ge(110) was studied with low energy electron microscopy (LEEM) and scanning tunneling microscopy (STM). The LEEM studies showed the formation of long, one-dimensional (1D) multi-height islands over the temperature range 430C-530C. During deposition, the length of the islands increases at a constant rate (~10^6 atoms/sec reaching ~20 microns) and constant width (100-200nm) for 9ML total deposition. Stochastic diffusion cannot account for these very high island growth rates. When smaller islands decay, the rate is ~$2x10^7$ atoms/sec, which is also exceedingly fast based on the Ag diffusion and detachment barriers. These high rates are not consistent with independent adatom events and imply multi-atom correlated diffusion. Such collective mass transport must be related to the mobility of the wetting layer. STM images show the crystalline structure of the 1D Ag islands and also indicate that the reconstructed regions between the islands consist of bare Ge. These data are corroborated by LEEM IV curves. Together, they confirm that the wetting layer provides the material for the islands to grow at these high rates.

LEEM was also used to study the growth of Au on Ge(110) in order to control the growth of low-dimensional nanostructures and understand the temperature induced motion of islands. Ge(110) was dosed with 0.5-5 ML of Au and heated to 850°C. During deposition, islands grew to ~1-2 μm in width and ~2-5 μm in length, all oriented along the (1,-1,0) direction. Above 750°C, the lack of a LEED pattern in the islands indicated a loss of crystalline structure and the formation of a Au/Ge liquid alloy. The larger islands began moving with speeds of 0.1-1.0 μm/s, absorbing smaller stationary islands upon collision and increasing in size up to ~60 microns in width and ~100 μm in length. This movement can be explained by a temperature gradient across the sample causing a Ge concentration gradient across the islands, inducing movement in the direction of increasing temperature. Optical microscopy confirmed that the large islands moved from the cooler edges of the sample toward the hotter center of the sample. Similar behavior has previously been observed for Pt/Si islands on Si(100) by PEEM [1]. As the temperature decreased, the island behavior was also studied and revealed rapid island contractions which left traces on the Ge(110) surface. Low Energy Electron Diffraction (LEED) showed a (4x1) reconstruction below 670°C, a

(4x4) reconstruction between 670°C and 750°C, and a (2x1) reconstruction above 750°C.

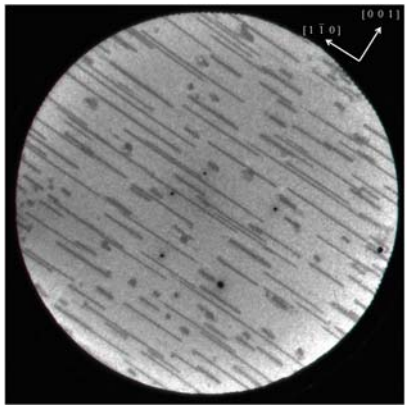

Figure 1: LEEM image of 1D islands of Ag on Ge(110). Island widths ~200nm, image FOV 10μm.

References

1. W.-C. Yang, H. Ade, and R. J. Nemanich. Phys. Rev. B 69, 045421 (2004).

Nanostructured graphene on cubic-SiC: synthesis, structure and transport properties

V.Yu. Aristov [1,2,3], H.-C. Wu [4], O.V. Molodtsova [2,5], S.V. Babenkov [2], A.N. Chaika [1,6]
[1] *Institute of Solid State Physics of Russian Academy of Sciences, 142432 Chernogolovka, Russia*
[2] *Deutsches Elektronen-Synchrotron DESY, D-22607 Hamburg, Germany*
[3] *Institut für Experimentelle Physik, TU Bergakademie Freiberg, 09596 Freiberg, Germany*
[4] *School of Physics, Beijing Institute of Technology, Beijing 100081, People's Republic of China*
[5] *National Research University of Inform. Technologies, Mechanics and Optics, Saint Petersburg, Russia*
[6] *CRANN and School of Physics, Trinity College, Dublin 2, Ireland*

Email: *victor.aristov@desy.de*
Key words: nanostructured graphene, cubic-SiC, synthesis, transport properties

Latest theoretical works [1] show that graphene nanodomain boundaries (NBs) with a periodic atomic structure along their length can perfectly reflect charge carriers over a large range of energies. Making use of this would provide a new way to control the charge carriers in graphene without the need to introduce an energy band gap. The main challenge is to produce self-aligned nanodomains with periodic NBs on a technologically relevant substrate. In this presentation we report a method to fabricate a few-layer graphene consisting of self-aligned nanodomains with periodic NBs on the semiconducting SiC/Si wafers compatible with silicon technologies.
The results of the studies of atomic and electronic structure and transport properties of such nanostructured graphene synthesized on low-index and vicinal surfaces of SiC(001) in UHV are reported as well. [2-4]. Atomic and electronic structure graphene layers on SiC (001) were studied by a number of modern experimental techniques (STM with atomic resolution, μ-LEED, LEEM, PEEM, μ-PES, AR-PES etc). Using the new dynamic-XPS end-station, based on the Argus spectrometer installed on the high-brilliance soft X-ray P04 beamline at PETRA III (DESY) [5] we control layer-by-layer graphene growth in real time following the evolution of the photoemission spectra with an acquisition time of ~ 0.1 sec/spectrum and break the process when the desired number of graphene layers is reached. The fine structure of the angle-resolved photoemission spectra suggests the Bernal stacking in the trilayer graphene on SiC(001) [6].
Electrical measurements conducted at low temperatures on the vicinal SiC(001) samples demonstrate the opening of a transport gap in the nanostructured trilayer

graphene up to 1.3 eV [6], which is induced by self-aligned periodic NBs. The transport gap opening produces high current on-off ratio of 104. This development may lead to new tuneable electronic nanostructures made from graphene on cubic-SiC, opening up opportunities for a wide range of new applications.

This work was supported by Beijing Institute of Technology Research Fund Program for Young Scholars, Science Foundation Ireland (SFI) (No. 12/IA/1264), National Plan for Science and technology of KSU (Nos. NPST 1598-02, NPST 1466-02, NPST 2529-02), Russian Foundation for Basic Research (Nos. 14-02-00949, 14-02-01234), SPP 1459 of DFG, Marie Curie IIF grant within the 7th EC Framework Programme.

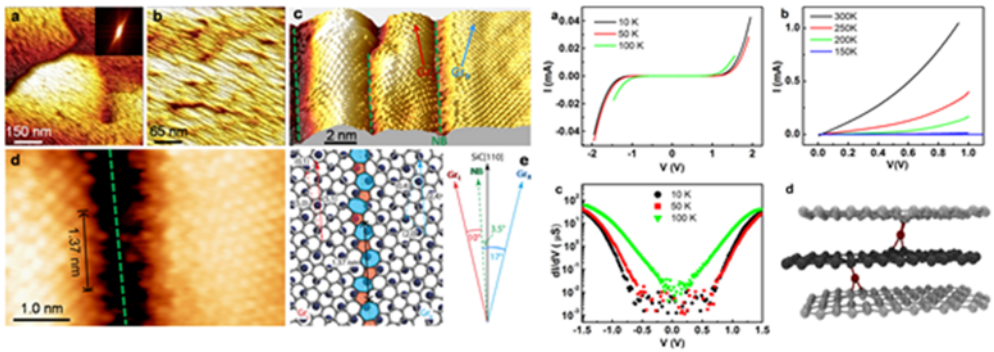

(1) (2)

Figure 1: (a) and (b) Large area STM images of graphene nanoribbons synthesized on the vicinal SiC(001). Inset in panel (a) shows the Fast Fourier Transform of the STM image proving one preferential direction of the NBs on the vicinal sample. (c) and (d) Atomically resolved STM images of graphene nanoribbons showing the system of domains rotated 17° clockwise (GrR) and 10° anticlockwise (GrL) relative to the NB (c) and the atomic structure of the NB (d). (e) Schematic model of the NB for the asymmetrically rotated nanodomains in panels (c) and (d).

Figure 2: (a) I-V curves measured at low temperatures. (b) I-V curves measured at 150 K - 300K. The current direction in (a,b) was perpendicular to nanodomain boundaries. (c) Corresponding dI/dV curves for temperatures below 150 K. The curves show the transport gap formation in nanostructured graphene on vicinal SiC(001) surface at indicated temperatures. (d) Schematic drawing of interstitial defects in trilayer graphene.

References

1. J. O.V. Yazev and S.G. Louie, Nat. Mater. 9, 806 (2010).
2. V.Yu. Aristov et al., Nano Letters 10, 992 (2010).
3. A.N. Chaika, O.V. Molodtsova et al., Nano Research 6, 562 (2013).
4. A.N. Chaika, O.V. Molodtsova, et al., Nanotechnology 25, 135605 (2014).
5. S.V. Babenkov, V.Y. Aristov, O.V. Molodtsova, et al., NIM A 777, 189 (2015).
6. H.-C. Wu, A.N. Chaika, T.-W. Huang et al, ACS Nano, 9, 8967 (2015).

A. Acun et al. “Atomically Controlled Surfaces Interfaces and Nanostructures”
edited by A. Bianconi, A. Marcelli (Superstripes Press, Rome 2016) isbn: 9788866830597

Gap opening on graphene sidewall nanoribbons

A. Tejeda[1,2], A. Taleb-Ibrahimi[2], C. Berger[3], W. de Heer[3] and E. H. Conrad[3]
[1]*Laboratoire de Physique des Solides, Université Paris-Sud, CNRS, Orsay, France*
[2]*Synchrotron SOLEIL, Gif sur Yvette, France,*
[3]*GeorgiaTech, Atlanta, United States*

Email: *antonio.tejeda@u-psud.fr*
Key words: 3-Electronic and optical properties of surfaces and interfaces; Graphene and other 2D materials

Armchair edged graphene nanoribbons are expected to present a controllable bandgap, suitable for graphene-based electronic devices. The gap relies on the fine control of the ribbon width and edge regularity at a level reaching a single atomic row, unattainable by state-of-the-art lithographic methods.

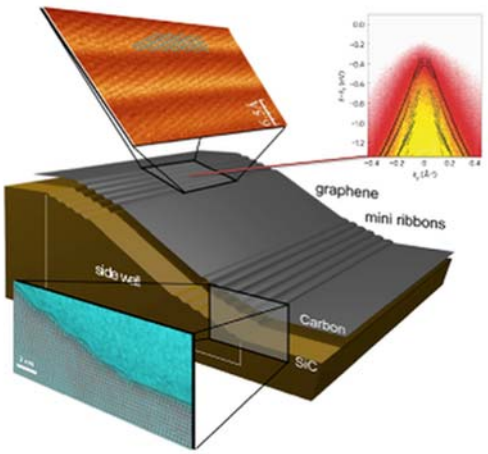

Figure 1: Stable facets at 27° from the [0001] direction of SiC favor the growth of graphene sidewall nanoribbons. These nanoribbons exhibit have a central part where graphene is decoupled from the substrate and are bordered by corrugated graphene, that follows the minifacets of the underlying substrate. In these corrugated regions, graphene is attached at some points and decoupled in between. A wide band gap is observed by photoemission from these regions.

Methods for producing semiconducting–metallic graphene networks suffer from scalability problems, stringent lithographic demands and process-induced disorder in

the graphene. These problems can be overcome by taking advantage of graphene grown on patterned SiC steps [1], where the edge is settled by growth instead by cutting an already existing graphene sheet.
This scalable bottom-up approach produces graphene nanoribbons. We have focused on the electronic properties of ribbons of graphene grown on facets of the SiC(0001) surface. We have observed by photoemission a region with a gap opening greater than 0.5 eV in an otherwise continuous metallic graphene sheet [2]. Our morphological characterization by STM and cross sectional TEM allows to understand the origin of the band gap in mini-ribbons bordering a central extended ribbon [3]. On the nanoribbon, where our STM measurements show a well-defined edge [4], transport measurements have also shown that charge carriers travel at room temperature on a length scale greater than ten micrometers [4], which is similar to the performance of metallic carbon nanotubes, and opens a promising future for graphene electronics.

References

1. M. Sprinkle et al., Nature Nanotechnology 5, 727 (2010).
2. I. Palacio et al., NanoLett. 15, 182 (2015).
3. J. Hicks et al., Nature Physics 9, 49 (2012).
4. J. Baringhaus et al., Nature 506, 349 (2014).

Mo3T session

Revisiting the structural transitions and metallization of monoclinic vanadium dioxide under high pressure

Bingbing Liu
State Key Lab of Superhard Materials, Jilin University, Changchun 130012, P.R.China

Email: *liubb@jlu.edu.cn*
Key words: monoclinic vanadium dioxid; high pressure； phase transition

Monoclinic Vanadium dioxide (VO_2 (M1)) is a prototypical strongly correlated electron oxide, for which pressureinduced metallization (PIM) and structure transition have attracted lots of interest and intrigued many researches, however, the metallicity of these samples under high pressure is still controversial.
In this study, high_pressure behavior of VO_2 (M1) was revisited using infrared reflecti vity (IR) spectroscopy, Raman spectroscopy and in situ synchrotron X_ray diffraction (XRD) up to 64.7 GPa. Upon compression, VO_2 (M1) follows the expected structure tra nsition sequence, M1→M1'→X, whereas we found that the M1' phase
is a semiconductor within the pressure region of 11.4 -
43.2 GPa and became metallic with further compression. We also verified that the X ph ase is metallic. Upon decompression, the metallic X phase is stable above 21.7 GPa, a metal-insulator
transition occurs at this pressure, together with a structural transition from the X phase to a new monoclinic structure (space group p21/c). These results provide further insigh into the PIM of VO_2 (M1).

A. Acun et al. “Atomically Controlled Surfaces Interfaces and Nanostructures”
edited by A. Bianconi, A. Marcelli (Superstripes Press, Rome 2016) isbn: 9788866830597

Spontaneous oxidation of Ni clusters grown on highly ordered MgO/Ag(100) monolayers

Marco Smerieri[1]
[1]*Istituto dei Materiali per l’Elettronica ed il Magnetismo del Consiglio Nazionale delle Ricerche (IMEM - CNR)*

Email: *marco.smerieri@imem.cnr.it*
Key words: Metal-oxide interface; Ultrathin oxide films and nano-clusters; Interface oxygen; STM and DFT.

In spite of the relevance of ultrathin MgO films for the study of model systems as well as for technological applications, the growth of extended, well-ordered, ultrathin films has been hard to achieve so far. By combining scanning tunnelling microscopy with X-ray photoemission and vibrational spectroscopy an with *ab-initio* calculations, we demonstrate that the morphology of sub-monolayer MgO/Ag(100) film strongly depends not only by the growth conditions but also by after-growth treatments. Moreover, we prove that accumulation of oxygen atoms at the MgO/Ag interface may occur.[1,2] Its presence reduces the compressive stress of the oxide film, favouring the formation of extended terraces. The result is the ability to tune the morphology of the films from small monolayer islands with irregular borders, to perfectly square bilayer islands of some 10nm size, to extended MgO monolayer limited only by the width on the Ag terrace underneath. Due to their almost perfect structure and to the presence of a band-gap already compatible to the one of bulk oxide, this last geometry is a very good candidate substrate for the deposition of further nano-objects. We tested it by depositing Ni nanoclusters at 100 K<T<300 K.[3] In the limit of low Ni coverage, the typical clusters of a few tens of atoms coexist with small aggregates of four to six atoms in size. The latter are flat rather than 3D, as expected for Ni tetramers, pentamers, or hexamers. Both the shape of these nanoclusters and the interatomic distance between neighbouring Ni atoms are indicative that the nanoparticles do not consist of pure metal atoms. Instead, a Ni_yO_x structure has formed thanks to the availability of atomic oxygen accumulated at the MgO/Ag interface, with Ni clusters acting as oxygen pumps. Besides being of relevance in view of the use of metal nanoclusters in catalysis and other applications, this finding gives a further proof of the peculiar behaviour of ultrathin oxide films.

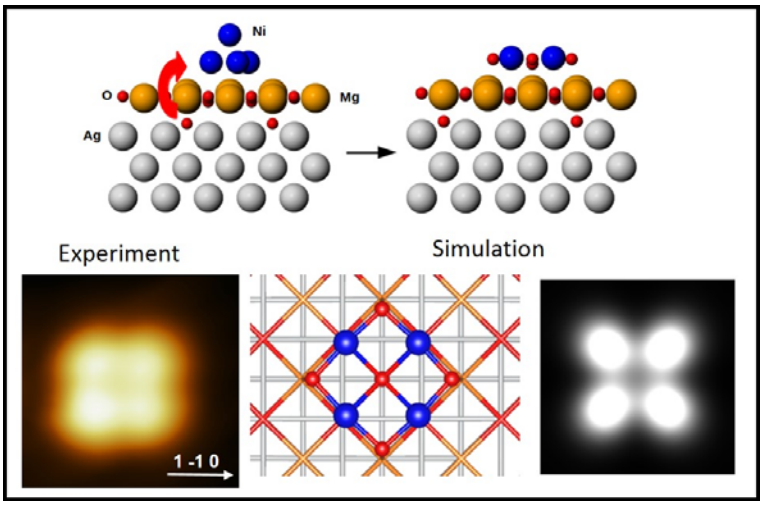

Figure 1. Top: Schematic model of the formation mechanism of Ni_4O_5 nano-clusters. Bottom: High-resolution experimental STM image of a Ni_4O_5 tetramer (8 Å × 8 Å), corresponding optimized DFT geometry and simulated STM image.

References

1. J. Pal, M. Smerieri, E. Celasco, L. Savio, L. Vattuone, M. Rocca, *Phys. Rev. Lett.* 112, 126102 (2014). http://dx.doi.org/10.1103/PhysRevLett.112.126102
2. J. Pal, M. Smerieri, E. Celasco, L. Savio, L. Vattuone, R. Ferrando, S. Tosoni, L. Giordano, G. Pacchioni, M. Rocca, *J. Phys. Chem. C*, 118, 26091 (2014). http://dx.doi.org/10.1021/jp507718n
3. M. Smerieri, J. Pal, L. Savio, L. Vattuone, R. Ferrando, S. Tosoni, L. Giordano, G. Pacchioni, M. Rocca, *J. Phys. Chem. Lett.* 6, 3104 (2015). http://dx.doi.org/10.1021/acs.jpclett.5b01362

Highly flexible and transferable SWNTs/VO_2/Mica hierarchical films for high-performance thermochromic devices

Y. L. Chen[1] , S. Chen[1], H. Ren[1] and C. W. Zou[1]
[1]*National Synchrotron Radiation Laboratory, University of Science and Technology of China*

Email: *tower@mail.ustc.edu.cn*
Key words: 3- Electronic and optical properties of surfaces and interfaces; 11- Oxides, nitrides and high-k dielectrics; 13- Nanotubes and other 1D materials

The chromogenic technologies as one of the most promising practical applications have been studied for several decades, including thermochromic (depending on temperature), electrochromic (depending on voltage or charge), photochromic (depending on irradiation), and gasochromic (depending on exposure to reducing or oxidizing gases).[1] Vanadium dioxide (VO_2) with reversible metal-insulator transition (MIT) is a promising thermochromic material for next-generation smart windows and infrared devices. However, the specific applications are largely limited by the relatively high critical temperature as well as the weak of flexible and the non-transferable grown-substrates.[2] Herein, we report such limitations can be overcome by growing VO_2 on layered mica under high temperature directly, together with integration of high transparent single-walled carbon nanotube films. The SWNTs/VO_2/Mica hierarchical films can be peeled-off to form a free-standing ultra-thin optical window and transferred onto any desired substrates with high flexibility and transparency. Through the self-heating SWNTs/VO_2 layer, the MIT process of VO_2 layer can also be facilely modulated by applying bias current, achieving the dynamical regulation of the infrared transmission with excellent stability and reversibility. Furthermore, by adjusting the bias current, it is possible to change the starting local temperature and shift the initial situation close to the "phase transition boundary", resulting in the decreased energy barrier to trigger MIT behavior. This fascinating strategy overcomes the high critical temperature limit of VO_2 and avoids the bottle-neck problem in practical applications of VO_2 material, which demonstrates wide applications of this kind of device in the future.

References

1. C. Granqvist, P. Lansåker, N. Mlyuka, G. Niklasson, E. Avendaño, Solar Energy Materials and Solar Cells 93, 2032 (2009).
2. H. Kim, Y. Kim, K. Kim, H. Jeong, A. Jang, S. Han, D. Yoon, K. Suh, H. Shin, T. Kim, W. Yang, ACS nano 7, 5769 (2013).

A. Acun et al. "Atomically Controlled Surfaces Interfaces and Nanostructures"
edited by A. Bianconi, A. Marcelli (Superstripes Press, Rome 2016) isbn: 9788866830597

Effect of Oxygen doping on Chemical Bonding and Mechanical Properties of CVD-grown DLC Films

Rintaro Sugimoto[1] , Hiro Abe[2], Shuichi Ogawa[1], Takanori Takeno[2], Koushi Adachi[2], Yuji Takakuwa[1]
[1]IMRAM, Tohoku University, [2]Department of Engineering, Tohoku University

Email: *rin817@mail.tagen.tohoku.ac.jp*
Key words: Diamond-like Carbon, Photoemission-assisted Plasma-enhanced CVD, O doping, Raman specroscopy, XPS

Diamond-like carbon (DLC) films with high hardness and flat surface morphology are useful as a low friction coating materal. Such mechanical properties are widely controlled by changing the composition ratio among sp^3/sp^2/H of DLC. Furthermore, oxygen or nitrogen can be doped to DLC films to improve their mechanical properties [1]. However, the doping efficiency depends on the kind of CVD process, for example, microwave or radio frequency plasma-enhanced CVD [1]. In this study, a photoemission-assisted plasma-enhanced CVD (PA-PECVD) with a CH_4/CO_2/Ar gas mixture, in which photoelectrons emitted from a UV-irradiated substrate are utilized as a trigger to generate a DC discharge plasma, was employed to synthesize O-doped DLC films [2, 3]. Owing to the assistance of photoelectron, a high density plasma can be generated very close to the substrate, making it possible to that radicals such as O and CO radicals as well as CH_x radicals reach the substrate without collisions between them resulting in production of O_2, CO_2 and soot. As previously reported [2, 3], the efficient O doping and the high growth rate were achieved at the same time by PA-PECVD. In this report, the CO_2 concentration (n_{CO2}) and DLC thickness (d_{DLC}) dependence of the chemical bonding were investigated by Raman spectroscopy, XPS, SIMS, and AFM. Mechanical properties of hardness and friction coefficient were also measured. Based on the correlation between them, a crystal structure model of O-doped DLC and a PA-PECVD growth mechanism are considered.

From Raman spectra and intensity ratios of D bands to G bands in Figs. 1 and 2(a), respectively, the growth of nanographite is enhanced by increasing n_{CO2} at growth temperature of 150℃ and the Raman spectrum at n_{CO2} of 14.3% is similar to that grown at ca. 600℃ without CO_2. However C 1s photoelectron spectra showed that sp^3/sp^2 was maintained almost unchanged independent of n_{CO2}, whereas the doped O amount increased in proportion to n_{CO2} as indicated from the O/C ratio in Fig. 2(b). These results suggests that the nanographite particles are embedded in sp^3-rich O-doped DLC matrix. Here it is noted that the H concentration was almost the same for all samples. The hardness of the O-doped DLC filsm was measured as ca. 10 GPa regardless of n_{CO2}. Such a mechanical property is in good agreement with the chemical bonding described above. Thus the O doping to DLC is efficiently achieved by PA-PECVD with nontoxic and nonexplosive CO_2 gas. The d_{DLC} dependence of chemical composition and mechanical properties as well as the aging effect will be presented.

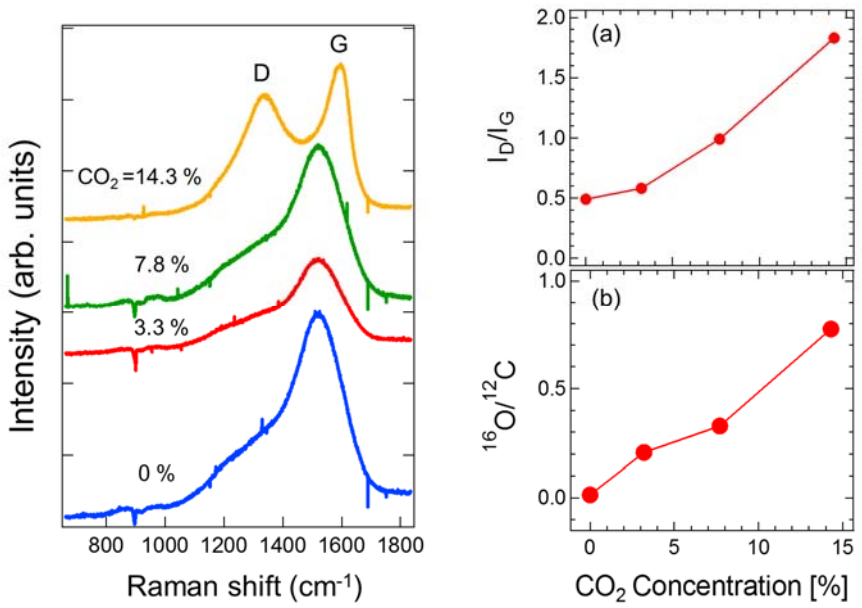

Figure 1: CO_2 concentration dependence of Raman spectra for O doped DLC films with thickness of ca. 200 nm grown at 150 ºC.
Figure 2: CO_2 concentration dependence of (a) Raman intensity ratio of D bands to G bands and (b) SIMS intensity ratio of ^{16}O to ^{12}C.

References

1. S. Yamamoto *et al*., Surf. Coat. Technol. 210 (2012) 1-9. http://dx.doi.org/10.1016/j.surfcoat.2012.07.005.
2. M. Yang *et al., Thin Solid Flm* 523 (2012) 25. http://dx.doi.org/10.1016/j.fts.2012.05.059.
3. S. Takabayashi *et al*., Diamond Relat. Phenomen. 53 (2015) 11-17. http://dx.doi.org/10.1016/j.diamond.2015.01.011.

Mo3S session

A. Acun et al. “Atomically Controlled Surfaces Interfaces and Nanostructures”
edited by A. Bianconi, A. Marcelli (Superstripes Press, Rome 2016) isbn: 9788866830597

Target-size single-crystalline quasi free-standing graphene on Ni(111)

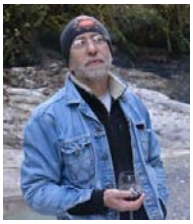

K.N. Eltsov , S.L. Kovalenko, T.V. Pavlova, B.V. Andryushechkin
A.M. Prokhorov General Physics Institute RAS, 38, ulitsa Vavilova, 119991 Moscow, Russia

Email: - *eltsov@kapella.gpi.ru*
Key words: Graphene and other 2D materials

In this work, we report the method of the growth of the quasi free-standing single-crystalline graphene monolayer on Ni(111). We have obtained that the adsorption of propene on Ni (111) at 25 °C and the subsequent annealing at 500 °C results in the growth of the epitaxial graphene monolayer. Since no rotated domains or other defects were observed in STM, we can conclude that the single-crystalline graphene monolayer covering all the sample area (6×6 mm) has been grown on Ni(111).

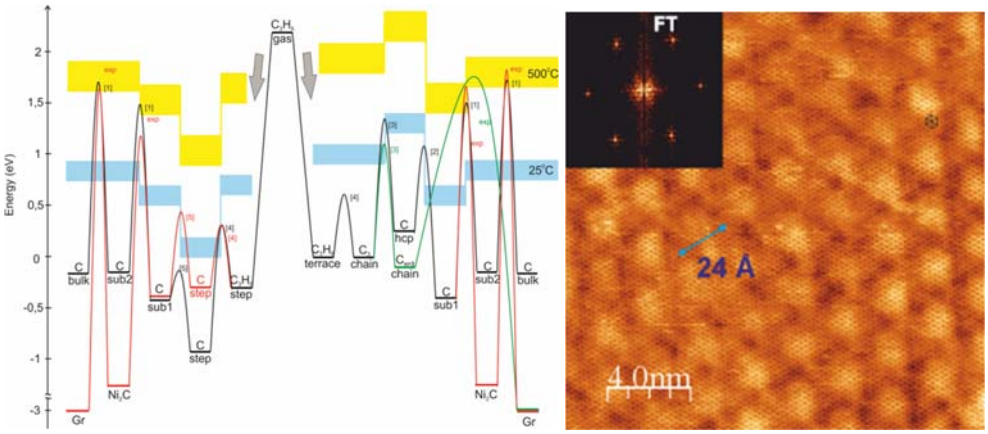

Figure 1. a) Energy diagram of C_3H_6 transformation and carbon structures formation on Ni(111) during propene adsorption at 25 °C/annealing at 500°C cycle; b) STM image of Gr/Au/Ni(111) after gold intercalation: dislocation loop superstructure Ni(111))-9.5×9.5-Au and graphene atomic structure are clearly seen. Fourier transform image is presented as an insert.

Our experimental STM data combined with DFT calculations indicate that the mechanism of the graphene growth includes following steps.
At 25 °C:
- The dehydrogenation of propene molecules at terraces and the complete dissociation at step edges;

- Formation of carbon atomic chains on terraces;
- Diffusion of carbon atoms into subsurface region through step edges and their accumulation between nickel atomic layers;
At 500 °C (annealing):
-The segregation of carbon atoms on surface of Ni(111), formation of the carbide phase (Ni_2C) and the subsequent transformation into graphene

To detach the graphene monolayer from the Ni(111) substrate, we used the intercalation by gold. The Au intercalation process included the deposition of gold onto the graphene monolayer on Ni(111) and the subsequent annealing at 450 °C. As a result, the network of dislocation loops Ni(111)-(9.5×9.5)-Au was formed, being a good indication of the penetration of gold atoms underneath of graphene.

Figure 1a shows energy diagram of propene molecule dehydrogenation (on terraces) and dissociation (on steps) at RT (25 °C) adsorption and following carbon atoms transformation into nickel carbide and graphene at 500 °C on Ni(111). The all energy levels and potential barriers have been calculated within DFT and with Nudged Elastic Band (NEB) approach. In Fig.1b, the resulting graphene monolayer on Ni(111)-9.5×9.5-Au is presented.

ARPES measurements show perfect Dirac cone in electron dispersion corresponding to quasi free-standing graphene.

A. Acun et al. “Atomically Controlled Surfaces Interfaces and Nanostructures”
edited by A. Bianconi, A. Marcelli (Superstripes Press, Rome 2016) isbn: 9788866830597

Nano-sized cobalt germanide islands on Ge(001): Morphology and chemical composition

Jens Falta[1,2,*], Moritz Ewert[1], Thomas Schmidt[1], Jan Ingo Flege[1,2], Inga Heidmann[1], Thomas Grzela[3], Wolfgang M. Klesse[3], Michael Foerster[4], Lucia Aballe[4], and Thomas Schroeder[3,5]

[1] *Institute of Solid State Physics, University of Bremen, Otto-Hahn-Allee 1, 28359 Bremen, Germany*

[2] *MAPEX Center for Materials and Processes, University of Bremen, Bibliothekstr. 1, 28359 Bremen, Germany*

[3] *IHP, Im Technologiepark 25, 15236 Frankfurt (Oder), Germany*

[4] *ALBA Synchrotron Light Facility, Carretera BP 1413, km 3.3, Cerdanyola del Vallès, Barcelona 08290, Spain*

[5] *BTU Cottbus-Senftenberg, Institute fo Physics and Chemistry, Konrad-Zuse-Str. 1, 03046 Cottbus, Germany*

Email: * *falta@ifp.uni-bremen.de*

Key words: Atomic and nanoscale structure of surfaces and interfaces: advanced methods; Nanoscale structure, growth processes and strain in thin layers and interfaces; Frontiers aspects of semiconductor, surfaces and interfaces]; Scanning probe and surface microscopy

Contact formation is a key issue when implementing Ge-based structures into established Si device technology. *In-situ* x-ray absorption spectroscopy photoemission electron microscopy (XAS-PEEM), micro-illumination low-energy electron diffraction (μ-LEED), and *ex-situ* atomic force microscopy (AFM) have been employed for a detailed study of reactive cobalt germanide growth on Ge(001) [1] . Ultra-thin films were grown by Co deposition at elevated temperatures. At a deposition temperature of 670°C, a rich morphology with different island shapes and dimensions is observed (fig. 1(a)), and a correlation between island morphology and stoichiometry is observed (fig. 1(b)). The combination of XAS-PEEM and μ-LEED reveals that a large part of the islands consists of $CoGe_2$. Many of these islands have an unusual epitaxial relationship, i.e. $CoGe_2[\bar{1}10](111) \parallel Ge[\bar{1}10](001)$, an orientation that has not been reported so far. The side facets of these islands were identified to be of (112) and (113) orientation. Additionally, two more phases were found, most likely Co_5Ge_7 and CoGe. Remarkably, a comparison of growth on Ge(001) single crystals and on Ge(001)/Si(001) epilayer substrates shows that the occurrence of such intermediate phases is strongly suppressed on single-crystal substrates, as compared to Ge epilayer substrates, which leads to the conclusion that these intermediate phases are likely promoted by defects or residual strain or both. It should be noted that this is not a general trend, since on amorphous Ge, for instance, the finding of $CoGe_2$ has been

reported without formation of any CoGe [2]. With respect to applications, an important conclusion is that the defect structure and defect density, as well as the strain of Ge layers on Si might play a significant role here and have to be taken into account when trying to transfer results from single-crystal based research to device development.

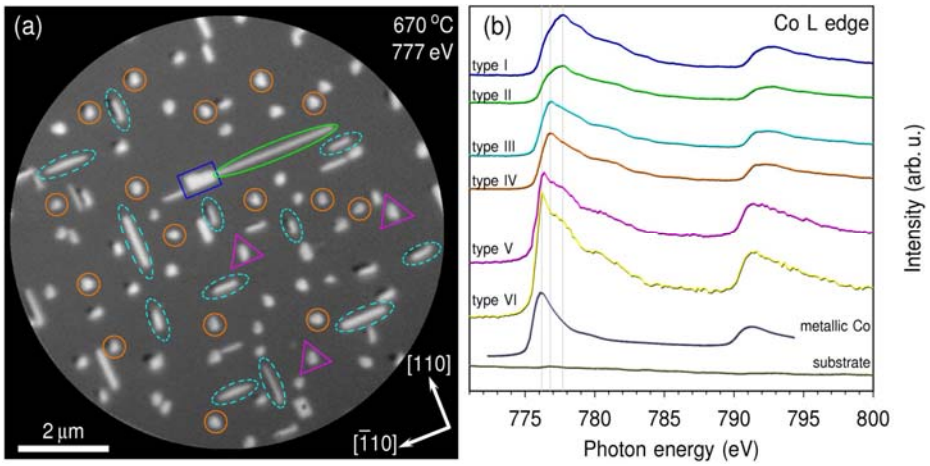

Figure 1: (a) XAS-PEEM image after Co deposition on a Ge(001) epilayer at 670°C. Islands of various types are found; (b) Local x-ray absorption spectra for the different island types (I to VI as indicated by the colored symbols in (a)) reveal that islands of different morphology consist of distinct stoichiometric composition, i.e. $CoGe_2$, Co_5Ge_7, and CoGe; the metallic spectrum has been taken from a Co layer deposited at RT (without annealing).

References

1. M. Ewert, Th. Schmidt, J. I. Flege, I. Heidmann, T. Grzela, W. M. Klesse, M. Foerster, L. Aballe, T. Schroeder, and J. Falta, submitted to Nanotechnology, 2015; published online under *http://arxiv.org/abs/1602.04680*.
2. K. Opsomer, D. Deduytsche, C. Detavernier, R. L. van Meirhaeghe, A. Lauwers, K. Maex, and C. Lavoie, Appl. Phys. Lett., 90 031906 (2007)

Atomic and electronic structure of corrugated silicene

Agata Podsiadły-Paszkowska[1] , Mariusz Krawiec[1]
[1]*Maria Curie-Skłodowska University in Lublin*

Email: *agata.podsiadly@gmail.com*
Key words: silicene, 1D corrugation

Silicene, a two-dimensional material composed of Si atoms, is known as a counterpart of graphene, because of its similar atomic arrangement (honeycomb lattice) and energetic structure. Both freestanding flat graphene and low-buckled silicene behave as zero-gap semiconductors with linear bands around the Fermi level [1,2]. However, this perfect picture can easily be disturbed by any factor, which arise naturally in experiment, such as finite temperature or interaction with a substrate, leading to distortion of the atomic arrangement and influencing the band structure [3,4].

We give a systematic analysis of the atomic and electronic structure of silicene subjected to one-dimensional structural modulation in the armchair or zigzag direction. Our first principles density functional theory calculations show the structural deformation dependent anisotropic Dirac cone with different group velocities in the band structure. We also discuss our results in connection with graphene.

This work has been supported by the National Science Centre (Poland) under Grant No. DEC-2014/15/N/ST3/03816.

References

1. K. S. Novoselov, A. K. Geim, S. V. Morozov, D. Jiang, Y. Zhang, S. V. Dubonos, I. V. Grigorieva, A. A. Firsov, Science 306, 666 (2004).
2. S. Cahangirov, M. Topsakal, E. Aktürk, H. Sahin, S. Ciraci, Phys. Rev. Lett. 102, 236804 (2009).
3. S. Okada and T. Kawai, Jpn. J. Appl. Phys. 51, 02BN05 (2012).
4. H. Liu, J. Gao, J. Zhao, J. Phys. Chem. C 117, 10353 (2013).

Investigation of the influence of deposition temperature and substrate type on physical and morphological characteristics of GaN thin films synthesized in APCVD

Gulnar Sugurbekova[1], Murat Baisariyev[1], R.J. Iskakov[1], N.K. Akhmetov[1]
[1]*National Laboratory Astana, Nazarbayev University*
Center of Energy and Advanced Materials Science

Email: *gulnar.sugurbekova@nu.edu.kz*
Key words: GaN semiconductors, nanorods, hexagonal platelets, CVD, heteroepitaxy, SEM, Raman scattering, optical phonons

GaN is a semiconductor material with wide direct band gap that has many potential applications in wide range of industries. The unique properties such as structural stability under harsh chemical and physical environments as well as its broad range of electronic properties such as high dielectric breakdown makes it an active area of research. However the wide implementation and market penetration is hindered with high cost of production and difficulty of epitaxial growth of GaN single crystals. The most important reason for that is the lack of lattice matched substrates that can withstand aggressive synthesis environments [1]. Since the inception of research on GaN semiconductors different fabrication methods have been employed such as MOCVD, Magnetron Sputtering and Molecular Beam Epitaxy. Among other fabrication methods our group have chosen the hot-wall horizontal tube CVD process to fabricate GaN thin films due to the low cost of equipment and simplicity of experimental procedure. The samples were grown in multi zone temperature CVD chamber with the use of pure Ga metal and NH_4Cl as main reactants in N2 carrier gas environment without catalysts. The aim of this study is to analyze the effect of growth temperature and substrate type on crystal quality, morphology and other physical properties of obtained GaN thin films and nanostructures. The samples were characterized by SEM, EDX, XRD, Raman and Vis-NIR spectroscopies. The SEM analysis of the images showed that the morphology of thin films on different substrates were substantially different from each other. The deposition of GaN on quartz substrate resulted in growth of nano-micro sized hexagonal rods that resemble the hedgehog fur while films grown on Si substrate exposed to 844-852^{o}C resulted in hexagonal platelets with outgrown whiskers. It was observed that the size of the hexagonal platelets decreases as the temperature of the Si substrate increases. It was also found that the average surface area of the platelets decreased as the temperature of the substrates increased. Raman spectra analysis revealed the presence of E_2 (high) and A_1(LO) modes in all the samples which are two-symmetry allowed modes of hexagonal wurtzite GaN. Additionally, an appearance of zone boundary phonon modes was noticed at ~250cm^{-1} and ~410cm^{-1} which could be attributed to surface disorder, quantum confinement effect and acoustic overtone as reported by several research

groups [2,5-6]. Figure 2b. shows the comparative Raman spectra of the thin films grown on silicon and quartz substrates. The elevated peak intensity of E_2 (high) mode of Si#2 sample relative to other samples indicates the film's higher crystallinity. The degree of the internal stresses in the films was calculated by employing the equation modeled by Kozawa et al. [3]. The calculation results reveal that all the thin films that were deposited were in tensile stress due to the lattice mismatch between substrate and deposited layer as well as due to involuntary incorporation of the impurities as evidenced by EDX data.

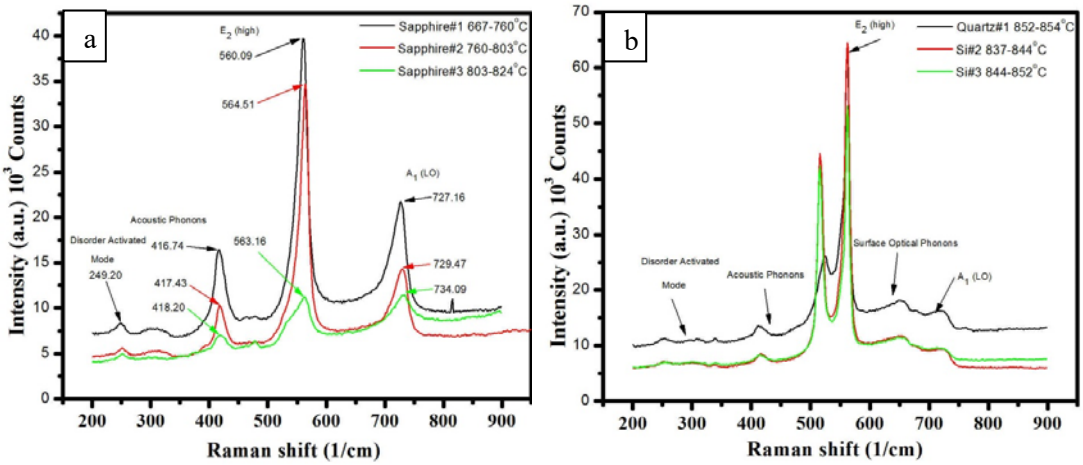

Figure 2: The Raman spectroscopy patterns for GaN samples. The above images of the Raman spectra correspond to data from thin films deposited on (a) sapphire substrates, (b) comparison of silicon and quartz substrates

References

1. M.H. Kane, N. Arefin GaN on Si substrates for LEDs, p99, Woodhead Publishing Limited 2014
2. C.-C. Chen, C.-C. Yeh, C.-H. Chen, M.-Y. Yu, H.-L. Liu, J.-J. Wu, et al., J. Am. Chem. Soc. 123 (2001) 2791.
3. H. Harima, H.Sakashita, T.Inoue, S.I. Nakashima, J.Cryst.Growth 189 (1998) 672
4. T. Kozawa, T. Kachi, H. Kano, Y. Taga, M. Hashimoto, N. Koide, et al., J. Appl. Phys. 75 (1994) 1098.
5. H-L. Liu, C.-C. Chen, C.-T. Chia, C.-C. Yeh, C.-H. Chen, M.-Y. Yu, et al., Chem. Phys. Lett. 345 (2001) 245.
6. X.-F. Wei, F. Shi, Appl. Surf. Sci. 257 (2011) 9931.

Mo4T session

Hybrid materials for Optoelectronics

Aurora Rizzo,[1] Silvia Colella,[1,2] Andrea Listorti,[1,2] Sofia Masi,[1,2,3] Alessandro Cannavale,[1,2] Pierluigi Cossari,[1,2] Marco Mazzeo,[1,2] Luisa De Marco,[1,3] Armando Genco,[1,2] Fabrizio Mariano[1,2] and Giuseppe Gigli.[1,2]
[1]Istituto di Nanocienze, CNR-NANOTEC
[2]Dipartimento di Matematica e Fisica, University of Salento
[3]Center for Bio-Molecular Nanotechnology - Fondazione Istituto Italiano di Tecnologia IIT

Email: *giuseppe.gigli@unisalento.it*
Key words: 19- Frontiers aspects of semiconductor, surfaces and interfaces; 4-Growth and applications of thin films; 29- Nanomaterials for energy

The exploration of innovative materials and device architectures is constantly fostering our research activity on novel generation optoelectronic devices, aiming at low cost and highly efficient solutions.
From conceptually new devices based on self-assembling hybrid perovskites,[1] to bulk heterojunction architectures based on versatile nanocrystals,[2] we have been exploring viable routes for an effective market impact of last generation photovoltaic and emitting devices.
Our vision is based on low cost processable materials, matching the requirements of existing technologies, for large-scale device production at reasonable production costs. Furthermore we pursuit the implementation of solar converting components into multifunctional devices, an example we conceived on this line, is a photovoltachromic cell integrating both photovoltaic and photoelectrochromic functionalities, targeting building integration.[3]

References

1. S. Masi, S. Colella, A. Listorti, V. Roiati, A. Liscio, V. Palermo, A. Rizzo, G. Gigli Sci Rep. 5: 7725 (2015); b) S. Masi, A. Rizzo, F. Aiello, F. Balzano, G. Uccello-Barretta, A. Listorti, G. Gigli, S. Colella Nanoscale ,7, 18956-18963 (2015)
2. C. Giansante, R. Mastria, G. Lerario, L. Moretti, I. Kriegel, F- Scotognella, G. Lanzani, S. Carallo, M. Esposito, M. Biasiucci, A. Rizzo, G. Gigli Adv. Funct. Mater. 25, 111-119 (2015); b) R. Mastria, A. Rizzo, C. Giansante, D. Ballarini, L. Dominici, O. Inganäs, G. Gigli J. Phys. Chem. C, 119, 14972- 14979 (2015).
3. A.Cannavale, G. E. Eperon, P. Cossari, A. Abate, H. J. Snaith, G. Gigli, Energy Environ. Sci. 8, 1578 (2015)

A. Acun et al. “Atomically Controlled Surfaces Interfaces and Nanostructures”
edited by A. Bianconi, A. Marcelli (Superstripes Press, Rome 2016) isbn: 9788866830597

Atomistic Origin of Dipole Layers at High-k/SiO_2 Interfaces

Takanobu Watanabe
Faculty of Science and Engineering, Waseda University

Email: *watanabe-t@waseda.jp*
Key words: High-k dielectrics, Interface dipole, Molecular dynamics, Ion migration

The introduction of high-k/metal gate stacks into CMOS devices causes anomalous shifts of the threshold voltage (V_{TH}). Recent studies have shown that these anomalous V_{TH} shifts are caused by an electric dipole layer formed at the high-k/SiO_2 interface [1]. Several mechanisms have been proposed to explain the origin of the interface dipole layer, but a unified view has not yet been reached. The proposed mechanisms can be roughly classified into two groups: (1) electronic redistribution around the interface [2,3] and (2) redistribution of ions across the interface [4]. This talk will focus on the latter model by presenting a series of molecular dynamics (MD) simulations performed by the author’s group [5–7].

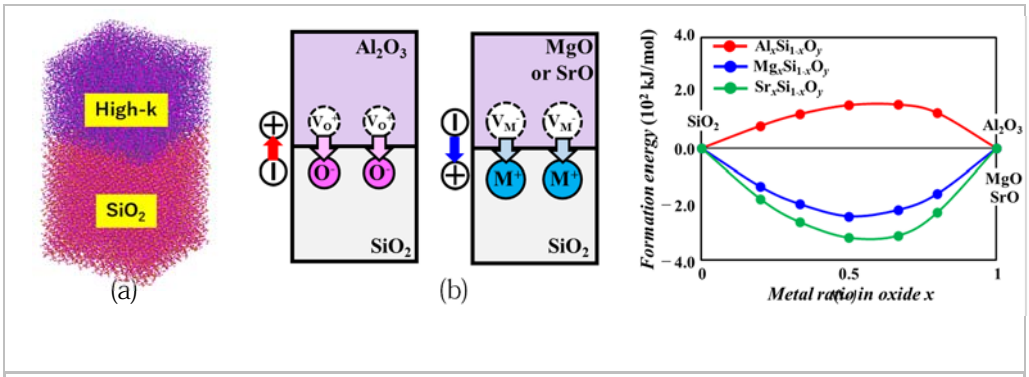

Figure 1: (a) High-k oxide/SiO_2 stack structure used in the MD simulation. (b) Schematic mechanism of dipole layer formation. (c) Formation energy of silicates.

This group has conducted MD simulations of Al_2O_3/SiO_2, MgO/SiO_2, and SrO/SiO_2 interfaces (Fig. 1(a)), employing a simple two-body ionic interaction model of the Born-Mayer-Huggins potential. As a result, experimentally observed flatband voltage (V_{FB}) shifts have been successfully reproduced for all three systems. In the case of the Al_2O_3/SiO_2 interface, a dipole layer is formed by the migration of O ions from the Al_2O_3 side to the SiO_2 side. The direction of the dipole leads to a positive V_{FB} shift, so the orientation of the dipole appearing at the Al_2O_3/SiO_2 interface can be defined as positive. This result seems to coincide with the oxygen density accommodation model proposed by Kita and Toriumi [4], but it differs in the sense that O ion migration is

driven by some systematic force rather than by a simple diffusion induced by the O density gradient across the interface. In this talk, the driving force of O ion migration at high-k/SiO_2 interfaces in terms of the multipole moment around cations will be discussed. In contrast, opposite (negative) dipoles appear at the MgO/SiO_2 and SrO/SiO_2 interfaces (Fig. 1(b)). The orientation of the dipole at the MgO/SiO_2 interface cannot be explained by the oxygen density difference model [4] because the oxygen density of MgO is higher than that of SiO_2. However, MD simulation can correctly reproduce the direction of the experimentally observed V_{FB} shift at the MgO/SiO_2 interface. The negative dipoles at the MgO/SiO_2 and SrO/SiO_2 interfaces are formed by a preferential migration of metal cations from the high-k oxide toward the SiO_2 layer, and silicate layers are formed at these interfaces. Figure 1(c) shows the formation energy of silicates estimated by the employed interatomic potential. The Mg and Sr silicates become more energetically stable at an intermediate composition, whereas the Al silicate is unstable. The formation energy of the Sr silicate is lower than that of the Mg silicate, suggesting that the ease of silicate formation is the driving force of negative dipole formation.

In conclusion, the dipole formation at high-k/SiO_2 interfaces can be explained by the ion redistribution model. The negative dipoles at the MgO/SiO_2 and SrO/SiO_2 interfaces are formed by a preferential migration of metal cations from the high-k oxide toward the SiO_2 layer during the formation of a stable silicate phase. Thus, the migration of metal cations as well as the migration of oxygen ions must be taken into account when considering the mechanics of the dipole layer formation.

Acknowledgement: This work was supported by JST-CREST and a Grant-in-Aid for Scientific Research (B) (15H03979) from the Ministry of Education, Culture, Sports, Science, and Technology of Japan.

References

1. A. Toriumi and T. Nabatame, in High Permittivity Gate Dielectric Materials, ed. S. Kar (Springer, Heidelberg, 2013) Vol. 43, Chap. 6.
2. K. Kakushima, K. Okamoto, M. Adachi, K. Tachi, P. Ahmet, K. Tsutsui, N. Sugii, T. Hattori, H. Iwai, Solid-State Electron. 52, 1280 (2008). http://dx.doi.org/10.1016/j.sse.2008.04.015.
3. X. Wang, K. Han, W. Wang, S. Chen, X. Ma, D. Chen, J. Zhan, J. Du, Y. Xiong, and A. Huang, Appl. Phys. Lett. 96, 152907 (2010). http: //dx.doi.org/10.1063/1.3399359.
4. K. Kita, and A. Toriumi, Appl. Phys. Lett. 94, 132902 (2009). http://dx.doi.org/10.1063/1.3110968.
5. R. Kuriyama, M. Hashiguchi, R. Takahashi, A. Ogura, S. Satoh, and T. Watanabe, Jpn. J. Appl. Phys. 53, 08LB02 (2014). http://dx.doi.org/10.7567/JJAP.53.08LB02.
6. T. Watanabe, R. Kuriyama, M. Hashiguchi, R. Takahashi, K. Shimura, A. Ogura, S. Satoh, ECS Trans. 64, 3–15, (2014). http://dx.doi.org/10.1149/06408.0003ecst.
7. K. Shimura, R. Kunugi, A. Ogura, S. Satoh, J. Fei, K. Kita, T. Watanabe, Jpn. J. Appl. Phys. 55, 04EB03 (2016). http://dx.doi.org/10.7567/JJAP.55.04EB03.

Ultrathin films for model catalysis studies

Mingshu Chen , Xuefei Weng, Huan Li, Hong Zhang,
Yanping Zheng, Huilin Wan
State Key Laboratory of Physical Chemistry of Solid Surfaces,
Department of Chemistry, Xiamen University
Xiamen, Fujian, China

Email: *chenms@xmu.edu.cn*
Key words: Growth and applications of thin films; Model Catalysis; In-situ Spectroscopies;

Fundamental understanding of catalysts and how they function under the reaction conditions is the foundation for design high efficient catalysts and improved current catalytic conversion processes. Among such researches, *in-situ* studies on the model catalyst surfaces may provide more direct evidences of the structure ~ activity relationship, better understand the nature of the active sites. Metal oxide thin films grown on a refractory metal substrate are idea models for thoroughly investigating the structure and property of oxide supports and oxide catalysts. Moreover, it is also a prototype system to study the metal-support interaction, as well as the strong metal support interaction (SMSI).

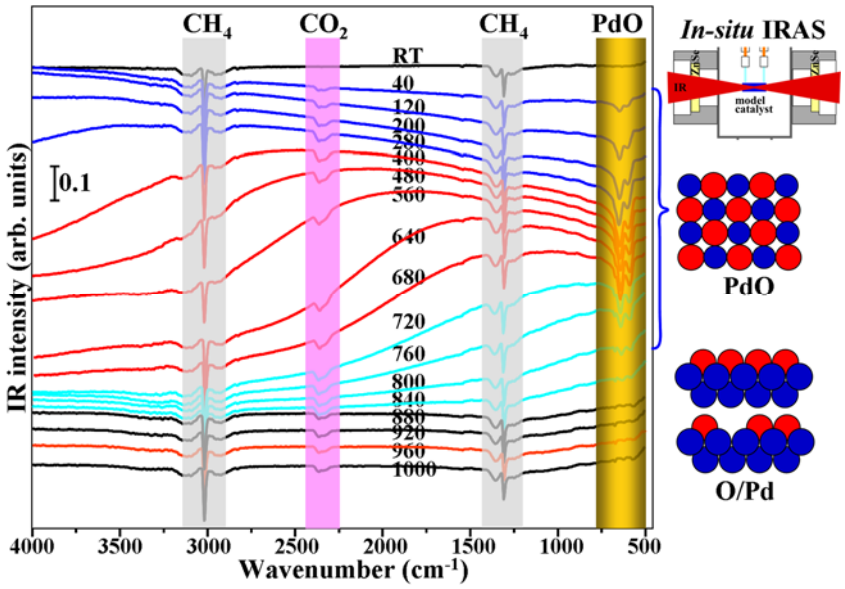

Figure 1: In situ IRAS spectra displaying the formation and reduction of surface palladium oxide during CH_4 oxidation as a function of the reaction time, i.e., O_2 partial pressure.

In this presentation, several systems of oxide/metal, TiO_x/Pt(111), VO_x/Pt(111), TiO_x/Ni(111), MnO_x/Rh(111), FeO_x/Rh(111), etc. were prepared, characterized and tested for CO oxidation, CO hydrogenation, and alkane oxidation.
New development of *in-situ* infrared spectroscopies with a spectral range of 4000~400 cm^{-1} is capable of measuring both the surface species and changes specific to the interface, providing useful information for metal-oxide interaction

References

1. Basic research needs: Catalysis for Energy, Report from the US Department of Energy, 2007.
2. M. S. Chen, X. V. Wang, L. H. Zhang, Z. Y. Tang, H. L.Wan, Langmuir 26, 18113 (2010).
3. Y. P. Zheng, L. H. Zhang, S. L. Wang, D. Ding, M. S. Chen, H. L. Wan, Langmuir 29, 9090 (2013).
4. F. Weng, H. J. Ren, M. S. Chen, H. L. Wan, ACS Catal. 4, 2598 (2014).

Characterization and engineering of the interface and surface of nanoscale multilayers for EUV and X-ray Optics

Qiushi Huang[1], Zhong Zhang[1], Wenbin Li[1], Igor V. Kozhevnikov[2], Philippe Jonnard[3,4], Zhanshan Wang[1]
[1]*Key Laboratory of Advanced Micro-Structured Materials MOE, Institute of Precision Optical Engineering, School of Physics Science and Engineering, Tongji University, Shanghai 200092, China*
[2] *Shubnikov Institute of Crystallography, Russian Academy of Sciences, Leninskiy pr. 59, Moscow 119333, Russia*
[3] *Sorbonne Universités, UPMC Univ Paris 06, Laboratoire de Chimie Physique - Matière et Rayonnement, 11 rue Pierre et Marie Curie, F-75231 Paris cedex 05, France*
[4] *CNRS UMR 7614, Laboratoire de Chimie Physique - Matière et Rayonnement, 11 rue Pierre et Marie Curie, F-75231 Paris cedex 05, France*

Email: *huangqs@tongji.edu.cn*
Key words: 1-Nanoscale structure of interface and surface; 4-Growth and applications of thin films

Nano-scale multilayers are vital optical components in the extreme ultraviolet (EUV) and X-ray wavelength range which enable the reflection beyond the total reflection region. They have been widely used in the astronomical observation, accelerator-based radiation facility, plasma diagnostics and EUV photolithography. To achieve the ideal optical performance, the nanoscale multilayer structure has to be made with atomically smooth and sharp interfaces. Here, some recent development of the multilayer optics in the Institute of Precision Optical Engineering (IPOE) in Tongji University will be presented.

The interface width of the EUV and X-ray multilayers contains two types of defects, the interface roughness and interdiffusion. These two defects are highly dependent on the layer growth mechanism which is affected by the material property, layer thicknesses, crystallization, and interfacial reaction. Thus, it is necessary to study the layer growth of certain materials before using them to fabricate a high reflectance mirror. For example, Cr/V multilayer is an ideal candidate working in the the water window region (λ=2.3-4.4 nm) for soft X-ray imaging. The period of the multilayer is only 1.2-1.8 nm which poses a challenge for fabrication. We studied the multilayer structure with varied layer thickness from 0.6 nm - 4.0 nm, using grazing incidence X-ray reflectometry (GIXR), atomic force microscopy (AFM) and transmission electron microscopy (TEM). It was found that the Cr and V layers can crystallize even with only 0.6 nm thickness and the larger thicknesses induced a columnar growth the polycrystalline structure and a large interface width. To reduce the interface width, we introduce ultrathin B_4C barrier layers at the interfaces which significantly suppressed the crystallization and improved the interface sharpness [1]. To further understand the chemical change inside the layer structure with B_4C barrier, depth profile X-ray

photoelectron spectroscopy (XPS) was performed which showed that the compound formation of VB_2, VC and B_4C contribute to the suppression of interdiffusion and crystallization. The second example is the Pd/Y multilayer which exhibits the highest theoretical reflectance at 8-12 nm waveband. However, the interfaces between Pd and Y are very poor due to the severe interdiffusion and reaction. In this case, we added nitrogen in the sputtering process which successfully passivated the interface. The XPS depth profile exhibited an obvious improvement of the elemental contrast between Pd and Y and the TEM result confirmed the YN formation in the layers which explained the passivation effect [2].
To better fabricate the multilayer optics, accurate characterization of the nanoscale structure especially in a nondestructive way is required. X-ray standing wave is an effective method to probe the interface structure with high resolution. Combined with fluorescence method, we investigated the Ti/Ni/Ti trilayer and determined the interface width at the two interfaces separately [3].

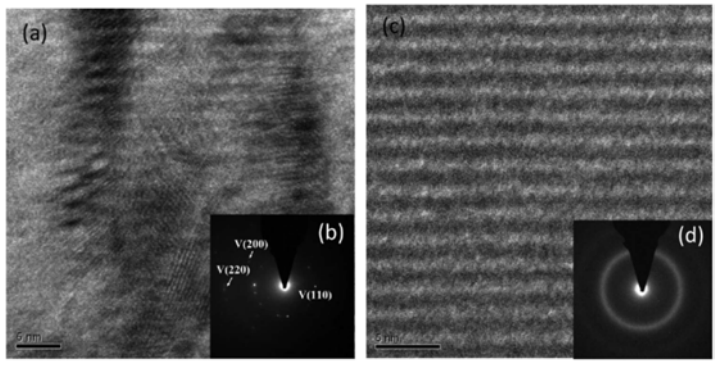

Figure 1: TEM images of the 1.8 nm-period Cr/V multilayer with no barrier layer (a, b) and with B_4C barrier layers (c, d).

References

1. Q. Huang, J. Fei, Y. Liu, et al., Opt. Lett. 41(4), 701 (2016).
2. D. Xu, Q. Huang, Y. Wang et al., Opt. Express, 23(26), 33018 (2015).
3. W. Li, J. Zhu, H. Li, et al, ACS Appl. Mater. Interfaces 5, 404 (2013).

Mo4S session

A. Acun et al. “Atomically Controlled Surfaces Interfaces and Nanostructures”
edited by A. Bianconi, A. Marcelli (Superstripes Press, Rome 2016) isbn: 9788866830597

Coupled surface-plasmon/thermoelectric power generators based on TCO nanowires

Alessandra Catellani,[1] Alice Ruini,[1,2] Marco Buongiorno Nardelli,[3] and Arrigo Calzolari,[1,3]
[1] *Istituto Nanoscienze CNR-NANO-S3, via Campi 213A, I-41125 Modena, IT*
[2] *Dip. FIM, Univ. Modena e Reggio Emilia, via Campi 213A I-41125, Modena IT*
[3] *Department of Physics, University of North Texas, Denton, TX 76203, USA*

Email: *arrigo.calzolari@nano.cnr.it*
Key words: thermoelectric, plasmonics, ZnO nanowires, Transparent Conductive Oxides, DFT

Sunlight energy conversion throughout exciton dissociation in nanoscale systems (e.g. nanoparticles, nanowires, tetrapods, hierarchical structures, etc.) is a valuable alternative to carbon-based sources for green and low cost power generators. Yet, the shrinking of the solar cell dimensions causes relevant problems, especially for the local thermal dissipation that limits the efficiency of photovoltaic systems. On the contrary, thermophotovoltaic converters, which directly convert the energy of photons emitted by a thermal source into electrical energy, are limited to photons with energy above the bandgap, thus reducing the range of solar spectrum available for photoconversion.
The design of mixed architectures that could positively exploit both light and heat conversion would represent an important step forward in the realization of more efficient devices. Particularly promising are recent prototypical systems that couple a plasmonic heater to a thermoelectric device [1] for the realization of power generators (Fig. 1). Despite the simple schematization of Figure 1, the realization of this kind of device necessitates the solution of a huge number of theoretical and techno- logical problems, among which the choice of the materials is one of the most crucial. In order to maximize the thermal trans- fer across the vacuum gap, the two systems should be prepared with the same material; however, the search for nanostructured materials, which are simultaneously plasmonic and thermoelectric, is a tremendous challenge.
Here, using calculations from first principles based on DFT, we demonstrate that In-doped ZnO nanowires [2] exhibit the unique property of being simultaneously thermoelectric transparent conducting oxides (TCOs) [3] and low-loss plasmonic materials in the near-IR and visible range [5]. The analysis of their geometrical and optoelectronic properties shows that In doping does not perturb significantly the structure of the nanowire, while gives rise to a good electrical conductivity. The calculated charge density injected into the conduction band of the host (> 1019 cm−3) is sufficient to sustain a surface-plasmon excitation, whose energy decay could generate a temperature gradient in the wire. This effect, coupled with the quenching of the thermal conductivity (also calculated by first principles [5]) due to surface scattering and the enhanced thermoelectric figure of merit with respect to the bulk

material, establishes the potential of In-doped ZnO nanowires as novel nanostructured energy converters in the form plasmon-heater/thermoelectric generators [2].

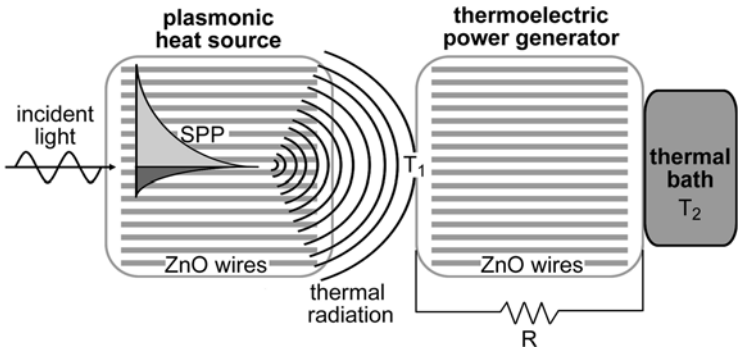

Figure 1: Schematic model of a coupled surface-plasmon/thermoelectric power generator based on ZnO nanowires.

References

1. Y. Xiong, R. Long, D. Liu, X. Zhong, C. Wang, Z.-Y. Li and Y. Xie, *Nanoscale*, 4, 4416–4420 (2012).
2. A. Catellani, A. Ruini, M. B. Nardelli and A. Calzolari, *RSC Advances,* 5, 44865-44872 (2015).
3. M. Bazzani, A. Neroni, A. Calzolari, A. Catellani, *Appl. Phys. Lett.*, 98, 121907 (2011).
4. A. Calzolari, A. Ruini, and A. Catellani, *ACS Photonics,* 1, 703-709 (2014).
5. A. Calzolari, T. Jayasekera, K.W. Kim, and M. Buongiorno Nardelli, *J. Phys. Cond. Matter.,* 24, 492204 (2012).

Improved high-bias stability of single-atom contacts formed by junction closing

Shin-saku Wakasugi, Shu Kurokawa, Akira Sakai
Department of Materials Science and Engineering, Kyoto University, Sakyo-ku, Kyoto, Japan

Email: *sakai.akira.4z@kyoto-u.ac.jp*
Keywords: single-atom contacts, high-bias stability

Single-atom contacts (SACs) are the smallest of metal contacts that consist only of one atom (or a single strand of atoms) yet form a conductive link between two electrodes. SACs are capable of sustaining a huge current density and would be a potential candidate of interconnects in future molecular- and atomic-scale devices. Studying the maximum ratings of SACs, their high-bias stability [1-3] in particular, is thus an endeavor not only of pure academic interest but also of much practical importance.

As for the stability of SACs, it is customary to discuss it using the following empirical equation [1] for the energy barrier W of the SAC break,

$$W = W_0 - \alpha V - \beta F, \quad (1)$$

where and V and F are the bias and the tensile force acting on an SAC, respectively, W_0, is the energy barrier at V=0 and F=0, and α and β are positive coefficients. When V increases, W decreases accordingly and vanishes at a break voltage V_b where the SAC ruptures. Majority of previous experiments on SACs have been made employing the break-junction method where SACs are formed by mechanically stretching macroscopic contacts. The resulting SACs are therefore subject to a tensile force and have F>0 in eq. (1). Because a positive F acts to reduce W, it tends to lower V_b and destabilize SACs as well. Smit *et al.* [1] showed that the average V_b of Au SACs is 1.2 V under F~0.95 nN at 4 K. This F amounts to 63% of the tensile strength of Au SACs. If we fabricate SACs under more reduced (or even negative, i.e. compressive) F, these SACs will show higher break voltage and exhibit improved high-bias stability than conventional SACs produced by junction breaking. In this work, we have tested this assumption by fabricating Au SACs not by breaking but by closing junctions and measure their V_b.

Atomic junctions of Au are first prepared by the conventional break-junction method. After once breaking a junction, its electrodes are made re-contact by slowly closing the junction. The re-contact is usually established abruptly through the jump-to-contact [4] which, for Au at 4 K, results in the formation of SACs with a nearly 100% probability.

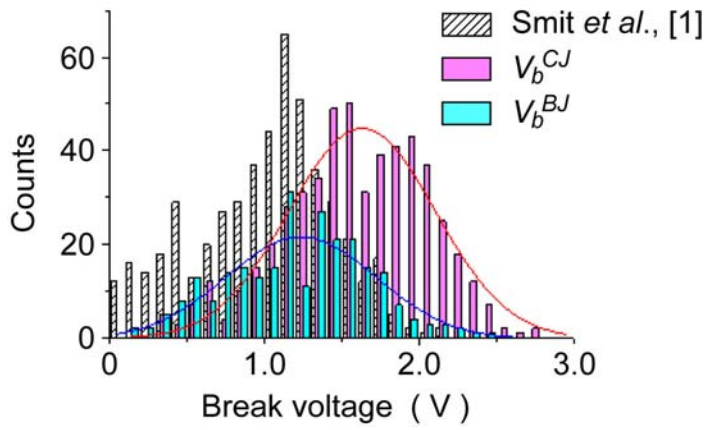

Figure 1: Distribution of the break voltage of Au SACs at 4 K. V_b^{CJ} and V_b^{BJ} are the break voltages measured at closing and breaking junctions, respectively. The previous break-voltage data reported by Smit *et al.* [1] is also shown for comparison.

Figure 1 shows the distribution of V_b^{CJ} obtained for Au SACs formed by closing junctions at 4 K. For comparison, the break voltage V_b^{BJ} acquired using the conventional break-junction method is also depicted. Our V_b^{BJ} is in good agreement with the previous data reported by Smit *et al.* [1] and shows a peak around 1.2 V. On the other hand, distribution of V_b^{CJ} shifts to higher biases and exhibits a peak at 1.6 V. Thus, as expected, SACs formed by closing junctions reveal better high-bias stability than conventional SACs prepared by breaking junctions. Our close-junction SACs should have lower F than break-junction SACs, but it is yet unclear how large F is acting on our SACs. If we use eq. (1) and α and β values reported in ref. [1], we can estimate F from V_b^{CJ}~1.6 V and obtain F~0.84 nN. However, a different data set of α and β [5] leads to F~0.55 nN. Furthermore, the formation of SACs through the not-so-simple jump-to-contact process makes it difficult to accurately evaluate F. Notwithstanding these quantitative uncertainties in the magnitude of F, the observed increment of V_b shown in Fig. 1 clearly indicates the critical importance of F in the high-bias break of SACs and provides an experimental ground for further improving the stability of SACs.

References

1. R. H. M. Smit, C. Untiedt, and J. M. van Ruitenbeek, Nanotechnology 15, S472 (2004).
2. D. Miura, K. Iwata, S. Kurokawa, and A. Sakai, e-J. Surf. Sci. Nanotech. 7, 891 (2009).
3. A. Sakai, in *Nanowires*, ed. K. Hashim (InTech, 2011), p. 439.
4. C. Untiedt, M. J. Caturla, M. R. Calvo, J. J. Palacios, R. C. Segers and J. M. van Ruitenbeek, Phys. Rev. Lett. 98, 206801 (2007).
5. M. Tsutsui, K. Shoji, M. Taniguchi, and T. Kawai, Nano Lett. 8, 345 (2008).

A. Acun et al. “Atomically Controlled Surfaces Interfaces and Nanostructures”
edited by A. Bianconi, A. Marcelli (Superstripes Press, Rome 2016) isbn: 9788866830597

Transport properties of nanoheterostructures, influence of interfaces on cathodoluminescence properties

Zamoryanskaya M.V.[1], Kuznetzova Ya.V.[1], Ivanova E.V.[1], Karavaev M.B.[1], Shustov D.B., Shkoldin V.A.[1] Chegodaev A.D.[1]
[1] *Ioffe Physical Technical Institute, St..Petersburg, Russia*

Email: *zam@mail.ioffe.ru*
Key words: nanogeterostructures, cathodoluminescence, interface, transport properties of nanogeterostructures

Active area of modern light emitting devices and laser structures is characterized by complicated design and contains a great number of layers. When trying to characterize quality and luminescent features of such devices it is difficult to choose only one parameter to compare. It is connected with the fact that the order, thickness and composition of the layers in structures can vary critical. Therefore development of new approaches to comparison of luminescent properties semiconductor structures is an important problem.

In this work we propose depth study of cathodoluminescent (CL) spectra under electron beam energy variation. CL spectra obtained by different energies of electron beam allows to determinate effective diffusion length of the charge carriers in the sample. This parameter depends on the quality of the upper and bottom layers and interfaces and makes possible the nondestructive investigation of the multilayer heterostructures to estimate transport properties of geterostructures and influence of interfaces on its.

The behavior of the CL intensity dependence can be simulated by the calculation of relative quantity of carriers transported into a quantum well (QW) or quantum dots (QD) from nearby layers of the structure and recombined producing the luminescence. It is assumed that all primary electron energy losses are spent to generation of the electron–hole pairs. In addition the valuable condition is that the CL intensity dependence on beam current must be linear with no saturation occurred.

At first stage we calculated CL depth distribution in multilayer structure. We supposed that CL depth distribution matches depth distribution of charge carriers in multilayer structure. It is a close approximation as typical times of charge carrier scattering and thermalization are by several orders of magnitude less than typical times of charge carrier diffusion. We used Monte-Carlo simulation in CASINO program package.

Next important experimental condition is the maintaining of continuity of excited electron-holes pairs quantity. This is achieved by keeping constant $E_0 \cdot I_0$ value (E_0 – energy of electron beam, I_0 – electron beam current).

For CL intensity dependence simulation we used following equation:

$$I_{CL}(E_e) = \int_0^{x_1} \frac{dE(E_e)}{dx} \cdot \exp\left(-\frac{|x - x_1|}{d_1}\right) \cdot dx + \int_{x_1}^{x_2} \frac{dE(E_e)}{dx} \cdot dx + \int_{x_2}^{\infty} \frac{dE(E_e)}{dx} \cdot \exp\left(-\frac{|x - x_2|}{d_2}\right) \cdot dx$$

Here $\rho(x, E)$ is CL depth distribution by electron beam energy E; x_1, x_2 – depth of charge carrier transport area, x_1, x_2 – parameters of exponential decay. The best fitting of this function to the experimental dependence of CL intensity on beam energy gives the position of the limits d_1, d_2 , x_1, x_2. This method gives the possibility to estimate
The quality of the heterostructures was evaluated basing on assessment of the carrier transport properties of the barrier/waveguide layers to QW/QD/active layer This technique were used for study the geterostructures based on AIIBIV, AIIIBV and nitride LED structures based on InAlGaN. The results of CL study correlate with the date of Transition Electron Microscopy.

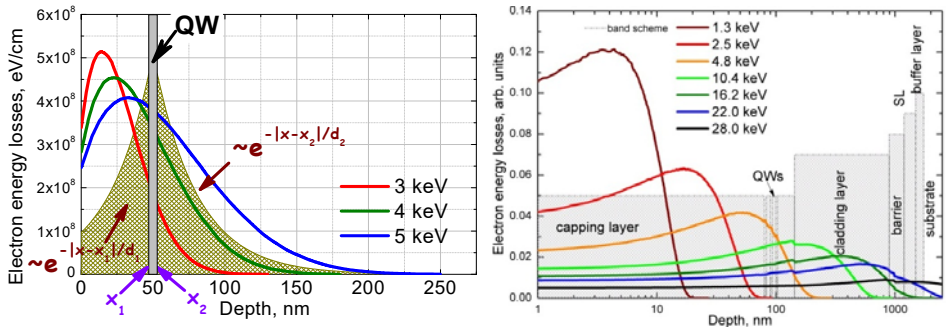

Fig.1 *Left:* Model equation permitting evaluation of charge carrier transport length. Chosen parameters in the model: d_1 and d_2 corresponds to the QWs borders; $x_1 > 0$; $x_2 > 0$, x_1
Right: Simulated CL depth distribution in LED structure.

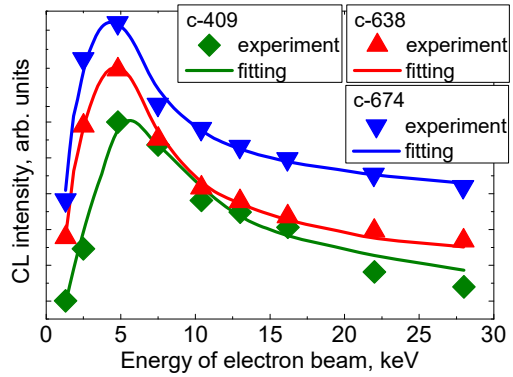

Fig. 2 Fitting of CL intensity depth dependence by model equation

Blue emission of Ce^{3+} in nanocrystalline heterojunction GaAs/SnO_2 and 2DEG photoinduced properties

Diego H. O. Machado[1], Luis V. A. Scalvi[1]
[1] *Physics Dept. – FC and POSMAT, UNESP São Paulo State University Bauru, Brazil.*

Email: *scalvi@fc.unesp.br*
Key words: heterojunction; gallium arsenide; tin dioxide; interface properties; photoluminescence

Tin dioxide (SnO_2) thin film, deposited by sol-gel-dip-coating, is coupled with gallium arsenide (GaAs) layer, deposited by resistive evaporation, forming the heterojunction GaAs/SnO_2. This assembly can be used in optoelectronic devices, when doped with rare-earth trivalent ions such as Eu^{3+} or Ce^{3+}. Eu^{3+} leads to efficient red emission whereas Ce^{3+} provides blue light. Photoluminescence (PL) data of GaAs/SnO_2:2at%Eu allow identification of three rare-earth transitions. Surface scanning electron microscopy (SEM) and a surface mapping of doping element concentration, done by energy dispersive X-ray (EDX) show Eu^{3+} concentration distribution in agglomerates around nanocrystalline particles, allowing the emission, not observable for films of sole deposited SnO_2 [1]. Concerning electrical properties, much higher conductivity was observed when compared to individual films, along with a smooth interface suggesting interfacial conduction due to small two-dimensional electron gas (2DEG) channels [2].

We report here results on GaAs/SnO_2 heterojunction, where the top layer is doped with Ce^{3+}. Fig. 1 shows dark resistance as function of temperature, and also recorded after illumination with distinct energies. Excitation with 1.55eV or 2.75eV, energies intermediate between GaAs and SnO_2 bandgap, shows that the electrical resistance is temperature-independent, suggesting that light excitation leads to electrons confined at interface region (2DEG). Electrons are not scattered by ionized impurities or phonons, since scattering centers and charge carriers are located at different space regions. The inset in fig. 1 shows PL of a SnO_2 layer deposited on quartz, and thermally treated at much higher temperature than the heterojunction. The excitation is done with a He-Cd laser (325nm). It is possible to observe a broad band emission between 375 and 500nm, with a peak about 420nm, coincident with Ce^{3+} transition, from level 5d to level 4f, sublevel $^2F_{5/2}$ [3]. This emission becomes clear about 250K and has higher intensity as the temperature is decreased. The mapping of heterojunction by EDX reveals the top layer distribution in this case.

Isolated SnO_2 films doped with rare earth, annealed at same temperature of the heterojunction, do not show emission, suggesting that heterojunction makes observable the rare-earth emission. This result, in conjunction with the 2DEG conductivity, is a remarkable result for the utilization of this assembly in optoelectronic devices.

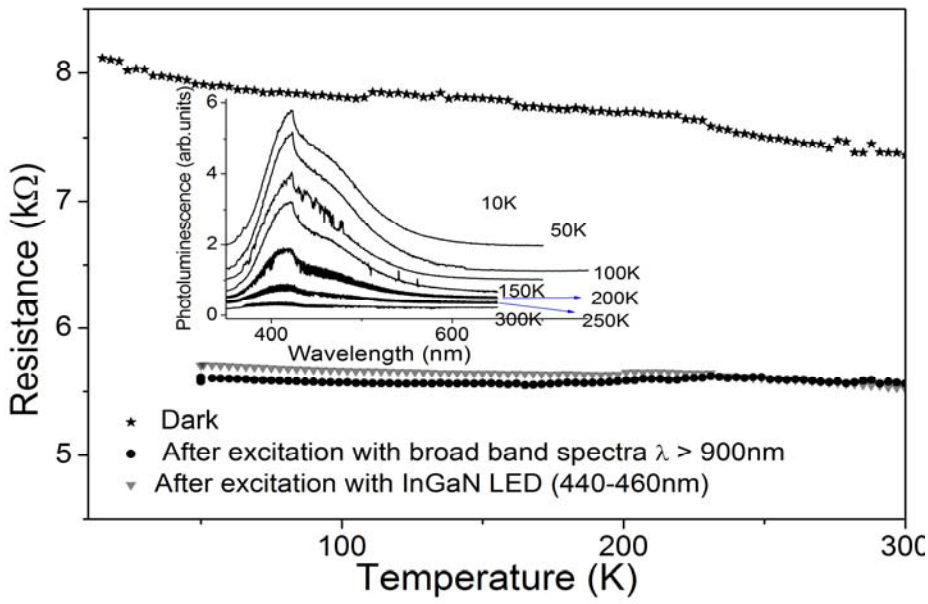

Figure 1: Resistance as function of temperature for the heterojunction GaAs/SnO_2 in the dark, and after excitation with distinct wavelengths (below and above GaAs bandgap). Inset: photoluminescence at different temperatures

References

1. C.F. Bueno, L. V. A. Scalvi, M. S. Li and M. J. Saeki, Opt. Mater. Express 5, 59 (2015)
2. T. F. Pineiz, E. A. Morais, L. V.A. Scalvi, C. F. Bueno, Appl. Surf. Scie. 267 200 (2013)
3. L. Bian, et al., J. Lum. 137, 1689 (2013).

Tu1T session

A. Acun et al. "Atomically Controlled Surfaces Interfaces and Nanostructures"
edited by A. Bianconi, A. Marcelli (Superstripes Press, Rome 2016) isbn: 9788866830597

NanoIR application in biology - chromosome (DNA) studies

Wojciech M. Kwiatek[1], Ewelina Lipiec[1], Anna Borkowska[1], Justyna Miszczyk[1],
[1]*Institute of Nuclear Physics, Polish Academy of Sciences, PL-31342 Krakow, Poland*

Email: *wojciech.kwiatek@ifj.edu.pl*
Key words: nanoIR, thermal spectroscopy, chromosome, DNA

The new, leading edge laboratory has been established and put into routine operation at the Institute of Nuclear Physics, Polish Academy of Sciences in Kraków, Poland. The laboratory is focused on multimodal studies of the cellular response to ionizing radiation and provides support and research facilities for the Bronowice Cyclotron Centre. Laboratory of Spectroscopic Imaging for Radiobiology, Therapy and of Complex Systems Research at the Institute of Nuclear Physics, Polish Academy of Sciences in Kraków was founded in order to apply physical methods in eradication cancer and other pathologies studies.

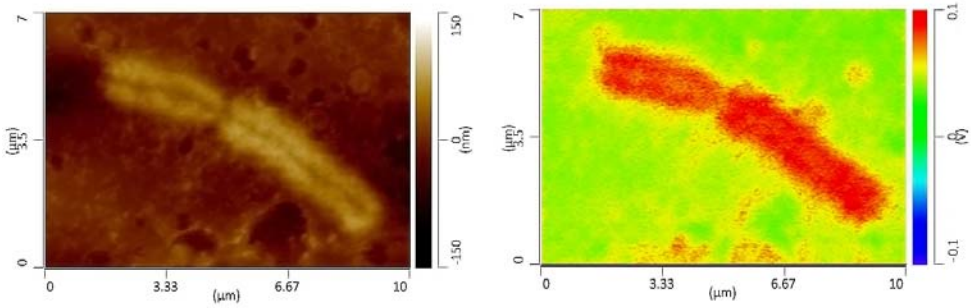

Figure 1: AFM topography image and corresponding 2D map of 1240 cm^{-1} band distribution.

We have developed and applied infrared nano-spectroscopy (nanoIR) to explore the detailed composition of chromosomes. NanoIR2 system has been applied to image local IR absorption with nanometer resolution. The integrity of chromatin structure is essential for every process occurring within eukaryotic nuclei [1, 2]. It is known that tightly packed, methylated DNA forms heterochromatin, which is transcriptionally inactive, but indispensable for the maintenance of structural integrity [3, 4]. However, lightly packed unmethylated euchromatin contains most genetic information [3, 4]. NanoIR coupled with the Principal Component Analysis (PCA) has confirmed that chromosome areas containing euchromatin and/or heterochromatin are distinguishable based on differences in degree of methylation. Heterochromatin has significantly more

methylated sites than euchromatin as previously described [3,4]. We will present the new, robust and reproducible approach for detection of DNA methylation sites in human chromosomes providing the location of the heterochromatin–euchromatin boundaries at a spatial resolution below 100 nm. Given the importance of DNA methylation in the development of nearly all types of cancer [5] there is potential of nanoIR approach [6] to be used as an early screening tool for malignancy.

A combination of AFM and InfraRed Spectroscopy (NanoIR2 setup) was successful in characterization molecular changes occurring in the nuclear environment following cellular irradiation. Particularly useful information acquired was the observation of changes in distribution of macromolecules with a spatial resolution as presented in Figure 1.

The laboratory of spectroscopic imaging has been co-funded by the Malopolska Regional Operational Program Measure 5.1 Krakow Metropolitan Area as an important hub of the European Research Area for 2007-2013. Project No. 2014/15/B/ST4/04839.

References

1. Luger, K., Mader, A. W., Richmond, R. K., Sargent, D. R. & Richmond, T. J. *Nature* 389, 251-260 (1997).
2. Jenuwein, T. & Allis, C. D. *Science* 293, 1074-1080 (2001).
3. Sproul, D. Gilbert N. &. Bickmore, W. A. *Nature Reviews Genetics* 6, 775-781 (2005).
4. Huisinga, K. L., Brower-Toland, B. & Elgin S. C. R. *Chromosoma* 115, 110–122. (2006).
5. Issa, J. P. *Clin Cancer Res.* 13, 1634–1637 (2007).
6. Ewelina Lipiec, Carine Benadiba, Francesco Simone Ruggeri, Justyna Miszczyk, Bayden R. Wood, Andrzej Kulik, Giovanni Dietler and Wojciech M. Kwiatek, *Nature Nanotechnology,* submitted (2016).

A. Acun et al. “Atomically Controlled Surfaces Interfaces and Nanostructures”
edited by A. Bianconi, A. Marcelli (Superstripes Press, Rome 2016) isbn: 9788866830597

Non-equilibrium Surface Dirac Fermion Dynamics of Topological Insulators

Akio Kimura
Graduate School of Science, Hiroshima University

Email: *akiok@hiroshima-u.ac.jp*
Key words: Topological insulators; Nonequilibrium surface Dirac fermion dynamics

Three-dimensional topological insulators (3D TIs) with surface Dirac fermions in a bulk energy gap induced by a strong spin-orbit coupling have attracted much attention as key materials to revolutionize current electronic devices. A spin helical texture of surface Dirac fermions, where the electron’s spin is locked to its momentum, is a manifestation of a 3D TI.

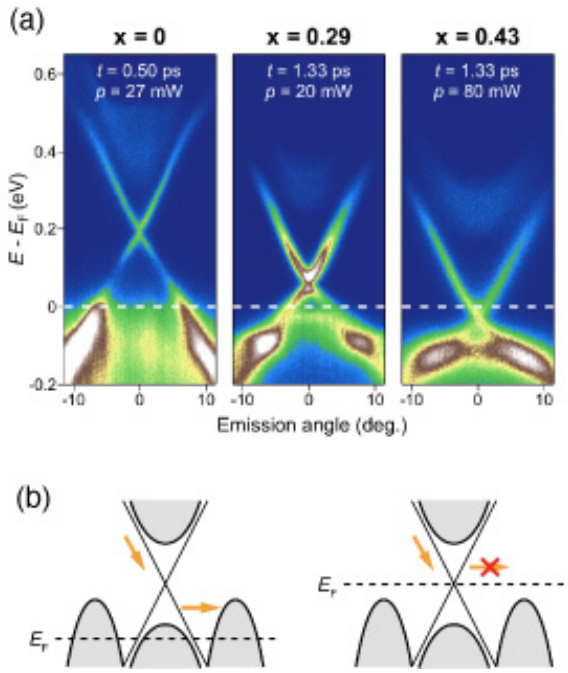

Figure 1: (a) Band dispersions acquired at certain pump-and-probe delay times. (b) Schematics of the relaxation processes in bulk metallic and bulk insulating TIs.

To unveil its Dirac fermion dynamics is crucial for the future development of (opto-) spintronic devices incorporating topological insulators. Angle-resolved photoemission spectroscopy implemented by a pump-and-probe method is powerful tool to study both occupied/unoccupied states as well as hot carrier dynamics [1].
Here, the surface Dirac fermion dynamics in the “carrier tuned” topological insulator $(Sb_{1-x}Bi_x)_2Te_3$ have been explored. Sb_2Te_3 (x=0) has a Dirac node completely located above the Fermi energy [Fig.1(a)]. The excited electrons in the upper Dirac cone are found to stay longer than those below the Dirac node to form an inverted population. This is attributed to a reduced density of states near the Dirac node [2]. Once the Fermi energy gets into the bulk energy gap by an appropriate Bi doping gap by an appropriate Bi doping (x=0.43) as shown in Fig.1(a), the duration of the nonequilibrium surface electronic state exceeds >400 ps. The keys for the prolonged nonequilibration are the bulk insulation and further tuning of the Fermi level to the Dirac point of the topological surface state [Fig.1(b)]. These findings expand the pathways to high-mobility opto-spintronic applications.

References

1. Y. Ishida et al., Rev. Sci. Instrum. 85, 123904 (2014).
2. S. Zhu et al., Sci. Rep. 5, 13213 (2015).

Terahertz optical properties of Topological Insulators

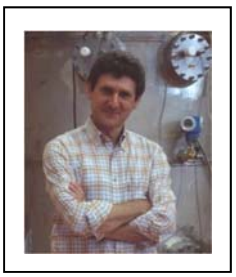

Stefano Lupi[1]
[1]*INFN and Department of Physics, Sapienza University of Rome*

Email: *Stefano.lupi@roma1.infn.it*
Key words: Topology, Dirac surface states, Plasmons

Topological Insulators (TIs) like Bi_2Se_3, are one of the most intriguing issues at focus in Condensed Matter Physics. TIs exhibit a band gap in the bulk like ordinary insulators, but have intrinsic 2D conducting states on their edge and surface. The edge states arise from a strong spin-orbit coupling, and they are backscattering protected, i.e. not sensitive to disorder (except that coming from magnetic impurities). Such as graphene, TIs surface charge transport is carried out by Dirac fermions, with a very high surface carrier density ($n \geq 1013$ cm^{-2}), compared to typical values on metal surfaces. Dirac fermions in TIs sustain both single-particle and plasmonic modes [1,2,3,4], whose properties can be used for photonics (terahertz) applications at the nanoscale and for producing non linear effects like electromagnetic transparency and harmonic generation process. In this talk, after a general review on the properties of Topological Insulators, I will discuss the linear response of Dirac excitations in TIs and their behavior under a strong magnetic field up to 30 T. The appearance of strong non-linear optical effects [5], when the THz electric field reaches values on the order of 1 MV/cm, will be also discussed. Both the linear and non-linear experiments provide a unifying picture of single particle and collective electronic excitations in Topological Insulators, indicating the strong specificity of Dirac carriers in Condensed Matter Physics.

References

1. P. Di Pietro et al., Nature Nanotechnology 8, 556 (2013).
2. M. Autore et al., Advanced Optical Materials, DOI: 10.1002/adom.201400513
1. (2015).
2. M. Autore et al., Nanoscale 8, 4667 (2016).
3. M. Autore et al., ACS Photonics, DOI: 10.1021/acsphotonics.5b00036, (2015).
4. F. Giorgianni et al., Nature Communications, 7 Article Number: 11421 (2016).

A. Acun et al. “Atomically Controlled Surfaces Interfaces and Nanostructures”
edited by A. Bianconi, A. Marcelli (Superstripes Press, Rome 2016) isbn: 9788866830597

Acoustic surface plasmons at gold surfaces: anomalous slope and effect of steps

Mario Rocca [1,2]
[1] *University of Genoa Department of Physics, Italy*
[2] *IMEM- CNR Genoa, Italy*
Via Dodecaneso 33, 16146 Genova

Email: *rocca@fisica.unige.it*
Key words: Growth and applications of thin films; Graphene and other 2D materials; Nanoelectronics, molecular electronics

Collective electronic excitation with acoustic dispersion (acoustic surface plasmons (ASP)) are important since they have a vanishing energy for vanishing wavevector and a constant group velocity.

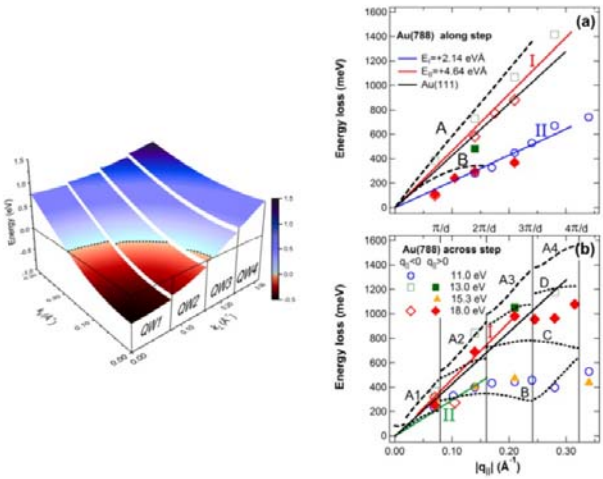

Figure 1: Quantum well states on Ag(788) and acoustic plasmon dispersion along and across the steps

The former characteristic allows, at least in the low wavelength limit, the thermal excitation and the interaction with surface phonons, thus allowing the ASP to have a role in energy dissipation in gas surface interaction and in chemical reactions and to envisage applications is Terahertz detectors. The independence of the group velocity of wave vector, on the other hand, makes the ASP interesting for applications in plasmonics since the ASP would propagate on the surface without distortion. The ASP corresponds to the excitation of a 2-dimensional electron gas oscillating in counter-

phase with an underlying 3D gas. Such excitation has been predicted theoretically [1] and reported experimentally for Be(0001) [2], Cu(111) [3,4] and Au(111) [5,6]. The ASP is a relatively robust excitation: it survives indeed to some extent to surface nanostructuring [7] and is present also on regularly stepped surfaces [8]. Interestingly on noble metal surfaces the ASP falls unexpectedly within the continuum of electron hole pair excitations maintaining, however, a narrow width. In presence of steps, the ASP propagates across them when its wavelength exceeds the terrace width and is otherwise localized.

References

1. J.M. Pitarke, V.M. Silkin, E.V. Chulkov and P.M. Echenique, Rep. Prog. Phys. 70, 1 (2007).
2. B. Diaconescu, K. Pohl, L. Vattuone, L. Savio, P. Hofmann, V.M. Silkin, J.M. PItarke E.V Chulkov, P.M. Echenique, D. Farias and M. Rocca, Nature 448, 57 (2007).
3. K Pohl K. B. Diaconescu, G. Vercelli, L. Vattuone, V.M. Silkin, E.V. Chulkov, P.M. Echenique, M. Rocca, Europhys. Lett. 90, 57006 (2010).
4. J. Pischel, E. Welsch, O. Skibbe, and A. Pucci, J. Phys. Chem. C 117, 26964 (2013).
5. S.J. Park and R. E. Palmer, Phys. Rev. Lett. 105, 016801 (2010).
6. L. Vattuone, M. Smerieri, T. Langer, C. Tegenkamp, H. Pfnür, V. M. Silkin, E. V. Chulkov, P. M. Echenique, and M. Rocca, Phys. Rev. Lett. 110, 127405 (2013)
7. L. Vattuone, G. Vercelli, M. Smerieri, L. Savio and M. Rocca, Plasmonics 7, 323 (2012).
8. M. Smerieri, L. Vattuone, L. Savio, T. Langer, C. Tegenkamp, H. Pfnür, V. M. Silkin, and M. Rocca, Phys. Rev. Lett. 113, 186804 (2014).

A. Acun et al. “Atomically Controlled Surfaces Interfaces and Nanostructures”
edited by A. Bianconi, A. Marcelli (Superstripes Press, Rome 2016) isbn: 9788866830597

Gold-Nanorod Based SPASER

Carola Kryschi[1] , Hans-Peter Solowan[1]
[1]*University of Erlangen, Dept. Chemistry and Pharmacy*

Email: *carola.kryschi@fau.de*
Key words: Plexcitonic nanostructure, SPASER, laser-dye-coated gold nanorod, gold nanocluster coated gold nanorod

Upon resonant optical excitation noble-metal nanostructures exhibit spatially confined (localized) surface plasmons (LSP) that efficiently squeeze the electromagnetic field in nanoscale regions near the nanostructure surface and therewith, allowing for tailoring light-matter interactions at the nanoscale [1]. Optically excited excitonic systems, when located within 5 nm of the plasmonic surface, exhibit interfacial resonance excitation energy transfer. In case of an efficient feedback mechanism resonance energy transfer generates plasmons in the noble-metal nanostructure, and the resulting high local electromagnetic fields, in turn, excite the adjacent excitonic systems. Such plexcitonic nanostructures are suited for setting up a nanoscale laser, the so-called SPASER (i.e. surface plasmon amplification by stimulated emission of radiation). In the SPASER the plasmonic noble-metal nanostructure acts as a nanocavity, and incorporated or surface-coupled two-level emitters (i.e. excitonic systems) constitute the nanoscale gain medium. Resonant optical pumping of both, the gain medium and the plasmonic nanocavity, provides LSP stimulated excitation energy transfer between two-level emitters and the plasmonic nanostructure which enables the buildup of a macroscopic number of LSPs in a single mode and therewith, coherent local optical fields which drive the SPASER action.

In this contribution, we demonstrate that room-temperature SPASER emission can be achieved through amplifying longitudinal surface plasmon modes supported in gold nanorods and employing laser dyes or luminescent gold complexes and gold nanocluster that function as optical gain for compensation of plasmon losses. The central wavelength of the longitudinal surface plasmon resonance band was tuned between 650 to 670 nm via the aspect ratio that was adjusted through the synthesis procedure parameters. Suited laser dyes and properly synthesized gold complexes/nanocluster electrostatically attached within a 5 nm-distance at the gold nanorod surface at a high concentration provided an effective optical gain medium which facilitates SPASER emission in the red spectral range. These SPASER nanostructures were characterized using high-resolution transmission electron microscopy, uv/vis absorption spectroscopy, stationary and time resolved fluorescence spectroscopy and femtosecond transient absorption spectroscopy.

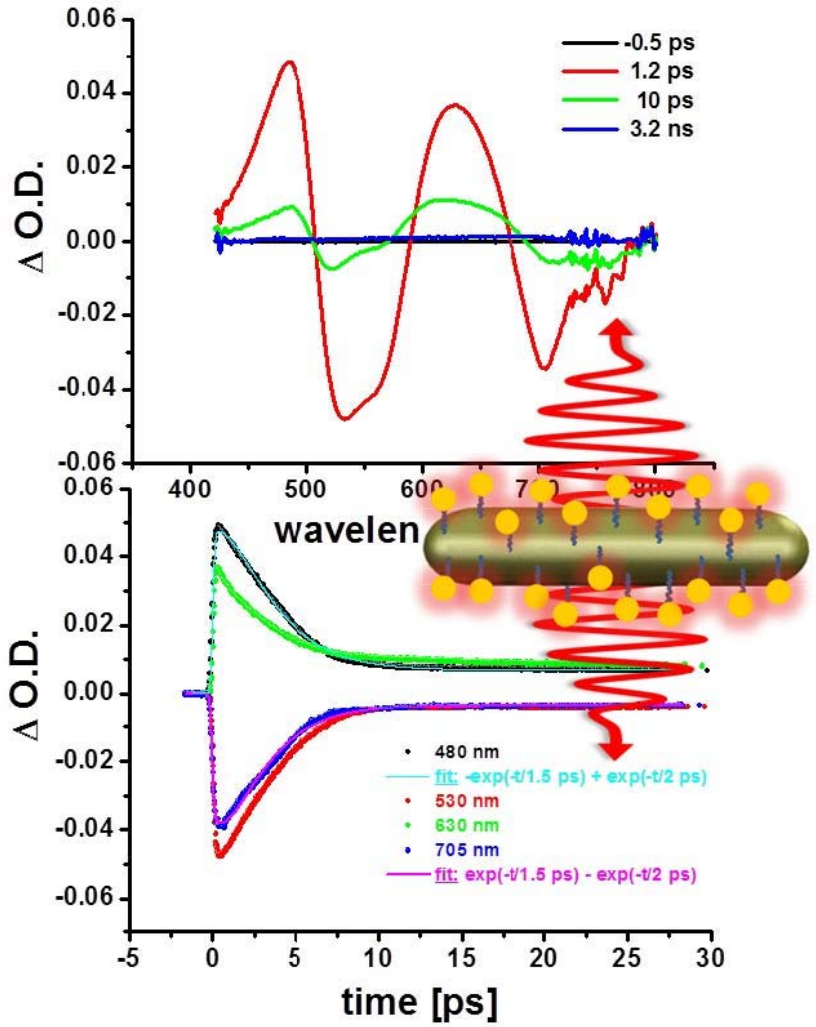

Figure 1: Time evolution of fs transient absorption spectra (top) with associated kinetics traces (bottom) of gold nanocluster coated gold nanorods.

References

1. V. Giannini, Antonio I. Fernandez-Domínguez, S. C. Heck, S. A. Maier, Chem. Rev. 111, 3888 (2011). http://dx.doi.org/10.1021/cr1002672.
2. D. J. Bergman, M. I. Stockman, Phys. Rev. Lett. 90, 027402-1 (2003). http://dx.doi.org /10.1103/PhysRevLett.90.027402.

Tu2T session

A. Acun et al. “Atomically Controlled Surfaces Interfaces and Nanostructures”
edited by A. Bianconi, A. Marcelli (Superstripes Press, Rome 2016) isbn: 9788866830597

Superconducting nanostructures to realize optimal configurations for room temperature superconductivity: Lifshitz transtions, shape resonances and BCS-BEC crossover

Andrea Perali [1,2],
[1]*University of Camerino, School of Pharmacy, Physics Unit, 62032, Camerino, Italy*
[2]*INFN – Sezione di Perugia, Italy*

Email: andrea.perali@unicam.it
Key words: Shape resonances, SuperStripes, Lifshtiz transitions, BCS-BEC crossover, high-Tc superconducting nanostructures.

The superconductivity in iron-based, magnesium diborides, and other novel high-Tc superconducting materials, possibly including the recently discovered superconducting hydrogen disulfide, has a strong multi-band and multi-gap character [1,2] and recent experiments support the possibility for a BCS-BEC crossover induced by strong-coupling and proximity of the chemical potential to the band edge of one of the bands, with evidences for Lifshitz transitions associated with changes in the Fermi surface topology [3, 4].

Here we study the simplest theoretical model which accounts for the BCS-BEC crossover in a two-band / two-gap superconductor, considering tunable interactions. When the gap is of the order of the local chemical potential, superconductivity is in the crossover regime of the BCS-BEC crossover and the Fermi surface of the small band is completely smeared by the gap opening. In this situation, small and large Cooper pairs coexist in the total condensate, which is the optimal condition for high-Tc or even for room temperature superconductivity [5]. Using available experimental data, our analysis shows that iron-based superconductors have the partial condensate of the small Fermi surface which is in the crossover regime of the BCS-BEC crossover [6], supporting in this way the recent ARPES findings [7, 8]. We also discuss different physical systems in which the multigap and multiband BCS-BEC crossover can be realized, pointing toward very high-Tc superconductivity.

Two examples are considered here: (i) superconducting stripes in which shape resonances and multigap physics at the band edge play a cooperative role in enhancing superconductivity in the crossover regime of pairing [9], and (ii) our prediction of high-Tc superconductivity using nanoribbons of doped graphene [10]. Finally, we focus on a key prediction of the above discussed physics: the isotope effect of the superconducting critical temperature in the vicinity of a Lifshitz transition, which has a unique dependence on the energy distance between the chemical potential and the Lifshitz transition point. Comparisons with available experimental data for superconducting cuprates and hydrogen disulfide will be discussed [2,11,12,13].

References

1. S.V. Borisenko et al., Symmetry 4, 251 (2012).
2. A. Bianconi, T. Jarlborg, EPL (Europhysics Letters) 112, 37001 (2015).
3. D. Innocenti, N. Poccia, A. Ricci, A. Valletta, S. Caprara, A. Perali, and A. Bianconi, Phys. Rev. B 82, 184528 (2010).
4. A. Bianconi, Nature Phys. 9, 536 (2013).
5. A. Perali, C. Castellani, C. Di Castro, M. Grilli, E. Piegari, and A. A. Varlamov, Phys. Rev. B 62, R9295 (2000).
6. A. Guidini and A. Perali, Supercond. Sci. Technol. 27, 124002 (2014).
7. Y. Lubashevsky, et al., Nat. Phys. 8, 309 (2012).
8. K. Okazaki et al., Sci. Rep. 4, 4109 (2014).
9. A. Perali, A. Bianconi, A. Lanzara, N.L. Saini, Solid State Comm. 100, 181, (1996)
10. A. Perali et al., in preparation.
11. A. Perali, D. Innocenti, A. Valletta, A. Bianconi, Supercond. Sci. Technol. 25, 124002 (2012).
12. A. Bianconi, Journal of Superconductivity 18, 625 (2005)
13. A. Bianconi, A. Valletta, A. Perali, and N. L. Saini, Solid State Commun. 102, 369 (1997).

Heterostructures at atomic limit for quantum coherence

Antonio Bianconi[1,2,3] ,
[1]*Rome International Centre for Material Science Superstripes, RICMASS, via dei Sabelli 119A, 00185 Rome, Italy*
[2] *National Research Nuclear University MEPhI (Moscow Engineering Physics Institute), Kashirskoe sh. 31, 115409 Moscow, Russia*
[3] *Institute of Crystallography, CNR, via Salaria Km 29.300, Monterotondo Roma, I-00015, Italy*

Email: *Antonio.bianconi@ricmass.eu*
Key words: surface XANES; surface EXAFS, superlattices of atomic wires, macroscopic quantum coherence at room temperature. multigap superconductor, BEC-BCS crossover, Lifshitz transition.

X-ray spectroscopies surface EXAFS [1] and surface XANES [2,3] developed since 1979 by using synchrotron radiation have provided new tools for the science of surfaces, interfaces and nanostructures. These modern methods have allowed our modern understanding of local conformational fluctuations in complex biological systems, and the complxity of surfaces, interfaces and nanostructures [4-7]. Recently new diffraction methods have taken advantage of advanced nano x-ray beams [8,9] and resonant x-ray scattering [10] at synchrotron radiation facilities. These novel fast, local and orbital symmetry selective experimental methods have provided advances to our understanding of quantum physics of living matter [11] and new venues to engineer oxides by manipulating oxygen sublattice nanostructures [12-14]. It has been possible to correlate the emergence of high temperature superconductivity with the formation of superlattices of wires at atomic level as shown in Fig.1. (figures of the patent in ref. 15)

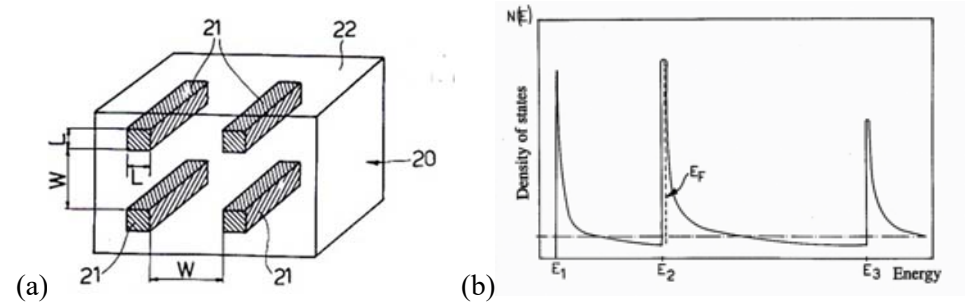

Figure 1: Controlling the structural parameters W, L, of a superlattice of quantum nanoscale wires (left panel a) and charge density it is possible to tune the Fermi level (E_F) at the Lifshitz transition i.e. at few meV above the bottom of a quantum subband where a peak in the Density of states appear (right panel b). [15-18].

This particular architecture of nanostructures (called Superstripes) which can be realized by atomic control and manipulation provides a particular case of multi-gap superconducting phase at the BCS-BEC crossover.

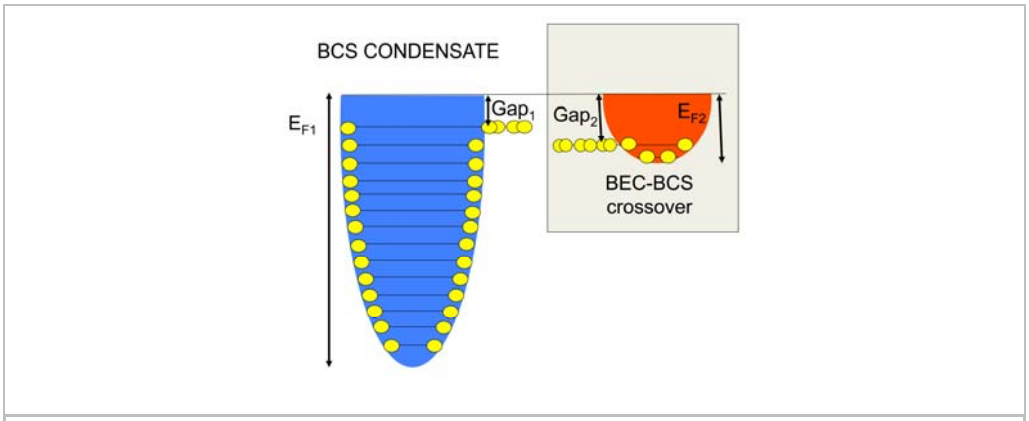

Figure 2: Pictorial view of the multigap superconductor in the clean limit [15-20] given by a superlattice of stripes (fig.1a) tuned at a Lifshitz transition. The electrons in the first subband (blue color) have a large Fermi surface E_{F1} are in a weak coupling regime and form cooper pairs forming a BCS-condensate. The second type of electrons in the second subband (red color) are in the strong coupling regime and tuned at a peak in the DOS(Fig.1b), in a polaronic regime where the Fermi energy is of the same order as the energy of the superconducting gap giving a second condensate in the BEC-BCS crossover near a Lifshitz transition. A Fano Feshbach resonance between the two different pairing channels

Here by tuning the Fermi level relative to the bottom of a band novel physical properties emerges of a particular superconducting phase at the BCS–BEC crossover in a two-band superconductor [15-20]. It was recently found that is in this particular physical state the system made of two electronic components is unstable toward phase separation and give a complex multiscale scenario called superstripes [8,9,21,22] where short range CDW order and short range superconducting order compete [23].

References

1. A. Bianconi and R. Z. Bachrach, Al surface relaxation using surface extended X-Ray-absorption fine structure. *Phys. Rev. Lett.* 42, 104 (1979), doi:10.1103/physrevlett.42.104.
2. A. Bianconi, Surface X-Ray absorption spectroscopy: Surface EXAFS and surface XANES. *Applications of Surface Science* 63, 392-418 (1980). doi:10.1016/0378-5963(80)90024-0
3. A. Bianconi, A. Marecllli Surface X-Ray Absorption Near-Edge Structure: XANES in Bachrach, R. Z. *et al. Synchrotron radiation research: advances in surface and interface science techniques* (Springer US, Boston, MA, 1992). doi:10.1007/978-1-4615-3280-4.

4. S. Della Longa, A. Soldatov, Pompa, and A. Bianconi, Computational Materials Science 4, 199 (1995), doi:10.1016/0927-0256(95)00027-n.
5. A. Bianconi, S. Doniach, and D. Lublin, *Chemical Physics Letters* 59, 121 (1978), doi: 10.1016/0009-2614(78)85629-2.
6. J. Garcia, A. Bianconi, M. Benfatto, and C. R. Natoli, *Le Journal de Physique Colloques* 47, C8 (1986), doi:10.1051/jphyscol:1986807.
7. A. Bianconi, *et al. Physical Review B* 44, 10126-10138 (1991). doi:10.1103/physrevb.44.10126.
8. N. Poccia, et al., *Proc. Nat. Acad. Sci.* 109, 15685 (2012). doi: 10.1073/pnas.1208492109.
9. Y. Drees, Z. W. Li, A. Ricci, et al., *Nature Communications* 5, 5731 (2014).
10. M. Dantz, *et al*. *Sci. Rep.* 6, 32896; doi: 10.1038/srep32896 (2016).
11. P. Turner, L. Nottale, J Supercond Nov Magn (2016). doi:10.1007/s10948-016-3756-z
12. N. Mathur, P. Littlewood, *Nature Materials* 3, 207 (2004). doi:10.1038/nmat1108.
13. E. W, Carlson, *Nature* 525, 329-330 (2015). doi:10.1038/525329a
14. D. Samal, G. Koster. *Journal of Materials Research* 30, 463–476 (2015).
15. A. Bianconi, “Process of increasing the critical temperature Tc of a Bulk Superconductor by Making Metal Heterostructures at the Atomic Limit” US Patent 6,265,019 (2001) priority date Dec 1993.
16. A. Bianconi, A. Valletta, A. Perali, N.L. Saini, “High Tc superconductivity in a superlattice of quantum stripes” *Solid State Communications* 102, 369 (1997) doi: 10.1016/s0038-1098(97)00011-2
17. A. Bianconi, Feshbach shape resonance in multiband superconductivity in heterostructures. *Journal of Superconductivity* 18, 625 (2005), doi:10.1007/s10948-005-0047-5
18. A. Bianconi, Feshbach shape resonance for high Tc superconductivity in superlattices of nanotubes. *Physica Status Solidi (a)* 203, 2950-2955 (2006). doi:10.1002/pssa.200567003.
19. A. Bianconi, *Nature.* Phys. 9, 536 (2013). doi:10.1038/nphys2738
20. A. Guidini, A. Perali, *Superconductor Science and Technology* 27, 124002+ (2014). URL http://dx.doi.org/10.1088/0953-2048/27/12/124002.
21. A. Bianconi, *et al. Physica C: Superconductivity* 341-348, 1719-1722 (2000). doi:10.1016/s0921-4534(00)00950-3.
22. A Bianconi *International Journal of Modern Physics* B 14, 3289-3297 (2000)
23. G. Campi, et al., Nature 525, 359 (2015). doi:10.1038/nature14987.

A. Acun et al. “Atomically Controlled Surfaces Interfaces and Nanostructures”
edited by A. Bianconi, A. Marcelli (Superstripes Press, Rome 2016) isbn: 9788866830597

Simulation of surfaces of simple and reactive oxides - dynamics and interactions

Kersti Hermansson , Jolla Kullgren, Peter Broqvist
Uppsala University, Department of Chemistry-Ångström

Email: *kersti@kemi.uu.se*
Key words: Multiscale modelling, water/metal oxide interfaces, redox processes, nanoparticles, ab initio MD simulations, force-field calculations.

Chemically active metal oxide surfaces and interfaces (e.g. as catalysts, sensors, or electrodes) play a crucial role in our society and in the development of new technologies. About 80% of all chemicals are produced via surface-assisted catalytic reactions. Such active surfaces and interfaces are often complex multi-component systems with nanosized (or smaller) defects or special structures which are essential for the surface activity.

Experimental progress over many years has moved the scientific frontier forward beyond surface science studies of ideal extended single crystals. New powerful experimental characterization techniques have emerged, also for rather complex surface and interface systems. On the *computational* side, large breakthroughs have also been achieved, but *the* largest bottleneck hindering a wider use of modelling in strategic material applications today is the lack of appropriate models to treat systems of large (realistic) complexity. This was recently demonstrated in a survey [1] conducted by the European Materials Modellling Council. Models of high accuracy and speed were requested as well as techniques to couple and link models and data over time and length scales (multiscale modelling).

I will discuss some of our efforts in the development of (multiscale and other) modelling approaches for metal oxide surfaces and interfaces – with and without interacting molecules. Compared to the prototypic MgO, the redox-active oxides constitute a particular challenge for both DFT calculations and for force-field simulations (e.g. [2]), where the model needs to capture chemical effects although no explicit electrons are present. In summary, we combine a range of theoretical methods including DFT, tight-binding-DFT [3], and reactive force-field simulations to examine the properties of metal oxide surfaces, nanoparticles and interfaces. I plan to focus on the following topics:

1. Multiscale modelling of metal oxide surface and interface systems (see Fig. 1).
2. DFT functionals for water/oxide interfaces and crystalline hydrates.
3. Dynamics on surfaces – simulating motion and spectra (e.g. vibrational [4]), and learning from it.

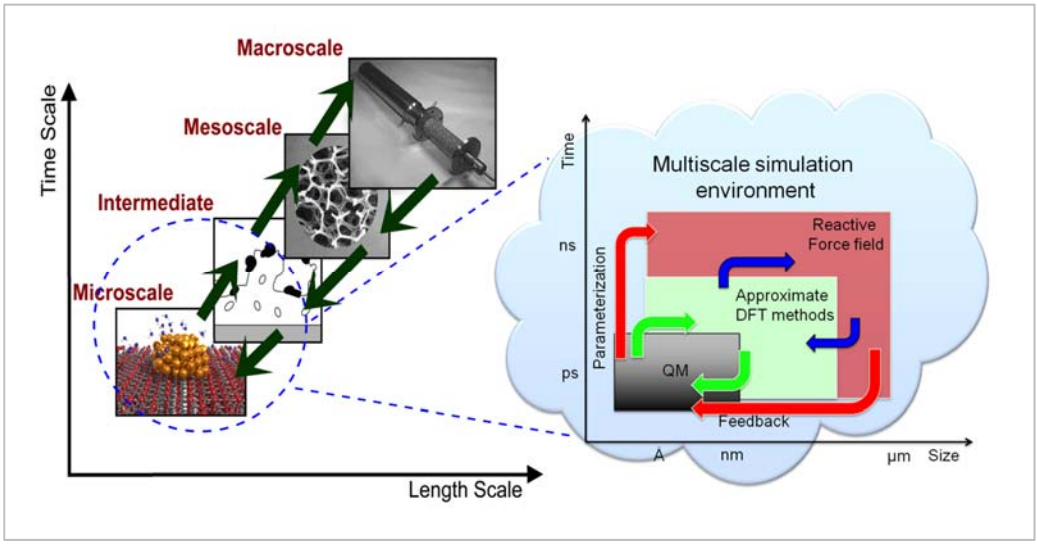

Figure 1: Overview of our multiscale modelling scheme.

References

1. https://emmc.info/wp-content/uploads/2016/05/Survey-materials-modelling-development_v05.pdf (2016).
2. P. Broqvist, J. Kullgren, M. J. Wolf, A. C. T. van Duin, K. Hermansson, A ReaxFF force-field for ceria bulk, surfaces and nanoparticles, J. Phys. Chem. C 119, 13598−13609 (2015).
3. M. Hellström, K. Jorner, M.Bryngelsson, S .E. Huber, J. Kullgren, Th. Frauenheim, P. Broqvist, An SCC-DFTB Repulsive Potential for Various ZnO Polymorphs and the ZnO-Water System, J. Phys. Chem. C 117, 17004 (2013).
4. S. Hu, Z. Wang, A. Mattsson, L. Österlund, K. Hermansson, Simulation of IRRAS Spectra for Molecules on Oxide Surfaces: CO on TiO_2(110), J. Phys. Chem. C 119, 5403 (2015).

From single magnetic impurities on superconductors to coupled spin chains

Michael Ruby[1], Benjamin W. Heinrich[1], Yang Peng[2], Felix von Oppen[2], Katharina J. Franke[1]
[1]*Fachbereich Physik, Freie Universität Berlin*
[2]*Dahlem Center for Complex Quantum Systems and Fachbereich Physik, Freie Universität Berlin*

Email: *franke@physik.fu-berlin.de*
Keywords: superconductivity, scanning tunneling spectroscopy, Shiba states

Magnetic adsorbates on conventional s-wave superconductors lead to exchange interactions that can induce bound states inside the superconducting energy gap. These states are known as Yu-Shiba-Rusinov states and can be resolved by scanning tunneling spectroscopy as a pair of resonances at positive and negative bias voltages in the superconducting gap. The exchange coupling strength determines the alignment of the states inside the energy gap. Recently, it has been suggested that proximity-coupled magnetic adsorbates induce a non-trivial superconducting state, which allows for the formation of Majorana bound states [1].
Here, we employ tunneling spectroscopy at 1.1 K to investigate magnetic atoms and chains on superconducting Pb surfaces. The single-atom junctions are stable over several orders of magnitude in conductance. We observe two different transport regimes: at large tip-sample distance, the tunneling current is dominated by single-electron processes. However, these require the relaxation of electrons/holes from the Shiba states into the superconductor. At small tip-sample distance, the relaxation processes are not fast enough for an efficient depopulation of the states, and thus Andreev processes become important, which resonantly transfer a Cooper pair into the superconductor [2]. When the atoms are brought into sufficiently close distance, the Shiba states hybridize, thus giving rise to states with bonding and anti-bonding character. It has been shown that the Pb(110) surface supports the self-assembly of Fe chains, which exhibit fingerprints of Majorana bound states [1]. Using superconducting tips, we resolve a rich subgap structure including peaks at zero energy and low-energy resonances, which overlap with the putative Majorana states [3].

References

1. S. Nadj-Perge, I. K. Drozdov, J. Li, H. Chen, S. Jeon, J. Seo, A. H. MacDonald, B. A. Bernevig, A. Yazdani, Science 346, 602 (2014).
2. M. Ruby, F. Pientka, Y. Peng, F. von Oppen, B. W. Heinrich, K. J. Franke, Phys. Rev. Lett. 115, 087001 (2015)
3. 3 M. Ruby, F. Pientka, Y. Peng, F. von Oppen, B. W. Heinrich, K. J. Franke, Phys. Rev. Lett. 115, 197204 (2015).

A. Acun et al. “Atomically Controlled Surfaces Interfaces and Nanostructures”
edited by A. Bianconi, A. Marcelli (Superstripes Press, Rome 2016) isbn: 9788866830597

Novel two-dimensional electron gases at the surface of transition-metal oxides

Andrés F. Santander-Syro[1]
[1]*CSNSM, Université Paris-Sud and CNRS/IN2P3, Bâtiments 104 et 108, 91405 Orsay, France.*

Email: *andres.santander@csnsm.in2p3.fr*
Key words: Electronic and optical properties of surfaces and interfaces; Oxides, nitrides and high-k dielectrics; Frontiers aspects of semiconductor, surfaces and interfaces; Transparent conducting interface; Quantum materials and devices; Engineering surface and interface for applications.

Transition-metal oxides (TMOs) show remarkable properties, such as high-temperature superconductivity or large magnetoresistance. The realization of two-dimensional electron gases (2DEGs) in TMOs, a field of current intense research, is crucial for harnessing the functionalities of these materials for future applications. Additionally, these 2DEGs offer the possibility to explore new physics emerging from the combined effects of electron correlations and low-dimensional confinement.

In this talk, I will first introduce our discovery that 2DEGs can be simply realized at the surface of various insulating transparent TMOs, such as the quantum paraelectric $SrTiO_3$ [1], the strong spin-orbit coupled $KTaO_3$ [2], or the photo-catalyst TiO_2 [3]. Then, I will show how the choice of the surface termination allows tailoring the electronic structure and symmetries of these 2DEGs [4-5], paving the way for the quest of topological states in correlated oxides. Furthermore, I will discuss our studies of magnetism in the 2DEG at the surface of oxygen-deficient $SrTiO_3$ [6]. These results show that confined electronic states at oxide surfaces can be endowed with novel properties, not present in the bulk, which are promising for technological applications. Finally, I will describe our recent development of a universal method to fabricate these 2DEGs in several oxides, which simultaneously protects the 2DEG from passivation in air and allows measuring its transport characteristics –and is thus promising for the realization of oxide devices [7].

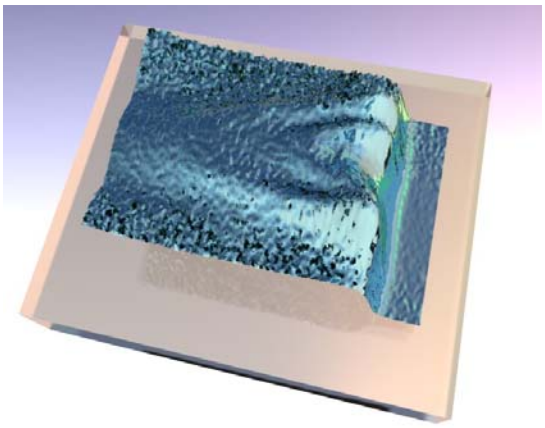

Figure 1: A metallic 2DEG, whose quantized energy bands form the parabolas shown in blue relief, emerges at the surface of insulating $SrTiO_3$ (transparent block). The probability of presence of electrons for a given energy and momentum, measured by angle-resolved photoemission spectroscopy (ARPES), falls off abruptly at the Fermi level, giving the impression of a cascade, demonstrating the metallic character of this surface electronic state. Adapted from Ref. [1].

References

1. A. F. Santander-Syro *et al*., Nature 469, 189 (2011).
2. A. F. Santander-Syro *et al*., Phys. Rev. B 86, 121107(R) (2012).
3. T. C. Rödel *et al*., Phys. Rev. B 92, 041106(R) (2015).
4. C. Bareille *et al*., Sci. Rep. 4, 3586 (2014).
5. T. C. Rödel *et al*., Phys. Rev. Applied 1, 051002 (2014).
6. T. Taniuchi *et al*, Nature Communications, *in press* (2016).
7. T. C. Rödel *et al*., Adv. Mater. doi:10.1002/adma.201505021 (2016).

Intermetallic charge transfer mechanism of solid solution alloy nanoparticle

Natalia Palina,[1] Osami Sakata,[1,2] Hirokazu Kobayashi,[3,4] Kohei Kusada,[3] and Hiroshi Kitagawa,[3,4,5]
[1] *Synchrotron X-ray Station at SPring-8, National Institute for Materials Science (NIMS), Japan*
[2] *Department of Materials Science and Engineering, Tokyo Institute of Technology, Japan*
[3] *Division of Chemistry, Graduate School of Science, Kyoto University, Japan*
[4] *Department of Chemistry, Faculty of Science, Kyushu University, Japan*
[5] *INAMORI Frontier Research Center, Kyushu University, Japan*

Email: *MUELLER.Natalia@nims.go.jp*
Key words: alloy nanoparticle, Hard X-ray Photoelectron Spectroscopy, charge transfer, catalytic activity

In this study, advanced synchrotron radiation (SR) characterisation techniques were utilized to assess changes in electronic structure of extremely small 1-1.5 nm solid solution RhCu alloy nanoparticles (NPs). Rh and RhCu alloy NPs have been investigated as cost-effective candidates for CO oxidation catalysts, namely CO removal from car exhaust or for preventing CO poisoning in fuel cell systems [1, 2]
Rh_xCu_y nanoparticles with a narrow size distribution were prepared by chemical reduction methods using Rhodium(III) acetate $Rh(AcO)_3$ and Cupper (II) chloride $CuCl_2$ as metal precursors, poly (N-vinyl-2-pyrrolidone) (PVP) as protective agent. Additionally, strong base $(CH_3)_3COK$ was added to control pH of Ethylene glycol EG solution [3].
The Hard X-ray Photoelectron Spectroscopy (HAXPES) core level (CL) and valence band (VB) spectra of RhCu NPs with various composition were recorded ex-situ at the NIMS (National Institute for Materials Science) contract undulator beamline, BL15XU and High-Energy X-ray Diffraction (HEXRD) data were acquired at the BL04B2 of SPring-8, Japan [4, 5].
The change in the electronic structure observed as a result of atomic-level alloying of Rh and Cu can be understood as concurrent reduction of Rh and oxidation of Cu. As can be seen from Figure 1 (a) and Figure 1 (b), CL peaks for Rh *3d* and Cu $3p_{3/2}$ are moved in opposite directions, indicating intermetallic charge transfer mechanism from Cu to Rh. Our characterisation reveals, that for pure Rh and Rh-rich alloy NPs formation of rhodium surface oxide with non-integer oxidation state ($Rh^{(3-\delta)+}$) is main factor which leads to the improvement of catalytic activity, in agreement with previously reposted data [6, 7]. Whereas, for alloy NPs with comparable Rh:Cu ratio a decreased fraction of catalytically active Rh $^{(3-\delta)+}$ oxide is compensated by charge transfer from Cu to Rh, hence ensuring a negligible change in the catalytic activities of those as compared to Rh-rich and pure Rh NPs.

In addition to that, HEXRD data (refer to talk materials), confirming that investigated samples can be divided into two groups, namely Rh-rich alloy NPs and NPs with comparable Rh:Cu ratio. Structural changes observed in HEXRD data are consistent with conclusions drawn from CL HAXPES data analysis.
We demonstrate capability of advanced SR-based characterisation to access, understand and possibly control physical properties of novel functional nanoscale materials.

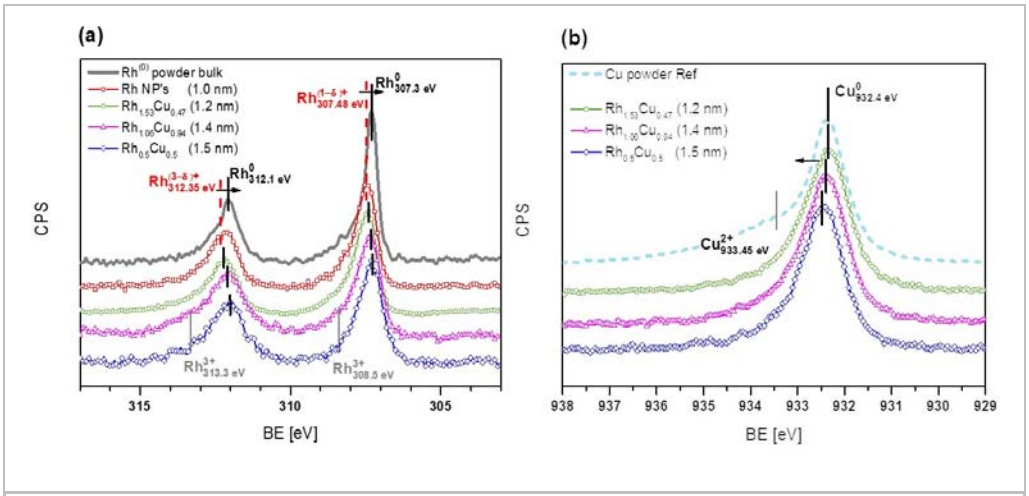

Figure 1: Rh *3d* and Cu $2p_{3/2}$ CL HAXPES spectra, (a) and (b) respectively, of reference Rh and Cu powder (solid and dashed lines, respectively), Rh NPs (red square scatters), $Rh_{1.53}Cu_{0.47}$ (green circle scatters), $Rh_{1.06}Cu_{0.94}$ (magenta triangle scatters) and $Rh_{0.50}Cu_{0.50}$ (blue diamond scatters) alloy NPs. The change in the electronic structure is understood as concurrent reduction of Rh and oxidation of Cu.

References

1. S. Kim, K. Qadir, S. Jin, A. S. Reddy, B. Seo, B. S. Mun, S. H. Joo, and J. Y. Park. Catalysis today 185, 131 (2012).
2. M.E. Grass, Y.W. Zhang, D.R. Butcher, J.Y. Park, Y.M. Li, H. Bluhm, K.M. Bratlie, T.F. Zhang, G.A. Somorjai. Angewandte Chemie-International Edition, 47, 8893 (2008).
3. H. Kobayashi, K. Kusada, & H. Kitagawa. Accounts of chemical research, 48(6), 1551 (2015).
4. S. Ueda. J. Electron Spectrosc. Relat. Phenom. 190, 235 (2013).
5. M. Isshiki, Y. Ohishi, S. Goto, K. Takeshita, & T. Ishikawa. Nucl. Instrum. Methods Phys. Res. A, 467, 663 (2001).
6. J. I. Flege and P. Sutter.Phys. Rev. B 78, 153402 (2008).
7. R. Westerström, J.G. Wang, M.D. Ackermann, J. Gustafson, A. Resta, A. Mikkelsen, J.N. Andersen, E. Lundgren, O. Balmes, X. Torrelles, J.W.M. Frenken, B. Hammer. J. Phys. Condens. Matter 20, 184018 (2008).

A. Acun et al. “Atomically Controlled Surfaces Interfaces and Nanostructures”
edited by A. Bianconi, A. Marcelli (Superstripes Press, Rome 2016) isbn: 9788866830597

Tu3T session

Silicene on metallic quantum wells

Mariusz Krawiec[1] , Agata Podsiadły-Paszkowska[1]
[1]*Maria Curie-Sklodowska University in Lublin*

Email: *mariusz.krawiec@umcs.pl*
Key words: Graphene and other 2D materials

Freestanding silicene, a new graphene-like two-dimensional material composed of Si atoms arranged in a honeycomb lattice, has been predicted to give rise to massless Dirac fermions [1,2]. However, due to the preferred sp^3 bonding, the freestanding silicene layer is not expected to be easily realized in experiment. Therefore it must be grown on a substrate [3,4], where the interaction between silicene and the substrate is of prime importance [5,6].
We discuss recently proposed efficient way of tuning the silicene-substrate interaction utilizing quantum size effect in the substrate [6]. As an example we consider silicene on ultrathin Pb(111) layers. Using first-principles density functional theory calculations, we demonstrate how the properties of silicene, including binding energy, properties of the Dirac cone, magnitude of the energy gap, can easily be manipulated by quantum well states of the substrate.
We also discuss a novel mechanism of protecting the Dirac electrons from the influence of the substrate. This is associated with a special arrangement of a part of Si atoms in silicene [6,7].
The above findings emphasize the essential role of interfacial coupling and open new routes to create silicene structures with controlled electronic properties.

This work has been supported by the National Science Centre (Poland) under Grant No. DEC-2014/15/B/ST5/04244.

References

1. K. Takeda, K. Shiraishi, Phys. Rev. B 50, 14916 (1994).
2. S. Cahangirov, M. Topsakal, E. Aktürk, H. Sahin, S. Ciraci, Phys. Rev. Lett. 102, 236804 (2009).
3. P. Vogt, P. De Padova, C. Quaresima, J. Avila, E. Frantzeskakis, M.C. Asensio, A. Resta, B. Ealet, G. Le Lay, Phys. Rev. Lett. 108, 155501 (2012).
4. A. Fleurence, R. Friedlein, T. Ozaki, H. Kawai, Y. Wang, Y. Yamada-Takamura, Phys. Rev. Lett. 108, 245501 (2012).
5. A. Podsiadły-Paszkowska, M. Krawiec, Phys. Chem. Chem. Phys. 17, 2246 (2015).
6. A. Podsiadły-Paszkowska, M. Krawiec, Phys. Rev. B 92, 165411 (2015).
7. A. Podsiadły-Paszkowska, M. Krawiec, Appl. Surf. Sci. 373, 45 (2016).

A. Acun et al. "Atomically Controlled Surfaces Interfaces and Nanostructures"
edited by A. Bianconi, A. Marcelli (Superstripes Press, Rome 2016) isbn: 9788866830597

Interplay between steps and vacancies on curved TiO_2(110)

J. Enrique Ortega[1,2,3], F Luis A. Miccio[1,2], Martin Setvin[4], Moritz Müller[1], Mikel Abadía[1], Ignacio Piquero[1], Jorge Lobo-Checa[1], Celia Rogero[1], Michael Schmid[4], Daniel Sánchez-Portal[1,2], Ulrike Diebold[4], Frederik Schiller[1]
[1] *Centro de Física de Materiales San Sebastián, Spain*
[2] *Donostia International Physics Center San Sebastián, Spain*
[3] *Universidad del País Vasco San Sebastián, Spain*
[4] *Institute of Applied Phys., Vienna Univ. of Technol., Austria*

Email: *enrique.ortega@ehu.es*
Keywords: Nanostructured oxides, vicinal surfaces

Vicinal surfaces exhibit distinct chemical and physical properties due to their high density of atomic steps, being also useful as nanoscale templates to control the growth of low dimensional structures, such as nanodots or nanostripes. In this context, a vast majority of studies on the chemistry and electronic properties of rutile r -TiO_2(110) have been carried out flat surfaces, whereas much less effort has been focused on stepped planes. Moreover, as low atomic coordination sites, the step edges are chemically and electronically very active, and hence stepped surfaces may become technologically relevant, e.g., as a way of tailoring new chemical properties of r-TiO_2. Using a curved r-TiO_2(110) crystal with a smooth variation of the density of atomic steps parallel to the [1-10] direction, we have performed a combined (STM-ARPES) and systematic study of stepped r-TiO_2(110) with [1-10]-oriented steps [1].
By means of Scanning Tunneling Microscopy (STM) we analyze the structure and distribution of steps and vacancies as a function of the average deviation (miscut α) from the (110) surface (Fig. 1 a). We observe the surface to smoothly evolve from wide terraces, containing O_{br} vac´s (Fig. 1 b), toward narrow (110) terraces, depleted of O_{br} vac´s (Fig. 1 c). We also observe the step edge morphology changing across the sample, from [1-11] zig-zag faceting to straight [1-10] steps. The [1-10] steps terminate with a pair of two-fold coordinated O atoms, which give rise to bright, triangular protrusions (S_t). The statistical analysis of the terrace width variation across the sample allows us to detect a step-bunching phase with a large α range, triggered by an optimal d~2.8 nm (110) terrace width, where all bridge-bonded O atom vacancies (O_{br} vac´s) vanish, but S_t-featured steps remain.
With Angle-Resolved Photoemission (ARPES) we focused on the Ti 3d-derived gap state (Fig. 1 d). The gap state intensity is observed to remain constant across the curved surface, directly correlating with the total density of S_t protrusions plus O_{br} vac´s measured with STM. This observation indicates that individual S_t protrusions (at steps) and O_{br} vac´s (at terraces) contribute to the crystal doping equally. The scan across the curved surface also reflects the transition from large O_{br}-filled terraces to the high density of S_t-featured steps through a 110 meV shift in apparent binding energy, which in turn suggests differences in the polaronic relaxation at terraces and steps. Density functional theory (DFT) calculations predict that S_t protrusions of [1-10] step edges are

favorable sites for the formation of O_{br} vac's in r-TiO_2(110), in accordance with previous studies on [1-11] steps [2]. Moreover, DFT indicates that the observed electron doping at the stepped part of the sample is not intrinsic to the step-edge, but stems from the presence of one O_{br} vacancy per S_t site.

We acknowledge financial support from the Spanish Ministry of Economy (MAT2013-46593-C6-4-P and MAT2013-46593-C6-2-P) and the Basque Government (IT621-13 and IT756-13), the ERC Advanced Grant "OxideSurfaces"., and the Marie Curie ITN "THINFACE".

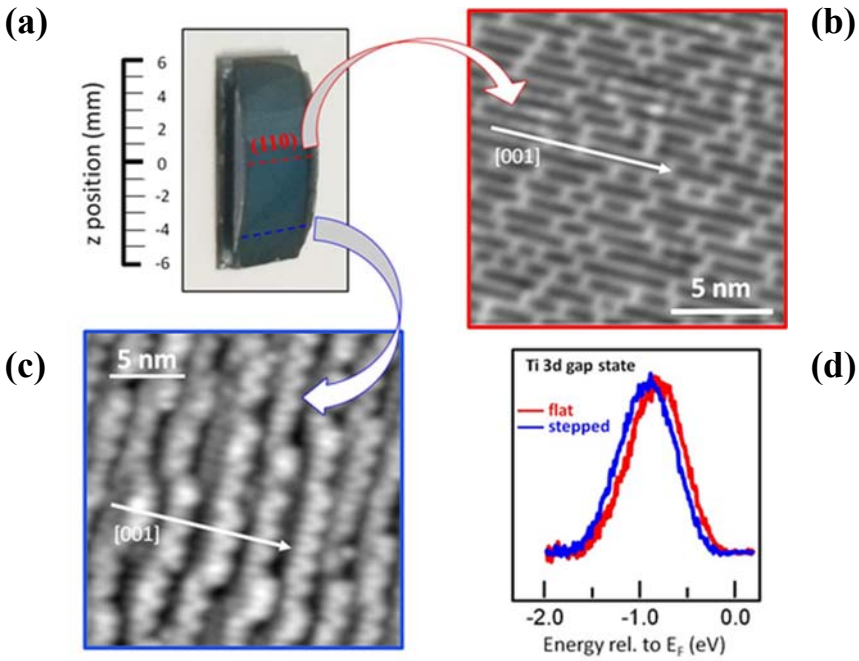

Figure 1. (a) Photography of the curved TiO_2(110) crystal used in the present work. Marked are the center of the crystal, with large (110) terraces and O_{br} vacancies [measured with STM in panel (b)], and the edge of the crystal, with a high density of steps featured with bright triangular protrusions [measured in panel (c)]. Despite the strong structural differences from flat to stepped areas of the crystal, the Ti 3d gap state peak [measured in ARPES and shown in panel (d)], shows no intensity change, but a small 110 meV binding energy shift.

References

1. L. A. Miccio et al., Nanoletters 16, 2017–2022 (2016).
2. U. Martinez, et al., Phys. Rev. Lett. 109, 155501 (2012).

A. Acun et al. “Atomically Controlled Surfaces Interfaces and Nanostructures”
edited by A. Bianconi, A. Marcelli (Superstripes Press, Rome 2016) isbn: 9788866830597

A precision surface electrical conductivity study of the Si(111)-In (4x1) – (8x2) phase transition

Shinichiro Hatta, Tetsuya Aruga
Department of Chemistry, Kyoto University

Email: *aruga.tetsuya.4e@kyoto-u.ac.jp*
Key words: Electronic and optical properties of surfaces and interfaces; Surfaces and interfaces for electronic devices; Frontiers aspects of semiconductor, surfaces and interfaces

There is an ever-growing interest in the transport properties of ultrathin films of, for instance, elemental metals, topological insulators and transition metal chalcogenides. Pioneering works of quantitative electrical conductivity measurement on semiconductor surfaces utilizing ultrahigh-vacuum (UHV) four-point probes (4pp) have been done for a number of superstructures and metallic monolayers [1]. A difficulty, however, has also been recognized in measurements varying the surface temperature, which should be due to the thermal instability of the probe–surface contacts during the temperature change. In order to overcome this difficulty, we have recently developed a highly-stable UHV 4pp system for the measurements of surface electrical conductivity in a wide temperature range (7–300 K) and applied it to Ge(111)-Pb-β(√3 x √3)R30°, showing unusually high electrical conductivity and weak electron–phonon coupling compared with bulk Pb [2].

The Si(111)-In-(4x1) system has been a benchmark of quasi-one-dimensional atomic nanowires. The system undergoes a (4x1) – (8x2) phase transition at around 120 K [3]. From an electronic-structure point of view, the transition corresponds to metal–insulator transition as revealed by ARPES [4]. After the years of controversy as to the nature of the phase transition,[5] the first-order nature of the transition has recently been revealed by an *ab initio* atomistic thermodynamic calculation and various diffraction experiments [6-9]. The LEED experiment [9] clearly demonstrated a hysteresis, showing the existence of an energy barrier in the transition and thus the first-order nature of the phase transition. Since the electrical conductivity is a macroscopic quantity, its temperature dependence should exhibit a characteristic behavior peculiar to first-order transitions. However, any indication of a hysteresis has not yet been found [10].

In this talk, we show the result of a precision electrical conductivity measurement during the (4x1) – (8x2) phase transition in Si(111)-In, which clearly shows the existence of the hysteresis. Thus the first-order nature of the phase transition is now supported also from the viewpoint of macroscopic electrical conductivity. Electrical transport in the metallic wires is also discussed.

References

1. S. Hasegawa, X. Tong, S. Takeda, N. Sato, T. Nagao, Prog. Surf. Sci. 60, 89 (1999). doi:10.1016/S0079-6816(99)00008-8
2. S. Hatta et al., Phys. Rev. B 90, 245407 (2014). doi: 10.1103/PysRevB.90.245407
3. H. W. Yeom et al., Phys. Rev. Lett. 82, 4898 (1999). doi: 10.1103/PhysRevLett.82.4898
4. J. R. Ahn et al., Phys. Rev. Lett. 93, 106401 (2004). doi: 10.1103/PhysRevLett.93.106401
5. P. C. Snijders and H. H. Weitering, Rev. Mod. Phys. 82, 307 (2010). doi: 10.1103/RevModPhys.82.307
6. S. Wippermann and W. G. Schmidt, Phys. Rev. Lett. 105, 126102 (2010). doi: 10.1103/PhysRevLett.105.126102
7. S. Hatta et al., Phys. Rev. B 84, 245321 (2011). doi: 10.1103/PhysRevB.84.245321
8. S. Wall et al., Phys. Rev. Lett. 109, 186101 (2012). doi: 10.1103/PhysRevLett.109.186101
9. F. Klasing et al., Phys. Rev. B 89, 121107(R) (2014). doi: 10.1103/PhysRevB.89.121107
10. See, for example: T. Uetake et al., Phys. Rec. B 86, 035325 (2012). doi: 10.1103/PhysRevB.86.035325

Spin scattering studied with scanning tunneling microscopy

Deung-Jang, Choi[1] , Carmen Rubio-Verdú[1], Miguel Moreno Ugeda[1], Jose Ignacio Pascual[1]
[1] *CIC nanoGUNE, Tolosa Hiribidea 78, Donostia-San Sebastian 20018, Spain*

Email: *d.choi@nanogune.eu*
Key words: Edge states, Shiba states

We use a low-temperature (1 K) scanning tunneling microscopy (STM) to study of magnetic impurities on different substrates. In the present contribution, we report on work on atomic Mn chains assembled on Cu_2N/Cu (100) surfaces. Besides their known magnetic spectra [2], we have found an electronic edge state on these chains whose properties depend on the magnetic ordering of the Mn chains [3]. We have also applied our techniques to the study of magnetic spectra on superconducting surfaces revealing the orbital properties of the Shiba states [4] associated with the magnetic impurities.

References

1. Cyrus F. Hirjibehedin, Chiung-Yuan Lin, Alexander F. Otte, Markus Ternes, Christopher P. Lutz, Barbara A. Jones, and Andreas J. Heinrich. Large magnetic anisotropy of a single atomic spin embedded in a surface molecular network. Science , 317: 1199 (2007).
2. D.-J. Choi et al. Submitted
3. K. J. Franke, G. Schulze, J. I. Pascual, Competition of superconducting phenomena and Kondo screening at the nanoscale, Science, 332: 940 (2011).

A. Acun et al. “Atomically Controlled Surfaces Interfaces and Nanostructures”
edited by A. Bianconi, A. Marcelli (Superstripes Press, Rome 2016) isbn: 9788866830597

Quasi-1D atomic-chains on vicinal surfaces: the role of defects and constrictions towards electronic transport

I. Miccoli[1] , F. Edler,[1] J. P. Stöckmann,[1] S. Demuth,[1] H. Pfnür,[1,2] S. Wippermann,[3] A. Lücke,[4] W. G. Schmidt,[4] and C. Tegenkamp[1,2]
[1]*Institut für Festkörperphysik, Leibniz Universität Hannover, Appelstraße 2, 30167 Hannover, Germany*
[2]*Laboratorium für Nano- und Quantenengineering (LNQE), Leibniz Universität Hannover, Schneiderberg 39, 30167 Hannover, Germany*
[3]*Grenzflächenchemie und Oberflächentechnik, Max-Planck-Institut für Eisenforschung GmbH, Max-Planck-Straße 1, 40237 Düsseldorf, Germany*
[4]*Lehrstuhl für Theoretische Physik, Universität Paderborn, 33098 Paderborn, Germany*

Email: *miccoli@fkp.uni-hannover.de*
Key words: Atomic-chains, metal-insulator transitions, interwire coupling, defects, lateral constrictions

Metallic atomic chain ensembles grown epitaxially on vicinal semiconductor surfaces are prototype quasi-1D systems with outstanding electronic properties for fundamental research studies, such as Peierls driven metal to insulator phase transition (MIT) or dimensional crossover from a Fermi to Luttinger liquid behavior [1]. Despite the intense studies over the last decades on several systems, e.g. Si(111)-4x1-In, Si(557)-Au and Si(553)-Au, the effect of native defects or induced defects by adsorption (e.g. O_2 and H_2) on the conductance along the wires, the interwire coupling or the transition temperature, are still under current debate.
Here, we present a systematic study on the transport properties of In- and Au-chains grown on various Si(hhk) surfaces by means of a temperature variable multi-tip STM/SEM system. The anisotropy of the conductivities along the wires and in the direction across the wires is quantified by the so-called rotational four-point-probe square method [2] (see Fig. 1a). Additionally, an extremely higher sensitivity of almost one order of magnitude towards atomic imperfections and both conductivity components was reached by a spatial constriction of the electron path [2] (see Fig. 1b-c).
In detail, the interwire coupling for the Si(111)-4x1-In system was re-analyzed in greater detail. In contrast to previous studies, we showed in agreement with DFT calculations, that the interwire coupling can be gradually tuned by adsorption of oxygen [3] (see Fig. 1d). Moreover, the transport properties of various Au-phases on Si(hhk) surfaces were studied. While the 0.48 ML Au on Si(553) turned out to be extremely robust and almost unaffected (up to 20 Langmuir), the 0.2 ML phase on Si(557) reacts strongly as seen by the exponential decrease and the adsorbates induce even a crossover of its conductivity components.

The adsorption behavior turns out to be strongly triggered by the presence of a Si-adatom chain, which is a characteristic building block for some the Au/Si(hhk) chain systems [4].

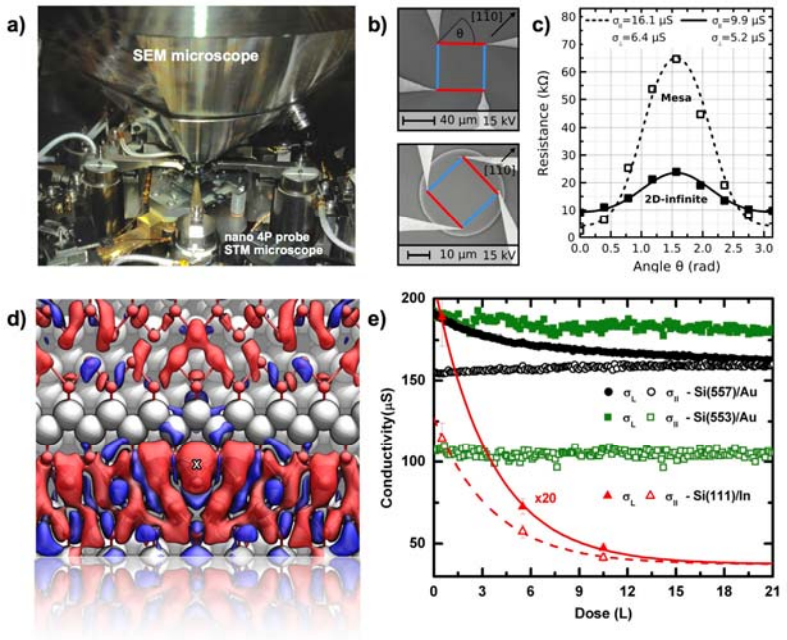

Figure 1: a) A photograph of a multi-probe STM system mounted in the focus of an SEM for the navigation and placement of the tungsten tips. b) SEM image of four W tips placed in square configuration on an unconfined In/Si(111) surface (above) and confined circular In/Si(111)-mesa structure (below). The resistance anisotropy on the spatially constricted 2D phase is significantly higher than for the quasi-infinite 2D case. (d) Difference of the local density of states (LDOS) within a 8 × 12 unit cell around an α-type oxygen defect (marked by a cross) compared to ideal, defect-free wires. (e) $\sigma_{\parallel}$ and $\sigma_{\perp}$ as a function of the O_2 dose for the Si(111)-4x1-In system, 0.48ML Au phase on Si(553) and 0.2ML Au phase on Si (557).

References

1. C. Zeng, P.R.C. Kent, T.H. Kim, A. Ping Li & H.H. Weitering, Nature Materials 7, 539 - 542 (2008). http://dx.doi.org./10.1038/nmat2209
2. I. Miccoli, F. Edler, H. Pfnür and C. Tegenkamp, J. Phys.: Condens. Matter 27 (2015) 223201 http://dx.doi.org./10.1088/0953-8984/27/22/223201
3. F. Edler, I. Miccoli, S. Demuth, H. Pfnür, S. Wippermann, A. Lücke, W.G. Schmidt, and C. Tegenkamp, Phys. Review B 92, 085426 (2015). http://dx.doi.org/10.1103/PhysRevB.92.085426
4. J. Aulbach, S.C. Erwin, R. Claessen, and J. Schäfer, Nano Letters 16, 2698 (2016). http://dx.doi.org/10.1021/acs.nanolett.6b00354

Strain induced quasi-one dimensional structure of rare earth silicides on Si substrates

J. Wollschläger[1,2], F. Timmer[1,2], R. Oelke[1,2], M. Franz[3], S. Appenfeller[3], C. Dues[4], W.G. Schmidt[4], S. Sanna[4], M. Dähne[3]
[1]*Fachbereich Physik, Universität Osnabrück, Osnabrück.*
[2]*Center of Physics and Chemistry of New Materials, University Osnabrück, Osnabrück.*
[3]*Institut für Festkörperphysik, Technische Universität Berlin, Berlin*
[4]*Departement Physik, Universität Paderborn, Paderborn*

Email: *jwollsch@uos.de*
Key words: rare earth silicide, superstructure, quasi-one dimensional structure, nanowire, strain induced structure

One dimensional (1D) systems have attracted a lot of attention since their physical properties, e.g., electronic and optical properties, Peierls instability, Tomonga-Luttinger liquid, are distinctively different from structures of higher dimensionality. Recently, a new class of quasi-1D systems based on rare earth silicides (RESi) has attracted attention since RESi monolayers form a large variety of different superstructures on Si substrates (cf. [1] for Si(111)). Some of these superstructures have large anisotropic quasi-1D structures. This effect has been attributed to strain induced effects due to different 'bulk' structures RESi and Si [2]. Here, we report on combined studies on quasi-1D structures by scanning tunneling microscopy STM), spot profile analysis of low-energy electron diffraction (SPA-LEED), grazing incidence x-ray diffraction (GIXRD) and density functional theory (DFT).

On one hand we observe a $2\sqrt{3}x\sqrt{3}$ superstructure depositing RE at elevated temperature on Si(111) (cf. Fig. 1) [3]. This structure is attributed to the formation of periodically arranged Si vacancies in different $RESi_2$ layers. The complex structure of this superstructure with buckled surface layer, $\sqrt{3}x\sqrt{3}$ superstructure in the first subsurface layer $2\sqrt{3}x\sqrt{3}$ superstructure in the second subsurface layer can only be analyzed applying the different techniques used here. The anisotropic character of this structure is emphasized by the formation of periodically arranged domain boundaries. The width of the RESi domains formed in two domains is roughly two unit cells.

On the other hand, we studied a sequence of different quasi-1D RESi structures on Si(001). A clear sequence from the (2x4) to the (2x7) reconstruction is observed where the latter consists of (2x4) and (2x3) subunits. The (2x7) surprisingly transforms back to the (2x4) before NWs are formed on top of this wetting layer. The NWs, however, show a clear (2x1) structure and have 1D metallic dispersion [4-6]. Finally, NW *bundles* are created at higher coverages with (2x*n*) signature in diffraction.

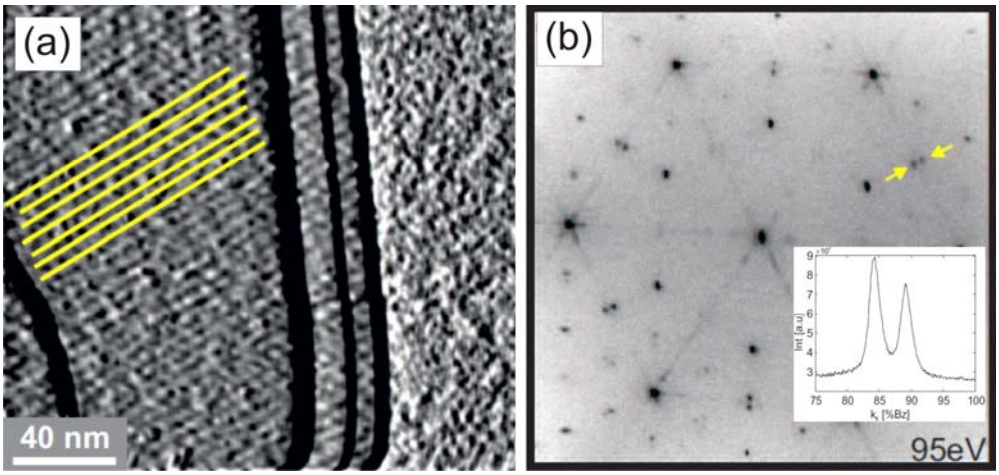

Figure 1: (a) STM micrograph of 2√3x√3 superstructure with domain walls (yellow lines). (b) SPA-LEED diffractogramm of the same superstructure with splitted odd order superstructure diffraction spots due to regularly arranged domain wall. Inset: Line scan through splitted superstructure diffraction spot.

References

1. S. Sanna et al., Phys. Rev. B93, 195407 (2016).
2. M. Dähne et al., J. Phys. Condens. Matter 25, 014012 (2013).
3. F. Timmer et al., in preparation.
4. M. Wanke et al., Phys. Rev. B79, 155428 (2009).
5. M. Wanke et al., J. Appl. Phys. 108, 064304 (2010).
6. M. Wanke et al., Phys. Rev. B83, 205417 (2011).

A. Acun et al. “Atomically Controlled Surfaces Interfaces and Nanostructures”
edited by A. Bianconi, A. Marcelli (Superstripes Press, Rome 2016) isbn: 9788866830597

Tu3S session

Spin Manipulation by Creating Single-Molecule Radical Cations

S. Karan[1], N. Li[2], Y. Zhang[3], Y. He[2], I. Hong[2], H. Song[3], J. Lü[4], Y. Wang [1,2,5], L. Peng[2], K. Wu[3], G. S. Michelitsch[6], R. J. Maurer[6], K. Diller[6], K. Reuter[6], A. Weismann[1], R. Berndt[1]
[1]*IEAP, Christian-Albrechts-Universität zu Kiel, Kiel, Germany*
[2]*Key Laboratory for the Physics and Chemistry of Nanodevices, Peking University, Beijing, People's Republic of China*
[3]*College of Chemistry and Molecular Engineering, Peking University, Beijing, People's Republic of China*
[4]*School of Physics, Huazhong University of Science and Technology, Wuhan, People's Republic of China*
[5]*Beida Information Research, Tianjin, People's Republic of China*
[6]*Lehrstuhl für Theoretische Chemie, Technische Universität München, Garching, Germany*

Email: *berndt@physik.uni-kiel.de*
Key words: STM, spin, organic molecule, manipulation, Kondo effect, magnetic field, very low temperature

All-trans-retinoic acid [1] and cholesterol [2], closed-shell organic molecules comprising only C, H, and O atoms, are investigated on a Au(111) substrate using scanning tunneling microscopy and spectroscopy. In dense arrays single molecules are switched to a number of states, several of which carry a localized spin as evidenced by conductance spectroscopy in high magnetic fields. The spin of a single molecule may be reversibly switched on and off without affecting its neighbors. We suggest that retinoic acid and cholesterol on Au are readily converted to a radical by the abstraction of an electron.

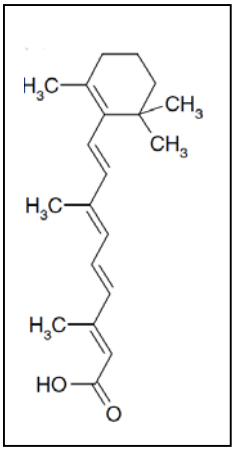

References

1. S. Karan et al., Phys. Rev. Lett. 116, 027201 (2016)
2. S. Karan and R. Berndt, Phys. Chem. Chem. Phys. 18, 9334 (2016)

A. Acun et al. “Atomically Controlled Surfaces Interfaces and Nanostructures”
edited by A. Bianconi, A. Marcelli (Superstripes Press, Rome 2016) isbn: 9788866830597

Thermodynamic balance of perylene self-assembly on Ag(110)

Kirill Bobrov, Nataliya Kalashnyk *and* Laurent Guillemot
Institut des Sciences Moléculaires d'Orsay, CNRS, Université Paris-Sud 11, F-91405 Orsay.

Email: *Kirill.Bobrov@u-psud.fr*
Key words: perylene, Ag(110), organic monolayer, self-assembly, epitaxy, surface mobility, thermodynamics, fluid phase, STM

We present a room temperature STM study of perylene adsorption on Ag(110) at the monolayer coverage regime. We found that structure and symmetry of the flat perylene monolayer is determined by thermodynamic balance of the three factors: (i) the site recognition effect, (ii) the intermolecular interaction and (iii) the thermal motion of the perylene molecules. The moderate strength of the site recognition and intermolecular interactions, of the same order of magnitude as kT ~25 meV, represented a key feature of the thermodynamic balance.
The thermodynamic balance bestowed to this system the unique quality to form a flexible monolayer of epitaxial as well as self-assembling character. The increasing perylene coverage induced gradual crystallization of the initially fluid monolayer (<0.1 ML) into the crystalline (2 5 3 -2)/(2 -5 3 2) monolayer (0.1053 ML). The crystalline monolayer further incorporated extra molecules modifying its structure and symmetry albeit maintaining its true commensurate character. The recognition effect of moderate strength was able to lock some of the perylene molecules into favorable adsorption sites of the (110) lattice providing a skeleton of the crystalline phases. We have found that the crystalline monolayer did not quench thermal motion of the included molecules but rather accommodated it modifying its skeleton by reselecting a new set of available adsorption sites favorable in terms of intermolecular interaction.
The ability of the perylene crystalline structure to accommodate its thermal motion made possible formation of the epitaxial and self-assembled perylene monolayer free of domain boundaries in the whole coverage range.

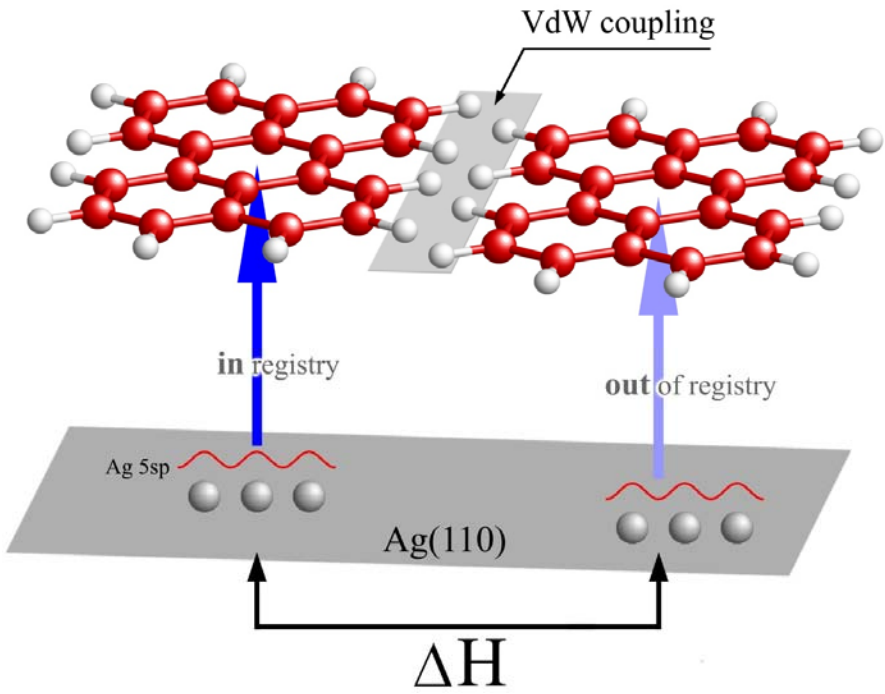

Fig.1 Perylene bonding on Ag(110)

A. Acun et al. “Atomically Controlled Surfaces Interfaces and Nanostructures”
edited by A. Bianconi, A. Marcelli (Superstripes Press, Rome 2016) isbn: 9788866830597

Identification of surface structures of titania nanoparticles by photoemission spectroscopy

P. Borghetti,[1] E. Meriggio,[2] G. Rousse,[1,3,4] G. Cabailh,[1] R. Lazzari,[1] and J. Jupille[1]
[1]*Institut des NanoSciences de Paris, UPMC University Paris 06 and CNRS, 4 Place Jussieu, 75005, Paris, France*
[2] *Dipartimento di Fisica, Università degli Studi di Genova, Via Dodecaneso 33, 16146 Genova, IT.*
[3] *Chimie du Solide et de l'Energie, Collège de France, 11, Place Marcelin Berthelot, 75231 Paris, France.*
[4] *Réseau sur le Stockage Electrochimique de l'Energie (RS2E), FR CNRS 3459, France.*

Email: *borghetti@insp.jussieu.fr*
Key words: Methods for structural identification; Titanium dioxide nanostructures; Photoemission spectroscopy; Auger transitions

The innumerous properties of titanium dioxide rely on its various polymorphs and crystallographic orientations, and quite often on mixtures of these. It is therefore crucial to set out surface-sensitive methods that allow the *in situ* structural identification. The present work reports on the ability of photoemission-based techniques performed with standard laboratory X-ray sources to identify the phase and surface orientation of TiO_2 nanostructured samples. Ti LMV Auger reference spectra of TiO_2 rutile (110), anatase (101) and anatase (001) single-crystals are singled out, by taking advantage of the presence of a valence level in the Auger transition. Indeed, differences in the Ti LMV transition derive from intrinsic structural aspects of the different titanium dioxide polymorphs and orientations. Ti LMV templates allow a quantitative analysis of phases and orientations involved in nanoparticle samples. As an example, the case of standard Degussa P-25 powder is analyzed, both in its as-received form and during the anatase-to-rutile transformation upon annealing. Comparison to X-ray diffraction measurements demonstrates the reliability of the Auger analysis and highlights its ability to detect crystallographic orientations and composition gradients.

A. Acun et al. "Atomically Controlled Surfaces Interfaces and Nanostructures"
edited by A. Bianconi, A. Marcelli (Superstripes Press, Rome 2016) isbn: 9788866830597

Theoretical investigations for strain relaxation and resultant growth mode of InAs thin layer on GaAs(111)A

Tomonori Ito[1] , Toru Akiyama[1], Kohji Nakamura[1]
[1]*Mie University*
[3]*Department of Physics Engineering*

Email: *tom@phen.mie-u.ac.jp*
Key words: Nanoscale structure, growth processes and strain in thin layers and interfaces; State of the art theoretical approaches on surfaces and interfaces

The InAs/GaAs system is crucial for fabricating semiconductor nanostructures such as quantum dots (QDs). Due to the 7 % lattice mismatch between InAs and GaAs, the InAs on the GaAs(001) produces three-dimensional (3D) QDs with Stranski-Krastanov (SK) growth mode. Despite a constant lattice mismatch, the InAs on the GaAs(111)A exhibits two-dimensional (2D) growth. Although many studies have been done to investigate the QD formation on the InAs/GaAs(001), there have been very few studies for the origin of 2D growth on the InAs/GaAs(111)A. In this study, the growth mode of the InAs/GaAs(111)A is systematically investigated using our macroscopic theory with the aid of empirical potential calculations to determine parameter values used in this study. Here, stacking fault tetrahedron (SFT) found in InAs/GaAs(111)A [1] and misfit dislocation (MD) formations are employed as strain relaxation mechanisms.

In our macroscopic theory, free energy F (eV/Å^2) for various growth modes such as 2D-coherent, SK-coherent, 2D-SFT, and 2D-MD is described as a function of layer thickness h as follows [2].

$$F = \gamma(1+\beta) + \frac{1}{2}M(1-\alpha)\varepsilon^2\left(1-\frac{l_0}{l}\right)h + \frac{E_d}{l}, \quad (1)$$

where γ (=0.042 eV/Å^2), β, M, α, ε (=0.072), l, l_0 (=58.76 Å), and E_d denote the surface energy, the effective increase in surface energy of the epilayer due to SK island formation, the effective elastic constant, the effective decrease in strain energy due to SK island formation, the intrinsic strain of the system, the average MD spacing, the MD spacing at which strain is completely relaxed, and the formation energy of the MD, respectively. In order to determine the values of M and E_d, the energy difference ΔE_{MD} between the 2D-coherent and the 2D-MD is estimated using empirical interatomic potential with a 14×14 planar unit cell.

The calculated ΔE_{MD} is shown in Fig. 1(a) as a function of InAs monolayers (MLs) h. This reveals that the ΔE_{MD} changes its sign from positive to negative at h = 8 MLs, where the strain in InAs thin layers is completely relaxed to stabilize the 2D-MD. Moreover, we found that the SFT formation makes surface atoms move upward to reduce the strain energy as described by $\Delta E_{\mathrm{SFT}} = 0.014h\text{-}0.0011h^2$ (eV). Therefore, the SFT in addition to the MD plays an important role for strain relaxation in InAs thin layers grown on GaAs(111)A. Using the parameter values of M ($=0.164 \times 10^{11}$ N/m^2),

E_d (=0.675 eV/Å), α (=0.74), and β (=0.08), calculated free energy differences ΔF between the 2D-coherent and various growth modes are shown in Fig. 1(b) as a function of h. This implies that the InAs growth on the GaAs(111)A proceeds along the lower energy path from the 2D-coherent ($h \leq 4$ MLs) to the 2D-MD ($h \geq 7$MLs) via the 2D-SFT (4 MLs $\leq h \leq$ 7 MLs). Although the SK-coherent and the 2D-MD are energetically competitive similarly to the InAs/GaAs(001) [3], it should be noted that 3D growth mode (the SK-coherent) does not appear due to the 2D-SFT formation preceding the SK-coherent. Consequently, 2D growth is preferable on the InAs/GaAs(111)A results from strain relaxation near the surface forming the SFT different from the InAs/GaAs(001).

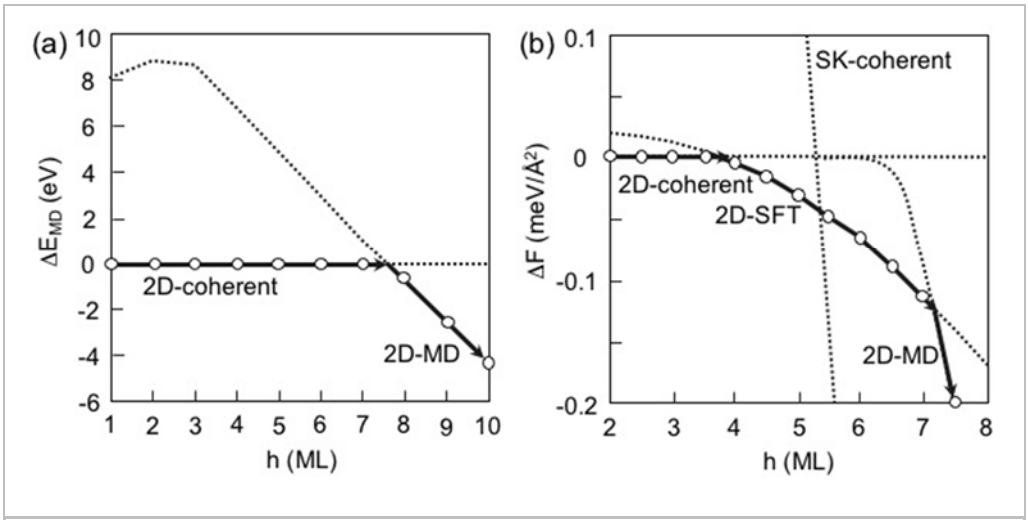

Figure 1: Calculated results for (a) system energy difference ΔE_{MD} between 2D-coherent and 2D-MD and (b) free energy differences ΔF between 2D-coherent and various growth modes as a function of layer thickness h.

References

1. K. Kanisawa, M. J. Butcher, Y. Tokura, H. Yamaguchi, and H. Hirayama, Phys. Rev. Lett. 87, 196804 (2001).
2. K. Shiraishi, N. Oyama, K. Okajima, N. Miyagishima, K. Takeda, H. Yamaguchi, T. Ito, and T. Ohno, J. Cryst. Growth 237-239, 206 (2002).
3. R. Kaida, T. Akiyama, K. Nakamura, and T. Ito, J. Cryst. Growth (submitted).

Ultrathin Sb layers on Pb quantum wells

Mieczysław Jałochowski , Agnieszka Stępniak-Dybala, Mirosław Stróżak, Mariusz Krawiec
Maria Curie-Skłodowska University in Lublin

Email: *mieczyslaw.jalochowski@umcs.lublin.pl*
Key words: Metal-semiconductor and insulator-semiconductor interfaces; Graphene and other 2D materials; Topological insulators

Antimony (Sb) show strong spin-orbit coupling and is proposed to be topological insulator (TI). However, Sb as bulk material is semimetal. According to theoretical predictions [1] 1 to 3 bilayer (BL) thick Sb(111) films are ordinary insulators and 4-5BL films are non-trivial insulators [1]. Calculations also show that with increasing film thickness surface splitting at the Γ point shrinks from 1.324 eV for 1BL film to 0.016 eV and 0.008 eV for 4BL and 5 BL films. Transition to topological semimetal should occur at thickness of 22BL [2]. As far as we know, tuning of topological properties of ultrathin Sb(111) film by manipulating solely electronic structure of substrate was not reported.
In our work electronic band structure of Sb(111) ultrathin films is tuned by deposition Sb on Pb(111) quantum wells (QW). Using scanning tunneling microscopy (STM), tunneling spectroscopy (STS), density functional theory (DFT) and reflection high energy electron diffraction (RHEED) methods we study electronic and crystal properties of Sb layers on Pb QW’s of different width. The QW fabricated on Si(111) and on Si(111)6x6Au surfaces served as controllable source of electronic states hybridizing with electron bands of ultrathin Sb(111) film. As thin as single and two BL thick continuous films on the top of Pb QW were fabricated and characterized.

This work was supported by National Science Centre, Poland, under Grant No. 2014/13/B/ST5/04442.

References

1. D. Wang, L. Chen, H. Liu, X. Wang, G. Cui, P. Zhang, D. Zhao and S. Ji, Phys. Chem. Chem. Phys. 17, 3577 (2015). DOI: 10.1039/C4CP04502E
2. P. F. Zhang, Z. Liu, W. H. Duan, F. Liu and J. Wu, Phys. Rev. B85, 201410(R) (2012). DOI: 10.1103/PhysRevB.85.201410

A. Acun et al. "Atomically Controlled Surfaces Interfaces and Nanostructures"
edited by A. Bianconi, A. Marcelli (Superstripes Press, Rome 2016) isbn: 9788866830597

Formation of a magnetite/hematite epitaxial bilayer generated with ion bombardment.

S. Ruiz-Gómez[1], A. Serrano[2], I. Carabias[1], M.A. García[2], A. Hernando[3], A. Mascaraque[1], L. Pérez[1], M.A. González[1], O. Rodríguez de la Fuente[1]
[1]*Universidad Complutense de Madrid*
[2]*Instituto de Cerámica y Vidrio-CSIC*
[3]*Instituto de Magnetismo Aplicado-UCM-CSIC*

Email: *oscar.rodriguez@fis.ucm.es*
Key words: Nanoscale structure, growth processes and strain in thin layers and interfaces; Heterojunctions and nanomagnetism

The fabrication of oxide heterostructures, with interfaces separating different oxides, is an important topic in the development of new materials. An oxide already displays a huge range of functionalities, but in combination with another oxide in the same material, it may give rise to novel phenomena not displayed by either of the constituent oxides alone. In this context, the continuous improvement of the existing techniques or the development of new methods for the synthesis of oxide heterostructures is mandatory.

An interesting subset of oxide interfaces is that formed by two simple oxides with the same cation but with a different oxidation state. In relation to this type of heterostructures (a sub-oxide on top of an oxide) we present in this work a novel approach to obtain such a system: Low Energy Ion Bombardment (LEIB). We have already successfully applied this growth technique to the TiO(001)/TiO_2(110) system [1], employing the technique to the surface of a single-crystal. Now we show the application of such approach to the case of iron oxides in the form of a thin film: we fabricate a magnetite/hematite (Fe_3O_4/α-Fe_2O_3) single-crystalline epitaxial bilayer on top of a metallic substrate. As far as we know, this system has not been synthesized yet in the form of a thin bilayer.

This novel fabrication method involves the transformation of the upper layers of a single-crystalline hematite thin film to single-crystalline magnetite, a process driven by the preferential sputtering of oxygen atoms. We show the reversibility of the transformation between hematite and magnetite, always keeping the epitaxial and single-crystalline character of the films. The magnetic characterization of the bilayer grown with this method shows that the magnetic response is mainly determined by the magnetite thin film.

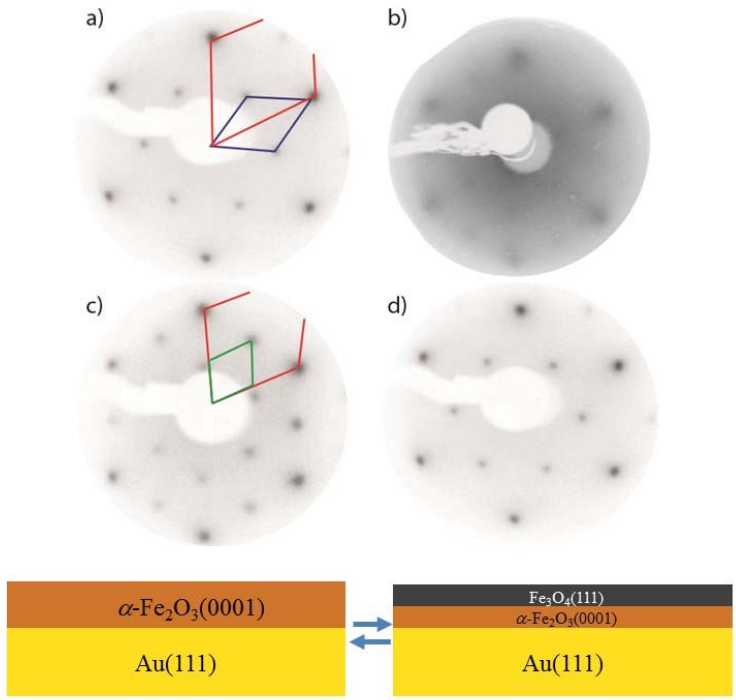

Figure 1. a) LEED pattern of the as-grown hematite thin film, which shows the expected symmetry (unit cell in blue) with respect to the original symmetry of the Au(111) substrate (in red). b) LEED pattern of a magnetite thin film after ion bombardment of the hematite thin film displayed in (a). While the spots are broad and diffuse and the background is bright, they already show an emerging new (2x2) symmetry. c) LEED pattern of the magnetite thin film after annealing the sample in (b). d) LEED pattern of hematite after the re-oxidation process of the magnetite film in (c). Bottom: Scheme of the transformation induced. The upper part of the hematite thin film is converted into magnetite after ion bombardment.

References

1. B.M. Pabón, J.I. Beltrán, G. Sánchez-Santolino, I. Palacio, J. López-Sánchez, J. Rubio-Zuazo, J.M. Rojo, P. Ferrer, A. Mascaraque, M.C. Muñoz, M. Varela, G.R. Castro, O. Rodríguez de la Fuente, Nature Communications 6, 6147 (2015). http://dx.doi.org/10.1038/ncomms7147

A. Acun et al. “Atomically Controlled Surfaces Interfaces and Nanostructures”
edited by A. Bianconi, A. Marcelli (Superstripes Press, Rome 2016) isbn: 9788866830597

Tu4T session

A. Acun et al. “Atomically Controlled Surfaces Interfaces and Nanostructures”
edited by A. Bianconi, A. Marcelli (Superstripes Press, Rome 2016) isbn: 9788866830597

Application of Kikuchi pattern to precise surface structure of GaN(0001) substrates at different polishing stages

Y. Shigeta[1] , Y. Hagiwara, T. Otaka J. Namkata[1], A. Tosaka[1] and K. Koyama[2]
[1] *Yokohama City University, 22-2 Seto, Kanazawa-ku, Yokohama 236-0027, Japan*
[2] *Namiki Precision Jewel. Co. Ltd., 3-8-22 Shinden, Adachi, Tokyo 123-8511, Japan*

Email: *shigeta@yokohama-cu.ac.jp*
Key words: Surface Structure Change by using Kikuchi pattern; Surface strain by polishin; GaN(0001) substrate

A precise in situ measurement of a lattice constant including the strain is very important, because the surface strain has a great influence on the electronic properties of the surface and the thin film growth on the surface. Though some diffraction methods by using X-ray and neutron are used as measurements of the strain, it is too difficult to measure the surface strain within a few nm in depth.
The reflection high-energy electron diffraction (RHEED) is very useful tool to investigate the structure within a few layers underneath the surface [1,2]. However the position shift of the RHEED spots is very small compare to the spot size. The spot size on the fluorescent screen is about 0.5 mm, which is resulting from the uncertainty of the camera length between the fluorescent screen and the sample. The irradiation region of the incident beam on the sample surface spreads to a few mm, because the glancing angle of the incident beam is very small (about 1° - 6°). So, the strain about a few % of the lattice constant is too difficult to measure from the position shift of the RHEED spot.
However, the change of the Kikuchi line is much larger than the shift of the RHEED spot, if the strain isn’t isotropic but anisotropic. The strain in the surface region is considered to be anisotropic, because a stress along to the surface normal and a stress parallel to the surface are different, generally. The Kikuchi pattern constructed from the Kikuchi lines is much useful to measure the anisotropic strain in the surface region. When the tensile strain is introduced to only the direction parallel to the surface plane, the reciprocal lattice for the surface region shrinks along the direction parallel to the surface. According to the change of the reciprocal lattice, the Kikuchi line changes anisotropic, as shown in Figs. 1(a) and 1(b), where 4% of tensile strain is introduced parallel to the surface. We had presented [3] that the sensitivity of the strain measurement by using the Kikuchi line is very high and the strain less than 1 %t is measurable.

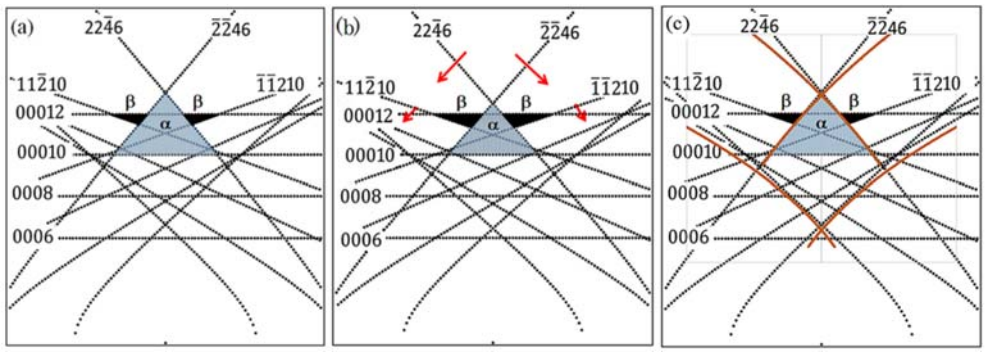

Figure 1: Simulated Kikuchi pattern of GaN(0001); (a) Kikuchi lines from strain free surface, (b) Change of Kikuchi lines with 4% of tensile strain paralell to the surface, and (c) Kikuchi envelopes are superinposed on the Kikuchi pattern.

In this paper, we have took the Kikuchi envelope into consideration, because the Kikuchi envelope is observed higher intensity than that of the Kikuchi line and is created by the two dimensional surface reciprocal rod [4]. So, the position of the Kikuchi envelope reflects a lattice constant of the top most surface layer. By using the Kikuchi envelope in the RHEED pattern, we can measure the lattice constant of the surface layer precisely, even on the surface during thin film growth.
We have applied the method to investigate difference between two GaN(0001) substrates, which are two different stages of Chemical Mechanical Polishing (CMP) after a mechanical polishing (MP) with the Diamond powder. It is reported that the MP substrate is composed of a strong damaged layer with the thickness of 200 nm on a weakly damaged layer with the thickness of 2000 nm in the surface region [5]. We measured the lattice constant of the weakly damaged layer after removing the strong damaged layer and that of the surface layer without any damaged layer removed by the MCP. We confirmed that the difference in the lattice constant between these two surface layers is about 1%.

References

1. Y. Fukaya and Y. Shigeta, Surf. Sci. 530, 175 (2003).
2. doi:10.1016/S0039-6028(03)00435-7
3. Y. Fukaya, Y. Shigeta, and K. Maki, Phys. Rev. B61, 13000 (2000).
4. http://dx.doi.org/10.1103/PhysRevB.61.13000
5. Y. Shigeta *et. al.*, The 13th European Vacuum Congress, 2014, at Aveiro, Spain.
6. A. Ichimiya, K. Kambe and G. Lehmpfuhl, *J. Phys. Soc. Jpn*. 49, 684 (1980).
7. http://dx.doi.org/10.1143/JPSJ.49.684
8. H. Aida, *et. al.*, J. Electrochem. Soc. 158 (2011) H1206.
9. doi: 10.1149/2.024112jes

Interaction between adjacent twin Si_4 atom switches

S. Yamazaki[1,2], K. Maeda[2], Y. Sugimoto[2], M. Abe[3], P. Pou[4], L. Rodrigo[4], R. Perez[4], P. Mutombo[5], P. Jelinek[5], S. Morita[6]
[1]*School of Science, Tokyo Institute of Technology,*
[2]*School of Engineering, Osaka Univ.,*
[3]*School of Engineering Science, Osaka Univ.,*
[4]*Cond. Matter Phys. Center, Univ. Autonoma de Madrid,*
[5]*Inst. of Phys., Academy of Science of the Czech Republic,*
[6]*The Inst. of Scientific and Industrial Research, Osaka Univ.*

Email: *yamazaki.s.aj@m.titech.ac.jp*
Key words: Atom manipulation; Atom switch; Silicone surface; Scanning tunneling microscopy; Atomic force microscopy

Various kinds of atom switches have been reported for the last several decades. While most of atom switches are induced by tunneling current injected from STM tip, buckled dimer rows (1D-like) on the Si(100) surface are switched by atomic force in unidirectional manner, as recently found in AFM studies[1]. We have introduced a bi-stable self-standing (0D-like) all-Si atom switch, Si tetramer (Si_4) [2], which can be fabricated on the well-known Si(111)-7x7 surface by atom manipulation at room temperature [3].

Structure models of bi-stable Si_4 in the ground state (Type-A and B) were constructed by first-principles simulation [Fig. (a), (b)], and confirmed by corresponding STM images using an Omicron LT QPlus-AFM/STM system operated at 80 K [Fig. (c), (d)]. Si_4 is switched between two mirror-symmetric equivalent configurations by both atomic force and tunneling current selectively.

STM tunneling current induces downward switching on Si_4, resulting in cross-like contrast (AxB) in apparent [Fig. (e)]. In contrast, AFM images at close tip-surface distances beyond the switching threshold clearly resolve four Si atoms of Si_4 [Fig. (f)]. Symmetric square-like contrast (A+B) is due to continuous upward switching during scan. Competition and transition between force-induced (upward) and current-induced (downward) switching is demonstrated. [2]

What happens if such well-defined single Si_4 atom switch stay next to another Si_4? It is intriguing question that they are still independent or interacting. To investigate interacting atom switchs, we intentionally increased density of Si_4 so that some of them stay next to another Si_4. Such two adjacent Si_4 atom switches is named "twin Si_4" [Fig. (g)].

At high-bias STM image, both Si_4 in twin Si_4 show cross-like image [Fig. (g)], while at low-bias STM image, they show one of ground states of Si_4, namely A type or B type [Fig. (h)-(k)]. Such apparent looks of STM image is same as single Si_4 atom switch.

However, it is found that twin Si_4 preferentially stay “On-On” state (Fig. (h)), meaning two adjacent Si_4 exhibits atom switch so that bright protrusion of both Si_4 stay closer to each other. In addition, even switching probability of one Si_4 of twin Si_4 increases when another Si_4 stay “On” state. Therefore, it is concluded that two adjacent Si_4 atom switches exhibits interaction, not only statically but also dynamically.

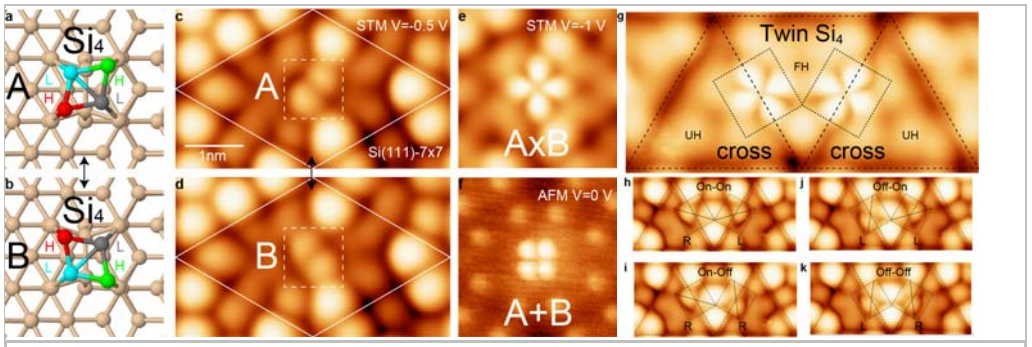

Figure 1: (a), (b) DFT model of A state and B state Si_4, respectively. (c), (d) STM images of A state and B state Si_4, respectively. (e) High-bias STM image of Si_4 showing cross pattern. (f) Close-distance AFM image of Si_4 showing square pattern. (g) STM image of twin Si_4 showing cross pattern. (h-k) STM image of twin Si_4 showing On-On, On-Off, Off-On, and Off-Off states, respectively.

References

1. Adam Sweetman, et al., Phys Rev. Lett. 106, 136101 (2011)
2. S. Yamazaki, et al., Nano. Lett. 15, 4356 (2015)
3. Y. Sugimoto, et al., Nat. Comm. 5, 4403 (2014)

A. Acun et al. "Atomically Controlled Surfaces Interfaces and Nanostructures"
edited by A. Bianconi, A. Marcelli (Superstripes Press, Rome 2016) isbn: 9788866830597

In situ observations of crystallization process in amorphous antimony nanoparticles by μs time- and pm spatial-scale using the ultra-high voltage electron microscope

H. Yasuda[1]
[1]*Research Center for Ultra-High Voltage Electron Microscopy, Osaka University*

Email: *yasuda@uhvem.osaka-u.ac.jp*
Key words: strain induced crystallization of amorphous structure, phase transition, nanoparticle, in situ observation

Fast in situ observation by TEM is one of useful techniques in researches on phase transitions of nanoparticles. In our previous study, it was evident that amorphous antimony nanoparticles can be crystallized with ease by stimulation from the outside. For example, when lead atoms are vapour-deposited onto amorphous antimony nanoparticles kept at room temperature, crystallization of the amorphous antimony nanoparticles is abruptly induced by an interfacial strain between an antimony nanoparticle and crystalline lead nanoparticles attached. On the other hand, knock-on displacements by high energy electron irradiation also become one of the stimulations for the crystallization of the amorphous nanoparticles. In the present study, electron-irradiation-induced crystallization processes of amorphous antimony nanoparticles have been studied by μs time- and pm spatial-scale in situ observations by ultra-high voltage electron microscope developed with JEOL Ltd. at Osaka University recently.

Amorphous antimony nanoparticles supported on thin amorphous carbon substrates were prepared by a vapour-deposition method. Electron irradiation experiments and the simultaneous in situ observations were carried out by JEM-1000EES ultra-high voltage electron microscope operating at an accelerating voltage of 1 MV and the electron flux of the order of approximately 10^{24} e m^{-2} s^{-1}, which was equipped with Gatan K2-IS electron direct detection CMOS camera. The time for one frame was 625 μs.

The figure 1 shows a typical example of atomic scale observations during crystallization in an approximately 20 nm-sized amorphous antimony nanoparticle. The figures 1(a)~(c) show the snapshots during crystal growth in about 20 nm sized nanoparticle. In fig, 1(a), 2 nm-sized crystalline nucleus appears on the surface of the particle, and the FFT pattern from the particle is in set. Week four spots are recognized as indicated by four arrows in the FFT pattern, and correspond to nucleation of the small crystal. In fig. 1(b), the nucleus grows up to approximately 5 nm in diameter, after that the amorphous nanoparticle is crystallized in the whole nanoparticle. In the FFT pattern, the week four spots change to an obvious net pattern, which is indexed as the [2-21] zone axis pattern of an antimony crystal. In this case of the 20 nm-sized nanoparticle, the velocity of interface migration is estimated to be approximately 20 μm s^{-1}. The velocity of the interface migration depends on the particle size, and it was

confirmed that the smaller the particle size is, the faster the velocity is. From the observation, the critical particle size for crystallization all over the nanoparticle is estimated to be approximately 5 nm. A strain on the interface between this crystalline nucleus and the amorphous nanoparticle may induce the crystallization all over the nanoparticle. A schematic illustration of crystallization mechanism in amorphous antimony nanoparticles is shown in the bottom of figure 1. The amorphous nanoparticle has to jump beyond the activation energy for the crystallization. At the early stage of the crystallization, small nucleus fluctuates between an appearance and a disappearance. However, when the size of the nucleus is larger than the critical size for crystallization, the strain energy of interface between this crystalline nucleus and the amorphous nanoparticle will be larger than the activation energy. It is suggested that the strain energy is a trigger for crystallization in amorphous antimony nanoparticles.

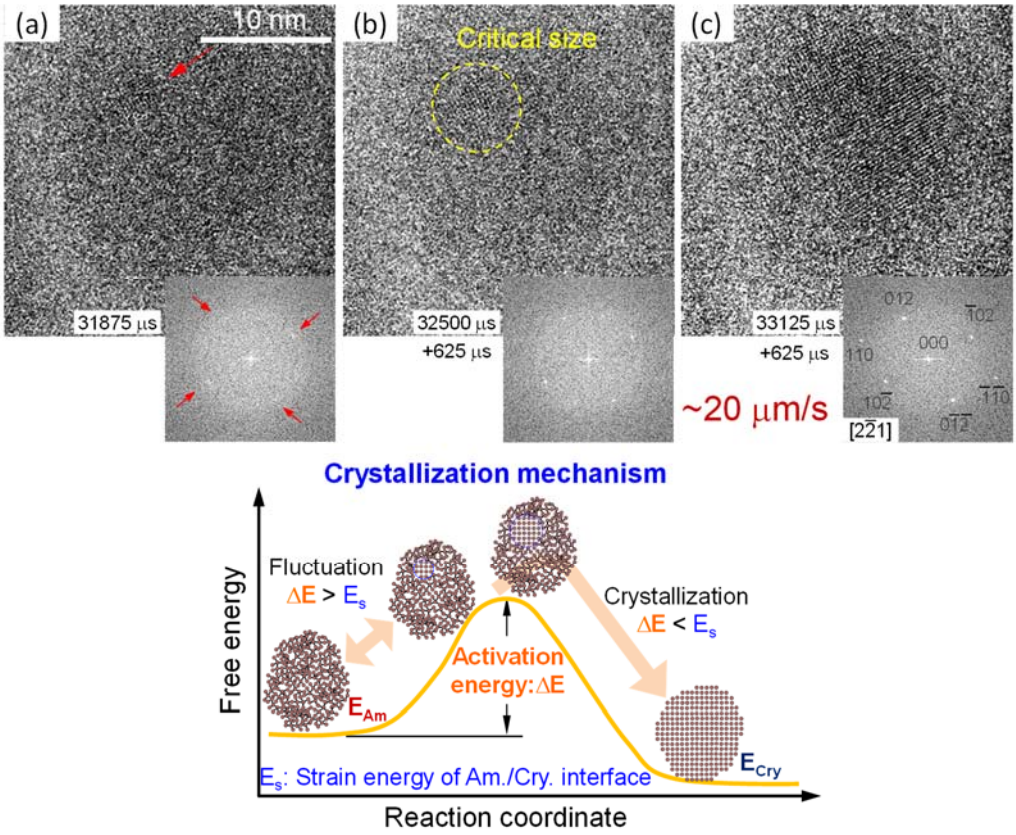

Figure 1: (a) ~ (c) Snapshots by an atomic scale observation during crystallization in about 20 nm sized nanoparticle, and a schematic illustration of crystallization mechanism of amorphous antimony nanoparticles.

A. Acun et al. "Atomically Controlled Surfaces Interfaces and Nanostructures"
edited by A. Bianconi, A. Marcelli (Superstripes Press, Rome 2016) isbn: 9788866830597

Evaluation of conduction mini-bands in semiconductor superlattice by visible-light photoelectron spectroscopy

Toru Ujihara[1,2], Fumiaki Ichihashi[2], Takahiko Kawaguchi[3], Xinyu Dong[2], Akito Inoue[2], Takahiro Ito[2], Makoto Kuwahara[1], Shunta Harada[1,2], Miho Tagawa[1,2]
[1]*Institute of Materials and Systems for Sustainability, Nagoya University*
[2]*Department of Materials Science and Engineering, Nagoya University*
[3]*Department of Electronics and Materials Science, Shizuoka University*

Email: *ujihara@nagoya.jp*
Key words: State-of-the-art theoretical approaches on surfaces and interfaces; Frontiers aspects of semiconductor; Surfaces and interfaces

One of the advantages of quantum structure is that we can design band structure. An occupied band structure, e.g. valence band in semiconductor, is easily evaluated by ultraviolet photoelectron spectroscopy (UPS). On the other hand, it is surprisingly difficult to evaluate an unoccupied band structure, e.g. conduction band in semiconductor. Recently we proposed a novel photoelectron spectroscopy method to reveal unoccupied band structures, which we call "visible-light photoelectron spectroscopy (VPS)."
In this method, we utilize negative electron affinity (NEA) surface by depositing Cs and O on a sample surface. Figure 1 shows the band diagram of p-type semiconductor around a NEA surface. At the NEA surface, the vacuum level quickly decreases below the bottom of the conduction band. The electrons excited by visible-light diffuse to the surface in the conduction band and emit to a vacuum by electron tunneling. The emitting electrons accelerated by external electric field reach hemi-sphere type analyzer. The energy from Fermi level in the specimen, E–E_F, can be determined from the following equation: [1]

$$E - E_F = E_m + \phi_{ana} - V_{bias}, \quad (1)$$

where E_m is the kinetic energy of the electron measured by analyzer, ϕ_{ana} is the work function of analyzer, and V_{bias} is the negative bias voltage between the specimen and the analyzer. The emitting electrons are analyzed by semi-sphere angle resolved analyzer.
We have actually evaluated the conduction band structures of GaAs and GaP utilizing the VPS method. Recently we revealed conduction mini-band structures in superlattce of InGaAs/GaAsP. However, the issue of determining wavenumber from angle values still remains. In this study, we established a smart determination method of wavenumber, and we actually evaluated the mini-band structure in superlattice semiconductor.
Figure 2(a) depicts the InGaAs/GaAsP superlattice specimen and the calculated mini-band structure. The specimen was grown by MOCVD method. Firstly, NEA condition was prepared by supplying Cs and O_2 gas to specimen surface alternately in the NEA

preparation chamber [2]. Next the sample was transferred to the sample chamber and the electrons excited by various visible laser lights (1.25 eV, 1.43 eV, 1.59 eV, 1.88 eV) were analyzed. The laser power is ~100 nW and the measuring time is about 10 min. Figure 2(b) shows the energy mapping and the energy distribution curve mapping. We successfully evaluated the energy dispersion of mini-band.

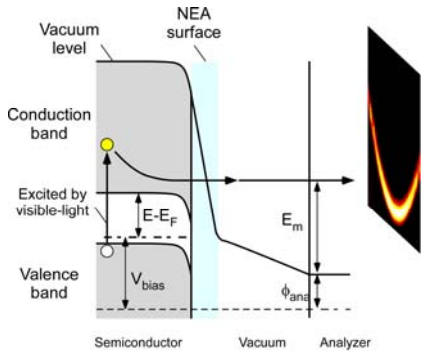

Figure 1: Band diagram of p-type semiconductor with NEA surface. External field is applied between sample and analyzer.

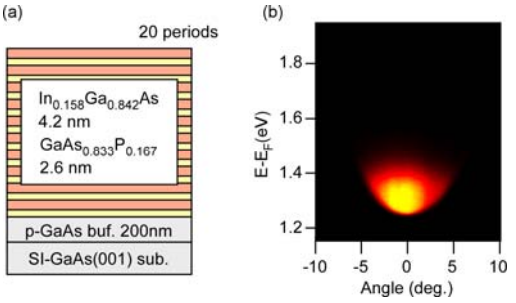

Figure 2: (a) Sample structure of InGaAs/GaAsP superlattice and (b) VPS energy distribution curves mapping.

References

1. F. Ichihashi, D. Shimura, K. Nishitani, T. Kawaguchi, M. Kuwahara, T. Ito, S. Harada, H. Katsuno, M. Tagawa, T. Ujihara, Proceedings of Photovoltaic Specialist Conference (PVSC) IEEE 40th, 2882 (2014).
2. K. Togawa, T. Nakanishi, T. Baba, F. Furuta, H. Horinaka, T. Ida, Y. Kurihara, H. Matsumoto, T. Matsuyama, M. Mizuta, S. Okumi, T. Omori, C. Suzuki, Y. Takeuchi, K. Wada, and M. Yoshioka, Nucl. Instr. and Meth. in Phys. Res. A 414, 431(1998).

Determination of structure of the rutile-TiO_2 (110)-(1×2) surface by using total-reflection high-energy positron diffraction (TRHEPD)

I. Mochizuki[1], H. Ariga[2], Y. Fukaya[3], K. Wada[4], A. Ichimiya[1], K. Asakura[2] and T. Hyodo[1]
[1]*Institute of Materials Structure Science, High Energy Accelerator Research Organization (KEK)*
[2]*Institute for Catalysis, Hokkaido University*
[3]*Advanced Science Research Center, Japan Atomic Energy Agency (JAEA)*
[4]*National Institute for Quantum and Radiological Science and Technology (QST)*

Email: *mochizu@post.kek.jp*
Key words: Atomic structure of surfaces; Oxides

Recently we developed a new TRHEPD (total-reflection high-energy positron diffraction) apparatus [1, 2] on the beam line (SPF-A3) of a linac-based intense positron beam at the Slow Positron Facility, KEK, Japan [3, 4]. TRHEPD is the positron counterpart of reflection high-energy electron diffraction (RHEED). The high intensity of the positron beam enables enhancement of the brightness of the beam [4] for the observation of clear diffraction patterns within a reasonable measurement time. It provides an ideal technique for the determination of the topmost- and immediate-sub-surface structure of a crystal [5-7].

Here we report a successful determination of the atomic arrangement of the rutile-TiO_2 (110)-(1×2) surface which is reconstructed from a well-known (1×1) surface by elevating the sample temperature above ~1100 K. Although many models were proposed for this structure during the past 30 years, it was under a long-lasting debate: meanwhile several models were proposed based on scanning tunnelling microscopy [8, 9], low-energy electron diffraction [10], and *ab initio* calculations [11,12], including Ti_2O_3 [8, 10, 12], Ti_3O_5 [9] and Ti_2O [11] compositions.

In order to address this issue, we analized the rocking curves, or the glancing angle dependence, of the TRHEPD 00-spot intensity, using a fully-dynamical diffraction theory [13]. The most plausible structure determined [14] is an asymmetric Ti_2O_3 structure, where the two Ti atoms with the surrounding O atoms in the Ti_2O_3 composition on the top have different height. This conclusion agrees well with a recent theoretical result by Wang *et al*. [12] employing a global optimization method using the USPEX code, where the atomic composition and the atomic arrangement of the model were concurrently stabilized.

Thus it is concluded that the structure of the rutile-TiO_2 (110)-(1×2) is represented by an asymmetric Ti_2O_3 model [14].

This work was partly supported by Grant-in-Aid for Scientific Research (S) No. 24221007 and that for Young Scientists (B) No. 26800170 from JSPS, and was

approved by the Photon Factory Program Advisory Committee (Proposal No. 2013U002).

References

1. A. Ichimiya, Solid State Phenom. 28/29, 143 (1992).
2. A. Kawasuso and S. Okada, Phys. Lett. 81, 2695 (1998).
3. K. Wada, *et al*., Eur. Phys. J. D 66, 37, (2012).
4. M. Maekawa, *et al*., Eur. Phys. J. D 68, 165, (2014).
5. Y. Fukaya, *et al*., Appl. Phys. Express 7, 056601 (2014).
6. Y. Fukaya, *et al*., Phys. Rev. B 88, 205413 (2013).
7. Y. Fukaya, *et al*., Carbon 103, 1 (2016).
8. H. Onishi and Y. Iwasawa, Surf. Sci., 313, L783 (1994).
9. C. L. Pang *et al*., Phys. Rev. B, 58, 1586 (1998).
10. M. Blanco-Rey *et al*., Phys. Rev. Lett., 96, 055502 (2006).
11. K. T. Park *et al*., Phys. Rev. B, 75, 245415 (2007).
12. Q. Wang *et al*., Phys. Rev. Lett., 113, 266101 (2014).
13. A. Ichimiya, Jpn. J. Appl. Phys. 22, 176 (1983).
14. I. Mochizuki *et al*., Phys. Chem. Chem. Phys., 18, 7085 (2016).

Tu4S session

A. Acun et al. "Atomically Controlled Surfaces Interfaces and Nanostructures"
edited by A. Bianconi, A. Marcelli (Superstripes Press, Rome 2016) isbn: 9788866830597

Gd-induced Defects in the (111) Surface of the Topological Insulator, Bi_2Te_3

Eun-Ha Shin[1], Jinsu Kim[2], Myung-Hwa Jung[2], Chanyong Hwang[3], Miyoung Kim[1], Hanchul Kim[1]
[1]*Sookmyung Women's University*
[2]*Sogang University*
[3]*Korea Research Institute of Standards and Science*

Email: *hanchul@sookmyung.ac.kr*
Key words: Growth and applications of thin films; Graphene and other 2D materials; Topological insulators

Three dimensional strong topological insulators (TIs), such as Bi_2Se_3, Bi_2Te_3 and Sb_2Te_3, have metallic surface states in contrast to the insulating bulk. The surface states are known to be topologically protected and robust for non-magnetic impurities [1].
Recently, Gd doped Bi_2Te_3 was studied to understand the effect of magnetic rare-earth element on the surface metallicity and magnetic property [2]. $Bi_{2-x}Gd_xTe_3$ showed a magnetic phase transition from paramagnetic to antiferromagnetic phase.
In this study, we report to the identification of the stable Gd-related defects in Bi_2Te_3 by comparing the scanning tunneling microscopy (STM) measurements and the simulated STM images using the first-principles calculations. We considered three Gd-related defect types: adsorption on the surface (Gd_{ad}), intercalation in the van der Waals (vdW) gap (I_{Gd}), and substitution for Bi (Gd_{Bi}) or Te (Gd_{Te}). The Gd_{Bi} is turned out to be the most stable among the considered structures. The Gd_{Bi} in second atomic layer of the surface QL (Gd_{Bi1}) is slightly more stable than Gd_{Bi} in fourth atomic layer of the surface QL (Gd_{Bi2}), and the energy difference is as small as 0.005 eV. Additionally, it is found that the I_{Gd} in the vdW gap tends to kick out one Bi atom to the vdW gap and take the Bi site, which results in the formation of a Gd_{Bi2}. This Gd_{Bi2}-intercalated Bi (I_{Bi}) pair has a lower formation energy than I_{Gd} by 0.3 eV.
In the simulated STM images, Gd_{Bi1} appears as a clover-shaped depression in both filled and empty states as shown Fig. 1(c). Similar appearance in the STM image has been observed for Fe doped Bi_2Te_3 [3], Mn doped Bi_2Te_3 [4]. On the other hand, Gd_{Bi2} is indistinguishable from the pristine surface at least in the simulated STM images [Fig. 1(d)], which is differernt from the other metallic substitional elements in TIs [3, 5]. The Gd_{Bi2}-I_{Bi} pair and I_{Gd} show a dark depression of a single Te atom in the empty state [Figs. 1(a) and 1(b)]. In the filled state, the vicinity of the Te atom is dimmer than in the pristine surface. The other considered Gd-related defects, Gd_{ad} and Gd_{Te}, are not observed at all negating their presence.
In addition, we found that an intrinsic defect, Bi anti-site defect (Bi_{Te}), is abundantly found in the annealed $Bi_{2-x}Gd_xTe_3$. Bi_{Te} manifest itself as a bright feature at both filled and empty states, which is in good agreement with the STM experiments. It is speculated that the volatile Te atoms are evaporated mainly from the surface upon annealing. Bi atoms migrate to occupy the Te vacancy site and form Bi_{Te}. A

subsequent migration of Gd atoms to vacant Bi site results in the formation of Gd_{Bi}. As a result, the annealing gives rise to the out-diffusion of Gd and Bi.

This work was supported by the National Research Foundation of Korea (NRF) grant funded by the Korea government(MSIP) (No. 2015R1A2A2A01005564). The computations were performed with the support from the Supercomputing Center/Korea Institute of Science and Technology Information (No. KSC-2015-C2-049).

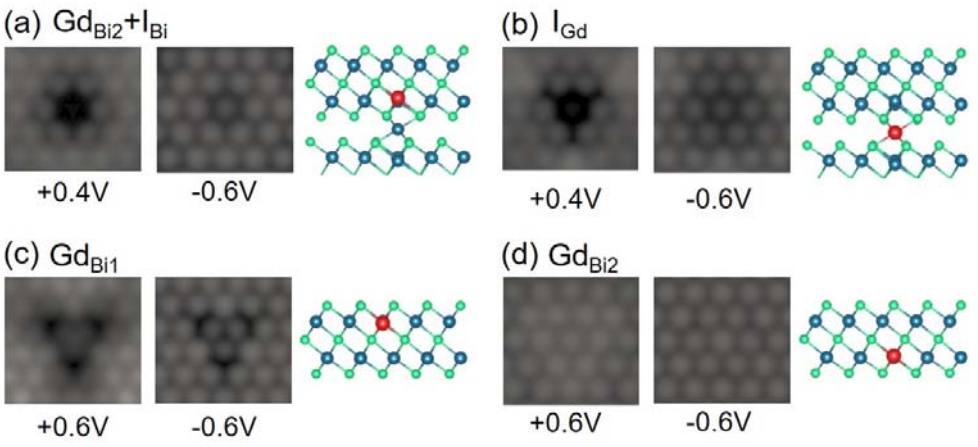

Figure 1: The simulated STM images and atomic structures of Gd-related defects on the Bi_2Te_3(111) surface. (a) Gd_{Bi2}-I_{Bi}, (b) I_{Gd}, (c) Gd_{Bi1}, and (d) Gd_{Bi2}. In each subfigure, the left, center, and right panels show the empty state STM image, the filled state STM image, and the atomic structure, respectively. The green, blue, and red circles represent Te, Bi, and Gd atoms, respectively.

References

1. M. Z. Hasan and C. L. Kane, Rev. Mod.Phys. 82, 3045 (2010).
2. J. Kim, *et al.*, Sci. Rep. 5, 10309 (2015).
3. C. –L. Song, *et al*., Phys. Rev. B. 86, 045441 (2012).
4. Y. S. Hor, *et al*., Phys. Rev. B. 81, 195203 (2010).
5. C. Mann, *et al*., Phys. Rev. B. 89, 155312 (2014).

The effect of a skin-deep surface zone on formation of two-dimensional electron gas at a semiconductor surface

Jacek J. Kolodziej[1] , Natalia Olszowska[1], Jakub Lis[1], Piotr Ciochon[1], Lukasz Walczak[2], Enrique G. Michel[2]
[1]*Faculty of Physics, Astronomy, and Applied Computer Science, Jagiellonian University, Lojasiewicza 11, 30-348 Krakow, Poland*
[2]Dpto. de Fisica la Materia Condensada and Condensed Matter Physics Center (IFIMAC),Universidad Autonoma de Madrid, 28049 Madrid, Spain

Email: *jj.kolodziej@uj.edu.pl*
Key words: 2D electron gas, electronic structure, angle resolved photoelectron spectroscopy, III-V semiconductor surfaces

Two dimensional electron gases (2DEGs) at surfaces and interfaces of semiconductors are described straightforwardly with a 1D self-consistent Poisson-Schroedinger scheme [1-3]. However, their band energies have not been modelled correctly in this way [2].

Using angle-resolved photoelectron spectroscopy we study the band structures of 2DEGs formed at sulfur-passivated surfaces of InAs(001) as a model system. Electronic properties of these surfaces are tuned by changing the S coverage, while keeping a high-quality interface, free of defects and with a constant doping density.

In contrast to earlier studies we show that the Poisson-Schroedinger scheme predicts the 2DEG bands energies correctly but it is indispensable to take into account the existence of the physical surface. The role of the surface, beyond the simple electrostatics, is setting nontrivial boundary conditions for the 2DEG wavefunctions.

These observations are crucial in the general context of the understanding and modeling of two-dimensional electron gases existing at surfaces and interfaces of semiconductors and oxides [2-6].

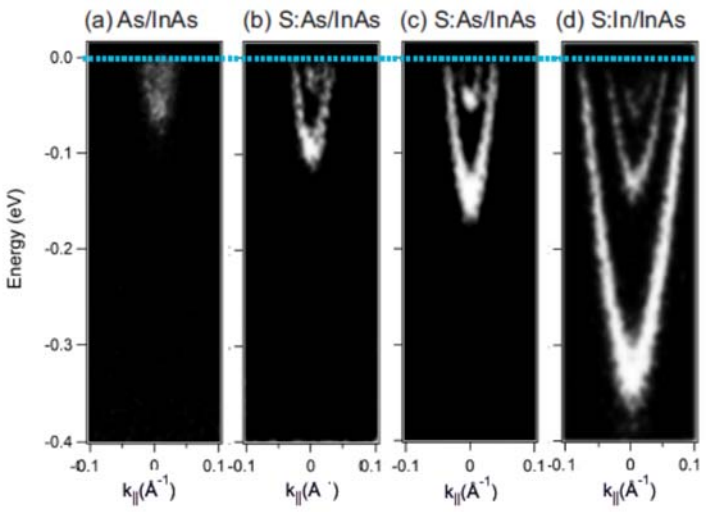

Figure 1: ARPES photocurrent maps reflecting 2DEG bands on several sulfur-passivated InAs (001) surfaces As-rich surfaces.

References

1. H. Ubensee, G. Paasch and J.P. Zolner, Phys. Rev. B 39,1955 (1989).
2. P.D.C. King et al., Phys. Rev. Lett. 104, 256803 (2010).
3. P.D.C. King, T.D. Veal and C.F. McConville, Phys. Rev B 77, 125305 (2008).
4. L. Colakerol et al., Phys. Rev. Lett. 97, 237601 (2006).
5. W. Meewasana, et al., Nature Mat. 10, 114 (2011).
6. M. Bianchi et al., Semicond. Sci. Technol. 27 124001 (2012).

Acknowledgements

We acknowledge financial support by Polish NCN (contract 2011/03/B/ST3/02070). The research was carried out with the equipment purchased thanks to European Regional Development Fund in the framework of the Polish Innovation Economy Operational Program (contract no. POIG.02.01.00-12-023/08). L.W. and E.G.M. acknowledge financial support by MINECO (grant MAT2014-52477-C5-5-P). J.L. wishes to thank prof. K. Rosciszewski for instructive discussion.

Bismuth reconstructions on Si(553) surface

Marek Kopciuszyński , Marek Dachniewicz, Anna Mandziak, Ryszard Zdyb
Institute of Physics, Maria Curie-Sklodowska University, Lublin, Poland

Email: *m.kopciuszynski@umcs.pl*
Key words: vicinal surface;Rashba effect; Si(553); Bi

Breaking of the inversion symmetry at a crystal surface may lift the spin degeneracy of the electronic states. This phenomenon, known as the Rashba effect, is responsible for the existence of spin polarized electronic bands on the Bi-reconstructed Si(111) surface [1,2]. The Rashba effect occurs also in one dimensional metallic structures formed on stepped surfaces. Strong potential gradient related to the atomic steps may induce an out-of-plane spin component [3,4].

Our goal was to constrain (√3×√3)-Bi superstructure to a form of quasi one dimensional stripes using stepped Si(553) substrate. It turns out that bismuth forms (√3×√3) structure on (111) terraces separated by steps. Diffraction measurements supported by scanning tunneling microscopy (STM) show two different Bi-induced reconstructions at 1/3 and 1 ML Bi coverage, resembling those obtained on the Si(111) surface, namely (√3×√3)-α and (√3×√3)-β. In the first case, it forms wide reconstructed (111) terraces separated by (331) facets. In the latter case, the β phase stabilizes Si(553) surface forming 26.6 Å wide (111) terraces separated by double height steps, similar to the order obtained on the bare Si(553) surface [5].

Angle resolved photoelectron spectroscopy (ARPES) measurements reveal electronic structure similar to that obtained for the flat Si(111) surface, however, with broken three-fold symmetry. It proves that the Si(553) surface may be used to obtain (√3×√3)-β reconstruction with preserved electronic properties but constrained to quasi 1D stripes separated by steps.

Acknowledgments
This work has been supported by the National Science Center under Grant No. 2013/11/B/ST3/04003.

References
1. I. Gierz, T. Suzuki, E. Frantzeskakis, S. Pons, S. Ostanin, A. Ernst, J. Henk, M. Grioni, K. Kern, and C. R. Ast, Phys. Rev. Lett. 103, 046803 (2009).
2. K. Sakamoto, H. Kakuta, K. Sugawara, K. Miyamoto, A. Kimura, T. Kuzumaki, N. Ueno, E. Annese, J. Fujii, A. Kodama, T. Shishidou, H. Namatame, M. Taniguchi,

T. Sato, T. Takahashi, and T. Oguchi, Phys. Rev. Lett. 103, 156801 (2009).
3. T. Okuda, K. Miyamaoto, Y. Takeichi, H. Miyahara, M. Ogawa, A. Harasawa, A. Kimura, I. Matsuda, A. Kakizaki, T. Shishidou, and T. Oguchi, Phys. Rev. B 82, 161410 (2010).
4. M. Krawiec, M. Kopciuszyński, and R. Zdyb, Appl. Surf. Sci. 373, 26 (2016).
5. M. Kopciuszyński, P. Dyniec, R. Zdyb, M. Jałochowski, Phys. Rev. B 91, 235420 (2015)

LEED, STM and ARPES studies of a 2D As/Ag(111) surface alloy

Jalil Shah , Hafiz M. Sohail, W. Wang and R. I. G. Uhrberg
Department of Physics, Chemistry and Biology, Linköping University, S-581 83 Linköping, Sweden.

Email: *jalsh37@ifm.liu.se*
Key words: Binary two dimensional (2D) surface alloys; Atomic and electronic structure; Low energy electron diffraction (LEED); Scanning tunneling microscopy (STM); Angle resolved photoelectron spectroscopy (ARPES).

Well ordered, two-dimensional (2D), binary surface alloys can in some cases be formed by replacing surface atoms of a substrate by atoms of a second element. Such 2D alloys are confined to the outermost atomic layer and may have unique physical and chemical properties. The Rashba type of spin split of surface electronic bands has been intensively studied due to a potential application in spintronics. In these studies, Ag(111) is an important substrate on which 1/3 monolayer of Bi, Pb, Sb, Sn and Ge all form a Ag_2E 2D surface alloy by replacing Ag atoms in an ordered way (E = Bi, Pb, Sb, Sn or Ge). Bi, Pb, Sb, and Sn all result in a well-ordered $\sqrt{3} \times \sqrt{3}$ R30° periodicity [1-4], while alloying with Ge leads to a complex striped structure superimposed on the $\sqrt{3} \times \sqrt{3}$ R30° periodicity [5]. In the case of Bi/Ag(111), there is a big Rashba split [1], while in the case of Sn/Ag(111) there is no observable split [4]. These findings are in accordance with the expected decrease of the Rashba split with decreasing atomic number. In the case of Ge/Ag(111), an unexpected split of the surface band was found at the $\overline{M}$ point along the $\overline{\Gamma}\,\overline{K}\,\overline{M}$ direction of a $\sqrt{3} \times \sqrt{3}$ surface Brillouin zone (SBZ) [5]. In order to further investigate this new kind of split of the surface bands, we have investigated the Ag_2As 2D surface alloy. Arsenic is the group V neighbor to Ge in the periodic table and it is interesting to find that Ag_2As shows the same kind of split as Ag_2Ge.

Low energy electron diffraction (LEED) reveals the existence of a $\sqrt{3} \times \sqrt{3}$ striped atomic structure. From scanning tunneling microscopy (STM) images of the surface alloy it is clear that there is a basic $\sqrt{3} \times \sqrt{3}$ structure with a superimposed long range modulation, see Fig. 1. Electronic structure data obtained by angle resolved photoelectron spectroscopy (ARPES) is also presented. The surface band spitting that appears at the $\overline{M}$ point as a result of the modification of the basic $\sqrt{3} \times \sqrt{3}$ periodicity is of particular interest.

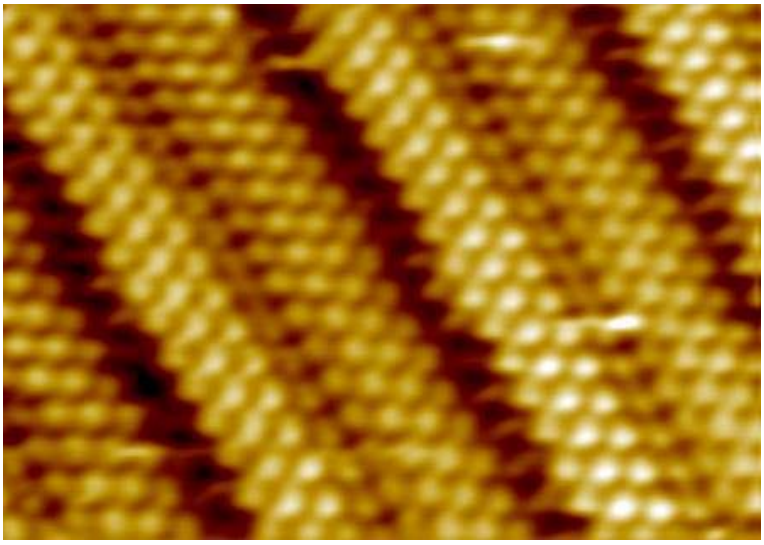

Figure 1: Atomically resolved filled state STM image (tunneling current of 200 pA and a sample bias of +0.3 V) of a 7.3×10.4 nm^2 area of the Ag_2As 2D surface alloy obtained at room temperature. The image shows a $\sqrt{3} \times \sqrt{3}$ striped structure.

References

1. C. R. Ast, J. Henk, A. Ernst, L. Moreschini, M. C. Falub, D. Pacilé, P. Bruno, K. Kern, and M. Grioni, Phys. Rev. Lett. 98, 186807 (2007).
2. D. Pacilé, C. R. Ast, M. Papagno, C. Da Silva, L. Moreschini, M. Falub, Ari P. Seitsonen, and M. Grioni, Phys. Rev. B 73, 245429 (2006).
3. L. Moreschini, A. Bendounan, I. Gierz, C. R. Ast, H. Mirhosseini, H. Höchst, K. Kern, J. Henk, A. Ernst, S. Ostanin, F. Reinert, and M. Grioni, Phys. Rev. B 79, 075424 (2009).
4. J. R. Osiecki and R. I. G. Uhrberg, Phys. Rev. B 87, 075441 (2013).
5. W. Wang, H. M. Sohail, J. R. Osiecki and R. I. G. Uhrberg, Phys. Rev. B 89, 125410 (2014).

A. Acun et al. “Atomically Controlled Surfaces Interfaces and Nanostructures”
edited by A. Bianconi, A. Marcelli (Superstripes Press, Rome 2016) isbn: 9788866830597

Graphene on iridium vicinal surface; a route to electronic band engineering

P. Pervan[1], I. Šrut Rakić[1], V. Mikšić Trontl[1], M. Kralj[1], P. Lazić[2], W. Sun[3],W. Jolie[4], F. Craes[4], C. Busse[4], J. Avila[5], M. C. Asensio[5]
[1] Institut za fiziku, Bijenička c. 46, 10000 Zagreb, Croatia
[2]Institut Ruđer Bošković, Bijenička c. 54, 10000 Zagreb, Croatia
[3]Massachusetts Institute of Technology, Massachusetts Avenue 77, Cambridge, USA
[4]Physikalisches Institut, Universität zu Köln, Zülpicher Straÿe 77, 50937 Köln,
[5]Synchrotron Soleil, L’Orme des Merisiers, Saint-Aubin - BP48, France

Email: *pervan@ifs.hr*
Key words: Nanoscale structure, growth processes and strain in thin layers and interfaces; Graphene and other 2D materials; State-of-the-art theoretical approaches on surfaces and interfaces

Graphene structural periodic patterning involving strain-engineering and/or added periodic potential is a promising route to modifications of its electronic band structure [1-9]. We have studied graphene grown on vicinal Ir(332), which can be benchmarked to a well-known graphene on Ir(111) recognized for a weak van der Waals (vdW) interaction. The system was studied with a range of experimental techniques which gave the insight into structural characteristics (scanning tunnelling microscopy (STM) and spectroscopy (STS) and low energy electron diffraction (LEED)) and electronic band structure (angle-resolved photoemission spectroscopy (ARPES) and density functional theory (DFT)). The graphene on Ir(332) caused a severe, yet reversible, surface restructuring, consisting of formation of large (111) terraces and (331) step bunches, giving the substrate and graphene a new periodicity.
The DFT calculations and STS showed that the nature of Gr-Ir interaction changes for the stepped surfaces where strong chemical binding occurs at step edges effectively anchoring graphene to each step, which provides the driving force for surface faceting. At step edges a severe orbital mixing occurs, and this local graphene chemisorption drives the surface restructuring in competition with the strain present in the system. This finding provides a general framework for the understanding of graphene mediated faceting of stepped substrates whenever the interaction of graphene to the corresponding low index surface is dominated by the vdW force.
Moreover, the identified chemical binding at step edges and accompanying charge transfer resulted in the strong n-type doping of graphene on (331) facets while on (111) facets graphene remained p doped.

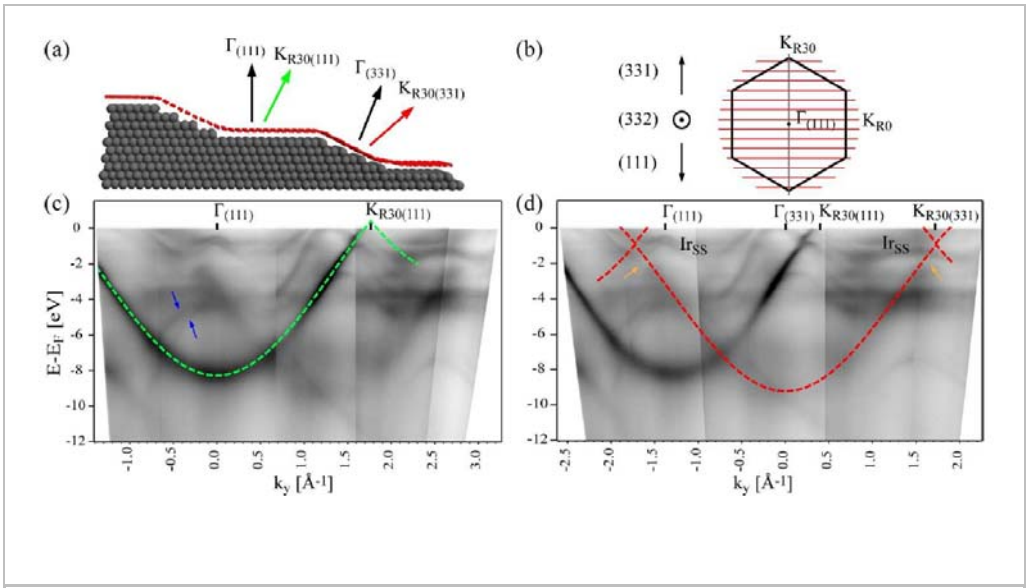

Figure 1: (a) A schematic representation of the mapped sample geometry in real space. (b) ARPES map of the □(111)-K_{R30}-M_{R30} direction with a green dashed line indicating contribution from R30 graphene on (111). (c) ARPES map of the □(331)-K_{R30}-M_{R30} direction with a red dashed line indicating contribution from R30 graphene on (331).

We propose that the periodically alternating (111) and (331) facets and the presence of pronounced boundary steps constitute a source of a 1D periodic potential which caused the observed graphene band modification. Measurements of the electronic band structure of the graphene on (111) facets showed the Dirac cone anisotropy with a severe Fermi velocity reduction in the direction parallel to the step edges consistent with the theory [10–12]. Additionally, the graphene π band is also tilted, which is likely an effect of graphene buckling, due to its periodical bending across step edges. [13]

Acknowledgements. This research was supported by Croatian Scence Fundation, project No. 2727 "Periodically strained graphene; structural and electronic properties"

References

1. I.I. Naumov et al., Phys. Rev. B 84 (2011) 245444.
2. A. Avsar et al., Nano Lett. 11 (2011) 2363.
3. Y. Wang et al., ACS Nano 5 (2011) 3645.
4. M.C. Wang et al., Nano Lett. (2015) 150213131149004.
5. J.-K. Lee et al., Nano Lett. 13 (2013) 3494.
7. J. Hicks et al., Nat. Phys. 9 (2013) 49.
8. T.M. Slipchenko et al., J. Opt. 15 (2013) 114008.
9. M. Farhat et al., Phys. Rev. Lett. 111 (2013) 237404.
10. D.C. Elias et al., Science 323 (2009) 610
11. S.-H. Phark et al., Phys. Rev. B 86 (2012) 1.
12. L.Z. Tan et al., Phys. Rev. B 81 (2010) 195426.
13. M. Krawiec, Appl. Surf. Sci. 304 (2014) 44.

We1T session

Advanced heterostructures in III-V nanowires

Anna Fontcuberta i Morral[1]
[1]*Laboratory of Semiconductor Materials, Institute of Materials, cole Polytechnique Fédérale de Lausanne, Switzlerand*

Email: *anna.fontcuberta-morral@epfl.ch*
Key words: Semiconductor nanowires, III-Vs, integration with Si, photovoltaics, nanoscale photonics, next generation solar cells

Thanks to their particular shape and small diameter, semiconductor nanowires exhibit very special optical properties in the optical and near-infrared domain. The small diameter also enables a quasi-defect-free integration with lattice-mismatched substrates or in lattice-mismatched junctions. Overall this results in an extremely high potential for semiconductor nanowires in next generation solar cells. We will review the theoretical aspects of nanowire-based solar cell design as well as some experimental demonstrations. Near-future and long term perspectives will also be discussed.
In this talk we report on the recent progress in our group concerning catalyst-free growth of III-V nanostructures. In particular we demonstrate how to obtain 100% vertical GaAs wires on silicon by controlling the thickness of the native oxide on the substrate and thereby the contact angle of the droplet (Figure 1 (a)-(b)). In the case of indium based wires we have found the density of stacking faults and twins can be reduced by incorporation of antimony. InAsSb nanowires with an antimony content above 25% are shown to be pure zinc blende twin-free over several hundred nanometers. Further we present the importance of surface passivation with a high-quality dielectric in order to achieve more reproducible electronic measurements and to enable the fabrication of top gates. A twin-free InAsSb nanowire with a 10nm alumina shell is shown in Figure 1 (c) and a top gated device in Figure 1 (d). Another approach to control defect formation is the growth of two dimensional nano-membranes. The membranes which are grown in (112) oriented openings on an oxide covered GaAs(111)B wafer are found to be defect-free. GaAs quantum wells can be defined by growing AlGaAs and GaAs shells around the membrane as shown in Figure 1 (e)-(f)..

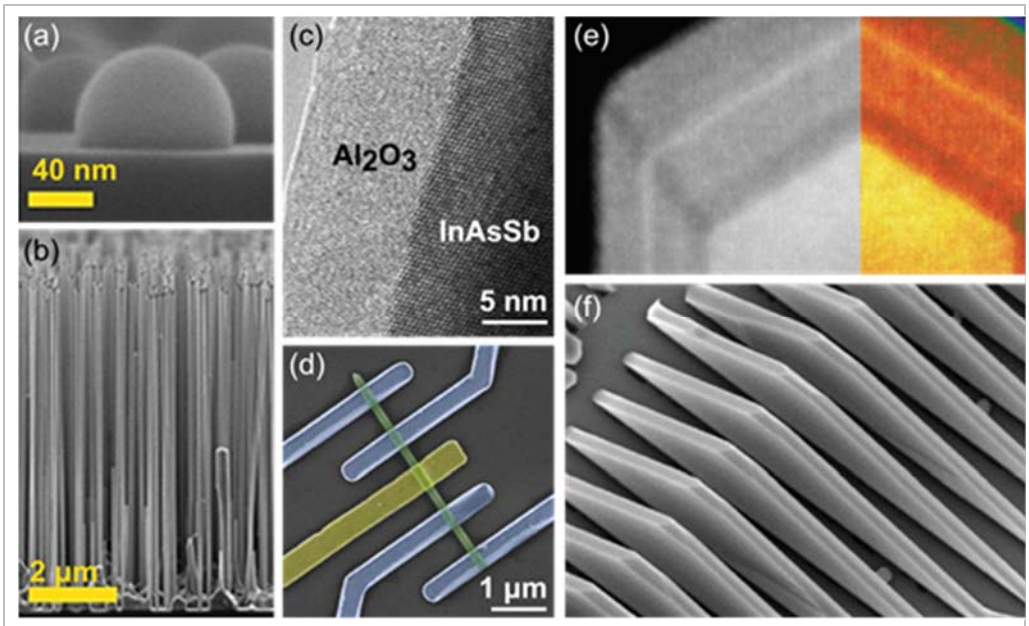

Fig1. (a)-(b) Gallium droplet and GaAs nanowire growth on a Si(111) wafer with optimized native oxide thickness for vertical wire growth [1]. (c) Twin-free InAsSb (35% Sb) nanowire coated with 10nm of alumina. (d) Top gated device based on an alumina coated wire (green: wire, blue: contacts, yellow: gate) [2]. (e)-(f) GaAs/AlGaAs nanomembrane heterostructure with a GaAs quantum well [3].

References

1. F. Matteini et al, Cryst. Growth Des. 15, 3105 (2015).
2. H. Potts et al, Nano Lett. 16, 637 (2016).
3. G. Tutuncuoglu et al, Nanoscale 7, 19453 (2015).

A. Acun et al. "Atomically Controlled Surfaces Interfaces and Nanostructures"
edited by A. Bianconi, A. Marcelli (Superstripes Press, Rome 2016) isbn: 9788866830597

Ultrafast Charge Injection at Complex Interfaces: Organic-Organic, Organic-Inorganic and Organic-Graphene

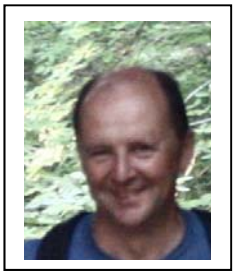

Alberto Morgante[1,2] , Dean Cvetko[1,3] Latha Venkataraman[4], A. Cossaro[1]
[1]CNR-IOM Triesteniversity of Rome [Times 11 italic]
[2]Physics Department University of Trieste
[3]Department of Materials Sciences
[3]Department of Materials Sciences

Email: *morgante@iom.cnr.it*
Key words: Growth and applications of thin films; Graphene and other 2D materials; Nanoelectronics, molecular electronics [Times 11]

Interface processes strongly affect the performances and efficiency of organic based devices. The integration of 2D materials like graphene in organic devices (for example as electrodes) is expected, on the other hand, to improve the overall device performances. There is a need therefore for a deeper understanding and control of processes like charge transfer (CT) at interfaces between organic films, graphene and metals. Charge injection across molecular junctions can occur at the femtosecond time scale or even shorter. In most cases this time frame is still out of reach of the pump probe spectroscopies. Here we use X-ray spectroscopies to investigate charge injection in complex hetero-structures that include organic molecules, graphene and metallic substrates. We show that the Core hole clock implementation of the Resonant Photoemission spectroscopy (RESPES) allows us to determine charge dynamics in both directions (to/from the molecule) at these interfaces and can give clues on the interface parameters that can increase/decrease the charge transfer efficiency. Examples of model systems will be discussed.
It will be shown how RPES allows us to elucidate the role of inter-molecular interaction on through-space charge transfer characteristics in π-stacked molecular systems [1], the electronic coupling, morphology and charge transfer rates at the donor-acceptor (D/A) interfaces between C60 and either flat- or contorted hexabenzocorones (HBC) [2] and the relation with improved internal (IQE) and external (EQE) quantum efficiency of devices based on these shape-matched molecular systems. The case of ammine and pyridine terminated organic overlayers will be discussed in connection with recent results of break junction experiments [3]. In this case we show how core-hole clock spectroscopy can be used to measure charge transfer through noncovalent interactions and map charge delocalization times from carbon and nitrogen sites on the molecules. Comparison of charge transfer rates between different substrates (metal, graphene and graphene nanoribbons) will be discussed elucidating the role of the local density of states of these materials and the level alignment in the charge transfer process [4].

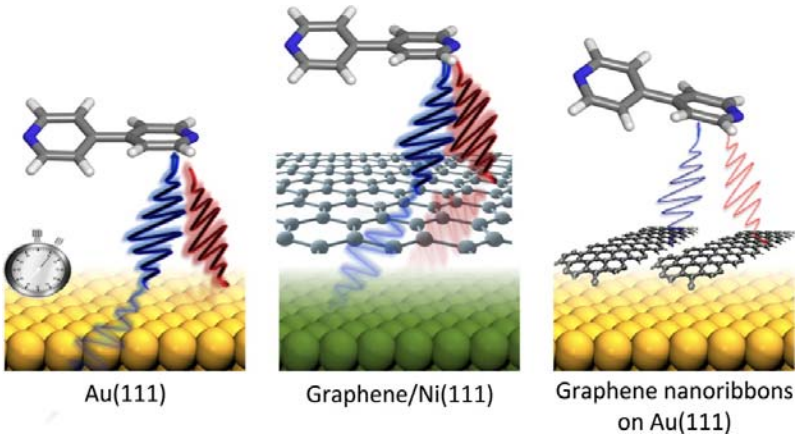

Figure 1: Comparison between charge transfer process from bipyridine and various substrates.

References

1. A. Batra, G. Kladnik, H. Vazquez, et al. Nature Communications. 3, 1086 (2012). http://dx.doi.org/10.1038/ncomms2083.
2. T. Schiro, et al., Advanced Energy Materials. 3, 894 (2013). http://dx.doi.org/10.1002/aenm.201201125.
3. G. Kladnik, et al, J. Phys. Chem. C 117, 16477 (2013). http://dx.doi.org/10.1021/jp405229b.
4. O. Adak, Nanoletters. 15, 8316 (2015). http://dx.doi.org/10.1021/acs.nanolett.5b03962

High resolution X-ray spectroscopy of electronic and atomic structure of TiO_2 nanostructures.

Federico Boscherini[1] , Lucia Amidani[2], Luca Pasquini[1], Giacomo Rossi[1], Marco Malvestuto[3] and Alberto Naldoni[4]
[1]*Department of Physics and Astronomy, University of Bologna, Italy*
[2]*ESRF, The European Synchrotron, Grenoble, France*
[3]*Elettra, Sincrotrone Trieste, Trieste, Italy*
[4]*CNR-ISTM, Milano, Italy*

Email: *federico.boscherini@unibo.it*
Key words: X-ray absorption spectroscopy, resonant inelastic x-ray scattering, titanium dioxide nanostructures, photocatalysis

Refined X-ray spectroscopy can play a key role in understanding the fundamental mechanisms responsible for the physical and chemical properties of advanced functional materials and devices. In this contribution, we will focus on TiO_2 – based nanostructures, which are actively studied for many applications, including photocatalysis. Despite many potential advantages, one limitation of TiO_2 is the wide band gap, which limits solar light absorption. By using high resolution XAFS and RIXS we have recently studied the atomic and electronic structure of two materials systems designed to overcome this limitation: nanostructures formed by close assembly of Au and TiO_2 nanoparticles [1] and V-doped TiO_2 [2].
Exploiting plasmonic Au nanoparticles to sensitize TiO_2 to visible light is a widely employed route to produce efficient photocatalysts. However, a description of the atomic and electronic structure of the semiconductor sites in which charges are injected is still not available. Such a description is of great importance in understanding the underlying physical mechanisms and to improve the design of catalysts with enhanced photoactivity. We investigated changes in the local electronic structure of Ti in pure and N-doped nanostructured TiO_2 loaded with Au nanoparticles during continuous selective excitation of the Au localized surface plasmon resonance with X-ray absorption spectroscopy (XAS) and resonant inelastic X-ray scattering (RIXS). Spectral variations strongly support the presence of long-lived charges localized on Ti states at the semiconductor surface, giving rise to new laser-induced lowcoordinated Ti sites.

Doping with transition metals is an effective method to enhance visible-light absorption in TiO_2 nanoparticles and to improve the efficiency of many photocatalytic processes under solar radiation. We have performed an in-depth XAFS study of V dopants in TiO_2 nanoparticles deposited by gas-phase condensation with a local structure similar to anatase, rutile, or intermediate. The combination of K- and Ledge spectra in the pre-edge, edge, and extended energy regions with full potential ab initio spectral simulations shows that V ions occupy substitutional cationic sites in the TiO_2 structure, irrespective of whether it is similar to rutile, anatase, or mixed. Very recently we have also performed RIXS measurements which highlight changes in the

occupation of electronic states localized on Ti and V induced by visible light absorption.

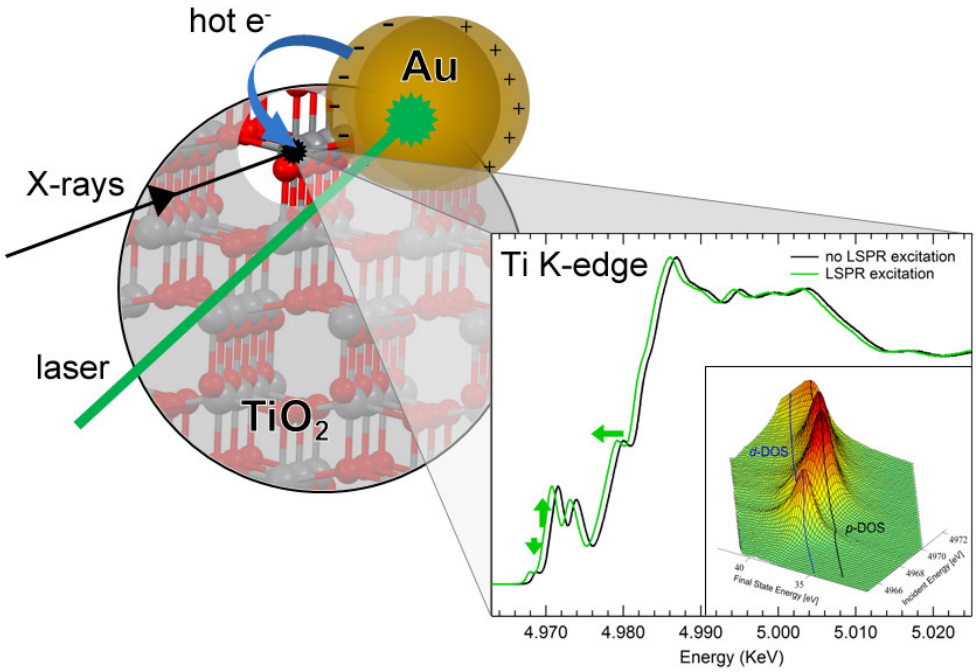

Figure 1: Graphical description of the experiment on Au:TiO2 and of hot electron charge transfer. The inset reports the effect of laser illumination on HERFD spectra and a typical RIXS plane.

References

1. L. Amidani, A. Naldoni, M. Malvestuto, M. Marelli, P. Glatzel, V. Dal Santo, and F. Boscherini, Angew. Chem. Internat. Ed. 54, 5413 5416 (2015). DOI: 10.1002/anie.201412030.
2. G. Rossi, M. Calizzi, V. Di Cintio, S. Magkos, L. Amidani, L. Pasquini, and F. Boscherini, Jour. Phys. Chem. C 120, 7457 (2015). DOI: 10.1021/acs.jpcc.5b12045

Nanodiamond particles, hydrosol and gel.

A.Ya. Vul[1] , E. D. Eidelman[1,2], A. E. Alekseenskiy[1], A.V.Shvidchenko[1], A.T.Dideikin[1], V.S.Yuferev[1], V.T.Lebedev[3], Yu.V. Kul’velis[3], M.V.Avdeev[4]
[1]Ioffe Physical-Technical Institute, 194021 St.Petersburg, Russia,
[2]St. Petersburg State Chemical–Pharmaceutical Academy, St. Petersburg, 197376 Russia
[3]B. P.Konstantinov Petersburg Nuclear Physics Institute, National Research Centre “Kurchatov Institute”, Gatchina, Leninradskaya Region, Russian Federation,
[4]Frank Laboratory of Neutron Physics, Joint Institute for Nuclear Research, Dubna 141980, Russian Federation

Email: *alexandervul @mail.ioffe.ru*
Key words: nanodiamond, hydrosol, hydrogel, detonation synthesis, deagglomeration, phase transitions in nanocarbons, viscosity, dynamic light scattering, suspension, DLVO theory.

Over the last few decades the application area of detonation nanodiamonds (DND) has been essentially restricted due to extreme strength of agglomerates that are formed from DND particles [1]. Recently developed methods for deagglomeration of DND and obtaining the stable hydrosols of diamond nanocrystals having size of 4-5 nm [2, 3] opened new application areas for this promising material. In this presentation, we report the results of study of the structure of the DND agglomerates, mechanism of deagglomeration, formation of stable hydrosols having positive and negative zeta potential.
We have revealed that the hydrogel is formed at increasing of concentration of DND particles higher than 4-7 wt. % and found that the concentration for hydrogel formation depends on sign of zeta potential. We have shown that stability of the hydrosol can be explained in the frame of DLVO theory [4]. However, there are some features, which have to take into account that double electric layer around every DND particle has not-spherical shape. The DLVO theory cannot be applicable in that case. We suggest new models for hydrogel formed from diamond nanoparticles. Characterization of suspension and gel by method of dynamic light scattering, small angle neutron scattering and by theoretical estimations supports the model.

The research was supported by the Russian Scientific Foundation (project 14-13-00795).

References

1. A.Kruger, F. Kataoka, M.Ozawa, T.Fujino, Y.Suzuki, A.E.Aleksenskii, A.Y.Vul', E. Osawa. Unusually tight aggregation in detonation nanodiamond: Identification and disintegration. Carbon 43, 1722–1730 (2005).

2. A. Williams, J. Hees, C. Dieker, W. Jager, L. Kirste, C. E. Nebel. Size-dependent reactivity of diamond nanoparticles. ACS Nano 4, 4824–4830 (2010).
3. A. E. Aleksenskiy, E.D. Eydelman, A.Y.Vul. Deagglomeration of detonation nanodiamonds. Nanosci. Nanotechnol. Lett., 3, 68–74 (2011).
4. Alain C. Pierre. Introduction to sol-gel processing. Springer. Kluwer Academic Publishers. Second Printing. (2002).

A. Acun et al. "Atomically Controlled Surfaces Interfaces and Nanostructures"
edited by A. Bianconi, A. Marcelli (Superstripes Press, Rome 2016) isbn: 9788866830597

Structural peculiarities of detonation nanodiamonds by small-angle neutron scattering

M.V. Avdeev[1] , O.V.Tomchuk[1,2]
[1]*Frank Laboratory of Neutron Physics, Joint Institute for Nuclear Research, Dubna, Moscow Reg., Russia*
[2]*Faculty of Physics, Taras Shevchenko National University of Kiev, Kiev, Ukraine*

Email: *avd@nf.jinr.ru*
Key words: nanoscale structures, nanodiamonds, scattering of thermal neutrons, small-angle scattering

Detonation nanodiamonds (DND) are one of the products of the detonation of organic explosives with an imbalanced carbon-oxygen ratio biased towards the carbon content. They are diamond crystallites with a typical size of less than 10 nm, which makes them a very attractive material for nanotechnology.

At present, of special interest is the combination of high specific surface and biocompatibility of DND. This is an important factor in the creation of nanocomposite materials for medical applications that use specific spectral properties of these nanoparticles. One of the main directions in the physical and chemical studies of DND concerns the purification and synthesis of their liquid suspensions in various solvents as a basis for the storage and subsequent chemical modification of nanoparticles. The availability of stable suspensions over a wide range of DND concentrations (up to 10 wt.%) makes it possible to apply [1-3] very effectively in structural research the method of small-angle neutron scattering (SANS) by using the contrast variation technique based on isotopic hydrogen-deuterium substitution in solvents. There are two fundamental aspects of the research presented: (I) structure of DND particles and their specific features at a nanoscale (characteristic size level of 10 nm); (II) cluster formation in the synthesis of DND and during their dispersion in liquid carriers (characteristic size level of 100 nm and higher).

It has been shown that DND particles reveal high size polydispersity (range from 2 to 10 nm) and exhibit a non-uniform inner structure. Thus, along with the predominant diamond component within the crystallites a graphite-like shell exists on the crystallite surface. This shell is also non-uniform and is characterized by a rather wide spatial diamond-graphite transition in terms of the radial distribution function of the scattering length density. It is responsible for the diffusive nature of the DND particle surface revealed in the scattering experiments as a specific deviation from the classical Porod law for particles with a smooth interface. To ensure a continuous diamond-graphite transition in DND, a characteristic diffusivity parameter is to be small, which can be observed in all the systems studied.

It has been shown that stable and reproducible fractal clusters with a wide size distribution from 10 to 100 nm and above (primary aggregation) are formed in liquid DND dispersions. The growth mechanism for the clusters characterized by a branched structure for both light and heavy cluster fractions is unique irrespective of the dispergation procedure and polar liquid carrier. By its structural characteristics it is similar to the mechanism of diffusion limited aggregation (DLA). The branched structure of the primary clusters determines their overlap in the secondary aggregates.

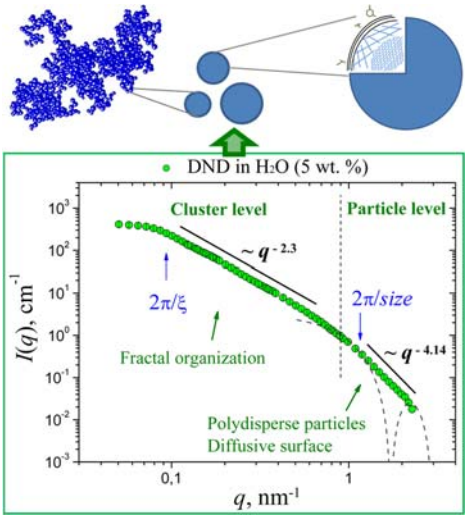

Figure 1: Characteristic structural peculiarities of DND in liquid suspensions as seen by SANS.

References

1. M.V.Avdeev, V.L.Aksenov, O.V.Tomchuk, L.A.Bulavin, V.M.Garamus, E.Osawa, *J. Phys. Cond. Matter* 25, 445001 (2013). http://dx.doi.org/10.1088/0953-8984/25/44/445001.
2. O.V.Tomchuk, L.A.Bulavin, V.L.Aksenov, V.M.Garamus, O.I.Ivankov, A.Ya.Vul', A.T.Dideikin, M.V.Avdeev, *J. Appl. Cryst.* 47, 642 (2014). http://dx.doi.org/10.1107/S1600576714001216.
3. O.V.Tomchuk, D.S.Volkov, L.A.Bulavin, A.V.Rogachev, M.A.Proskurnin, M.V.Korobov, M.V.Avdeev, *J. Phys. Chem. C* 119, 794 (2015). http://dx.doi.org/10.1021/jp510151b.

A. Acun et al. “Atomically Controlled Surfaces Interfaces and Nanostructures”
edited by A. Bianconi, A. Marcelli (Superstripes Press, Rome 2016) isbn: 9788866830597

We2T session

A. Acun et al. “Atomically Controlled Surfaces Interfaces and Nanostructures”
edited by A. Bianconi, A. Marcelli (Superstripes Press, Rome 2016) isbn: 9788866830597

Germanene, a germanium analogue of graphene

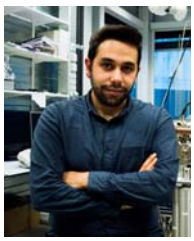

Adil Acun, Harold Zandvliet
University of Twente, Enschede, The Netherlands
Physics of Interfaces and Nanomaterials, MESA+ Institute for Nanotechnology

Email: *a.acun@utwente.nl*
Key words: Germanene, 2D materials, STM, DFT

Recently, several research groups have reported the growth of germanene, a new member of the graphene family. Germanene is in many aspects very similar to graphene, but in contrast to the planar graphene lattice, the germanene honeycomb lattice is buckled and composed of two vertically displaced sub-lattices.

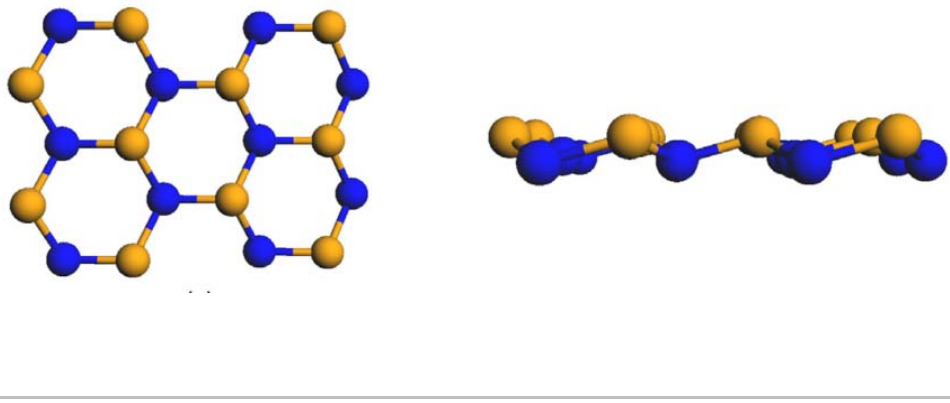

Figure 1: Buckled formation of a hexagonal 2D Dirac material composed of Ge-atoms: germanene

Density functional theory calculations have revealed that free-standing germanene is a 2D Dirac fermion system, i.e. the electrons behave as massless relativistic particles that are described by the Dirac equation, which is the relativistic variant of the Schrödinger equation. Germanene is a very appealing 2D material. The spin-orbit gap in germanene (~24 meV) is much larger than in graphene (<0.05 meV), which makes germanene the ideal candidate to exhibit the quantum spin Hall effect at experimentally accessible temperatures. Additionally, the germanene lattice offers the possibility to open a band gap via for instance an externally applied electrical field, adsorption of foreign atoms or coupling with a substrate. This opening of the band gap paves the way to the realization of germanene based field-effect devices. In this topical review we will (1) address the various methods to synthesize germanene (2) provide a brief overview of

the key results that have been obtained by density functional theory calculations and (3) discuss the potential of germanene for future applications as well for fundamentally oriented studies.

References

1. A Acun, L Zhang, P Bampoulis, M Farmanbar, A van Houselt, A N Rudenko, M Lingenfelder, G Brocks, B Poelsema, M I Katsnelson and H J W Zandvliet, JPCM 27, 44 (2015). http://dx.doi.org/10.1088/0953-8984/27/44/443002

A. Acun et al. “Atomically Controlled Surfaces Interfaces and Nanostructures”
edited by A. Bianconi, A. Marcelli (Superstripes Press, Rome 2016) isbn: 9788866830597

Band gap engineering in hydrogen functionalized graphene

Liv Hornekær
Dept. Physics and Astronomy and Interdisciplinary Nanoscience Center, Aarhus University

Email: *liv@phys.au.dk*
Key words: Graphene, band gap engineering, hydrogen functionalization.

Nanostructured hydrogen functionalization has been shown to open a band gap in graphene [1], but also to result in increased band broadening associated with scattering due to disorder induced by imperfect functionalization structures [1,2]. Here, we demonstrate band gap engineering in hydrogen functionalized graphene by changing the functionalization degree and the symmetry of the functionalization structures.

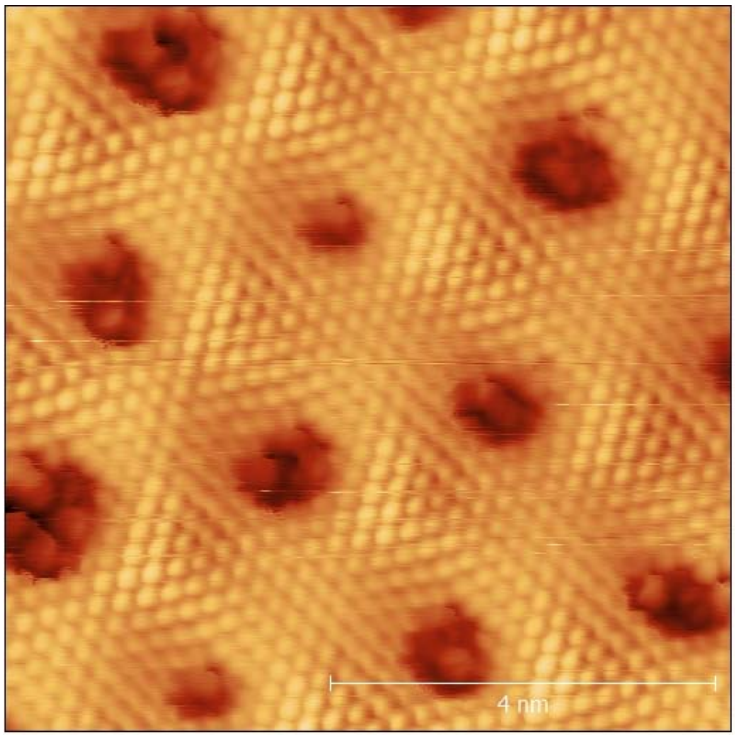

Figure 1: Scanning tunneling microscopy image of selective hydrogen functionalization of HCP regions in graphene on Ir(111).

This has been achieved by exploiting small differences in hydrogen adsorbate binding energies on graphene on Ir(111), which allow tailoring of highly periodic

functionalization structures favoring one distinct region of the moiré super-cell. Scanning tunneling microscopy (STM) measurements show that a highly periodic hydrogen-functionalized graphene sheet can thus be prepared by controlling the sample temperature during hydrogen functionalization. The associated reduction in the variation of hydrogen adsorption sites is evidenced by X-ray photoelectron spectroscopy (XPS). At deposition temperatures of 645 K and above hydrogen is observed to adsorb exclusively on the HCP regions of the graphene/Ir(111) moiré structure. This finding is rationalized in terms of a slight preference for hydrogen clusters in the HCP regions over the FCC regions as found by density functional theory (DFT) calculations. Angle-resolved photoemission spectroscopy (ARPES) measurements demonstrate that the preferential functionalization of just one region of the moiré super-cell results in a band gap opening with very limited associated band broadening. Thus, hydrogenation at elevated temperatures provides a pathway to efficient band gap engineering in graphene via the selective functionalization of specific regions of the moiré structure [3].

References

1. R. Balog, et al., Nature Materials 9, 315 (2010)
2. R. Balog, et al., ACS Nano 7, 3823–3832 (2013).
3. J. Jørgensen et al., Submitted (2016).

A. Acun et al. “Atomically Controlled Surfaces Interfaces and Nanostructures”
edited by A. Bianconi, A. Marcelli (Superstripes Press, Rome 2016) isbn: 9788866830597

Structure and electronic properties of 2D boron sheets

Qing Zhong, Baojie Feng, Hui Li, Lan Chen and Kehui Wu
Institute of Physics, Chinese Academy of Sciences
Beijing 100190, China

Email: *khwu@iphy.ac.cn*
Key words: 2D boron sheets, borophene, scanning tunneling microscopy

Since the discovery of graphene, intensive interest has been focused on two dimensional (2D) materials, especially mono-elemental 2D materials which may possess novel physical properties beyond that of graphene.

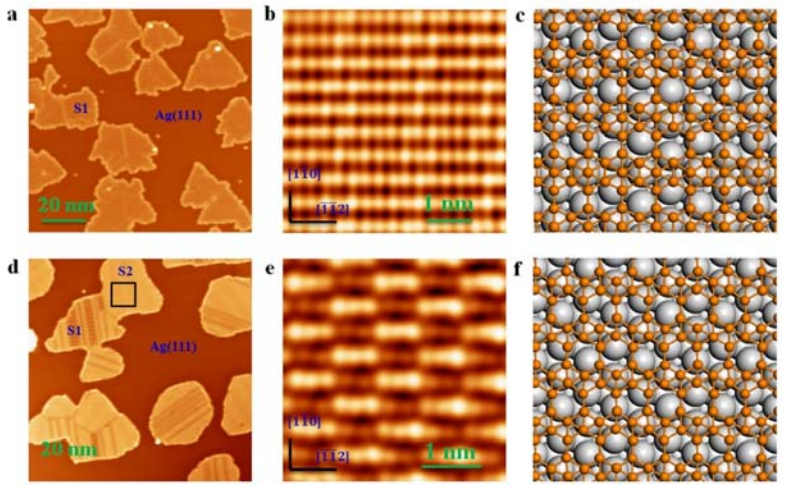

Figure 1: Two-dimensional boron sheets prepared on Ag(111) substrate. (a,d) are the large area STM image of the two 2D boron phases; (b,d) are high resolution STM images. (c,f) are their corresponding structure models.

In the periodic table of elements, elements sitting around carbon are group IV elements such as silicon, germanium and tin, as well as boron and nitrogen. 2D graphene-like materials such as silicene, germanene, stanene and black phosphors have recently been fabricated, but they are not stable in air. Boron possesses sp2 hybridized orbitals similar as carbon, which favors the formation of low dimensional nanostructures such as nanotube and fullerene. Theoretical studies revealed that 2D boron (borophene) is energetically stable. However, because of the extremely high melting point and low vapor pressure of boron, the experimental growth of borophene is very difficult, and the 2D form of boron has never been realized previously.

Here, we have experimentally realized 2D boron sheets (borophene) on Ag(111) surface for the first time [1]. We evaporated boron directly in a homemade molecular-beam epitaxy system. Two types of 2D B structures were found to formed on Ag(111) by using scanning tunneling microscopy. Combining with first principles calculations, it was revealed that boron atoms in our 2D B sheets are arranged in triangle lattices with periodic arrangement of holes, which accords with previous theoretical predictions very well. We also found that the 2D B sheets bonds to the Ag(111) substrate only weakly, and it remains chemically stable against oxidization in air. The experimental realization of such long expected 2D boron (borophene) structure provides a very exciting candidate for device applications in the future.
It should be noted that another parallel work was reported [2] by Mannix et al. at the same time (submission date later than ours). They also reported two boron sheet structures, one of which agrees with our work. Another structure, however, disagrees with our results. It is noted that several theoretical works have all supports our structures to be more stable ones.

References

1. Feng, B. J.; Zhang, J.; Zhong, Q.; Li W. B.; Li, S.; Li, H. Meng, S.; Chen, L.; Wu, K. H. Nat. Chem. DOI: 10.1038/nchem.2491.
2. Mannix, A. J. et al. Science 350, 1513–1516 (2015).
3. Gao, M.; Li, Q. Z.; Yan, X. W.; Wang, J.; arxiv.1602.02930
4. Penev, E. S.; Kutana, A., Yakobson B. I.; Nano Lett. DOI: 10.1021/acs. nanolett. 6b00070.
5. Zhang, Z.; Yao, Y.; Gao, G; Yakobson, B. I.; Angew. Chem. Int. Ed. 54, 13022 (2015).

A. Acun et al. "Atomically Controlled Surfaces Interfaces and Nanostructures"
edited by A. Bianconi, A. Marcelli (Superstripes Press, Rome 2016) isbn: 9788866830597

Electrical transport measured in chains of carbon atoms

F. Banhart[1] , A. La Torre[1,2], F. Ben Romdhane[1], A. Botello-Mendez[3], J.-C. Charlier[3]
[1]*Institut de Physique et Chimie des Matériaux de Strasbourg, Université de Strasbourg, France*
[2]*School of Chemistry, University of Nottingham, UK*
[3]*Institute of Condensed Matter and Nanoscience, Université catholique de Louvain, Belgium*

Email: *florian.banhart@ipcms.unistra.fr*
Key words: 1D materials; carbyne; carbon nanomaterials

The basic unit of sp^1 hybridized carbon is a linear chain of carbon atoms. The existence and stability of the bulk sp^1 phase carbyne is still controversial; however, isolated atomic carbon chains as the building blocks of carbyne and a perfectly 1D material have already been detected in several studies.

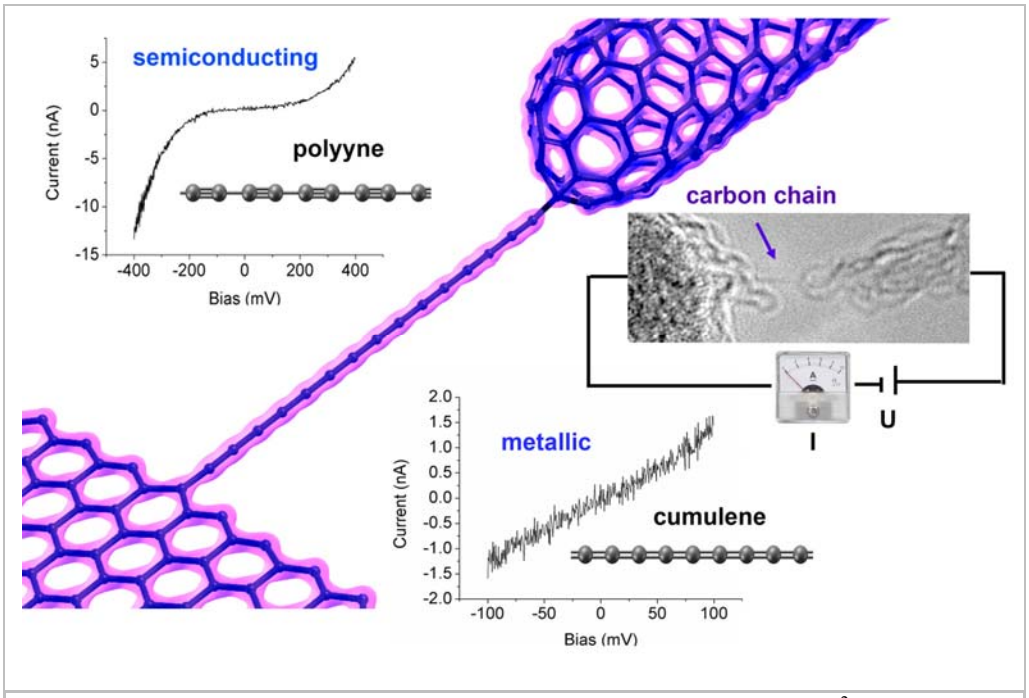

Figure 1: Model of a carbon chain spanning between a graphene ribbon (sp^2 contact) and a carbon nanotube (sp^3 contact). Experimental current-voltage curves are shown for semiconducting polyyne (top left) and metallic cumulene (bottom right). The TEM image shows a typical carbon chain. The principle of current-voltage measurement is indicated.

It has been predicted that carbon chains are unusual conductors that may occur either as metallic cumulene with double bonds or as semiconducting polyyne with alternating single and triple bonds. Now, it became possible to generate carbon chains in *in-situ* experiments in an electron microscope and to study some of their properties.
A scanning tunnelling microscopy setup integrated into the specimen holder of a transmission electron microscope allows to establish metal contacts to graphenic material and, by controlled retraction of the electrodes, to unravel chains of carbon atoms from graphene. At the same time, the electrical properties of the chains can be measured [1, 2]. By recording current-voltage curves of individual carbon chains, both cumulene and polyyne are identified.
It is found experimentally and by quantum conductance calculations that transport through narrow resonant states makes the conductivity much lower than predicted in previous theoretical work. When the 1D system is under strain, the chains exhibit a semiconducting behaviour, corresponding to polyyne. Conversely, when the chain is unstrained, an ohmic behaviour, corresponding to cumulene, is observed [3]. This confirms a recent theoretical prediction, namely that the Peierls distortion, which would stabilize polyyne, is suppressed by zero-point vibrations in an unstrained chain so that cumulene is the stable configuration. In the presence of strain, however, polyyne is favoured by the Peierls instability. Thus, a metal-insulator transition can be induced by adjusting the strain. Furthermore it is shown that these atomic chains can act as rectifying diodes when they are in a non-symmetric contact configuration.

References

1. O. Cretu, A. R. Botello-Mendez, I. Janowska, C. Pham-Huu, J.-C. Charlier and F. Banhart, Nano Lett. 13, 3487 (2013). doi: 10.1021/nl4018918.
2. A. La Torre, F. Ben Romdhane, W. Baaziz, I. Janowska, C. Pham-Huu, S. Begin-Colin, G. Pourroy and F. Banhart, Carbon 77, 906 (2013). doi: 10.1016/j.carbon.2014.06.004.
3. A. La Torre, A. Botello-Mendez, W. Baaziz, J.-C. Charlier, F. Banhart, Nature Comm. 6, 6636 (2015). doi:10.1038/ncomms7636.

C nanowire Field-Effect-Transistors etc.

Konstantinos Zekentes[1,2] , Edwige Bano[2]
[1] *IESL/ FORTH, Vassilika Vouton, PO Box 1385 Heraklion, Greece]*
[3] *Grenoble-INP, IMEP-LAHC, F-38000 Grenoble, France*

Email: *konstantinos.zekentes@imep.grenoble-inp.fr*
Key words: Nanowires, SiC, FET

Theoretical studies on the 3C-SiC NWFETs, in various transport regimes [1, 2, 3], have shown that the SiC NWFETs have similar performance to the Si-based ones while they offer the advantage of high temperature operation and eventually efficient heat dissipation. Thus, the use of SiC NWFETs will not degrade the electrical characteristics while it will address main issues in device scaling.

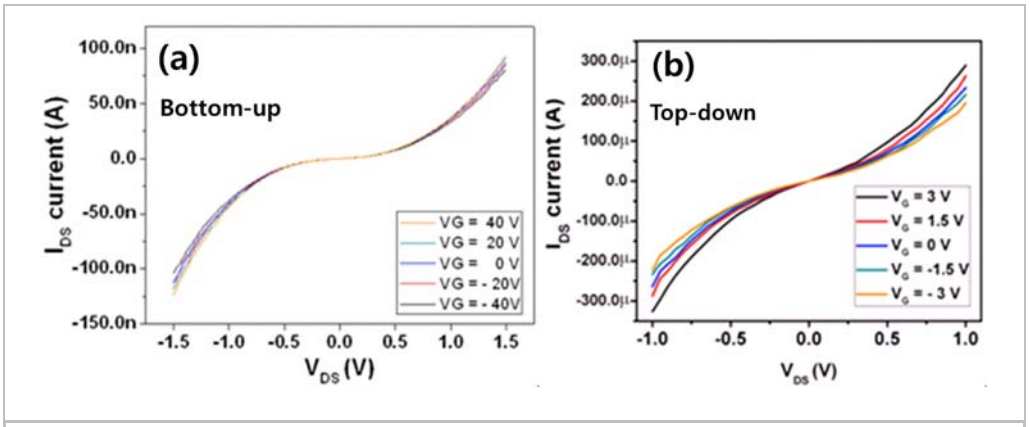

Figure 1: Output I-Vs of 3C-SiC NWFETs with: (a) bottom–up and (b) top-down grown SiC NWs.

Up to now, the potential advantages of SiC-based NWs have not been demonstrated mainly due to poor material properties of the grown materials (high density of planar defects and high residual doping) and the basic technology employed for fabricating SiC NWFETs resulting mainly in poor quality interface with gate dielectrics [1, 4, 5]. Back-gated NWFET geometries with ohmic contacts on the source and drain sides have been mainly employed. Most transistors exhibit weak gating effect (g_m<1 nS) and the device switching off is not achievable even for high negative gate voltages due to the high electron concentration. A better gating effect (g_m>1 nS) and device switching off have been achieved by using Schottky contacts [6]. The SiC NWFETs with ohmic source and drain contacts perform poorly due to the fact that the doping in the nanowire is too high preventing the nanowire of becoming fully-depleted in the off-

state. If nanowires with reduced doping could be grown then, the ohmic contact devices would outperform the SB devices by a wide margin [1, 6]. Since all SiC NWFETs related studies used SiC NWs produced by bottom up growth methods, a possible solution would be to form the NWs by a lithographic top-down approach. The recent effort is devoted to develop SiC NWFETs by using NWs formed by a top-down approach (“top-down” transistors) and compare their performance with that of SiC NWFETs with bottom-up grown NWs (“bottom-up” transistors).
The increased output currents (Fig.1) and transconductance value observed in the case of has top-down transistors confirmed partly the above hypothesis of high residual doping value, since a transistor switching off has not been possible. It is obvious, that to further improve the device performance of NWFET, it is strongly needed to control the gate dielectric/NW channel interface. Towards this purpose, a NW embedded top-gate geometry and eventually reliable high-k material deposition are necessary.

References

1. K. Rogdakis. Y. Lee, M. Bescond, S. K. Lee, E. Bano and K. Zekentes, IEEE Trans. Electron Dev., 55, 1970-1976 (2008)
2. K. Rogdakis, S. Poli, E. Bano, K. Zekentes and M. Pala, Nanotechnology 20 295202 (2009)
3. K. Rogdakis, S. Poli, E. Bano, K. Zekentes and M. Pala, Nanotechnology 20 295202 (2009)
4. H. K. Seong, H. J. Choi H J, S. K. Lee, J. I. Lee, D. J. Choi Doo, Appl. Phys. Lett. 15, 1256-1258, (2004)
5. M. Zhou, F. Fang, Z. Y. Hou, L. J. Yan, and Y. F. Zhang, IEEE Electron Device Lett. 27, 463-465, (2006)
6. K. Rogdakis, E. Bano, L. Montes, M. Bechelany, D, Cornu and K. Zekentes, IEEE Trans. On Nanotechnology, 10, 980-984 (2011)

A. Acun et al. “Atomically Controlled Surfaces Interfaces and Nanostructures”
edited by A. Bianconi, A. Marcelli (Superstripes Press, Rome 2016) isbn: 9788866830597

Extreme doping levels and many-body interaction in epitaxial graphene on SiC(0001)

Ulrich Starke
Max-Planck-Institut für Festkörperforschung, Stuttgart, Germany

Email: *u.starke@fkf.mpg.de*
Key words: Graphene, Intercalation, Electronic Structure, Many-body interactions, ARPES

Wafer scale epitaxial graphene grown on SiC single crystals is regarded as a suitable candidate for carbon based electronics. Although the presence of the SiC substrate has a strong influence on the electronic and structural properties of the graphene layers, these properties can be manipulated by functionalizing the graphene/SiC interface on an atomic scale. Intercalation under the first carbon honeycomb layer can relieve the strong covalent bonds of its atoms to the SiC(0001) substrate and manipulate the π-band structure in a large range of aspects. We have shown in recent years that this carbon layer can be turned into quasi-free standing monolayer graphene and that designed doping levels are accessible [1-4]. Here, I will demonstrate how extreme doping levels and drastic renormalization magnitudes give access to novel graphene properties that may promise applications such as plasmonics and superconductivity.

Intercalation of Cu induces a coincidence superstructure on top of the SiC surface, which originates from periodic regions of different bond configuration for the carbon atoms in the graphene layer [3]. A (13×13) graphene superlattice is seen in low-energy electron diffraction (LEED). As a result, a long range periodic potential is imposed onto the graphene layer, which leads to a profound modification of its electronic spectrum. A surprisingly strong doping and the development of mini-Dirac cones are observed in angle-resolved photoemission spectroscopy (ARPES).

Au intercalation yields two phases of different carrier type in SiC based graphene [4]. With the improved preparation quality of our furnace grown graphene layers, we retrieve a highly ordered graphene/intercalant/substrate system as demonstrated in ARPES by periodic replicas of the graphene π-bands. High resolution experiments reveal a significant renormalization of the graphene bands due to a strong electron-plasmaron interaction which can be used to estimate the tunability of graphene’s dielectric constant due to the intercalation. A sharp 2D band structure of its own can be resolved for the gold layer.

Extremely high doping regimes can be reached by the intercalation of lanthanide elements – in this case Gadolinium. As a result, the Van-Hove singularity in the π-band

structure at the M-point of pristine graphene is shifted towards the Fermi level so that spectral weight appears in ARPES along the KMK-line. Thus, the intercalation’s influence on the electronic structure of the graphene can be viewed as a topological transition from a situation with 2 hole pockets to one electron pocket. The doping is accompanied by a strong bending of the bands in the vicinity of the Fermi energy, which we attribute to a combination of hybridization with the Gd orbitals and electron-electron interaction. Additionally strong electron-phonon coupling is observed. We speculate that the high density of states at the Fermi level may potentially allow to access superconductivity in graphene.

References

1. C. Riedl, C. Coletti, T. Iwasaki, A.A. Zakharov, and U. Starke, Phys. Rev. Lett. 103, 246804 (2009).
2. K.V. Emtsev, A.A. Zakharov, C. Coletti, S. Forti, and U. Starke, Phys. Rev. B 84, 125423 (2011).
3. S. Forti, A. Stöhr, A.A. Zakharov, C. Coletti, K.V. Entsev, and U. Starke, 2D Materials, submitted.
4. I. Gierz, T. Suzuki, R.T. Weitz, D.S. Lee, B. Krauss, C. Riedl, U. Starke, H. Höchst, J.H. Smet, C.R. Ast, and K. Kern, Phys. Rev. B 81, 235408 (2010).

A. Acun et al. “Atomically Controlled Surfaces Interfaces and Nanostructures”
edited by A. Bianconi, A. Marcelli (Superstripes Press, Rome 2016) isbn: 9788866830597

We2S session

A. Acun et al. “Atomically Controlled Surfaces Interfaces and Nanostructures”
edited by A. Bianconi, A. Marcelli (Superstripes Press, Rome 2016) isbn: 9788866830597

Metal-insulator transition in a spinodally decomposed microstructure in the TiO_2–VO_2 system

Zenji Hiroi
ISSP, University of Tokyo

Email: *hiroi@issp.u-tokyo.ac.jp*
Key words: spinodal decomposition, metal–insulator transition, molecular orbital crystal, VO_2, TiO_2

The metal–insulator transition (MIT) of VO_2 is revisited with particular emphasis on the structural instability of the rutile compounds toward dimer structures. Ti substitution experiments reveal that the MIT is robust up to 20% Ti^{4+} substitution (hole doping) and occurs even in extremely thin V-rich lamellas of a few nm thick in spinodally decomposed TiO_2–VO_2 composites [1–3], as shown in Fig. 1, indicating that the MIT takes on an essentially local character and suggesting that either electron correlation or Peierls (Fermi-surface) instability plays a minor role on the MIT.

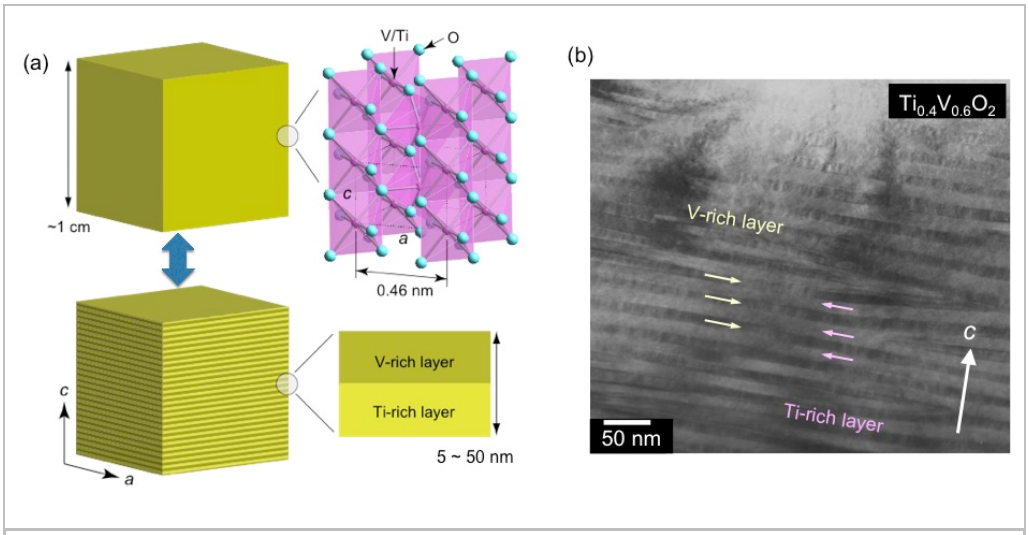

Fig. 1. (a) Schematic representation of a spinodal decomposition in the TiO_2–VO_2 system. A solid solution crystal between the two components are stable above 830 K, which crystallizes in the rutile structure with Ti/V atoms statistically occupying the position surrounded octahedrally by six oxide atoms. A spinodal decomposition occurs at lower temperatures, resulting ideally in such a natural superlattice crystal having a mega stack of alternate Ti- and V-rich layers along the *c* axis with periods of 5–50 nm. (b) electron micrograph showing a lamellar structure in which Ti-rich layers (bright bands with ~20 nm thickness) and V-rich layers (dark bands with ~15 nm thickness) alternate with an average periodicity of 33 nm along the *c* axis.

It is pointed out through a broad perspective of crystal chemistry on the rutile-related compounds that VO_2 and another MIT compound NbO_2 in the family happen to lie just on the borderline between the two structural groups with the rutile structure and the distorted structures characterized by the formation of dimer molecules with metal–metal bonding. It is also shown that the two compounds of the rutile form do not follow the general trends in structure observed for the other rutile compounds, giving clear evidence of an inherent structural instability in the two compounds. The MITs of VO_2 and NbO_2 are natural consequences of structural transitions between the two groups, as all the *d* electrons are trapped in molecular orbitals of dimers at low temperatures in the dimer phases. Dimer phases are ubiquitous in transition metal compounds with chain-like structures made of face- or edge-sharing octahedra, such as $MoBr_3$, $NbCl_4$, Ti_4O_7, and V_4O_7, the latter two of which also exhibit MITs probably of the same structural origin. In a broader sense, dimer phases belong to "molecular orbital crystals" in which virtual molecules made of transition metal atoms, such as dimers, trimers or larger ones, are stabilized by generating metal–metal bonding at low temperatures. Molecular orbital crystallisations are often observed in many transition metal compounds that comprise edge-sharing octahedron networks of various connectivities.

References

1. Z. Hiroi, H. Hayamizu, T. Yoshida, Y. Muraoka, Y. Okamoto, J. Yamaura, and Y. Ueda: Chem. Mater. 25, 2202 (2013). http://dx.doi.org/10.1021/cm400236p.
2. Z. Hiroi, Prog. Solid State Chem. 43, 47 (2015). http://dx.doi.org/10.1016/j.progsolidstchem.2015.02.001.
3. Z. Hiroi, T. Yoshida, J. Yamaura, and Y. Okamoto: APL Materials 3, 062508 (2015).http://dx.doi.org/10.1063/1.4919764.

A. Acun et al. "Atomically Controlled Surfaces Interfaces and Nanostructures"
edited by A. Bianconi, A. Marcelli (Superstripes Press, Rome 2016) isbn: 9788866830597

Creating and manipulating low-dimensional electron liquids at the surfaces of transition metal oxides

Zhiming Wang[1,2]
[1]*Swiss Light Source, Paul Scherrer Institute, Switzerland*
[2]*DQMP, University of Geneva, Switzerland*

Email: *zhiming.wang@psi.ch*
Keywords: Oxide surface and interface; low-dimensional electron liquid; ARPES; electron-phonon coupling; Fröhlich polaron

Surfaces and interfaces offer new possibilities for tailoring many-body interactions that dominate electrical and thermal properties of transition metal oxides (TMOs). Through photo-stimulated chemical doping of TMOs surfaces we can create quantum confined two-dimensional electron liquids (2DEL) at bare TMOs surfaces [1-5]. Here I will present our recent angle resolved photoemission spectroscopy (ARPES) experiments on 2DELs at the surfaces of $SrTiO_3$ and anatase TiO_2. Through carrier density control and lateral confinement, we will demonstrate how surface and interface engineering at atomic scale can be used to tailor properties of oxide 2DELs [3-5].

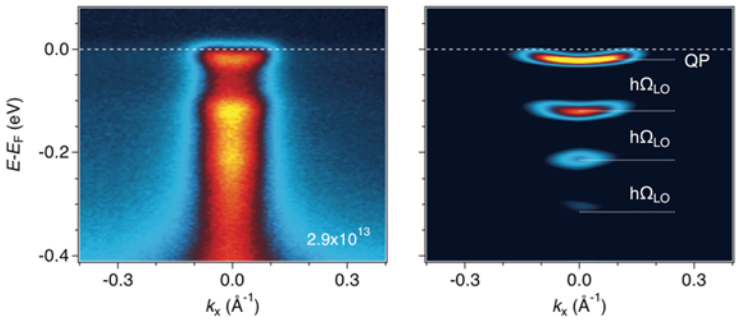

Figure 1: Energy–momentum intensity map and curvature plot, respectively, for a two-dimensional liquid of large polarons at the $SrTiO_3$(001) surface [4]. Note the dispersive replica bands at higher binding energy arising from strong coupling to the longitudinal optical (LO) phonon branch of $SrTiO_3$ with energy $h\Omega_{LO}$ approximately 100 meV.

In the first part, we will use the prototypical 2DEL at the $SrTiO_3$(001) surface [1-3] to reveal a remarkably complex evolution of electron-phonon coupling with the tunable carrier density of this system [4]. At low density, where superconductivity is found in the analogous 2DEL at the $LaAlO_3/SrTiO_3$ interface, our ARPES data show replica bands separated by 100 meV from the main bands. This is a hallmark of a coherent polaronic liquid and implies long-range coupling to a single longitudinal optical phonon branch. In the overdoped regime the preferential coupling to this branch

decreases and the 2DEL undergoes a crossover to a more conventional metallic state with weaker short-range electron-phonon interaction.

In the second part, we describe a bottom-up approach for the lateral confinement of a 2DEL with atomic scale precision on an unprecedented length scale comparable to the Fermi wavelength [5]. To this end, we use pulsed laser deposition to grow anatase TiO2 films terminated by a (1 × 4) in-plane surface reconstruction. Employing photo-stimulated chemical doping, we induce a 2DEL confined within only 2-3 unit cells below the TiO_2 surface. Subsequent *in-situ* ARPES experiments demonstrate that the (1 × 4) surface reconstruction provides a periodic lateral perturbation of the electron liquid. This causes strong backfolding of the electronic bands and the opening of unidirectional gaps at the reduced Brillouin zone boundaries, leading to a quasi-one-dimensional electronic structure. These findings open a new pathway for tailoring the electronic properties of oxide 2DELs.

References

1. A. F. Santander-Syro, *et al.*, Nature 469, 189 (2011).
2. W. Meevasana, *et al.*, Nat. Mater. 10, 114 (2011).
3. Z. Wang, *et al.*, Proc. Nat. Aca. Sci. USA 111, 3933 (2014).
4. Z. Wang, *et al.*, Nat. Mater. (2016) DOI:10.1038/nmat4623.
5. Z. Wang, *et al.*, Submitted.

Detecting Inorganic Molecules on reactive MoS2 defects by ab-initio Scanning Probe Microscopy Simulations.

C. González[1,2], B. Biel[1], Y. J. Dappe[2]
[1] *Facultad de Ciencias Universidad de Granada Granada E-18071, Spain*
[3] *SPEC/IRAMIS/CEA, CNRS, Université Paris Saclay, 91191 Gif-Sur-Yvette, France*

Email: *gonzalezcesar@ugr.es*
Key words: 2D-Materials, MoS_2, Gas sensing, DFT, AFM/STM

Since graphene was discovered some years ago [1], the interest in two dimensional (2D) materials has grown exponentially. The so-called transition-metal di-chalcogenides have recently attracted great attention due to their promising properties. One of the most studied compounds is MoS_2 due to its potential nanoelectronic, optoelectronic and spintronic applications [2].

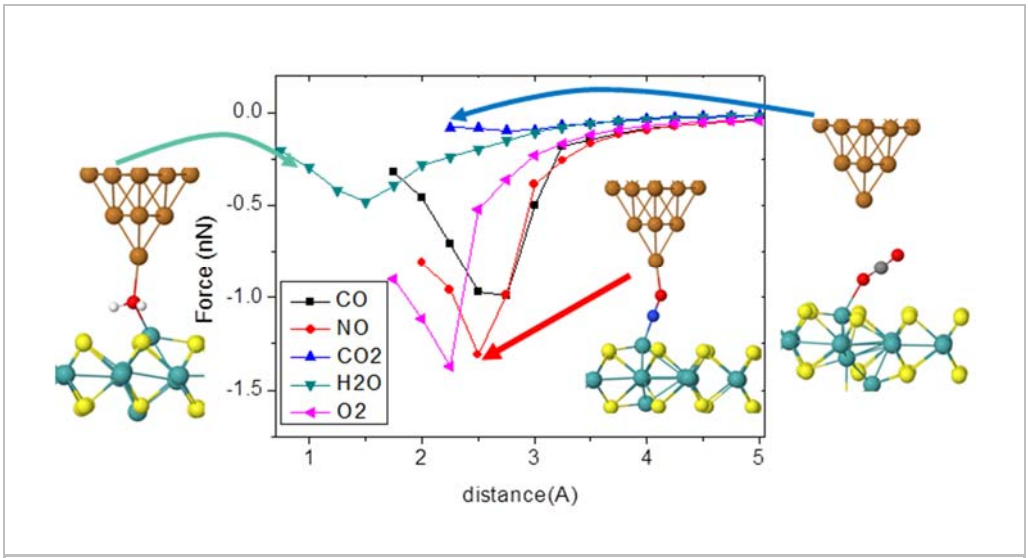

Figure 1: Force curves of a Cu tip contacting to different molecules adsorbed on a defect formed by the substitution of two S by two Mo atoms in the MoS2 monolayer. The ball and stick models of the contact point (minimum force) are shown for: a H_2O/CO_2 molecule (green/blue triangles), on the left/right side, and on the inset a NO molecule (red circles).

Very recently, this material has been proposed as a fundamental part in gas sensors [3]. In those cases, the molecules were weakly bonded by van der Waals (vdW) forces to

the poorly reactive MoS_2 substrate, changing the electric current measured in the sensor.

In this work, we have performed density functional theory (DFT) simulations using the VASP code [4] in order to find the most stable structures of small inorganic molecules (such as H_2O, N_2, O_2, CO, NO and CO_2) adsorbed on different point defects of the MoS_2 monolayer [5]. Our results show that the molecules can be bonded to the Mo atoms in the substitutional defects. In our analysis, the Sulphur divacancy occupied by two Mo atoms has been selected as the most interesting defect. Once the molecules are bonded to this point, they can be identified using the Scanning Probe Microscopies (SPM). Following the original idea of chemical identification proposed some years ago [6], each molecule will lead to a different force curve when an atomic force microscope (AFM) tip is approached. In figure 1, the forces of CO, NO, CO_2, H_2O and O_2 molecules are represented. The resulting value and position of the minimum force characterize the kind of molecule that has been scanned by the AFM. At the same time, the use of a metallic tip allows the calculation of the conductance as a second fingerprint of each molecule. This second parameter will help to elucidate the kind of molecule adsorbed in cases with comparable force (see in Figure 1 the similar values obtained for O_2 and NO). Using these parameters, a complete database would be created in order to identify molecules in future experimental measurements.

References

1. K. S. Novoselov et al., Science, 306, 666 (2004). doi: 10.1126/science.1102896
2. B. Radisavljevic et al., Nat. Nanotechnol., 6 (2011) 147. doi:10.1038/nnano.2010.279; J. Yoon et al., Small, 9, 3295 (2013). DOI: 10.1002/smll.201300134; Q. H. Wang et al., Nat. Nanotechnol., 7, 699 (2012). doi:10.1038/nnano.2012.193
3. H. Li, et al., Small, 8, 63 (2012). doi: 10.1002/smll.201101016; Q. Y. He, et al., Small, 8, 2994 (2012). doi: 10.1002/smll.201201224
4. G. Kresse and J. Hafner, Phys. Rev. B, 47 (1993) R558. http://dx.doi.org/10.1103/PhysRevB.47.558
5. C. González, B. Biel and Y. J. Dappe, sent to J. Phys. Chem. C
6. Y. Sugimoto et al., Nature, 446 (2007). doi:10.1038/nature05530

Local structural tuning of thermoelectric transport properties in oxides

Wei Xu[1,5], Yingcai Zhu[1], Sajid Butt[2], Yong Liu[3], and Augusto Marcelli[4,5]
[1]*Beijing Synchrotron Radiation Facility, Institute of High Energy Physics, Chinese Academy of Sciences, Beijing, 100049, China.*
[2]*Department of Materials Science and Engineering, Institute of Space Technology, Islamabad 44000, Pakistan.*
[3]*Beijing Institute of Aeronautical Materials，AVIC, Beijing 100095, China.*
[4]*INFN - Laboratori Nazionali di Frascati, Via E. Fermi 40, Frascati, 00044, Italy.*
[5]*RICMASS, Rome International Center for Materials Science Superstripes, Via dei Sabelli 119A, 00185 Rome, Italy.*

Email: *xuw@mail.ihep.ac.cn*
Key words: $Ca_3Co_4O_9$; In_2O_3; Thermoelectric properties; Local structure

Thermoelectricity is of great interests for energy conversion from waste heat to electricity, or electrical cooling of devices by dumping heat from hot side to a sink. To meet the demands for highly efficient thermoelectric performance, the community has been made tremendous endeavors to improve the figure of merit for thermoelectricity..

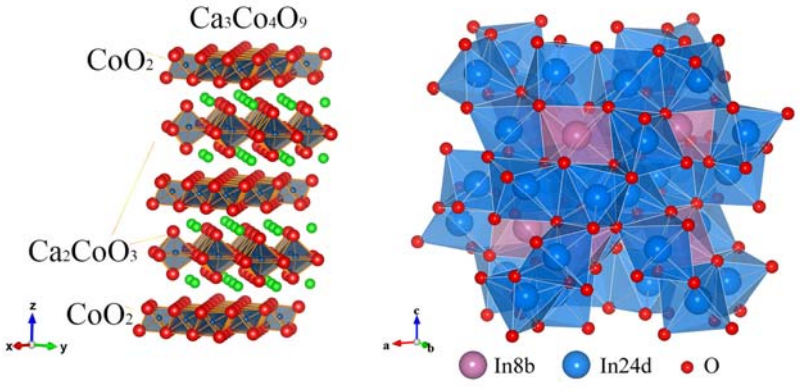

Figure 1: P-type thermoelectrics $Ca_3Co_4O_9$ and N-type thermoelectrics In_2O_3.

Oxides, quite stable form of matter in air, have been investigated as excellent candidates for thermoelectric applications, thanks to their relatively higher chemical and structural stability of oxides. Meanwhile, the interrations among cations and oxygen atoms are believed to play important role in regulating the carrier generation, charge tranport as well as lattice dynamics of oxides. Consequently, the thermoelectric transport properties, such as electrical conductivity, Seebeck coefficient and thermal conductivity, can be optimized via defect chemistry, hierarchically structural engineering approaches.

In this talk, we will present the recent progresses of such structural tuning of two typical thermoelectric oxides, e.g. $Ca_3Co_4O_9$ and In_2O_3.(Figure.1) The $Ca_3Co_4O_9$,[1-2] being a p-type thermoelectric material, has a misft structure consisting of two subsystems which are dominant for charge and heat transport, respectively. Furthermore, the In_2O_3,[3-4] representing a n-type thermoelectric material, possess cubic structure with two inequivalent indium sites. The local structure optimization of the thermoelectricity in those two families of oxides is envisaged to pave the way for obtaining oxides with higher thermoelectric performance. Combining the strategy in both p-type and n-type thermoelectrics is promising for manufacturing thermoelectric modules in future applications for both energy conversion and electrical cooling.

References

1. S. Butt, W. Xu, M. U. Farooq, G. K. Ren, F. Mohmed, Y. Lin, and C.-W. Nan, J. Am. Ceram. Soc. 98, 1230 (2015).
2. S. Butt, W. Xu, W. Q. He, Q. Tan, G. K. Ren, Y. Lin, and C. Nan, J. Mater. Chem. A 2, 19479 (2014).
3. Y. Liu, W. Xu, D.-B. Liu, M. Yu, Y.-H. Lin, and C.-W. Nan, Phys. Chem. Chem. Phys. 17, 11229 (2015).
4. W. Xu, Y. Liu, B. Chen, D.-B. Liu, Y. Lin, and M. Augusto, Phys. Chem. Chem. Phys. 15, 17595 (2013).

A. Acun et al. “Atomically Controlled Surfaces Interfaces and Nanostructures”
edited by A. Bianconi, A. Marcelli (Superstripes Press, Rome 2016) isbn: 9788866830597

BEEM and STM theories by the multiple scattering approach

Keisuke Hatada[1,2,3]
[1]*Département Matériaux-Nanosciences, Institut de Physique de Rennes, UMR UR1-CNRS 6251, Université de Rennes1, 35042 Rennes cedex – France*
[2]*Scienze e Tecnologie, Università di Camerino, Via Madonna delle Carceri 9, 62032 Camerino, Italy*
[3] *INFN Laboratori Nazionali di Frascati, 00044 Frascati, Italy.*

Email: *keisuke.hatada@univ-rennes1.fr*
Key words: Atomic and nanoscale structure of surfaces and interfaces: advanced methods, Metal-semiconductor and insulator-semiconductor interfaces, State-of-the-art theoretical approaches on surfaces and interfaces

The Ballistic Electron Emission Microscopy (BEEM) [1,2] is a powerful technique to investigate interfaces of bulk systems. The experimental setup of BEEM is basically based on the Scanning Tunneling Microscope (STM), so that the spatial resolution is in atomic scale as STM.

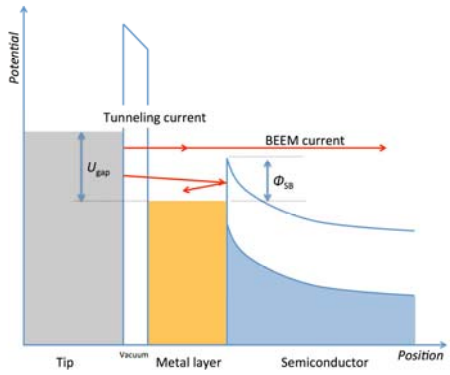

Figure 1: A scheme of BEEM current within an STM setup. Electrons on the tip is transported by tunneling effect to the metallic surface, then they meet Schottky barrier at the interface. Since the electrons have just about 1 eV of kinetic energy, they can be ballisticaly transported in the semiconductor.

When we cover the surface of a semiconductor with a metal thin layer, Schottky barrier is generated at the interface and behaves as an additional barrier to the tunneling barrier from the tip to the sample. Due to these two barriers, a hot electron, whose kinetic energy is about 1 eV, is created and travels in the bulk “ballistically”, namely the scattering should be elastic without loss by excitons or plasmons. (See Fig. 1)

Theoretical studies for BEEM have been done by means of k-space band calculation [3] and tight-binding method [4,5]. k-space band study is very convenient to understand the phenomena in qualitative way, however the diffusion process of the hot electron in real space out of periodicity can not be considered. While the tight binding method can treat the transport problem in the real space, the approximation is not suitable for the long traveling delocalized state due to the use of localized basis. Multiple scattering theory gives a good representation for a large-scale system within real space formalism. [6,7] We applied the full potential multiple scattering theory [8,9] to BEEM to describe the transport phenomena accurately.

References

1. W. J. Kaiser and L. D. Bell, *Phys. Rev. Lett*. 60, 1406 (1988).
2. L. D. Bell and W. J. Kaiser, *Phys. Rev. Lett*. 61, 2368 (1988).
3. M. Hervé, S. Tricot, Y. Claveau, G. Delhaye, S. Di Matteo, P. Schieffer, and P. Turban, *Appl. Phys. Lett.* 103, 202408 (2013).
4. P.L. de Andres, F.J. Garcia-Vidal, K. Reuter, and F. Flores, *Prog. in Surf. Sci.* 66, 3 (2001).
5. Y. Claveau, arXiv:1501.06458[cond-mat.mes-hall], PhD thesis (2014).
6. J. Xu, K. Hatada, D. Sébilleau and L. Song, arXiv:1604.04846[quat-ph].
7. J. Xu, P. Krüger, C. R. Natoli, K. Hayakawa, Z. Wu, and K. Hatada, *Phys. Rev. B* 92, 125408 (2015).
8. K. Hatada, K. Hayakawa, M. Benfatto and C. R. Natoli, *Phys. Rev. B* 76, 060102(R) (2007).
9. K. Hatada, K. Hayakawa, M. Benfatto and C. R. Natoli, *J. Phys. Cond. Matt.* 22, 185501 (2010).

A. Acun et al. “Atomically Controlled Surfaces Interfaces and Nanostructures”
edited by A. Bianconi, A. Marcelli (Superstripes Press, Rome 2016) isbn: 9788866830597

Effects of thermal disorder and zero-point motion on core levels in purple bronze

Thomas Jarlborg, DQMP, University of Geneva, Geneva, Switzerland

Email: *Thomas.jarlborg@unige.ch*
Key words: Electronic strucure, thermal disorder, Spetroscopy, core levels, low-dimensional system

The band structures of ordered and thermally disordered $Li_2Mo_{12}O_{34}$ are calculated by use of ab-initio DFT-LMTO method with focus on the behavior of the Mo 3d-core levels. High resolution photoemission have been used to measure the Mo 3d core spectra at low and high T. Comparison with possible XPS experiments should reveal what static and vibrational disorders are present in the real material. It is also useful to study core levels in magnetic materials for understanding of T-dependent spin moments.

A. Acun et al. “Atomically Controlled Surfaces Interfaces and Nanostructures”
edited by A. Bianconi, A. Marcelli (Superstripes Press, Rome 2016) isbn: 9788866830597

Th1T session

Multiple-probe STM study on materials that think

Tomonobu Nakayama[1,2], Rintaro Higuchi[1], Li Ming[1], Goswami Sherestarekha[1], Yoshitaka Shingaya[1]
[1]*International Center for Materials Nanoarchitectonics (WPI-MANA), National Institute for Materials Science, Japan*
[2]*Graduate School of Pure and Applied Science, University of Tsukuba, Japan*

Email: *nakayama.tomonobu@nims.go.jp*
Key words: Nanowires; multiple-probe scanning probe microscope; Neuromorphic networks; Complex networks; Nanoarchitectonics; Artificial intelligence

We have developed multiple-probe scanning probe microscopes (MP-SPMs) [1-3] which are not only useful in revealing physical properties of individual nanostructures and nanomaterials but also in investigating nanoarchitectonically assembled nanosystems. In this paper, we present our recent study using MP-SPM. Here, complex networks of nanowires are shown to exhibit interesting features such as a "small-world" and 1/f type fluctuation. Detailed analyses on the 1/f feature lead us to convince the complex networks to be neuromorphic networks which are, in the other words, materials that think.

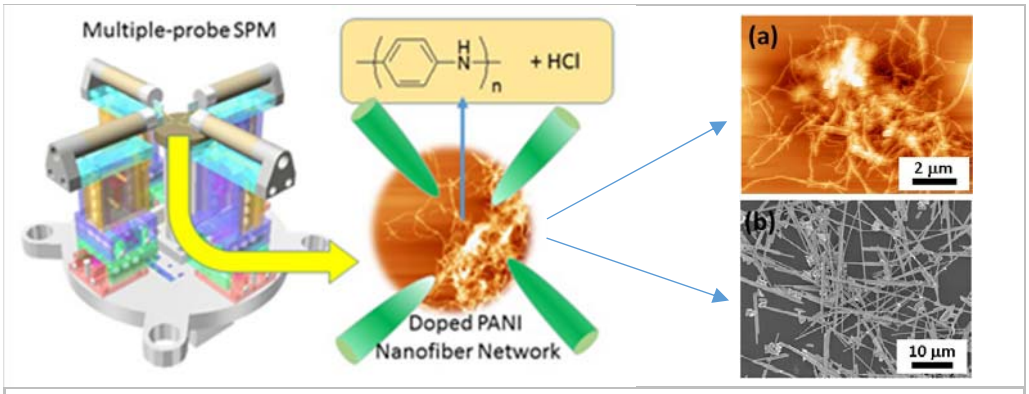

Figure 1: Schematic illustrations of (Left) multiple-probe SPM and (Center) four probe AFM measurements on a network of nanowires. In the right panel, MP-AFM image of doped-PANI and SEM image of Ag nanowire networks are shown.

The MP-SPMs [4] used in this study are home-built systems which equip independently-driven four AFM/STM probes. Each probe can be used as atomic force microscope (AFM) probe, a Kelvin force microscope (KFM) probe or a scanning tunneling microscope (STM) probe. For example, all the four probes are simultaneously operated in non-contact AFM mode to identify their locations on the structure of interest, then two of them are brought into contact with the structure as

source and drain electrodes. Another probe can be used for imaging the region of interest in a KFM mode to measure potential variation.

As samples to be measured, complex networks of nanowires were prepared on insulating substrates such as glass, mica, or SiO_2 on Si by drop-casting or spin-coating chemically prepared nanowires of conductive peptide [5], doped poly-aniline (PANI) [6] and sliver (Ag). Then, we used MP-SPM and other microscopes together with a semiconductor parameter analyzer for characterizing and monitoring morphological and electrical properties of the networks. Tuning fork type sensors having electrochemically etched tungsten tips [7] were used in MP-SPM measurements.

In the case of pseudo 2D networks of doped-PANI nanowires, the resistance did not show simple dependence against distances between two probes of MP-SPM, which was well-explained by a non-trivial topological feature known as a “small-world” property [8], indicating that the network is a complex network. Similar complex network could also be formed by Ag nanowires, and, interestingly it showed 1/f noise feature in power density spectra when flowing electrical current. This Ag nanowire network showed memristive property which were not confirmed for doped-PANI networks. Also, at individual cross point between Ag nanowires, an atomic switch [9] behavior was confirmed by MP-SPM measurements. From these results, the complex network of Ag nanowires would work as a neuromorphic materials network [10].

References

1. T. Nakayama, O. Kubo, Y. Shingaya, S. Higuchi, T. Hasegawa, C.-S. Jiang, T. Okuda, Y. Kuwahara, K. Takami, and M. Aono, Adv. Mater. 24, 1675 (2012).
2. O. Kubo, Y. Shingaya, M. Nakaya, M. Aono and T. Nakayama, Appl. Phys. Lett. 88, 254101 (2006).
3. D. K. Lim, O. Kubo, Y. Shingaya, T. Nakayama, Y. H. Kim, J. Y. Lee, M. Aono, H. Lee, D. Lee and S. Kim, Appl. Phys. Lett. 92, 203114 (2008).
4. Y. Shingaya et al, in preparation.
5. R. Creasey, Y. Shingaya, T. Nakayama, Mater. Chem. Phys. 158, 52 (2015).
6. R. Higuchi, Y. Shingaya, T. Nakayama, Jpn. J. Appl. Phys., in press
7. S. Higuchi, H. Kuramochi, O. Kubo, S. Masuda, Y. Shingaya, M. Aono and T. Nakayama, Rev. Sci. Instrum. 82, 043701 (2011).
8. D. J. Watts and S. H. Strogatz, Nature 393, 440 (1998).
9. K. Terabe, T. Hasegawa, T. Nakayama and M. Aono, Nature 433, 47 (2005).
10. A. Z. Stieg, A. V. Avizienis, H. O. Sillin, C. Martin-Olmos, M. Aono, J. K. Gimzewski, Adv. Mater. 24, 286 (2012).

A. Acun et al. "Atomically Controlled Surfaces Interfaces and Nanostructures"
edited by A. Bianconi, A. Marcelli (Superstripes Press, Rome 2016) isbn: 9788866830597

Co-GISAXS as a New Tool to Investigate Surface Growth Dynamics

M.G. Rainville[a], C. Wagenbach[a], J.G. Ulbrandt[b], S. Narayanan[c], A. Sandy[c], H. Zhou[c], M. Mokhtarzadeh[d], R.L. Headrick[b] and K.F. Ludwig[a],
[a]Div. of Materials Sci. & Eng.; Boston University
[b]Dept. of Physics; Univ. of Vermont
[c]Advanced Photon Source, Argonne National Laboratory
[d]Dept. of Physics; Boston University

Email: *ludwig@bu.edu*

Key words: Dynamical growth; thin films; Small-Angle X-ray Scattering; X-ray Photon Correlation Spectroscopy

The technique of X-ray Photon Correlation Spectroscopy (XPCS) [1] continues to grow in application. A detailed quantitative measurement of surface dynamics during thin film growth is a major experimental challenge. Recently we have used X-ray Photon Correlation Spectroscopy with coherent hard X-rays in a Grazing-Incidence Small-Angle X-ray Scattering (i.e. Co-GISAXS) geometry as a new tool to investigate nanoscale surface dynamics during sputter deposition of a-Si and a-WSi_2 thin films.

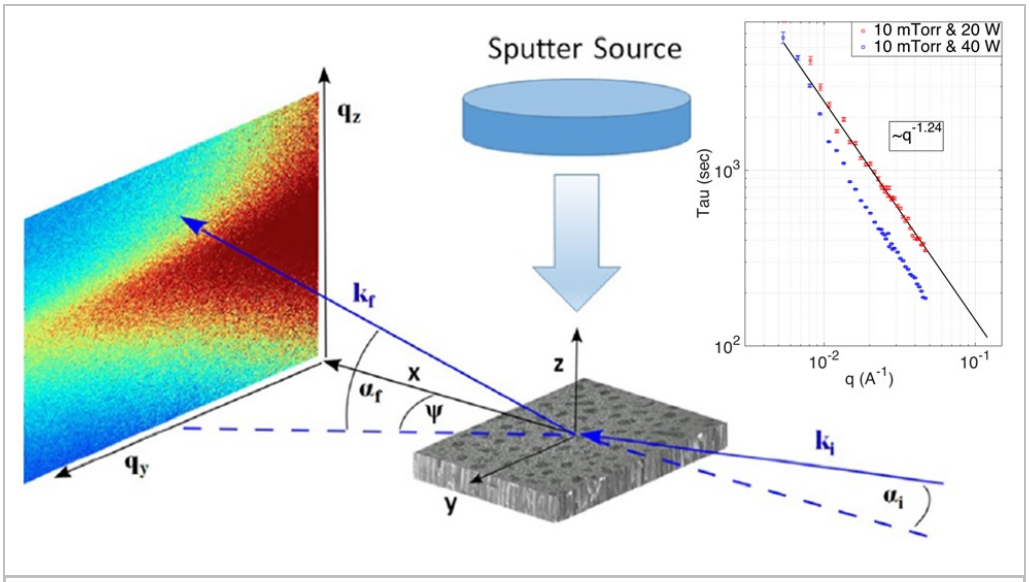

Figure 1: Schematic of Co-GISAXS experiment examining growth dynamics during sputter deposition of Si and WSi_2. Inset at top right shows that the measured correlation times tau are a power law in wavenumber q with an exponent independent of deposition rate.

For both films, kinetic roughening during surface growth reaches a dynamic steady state at late times in which the intensity autocorrelation function $g_2(q,t)$ becomes stationary. For the most surface-sensitive experimental conditions, the $g_2(q,t)$ functions

exhibit compressed exponential behavior at all wavenumbers studied. The overall dynamics are complex, but the structure factor and correlation time exhibit power law behaviors consistent with dynamical scaling [2]. Simulations were performed to better compare the observed kinetics with predictions of linear and nonlinear growth models. In contrast to the simple compressed exponential relaxation of $g_2(q,t)$ observed under surface-sensitive experimental conditions, more complex behavior is seen under conditions in which the X-ray signal comes from both the growth surface and the thin film bulk. In this case, oscillations in temporal correlations arise from coherent interference between scattering from stationary bulk features and from the ad-vancing surface. We observe evidence that elongated bulk features propagate upward at the same velocity as the surface [3].

This work was supported by the U.S. Department of Energy (DOE) Office of Science, Office of Basic Energy Sciences (BES) under DE-FG02-03ER46037 (BU) and DE-FG02-07ER46380 (UVM).

References

1. M. Sutton, *Coherent X-ray Diffraction*, in Third-Generation Hard X-ray Synchrotron Radiation Sources: Source Properties, Optics, and Experimental Techniques, edited by. Dennis M. Mills, John Wiley and Sons, Inc, New York, (2002).
2. M.G. Rainville, C. Wagenbach, J.G. Ulbrandt, S. Narayanan, A.R. Sandy, H. Zhou, R.L. Headrick and K.F. Ludwig, Phys. Rev. B 92, 214102 (2015).
3. J.G. Ulbrandt, M.G. Rainville, C. Wagenbach, S. Narayanan, A.R. Sandy, H. Zhou, K.F. Ludwig and R.L. Headrick, Nature Physics doi: 10.1038/nphys3708 (2016).

A. Acun et al. "Atomically Controlled Surfaces Interfaces and Nanostructures"
edited by A. Bianconi, A. Marcelli (Superstripes Press, Rome 2016) isbn: 9788866830597

Atomic-to-mesoscale structure of buried quantum electronic interfaces

Paul G. Evans[1]
[1]*Department of Materials Science and Engineering, University of Wisconsin-Madison, 1509 University Ave., Madison, WI 53706 USA*

Email: *pgevans@wisc.edu*
Key words: buried interface structure, distortion of quantum electronic materials, x-ray diffraction and scattering, synchrotron x-ray nanobeam diffraction, dynamics of structural phase transformation

Advanced x-ray nanobeam diffraction methods provide unique insight into the structure of the interfaces of emerging electronic materials. In materials for quantum devices, the confinement of electrons occurs at long lengthscales of hundreds of nanometers and can be affected by structural affects that are only beginning to be understood.

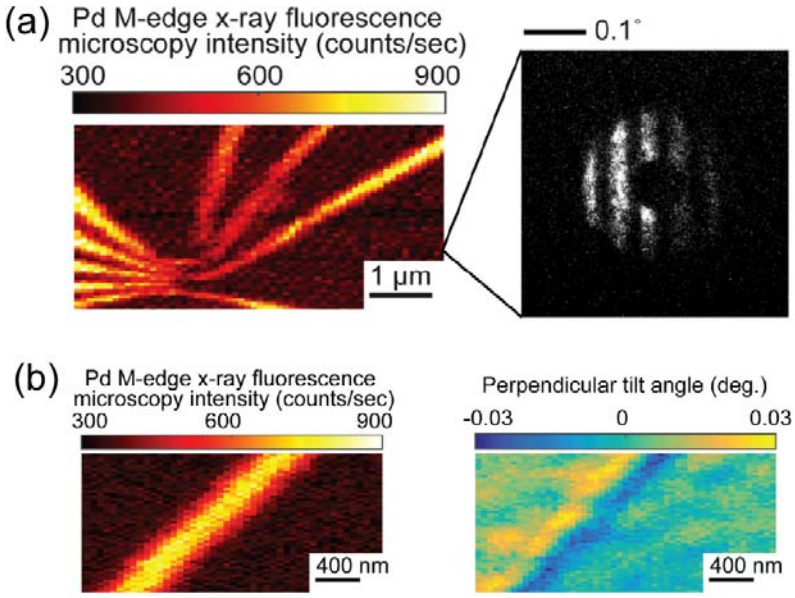

Figure 1: (a) Electrodes and x-ray diffraction pattern of a quantum dot defined by Pd electrodes deposited on a Si/SiGe heterostructure containing a Si quantum well. (b) Image and quantum well tilt in the region of a single electron. The tilt induces a strain that perturbs the confinement energy in the quantum well. After ref. [1].

At these scales, interfacial features include atomic steps, distortion and rotation due to relaxation during epitaxial growth, and stress induced by interfaces with electrodes and other device components. Synchrotron x-ray nanobeams allow these features electronic materials interfaces to be characterized, in both the heterostructures from which the devices are formed and in fully formed and patterned devices.

Key features of the interfaces of a Si quantum well within a Si/SiGe heterostructure are shown Figure 1. The device structure shown in Fig. 1(a) consists of a quantum dot defined by voltage gates formed from a patterned Pd thin film [1]. By analyzing the coherent diffraction patterns, as in Fig. 1(a), the bending and interface structure within the quantum well can be imaged, as for an isolated single electrode in Fig. 1(b). Our analysis includes the simulation of the complex nanobeam diffraction patterns created with the highly convergent x-ray focusing optics [2]. A key result of such simulation methods is that the transverse coherence of the focused beam results in the imprinting of structural information onto the scattered beam at angular resolutions much smaller than the total angular divergence of the focused beam.

Further applications of this approach include to other structural phenomena (including facet angles and reconstructions, e.g. in graphene/Ge [3]) and at interfaces in electronic materials such as compressively strained multiferroic $BiFeO_3$ that can be dynamically transformed between structural phases.

References

1. J. Park, Y. Ahn, K. C. Sampson, D. E. Savage, J. R. Prance, C. B. Simmons, M. G. Lagally, S. N. Coppersmith, M. A. Eriksson, M. V. Holt, and P. G. Evans, “*Electrode-stress-induced nanoscale disorder in Si quantum electronic devices*,” APL Mater. 4, 066102 (2016).
2. J. A. Tilka, J. Park, Y. Ahn, A. Pateras, K. C. Sampson, D. E. Savage, M. A. Eriksson, M. G. Lagally, M. V. Holt, and P. G. Evans, “*Combining Experiment and Optical Simulation in Coherent X-ray Nanobeam Characterization of Si/SiGe Semiconductor Heterostructures*,” J. Appl. Phys., in press (2016).
3. K. M. McElhinny, R. M. Jacobberger, A. J. Zaug, M. S. Arnold, and P. G. Evans, “*Graphene-induced Ge (001) surface faceting*,” Surf. Sci. 647, 90 (2016).
4. M. P. Cosgriff, P. Chen, S. S. Lee, H. J. Lee, L. Kuna, K. Pitike, W. D. Parker, L. Louis, H. Tajiri, S. Nakhmanson, J. Y. Jo, Z. Chen, L. Chen, and P. G. Evans, “*Nanosecond Phase Transition Dynamics in Compressively Strained Epitaxial $BiFeO_3$*,” Adv. Electron. Mater. 2, 1500204 (2016).

A. Acun et al. "Atomically Controlled Surfaces Interfaces and Nanostructures"
edited by A. Bianconi, A. Marcelli (Superstripes Press, Rome 2016) isbn: 9788866830597

Non-euclidean geometries in high temperature superconductors

Alessandro Ricci[1]
[1]*Deutsches Elektronen-Synchrotron DESY, Notkestraße 85, D-22607 Hamburg, Germany*

Email: *alessandro.ricci@desy.de*
Keywords: CDW inhomogeneity in HTS, nanoscale phase separation, correlated functional disorder in HTS

Functional materials like high temperature superconductors (HTS) and complex oxides are characterized by an *intrinsic complexity*. Indeed, they show the coexistence of multiple striped-orders like Charge-Density-Wave (CDW), Spin-Density-Wave (SDW) and defects that get organized in different striped nano-domains and exhibit a strong dynamic competition [1]. The study of the interplay among these multiple orders is challenging because their critical dynamics are strongly connected to the emerging of functional properties at the macroscopic scale. The first step to understand the competition between these multiple striped orders is the investigation of their spatial-organization. On this purpose we developed a set of innovative techniques like scanning micro X-ray diffraction (μXRD) and resonant scanning micro X-ray diffraction (RμXRD) to directly visualize the spatial-organization of the SDW, CDW and defects orders. We evidenced a common nanoscale phase separation scenario, characterized by the coexistence of competing scale-free networks of self-organized nano-domains promoting superconductivity [2-9]. Recently we discovered that the CDW stripes get self-organized in nano-domains defining a complex non-euclidean space available for the superconducting phase (Fig. 1) [10]. This open the way for completely new percolation theories for the interpretation of the microscopic mechanism of high temperature superconductivity.

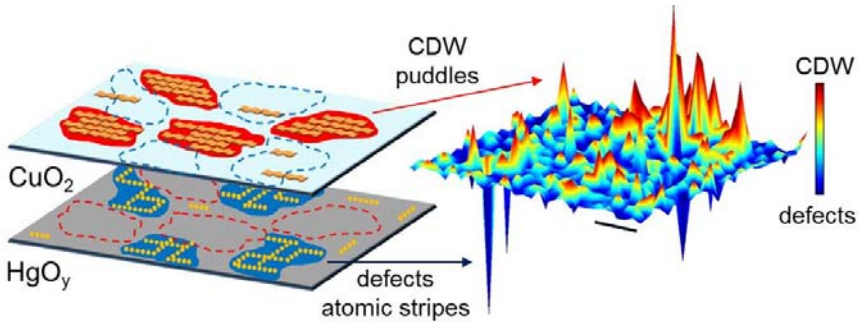

Figure 1: Spatial anti-correlation between CDW and defects domains [10].

References

1. A. Ricci, *Journal of Superconductivity and Novel Magnetism* 28, 1295-1298 (2015).
2. Y. Drees, Z. W. Li, A. Ricci, et al., *Nature Communications* 5, 5731+ (2014).
3. A. Ricci, et al., *New Journal of Physics* 16, 053030+ (2014).
4. A. Ricci, et al., *Scientific Reports* 3, 2383+ (2013).
5. N. Poccia, et al., *Nature Materials*, 10, 733-736 (2011).
6. A. Ricci, et al., *Physical Review B* 84, 060511+ (2011).
7. A. Ricci, et al. *Physical Review B* 91.2 020503 (2015).
8. M. Fratini, et al., *Nature* 466, 841 (2010).
9. N. Poccia, et al., *Proceedings of the National Academy of Sciences* 109, 15685 (2012).
10. G. Campi, et al. *Nature* 525, 359-362 (2015).

Molybdenum oxides films: conductivity properties vs. work function

Augusto Marcelli[1,2], Stefano Sarti[3], Bruno Spataro[1] and Giovanni Castorina[1,4]
[1]*INFN - Laboratori Nazionali di Frascati, Via E. Fermi 40, 00044 Frascati, Italy*
[2]*RICMASS, Rome International Center for Materials Science Superstripes, Via dei Sabelli 119A, 00185 Rome, Italy*
[3]*University of Rome Sapienza, Dipartimento di Fisica, 00185 Rome, Italy*
[4]*University of Catania, Dipartimento di Ingegneria Elettrica, Elettronica e Informatica, 95126 Catania, Italy*

Email: *marcelli@lnf.infn.it*
Key words: molybdenum films, annealed films, transport experiments, surface resistivity

As required by many different and extremely demanding applications, continuous efforts have been made in the last years to characterize and improve performances of metallic Transition Metal (TM) films and coatings. Indeed, morphology, structure and electronic properties of TMs films are very important in different technologies. However, these films are multiphase metallic films with not negligible contributions of several disordered oxide phases with different behaviors.
Among the many TM elements, Mo is a peculiar atom belonging to the Group 6 of the periodic table. It is characterized by a hot strength and a large creep resistance, has a Mohs hardness of 5.5, one of the lowest coefficients of thermal expansion and accounts for one of the highest melting point of any element. Although the solubility of oxygen in solid Mo is extremely low, the growth of Mo films is strongly affected by the presence of oxygen atoms and a complex phase diagram exist for the Mo–O system. With many phases corresponding to oxide compounds with both transparent and insulating phases, e.g., MoO_3, or metallic phases such as MoO_2 [1], molybdenum films and coatings are multiphase systems of high-interest for both fundamental and technological applications. Multiphase Mo films exhibit a resistivity less than one order of magnitude higher than the Mo bulk, actually comparable with MoO_x films.
All these films are characterized by percolative conductivity phenomena and make them extremely interesting to fabricate hard metallic coatings. However, different chemical and structural factors may affect their properties and, in particular, the work function. With the present day growing technology, it is actually difficult to control the properties of these films and also the work function. In order to tune TM oxides for specific applications, it is then mandatory to understand how chemical and structural factors affect their electronic properties. Recently, it has been demonstrated that, as a consequence of the relationship between defects and work function, many TM oxides tend to have decreased work functions near a metal/metal-oxide interface, a behavior useful to tune the work function according to applications [2].

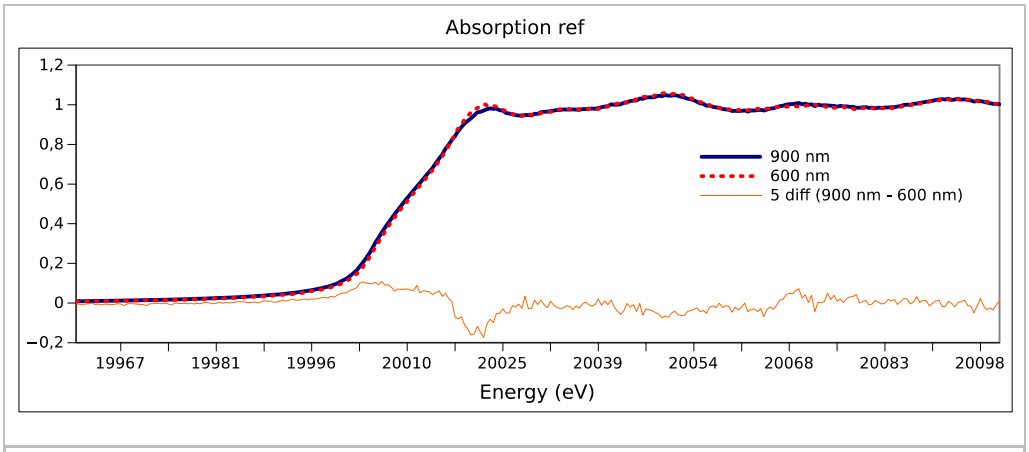

Figure 1: Comparison between two XANES spectra collected at the Mo K-edge of different thick films grown on copper. The lower curve is the difference of the two normalized spectra enhanced by a factor 5.

The interplay of nano- and micrometer-scale factors is typically at the origin of the properties and the macroscopic behavior of the TM systems such as Mo oxides, so that the capability to probe morphology and phase distribution of these complex systems at multiple length scale is mandatory. [3] Being a fast and local probe of a selected atom, X-ray Absorption Near Edge Spectroscopy (XANES) is a powerful technique suited to investigate the distribution of multi-scale/multi-phase highly correlated systems down to the micrometer scale and below using small spots. In the attempt to optimize Mo films to design and manufacture advanced high frequency accelerating structures characterized by performances well beyond those of the present copper based devices, [4] here we will present and discuss XANES data of Mo films of different thickness and discuss these results with transport properties measured on the same films. [5]

References

1. R. Goswami, H. Herman, S. Sampath, X. Jiang, Y. Tian, G. Halada, Surf. Coat. Technol. 141, 220–226 (2001)
2. Mark T. Greiner, Lily Chai, Michael G. Helander, Wing-Man Tang and Zheng-Hong Lu, Adv. Funct. Mater. 23, 215–226 (2013)
3. N. Poccia, M. Chorro, A. Ricci, Wei Xu, A. Marcelli, G. Campi and A. Bianconi, Appl. Phys. Lett. 104, 221903-1/ 221903-5 (2014)
4. S. Bini, B. Spataro, A. Marcelli, S. Sarti, V.A. Dolgashev, S. Tantawi, A.D. Yeremian, Y. Higashi, M.G. Grimaldi, L. Romano, F. Ruffino, R. Parodi, G. Cibin, C. Marrelli, M. Migliorati and C. Caliendo, Chinese Physics C 37, 097005-7 (2013)
5. A. Marcelli, B. Spataro, S. Sarti, V.A. Dolgashev, S. Tantawi, D.A. Yeremian, Y. Higashi, R. Parodi, A. Notargiacomo, Junqing Xu, G. Cappuccio, G. Gatti, G. Cibin, Surface & Coatings Technology 261, 391-397 (2015)

Th2T session

A. Acun et al. "Atomically Controlled Surfaces Interfaces and Nanostructures"
edited by A. Bianconi, A. Marcelli (Superstripes Press, Rome 2016) isbn: 9788866830597

Carbon nanotubes/silicon hybrid heterojunctions for solar cell applications

P. Castrucci,[1,] F. De Nicola,[1,$] M. Reali, [1,#] M. Salvato,[2,3] I. Cacciotti, [4] F. Nanni, [5] F. De Matteis, [6] P. Prosposito, [6] M. Crivellari, [7] M. Boscardin, [7] M. De Crescenzi [1]
[1]*Dipartimento di Fisica, Università di Roma Tor Vergata, via della Ricerca Scientifica 1, 00133 Roma, Italy*
[2] *Dipartimento di Fisica and MINAS Laboratory, Università di Roma Tor Vergata, Via della Ricerca Scientifica 1, 00133 Roma, Italy*
[3] *CNR-SPIN Salerno, Università di Salerno, Via Giovanni Paolo II 132, 84084 Fisciano, Italy*
[4] *Dipartimento di Ingegneria, Università di Roma Niccolò Cusano (INSTM-UdR), Via Don Carlo Gnocchi 3, 00166 Roma, Italy*
[5] *Dipartimento di Ingegneria dell'Impresa, Università di Roma Tor Vergata (INSTM-UdR Roma Tor Vergata), Via del Politecnico 1, 00133 Roma, Italy*
[6] *Dipartimento di Ingegneria Industriale and INSTM, Università di Roma Tor Vergata, Via del Politecnico 1, 00133 Roma, Italy*
[7] *Fondazione Bruno Kessler (FBK), Via Sommarive 18, 38123 Trento, Italy*

Email: *castrucci@roma2.infn.it*
Key words: Nanomaterials for energy; Nanotubes and other 1D materials

The significant growth of the Si photovoltaic industry has been so far limited due to the high cost of the Si photovoltaic system. In this regard, the most expensive factors are the intrinsic cost of silicon material and the Si solar cell fabrication processes. Conventional Si solar cells take advantage of *p-n* junctions for an efficient extraction of light-generated charge carriers. However, the *p-n* junction is normally formed through expensive processes requiring very high temperature (~1000°C). Therefore, several systems are currently under study to form heterojunctions at low temperatures. Among them, carbon nanotube (CNT)/Si hybrid solar cells are very promising, with power conversion efficiency (PCE) up to 17% for single wall carbon nanotubes (SWCNT) [1] and 10% for multiwall carbon nanotubes (MWCNT) [2]. In these cells, the *p*-type Si layer is replaced by a semitransparent CNT film deposited at room temperature on the *n*-doped Si wafer, thus giving rise to an overall reduction of the total Si thickness and to the fabrication of a device with cheaper methods at low temperatures. In particular, the CNT film coating the Si wafer acts as a conductive electrode for charge carrier collection and establishes a built-in voltage for separating photocarriers. Moreover, due to the CNT film optical semitransparency, most of the incoming light is absorbed in Si; thus the efficiency of the CNT/Si device is in principle comparable to that of a conventional Si one. However, one of the primary obstacles in realizing practical applications are the poor operational life-time of CNT/Si devices. In this work an overview of our recent PCE records for air-stable SWCNT and MWCNT/Si solar cells is reported. For these devices the CNT network on n-Si substrates is deposited by a simple, rapid, reproducible, and inexpensive

vacuum filtration process at room temperature. Moreover, a detailed discussion of the main factors at the basis of this device will be given.

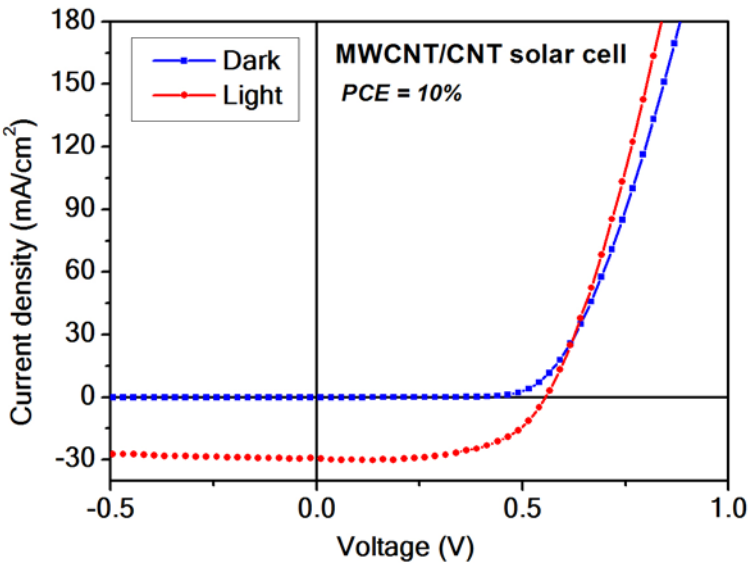

Figure 1: Best MWCNT/Si heterojunction solar cell in dark and light states after chemical doping by HNO_3 chemical exposition for 60s.

References

1. F. Wang, D. Kozawa, Y. Miyauchi, K. Hiraoka, S. Mouri, Y. Ohno & K. Matsuda, *Nature Comm*. 6, 6305 (2015).
2. F. De Nicola, M. Salvato, C. Cirillo, M. Crivellari, M. Boscardin, M. Scarselli, F. Nanni, I. Cacciotti, M. De Crescenzi, P. Castrucci, *Carbon* 101, 226-234 (2016).

[$] present address: IIT-Istituto Italiano di Tecnologia, Via Morego 30, Genova, 16163, Italy

[#] present address: INRS-Centre Énergie, Matériaux et Télécommunications, 1650 Blvd. Lionel-Boulet, C.P. 1020, Varennes, Québec J3X-1S2, Canada

A. Acun et al. "Atomically Controlled Surfaces Interfaces and Nanostructures"
edited by A. Bianconi, A. Marcelli (Superstripes Press, Rome 2016) isbn: 9788866830597

Self-Assembly and Surface Electronic Structure: the Case of Pentacene and Tetracene on noble metal (110) surfaces

E.G. Michel
[1]*Dto. de Física de la Materia Condensada and Condensed Matter Physics Center (IFIMAC)*
Universidad Autónoma de Madrid, 28049 Madrid, Spain

Email: *enrique.garcia.michel@uam.es*
Key words: Electronic and optical properties of surfaces and interfaces; Supramolecular structures and functionalization of surfaces and interfaces

Supramolecular chemistry is an interesting pathway to functionalize surfaces for a number of applications. The relative importance of molecule-molecule vs. molecule-substrate interaction in the formation of ordered structures of molecules on metal surfaces has deserved ample attention. Planar aromatic hydrocarbon molecules like pentacene lack the ability to form hydrogen bonds. Despite this fact, it has been proved that pentacene molecules interact with each other to form well-ordered structures on noble metal surfaces, and notable on (110)-oriented surfaces of Cu, Ag and Au. The complex behavior observed has been explained considering the different interactions present, and more exotic models [1-5].

We investigate whether the process of pentacene and tetracene self-assembly on Cu(110) and Ag(110) depends on the shape of the molecule and its detailed atomic structure, or whether it can be forced by the morphology and/or the electronic structure of the substrate. Angle-resolved photoemission with synchrotron radiation, scanning tunneling microscopy, and low-energy electron diffraction are combined with theoretical calculations in the DFT approximation to provide us with a complete data set on the behavior of pentacene and tetracene molecules in the low to intermediate coverage range.

We have observed that pentacene tends to form 1D wires running along the [1-10] direction even for very low coverages. Increasing the coverage results in different ordered arrays of molecular rows evenly spaced, and finally in a compact layer. The adsorption process modifies dramatically the Shockley surface state, which resides at the surface Y point on the clean (110) surfaces of Cu and Ag.

Additional modifications of the surface electronic structure are detected along the surface ΓX direction. From STM, angle resolved photoemission and theoretical calculations we discuss the role of the surface electrons in the molecule-molecule interaction, and the way they affect the self-assembling process

References

1. A. Scheybal et al. Phys. Rev. B 79, 115406 (2009).
2. Th. Ules et al, Phys. Rev. B 90, 155430 (2014).
3. P. Puschnig et al, Science 326, 702 (2009).
4. H. Yamane et al. Phys. Stat. Sol. (b) 5, 793 (2008).
5. M. Sauvage-Simkin et al, J.Phys. Chem. 118, 27815 (2014).

A. Acun et al. “Atomically Controlled Surfaces Interfaces and Nanostructures”
edited by A. Bianconi, A. Marcelli (Superstripes Press, Rome 2016) isbn: 9788866830597

Nonlinear response on solids by intense THz wave

Akinori Irizawa[1] , Takeshi Nagashima[2], Keigo Kawase[1], Kazuyuki Sakamoto[3], Shin-ichi Kimura[4], Atsushi Higashiya[2], Masaki Fujimoto[1], Goro Isoyama[1], and Shigemasa Suga[1]
[1]*ISIR, Osaka University, Japan*
[2]*Setsunan University, Japan*
[3]*AIS, Chiba University, Japan*
[4]*FBS, Osaka University, Japan*

Email: *irizawa@sanken.osaka-u.ac.jp*
Key words: nonlinear response; solids; far infrared; THz; FEL

Terahertz wave or far infrared light is on the boundary of radiowave and light in the energy scale of electromagnetic wave. It behaves as a high frequency radiowave and also a low energy photon. It consists of hundreds of fs or a few ps cycles of an electromagnetic field alternation in view of electromagnetic wave, and also is a several meV photon which is comparable to the energy scales of Drude response, phonon absorption in solids, and vibration and/or rotation in molecules.

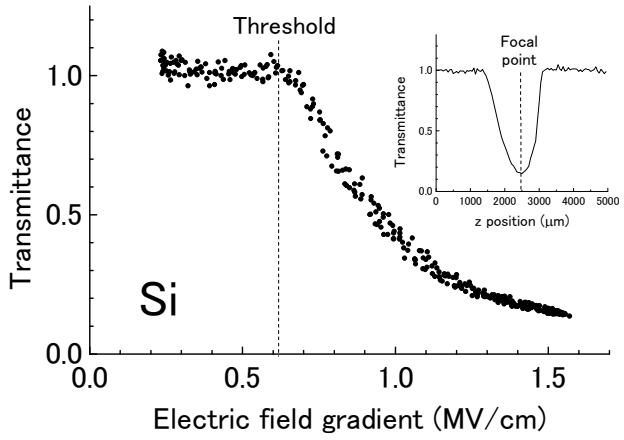

Figure 1: Nonlinear transmittance of Si.

Thus, the intense THz wave, i.e. the bright FIR light may cause novel final states on materials that must be quite different from those derived from high energy photons such as VIS, UV, and x-ray. THz free electron laser (FEL) has been developed at The Institute of Science and Industrial Research (ISIR) in Osaka University.[1] The wavelength can be controlled from 150 to 25 μm (2 to 12 THz). It consists of 5 Hz repeated macro pulses that include a micro pulse structure. The micro pulse length will be less than 20 ps

In this work nonlinear behaviors on typical semiconductors were derived by the monochromatic pulse THz FEL irradiation. The THz light was focused into 4σ~140 μm at the wavelength of 70 μm. The estimated electric field gradient was above 3 MV/cm. The z-scan method was employed for determining nonlinearity on samples. The change of transmittance was measured with changing the sample position along the optical axis, i.e. z axis. The FEL beam size at focal point was measured using knife edge. The beam profile was also observed at an off focal point using the THz viewer. It was resulted in a simple concentric distribution. Finally thresholds of nonlinearity was estimated with changing the intensity of THz FEL. Figure 1 shows the experimental results of z scanning and transmittance change of Si. The transmittance was suddenly decayed above the threshold of 0.6 MV/cm. The similar nonlinearities were observed for other semiconductors. Some of them were also accompanied by luminescence on the surfaces. The possible scenario is that the high electric field accelerates electrons during the half cycle of THz frequency, and the obtained kinetic energy is transformed to the potential energy. [2] The kinetic excitation of electrons should involve an impact ionization process which links to the decay process. We will touch the results of other samples in the presentation.

References

1. K. Kawase, R. Kato, A. Irizawa, et al., Nucl. Instrum. Meth. Phys. Res. A 726 (2013) 96-103. doi:10.1016/j.nima.2013.05.183.
2. H. Hirori, et al., Nature Commun. 2:594, Dec. 2011. doi:10.1038/ncomms1598.

A. Acun et al. "Atomically Controlled Surfaces Interfaces and Nanostructures"
edited by A. Bianconi, A. Marcelli (Superstripes Press, Rome 2016) isbn: 9788866830597

Photon induced ionization and fragmentation of isolated (endohedral) fullerenes by XUV radiation

Stefan Schippers[1]
[1]*I. Physikalisches Institut, Justus-Liebig-Universität Gießen, 35392 Giessen, Germany*

Email: *stefan.schippers@physik.uni-giessen.de*
Key words: fullerenes, endohedral fullerenes, gas phase, photoabsorption, photoionization, confinement resonances

Absorption of a single photon by an atoms, a molecules or a nanoparticle induces a complicated dynamics which may lead to the correlated emission of electrons by true many-body interactions [1-4] or to molecular breakup resulting in complex fragmentation patterns [5-7]. The photon-ion merged-beams techniqueis a sensitive tool for studying such elementary interactions by merging a beam of ionized atoms, molecules and mass-selected nanoparticles with a beam of energetic photons from a synchrotron radiation source (see [1] for a recent introductory review). In my talk I will present recent results from measurements on fullerene [3-5] and endohedral fullerene ions [6-9].

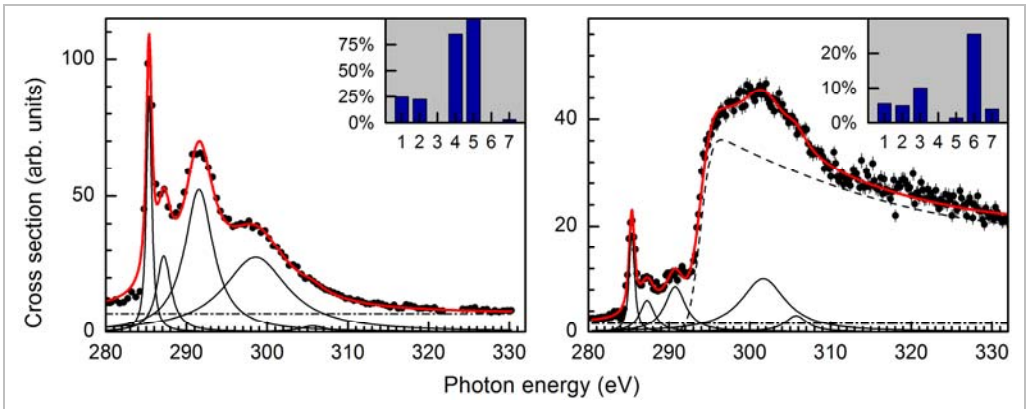

Figure 1: Measured (symbols) and fitted (lines) cross sections for single (left) and double (right) photoionization of $Lu_3N@C_{80}^+$ [7].

As an example, figure 1 shows measured cross sections for single and double ionization of $Lu_3N@C_{80}^+$ ions [7]. The single ionization cross section is dominated by resonant ionization processes while the double ionization cross section, in addition, exhibits a marked threshold due to the onset of direct K-shell ionization. Several common resonance features could be identified and their relative contributions to the

different cross sections were quantified. Further results include the first experimental study of confinement resonances in charged $Xe@C_{60}$ [8,9], a quantum mechanical interference phenomenon which - due to the high symmetry of this particular endohedral fullerene - manifests itself by distinct resonance features in the photoabsorption cross section.

References

1. S. Schippers, A. L. D. Kilcoyne, R. A. Phaneuf, and A. Müller, Contemp. Phys. 57, 215 (2016). http://dx.doi.org/10.1080/00107514.2015.1109771.
2. A. Müller et al., Phys. Rev. Lett. 114, 013002 (2015), http://dx.doi.org/10.1103/PhysRevLett.114.013002.
3. S. W. J. Scully et al., Phys. Rev. Lett. 94, 065503 (2005), http://dx.doi.org/10.1103/PhysRevLett.94.065503.
4. R. C. Bilodeau et al., Phys. Rev. Lett. 111, 043003 (2013), http://dx.doi.org/10.1103/PhysRevLett.111.043003.
5. K. K. Baral et al., Phys. Rev. A 93, 033401 (2016). http://dx.doi.org/10.1103/PhysRevA.93.033401.
6. A. Müller et al., Phys. Rev. Lett. 101, 133001 (2008). http://dx.doi.org/10.1103/PhysRevLett.101.133001.
7. J. Hellhund, A. Borovik Jr., K. Holste, S. Klumpp, M. Martins, S. Ricz, S. Schippers, and A. Müller, Phys. Rev. A 92, 013413 (2015). http://dx.doi.org/10.1103/PhysRevA.92.013413.
8. A. L. D. Kilcoyne et al., Phys. Rev. Lett. 105, 213001 (2010). http://dx.doi.org/10.1103/PhysRevLett.105.213001.
9. R. A. Phaneuf et al., Phys. Rev. A 88, 053402 (2013), http://dx.doi.org/10.1103/PhysRevA.88.053402.

A. Acun et al. "Atomically Controlled Surfaces Interfaces and Nanostructures"
edited by A. Bianconi, A. Marcelli (Superstripes Press, Rome 2016) isbn: 9788866830597

Epitaxial Silicene: Application to Nanoelectronics

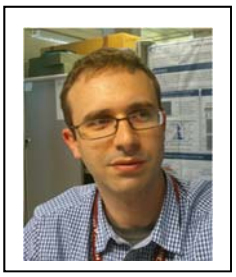

Alessandro Molle[1] , Carlo Grazianetti[1], Eugenio Cinquanta[1], Li Tao[2], Deji Akinwande[2]
[1] *CNR-IMM, Laboratorio MDM, via C. Olivetti 2, 20864 Agrate Brianza (MB), Italy*
[2] *Microelectronics Research Centre, The University of Texas at Austin, Texas 78758, USA*

Email: *alessandro.molle@mdm.imm.cnr.it*
Keywords: 2D materials, nanosheets, silicon, graphene

Realizing nanoelectronic devices based on atomically thin layers as active building blocks can pave the way to an ultimate scaling of the size features in line with the miniaturization trends, and can also envision new concepts and paradigms in nanoelectronics that may upset the current mainstream.[1,2] From both aspects, silicon at the two dimensional (2D) limit is a target material because of its natural affinity with the quite ubiquitous Si-based standards in nanotechnology. The recent rise of silicene[3] (i.e. the graphene counterpart of silicon illustrated in Fig. 1(a) as a buckled 2D lattice) constitutes a promising breakthrough in this sense which may concomitantly lead to the exploration of new and exotic physical scenarios such as the realization of 2D topological insulator. The epitaxy of silicene is here reported from the monolayer to the multilayer regime of growth on Ag(111)-based substrates.[4,5] A representative scanning tunneling microscopy image of the atomic structure of a silicene monolayer on Ag(111) is reported in Fig. 1(b). A methodology for the silicene encapsulation, delamination, and isolation is presented as enabling technology for device integration as illustrated in the sketch of Fig. 1(c).[6] Room temperature operation of field effect transistors incorporating silicene monolayer and multilayer as active channels for the carrier conduction is demonstrated. An ambipolar transport is presented as the hallmark of the electrical response from the silicene transistors opposed to other nanoscale silicon phases.
On the other hand, template engineering is also explored as alternative approach to create a metal-free platform for the technological implementation of silicene.[7] As a representative case, the epitaxy of silicene on MoS_2 templates is reported and the electronic band alignment between the two terms described. Silicene-on-MoS_2 is then integrated into a heterosheet junction transistor making evidence of an effective electrical transport at the Si/MoS_2 interface.
Possible advances in the functionalization of silicene are discussed which pave the way to multifunctional applications based on the same silicene platform. Finally, an overview of silicene contemporaries, germanene, stanene, borophene, etc., is discussed aiming at the exploration of the emerging class of 2D elementary materials and their potential impact on the nanotechnology framework.

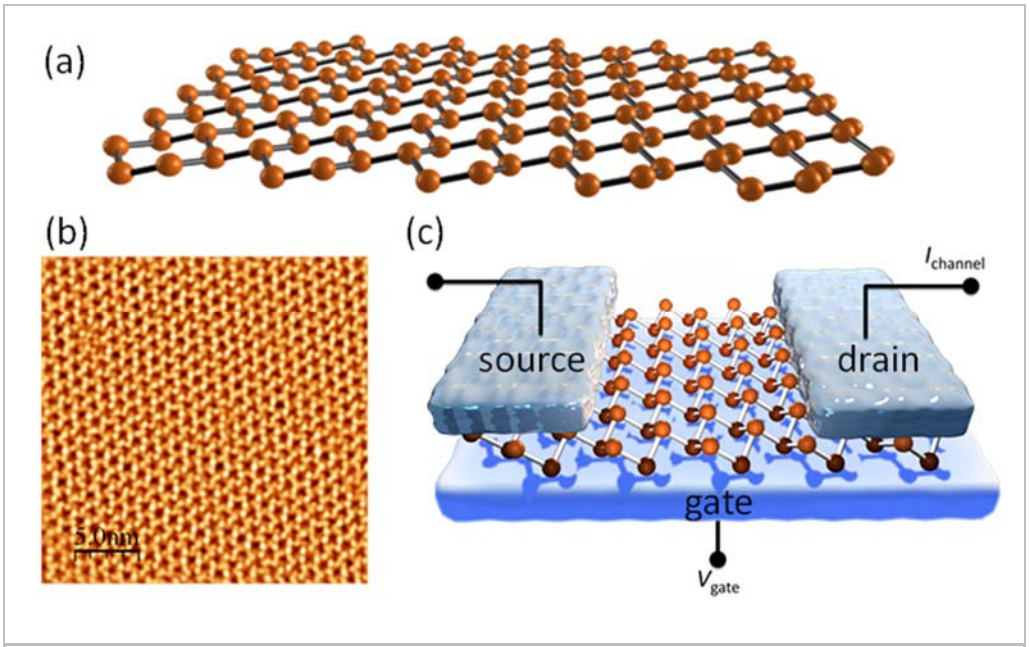

Figure 1: (a) Hard sphere model of a free-standing silicene sheet; (b) Scanning tunneling microscopy of a buckled sillicene phase supported by Ag(111); (c) Schematic picture of a silicene-based field effect transistor where the source and drain contacts are made of native Ag and the gate electrode consists of a SiO_2/Si substrate.

References

1. C. Grazianetti, E. Cinquanta, and A. Molle, *2D Materials* 3, 012001 (2016).
2. M. Houssa, A. Dimoulas, and A. Molle, *J. Physics: Condensed Matter* 27, 253002 (2015).
3. P. Vogt, P. de Padova, *et al.*, *Phys. Rev. Lett.* 108, 155501 (2012).
4. D. Chiappe, C. Grazianetti, *et al.*, *Adv. Mater.* 24, 5088 (2012).
5. C. Grazianetti, D. Chaippe, *et al.*, *J. Phys.: Condensed Matter* 27, 255005 (2015).
6. L. Tao, E. Cinquanta, et al., Nat. Nanotech. 10, 227 (2015)
7. A. Molle, A. Lamperti, *et al.*, *Adv. Mater. Interf.* (2016), DOI:10.1002/admi.201500619

Spin-Split Metallic Surface States of 2D Alloys and Compounds on.

A. A. Saranin[1,2], D. V. Gruznev[1,2], L. V. Bondarenko[1,2], A. V. Matetskiy[1,2], A. Y. Tupchaya[1,2], A. V. Zotov[1,2,3], S.V. Eremeev[4], J.-P. Chou[5], C.-R. Hsing[5], C.-M. Wei[5], S. Ichinokura[6], R. Hobara[6], A. Takayama[6], and S. Hasegawa[6]
[1]*Institute of Automation and Control Processes FEB RAS, Vladivostok, Russia*
[2]*Far Eastern Federal University, School of Natural Sciences, Vladivostok, Russia*
[3]*Department of Electronics, Vladivostok State University of Economics and Service, Vladivostok, Russia*
[4]*Institute of Strength Physics and Materials Science, Tomsk, Russia*
[5]*Institute of Atomic and Molecular Sciences, Academia Sinica, Taipei, Taiwan*
[6]*Department of Physics, University of Tokyo, Tokyo, Japan*

Email: *asaranin@gmail.com*
Key words: Atomic and nanoscale structure of surfaces and interfaces: advanced methods; Superconductors at nanoscale

The Rashba spin splitting [1] in the two-dimensional electron gas systems on semiconductors is considered to be the key concept for many promising spintronics applications. To combine Rashba-effect based spintronics with a silicon technology metallic surface states with a strong spin-orbit coupling on a silicon surface [2] are demanded. Unfortunately, the most of the metal/silicon systems with spin-split surface state bands (e.g., Bi/Si(111)$\sqrt{3}\times\sqrt{3}$, Tl/Si(111)1×1, Sb/Si(111)$\sqrt{3}\times\sqrt{3}$ and Pt/Si(110)"6"×5) are semiconducting. The only known exceptions are the Tl/Si(111)1×1 modified by adsorption of additional Tl [4]) and Au/Si(111)$\sqrt{3}\times\sqrt{3}$ modified by adsorption of In, Tl, Cs or Na [3]). It is worth noting that in both cases adsorbates do not alter the basic atomic arrangement of the pristine surface and their effect resides just in eliminating or generating surface defects (as in Au/Si(111) and Tl/Si(111), respectively) and doping electrons to the available surface-state bands. In the present study, we propose a strategy for tailoring the spin-split metallic surface states. The main concept resides in taking the surfaces with spin-split non-metallic surface-state bands and by alloying them with suitable metals to obtain dense reconstructions with spin-split metallic bands. Validity of the approach is demonstrated with Bi/Si(111)$\sqrt{3}\times\sqrt{3}$ alloyed with Na and Tl/Si(111)1×1 alloyed with Pb [5].

Recently we succeeded in the formation of a number of 2D alloys and compounds on the Si(111) surface with metallic spin split states: (i) sandwichlike structure made of one monolayer of Tl and one monolayer of Sn on Si(111) [6], (ii) Tl_xBi_{1-x} compound which represents a quasi-periodic tiling structures that are built by a set of tiling elements as building blocks [7] and (iii) Si(111)2×2-(Au,Al) with unusual spin texture [8]. We demonstrated that one atom layer Si(111)$\sqrt{3}\times\sqrt{3}$-Tl,Pb exhibits a giant Rashba-type spin splitting of metallic surface-state bands together with two-dimensional (2D) superconducting transport properties [9].

The work was supported by Russian Scientific Foundation (Grant 14-12-00479).

References

1. Y.A. Bychkov and E.I. Rashba, JETP Lett. 39, 78 (1984).
2. K. Yaji, Y. Ohtsubo, S. Hatta, H. Okuyama, K. Miyamoto, T. Okuda, A. Kimura, H. Namatame, M. Taniguchi, and T. Aruga, Nat. Commun. 1, 17 (2010).
3. L.V. Bondarenko, D.V. Gruznev, A.A. Yakovlev, A.Y. Tupchaya, D. Usachov, O. Vilkov, A. Fedorov, D.V. Vyalikh, S.V. Eremeev, E.V. Chulkov, A.V. Zotov, and A.A. Saranin, Sci. Rep. 3, 01826 (2013).
4. K. Sakamoto, T.-H. Kim, T. Kuzumaki, B. Müller, Y. Yamamoto, M. Ohtaka, J.R. Osiecki, K. Miyamoto, Y. Takeichi, A. Harasawa, S.D. Stolwijk, A.B. Schmidt, J. Fujii, R.I.G. Uhrberg, M. Donath, H.W. Yeom, and T. Oda, Nat. Commun. 4, 1 (2013).
5. D. V. Gruznev, L. V. Bondarenko, A. V. Matetskiy, A.A. Yakovlev, A.Y. Tupchaya, S. V. Eremeev, E. V. Chulkov, J.-P. Chou, C.-M. Wei, M.-Y. Lai, Y.-L. Wang, A. V. Zotov, and A.A. Saranin, Sci. Rep. 4, 04742 (2014).
6. D. V Gruznev, L. V Bondarenko, A. V Matetskiy, A.Y. Tupchaya, A.A. Alekseev, C.R. Hsing, C.M. Wei, S. V Eremeev, A. V Zotov, and A.A. Saranin, Phys. Rev. B 91, 035421 (2015).
7. D. V. Gruznev, L. V. Bondarenko, A. V. Matetskiy, A.Y. Tupchaya, E.N. Chukurov, C.R. Hsing, C.M. Wei, S. V. Eremeev, A. V. Zotov, and A.A. Saranin, Phys. Rev. B 92, 245407 (2015).
8. D. V. Gruznev, L. V. Bondarenko, A. V. Matetskiy, A.N. Mihalyuk, A.Y. Tupchaya, O.A. Utas, S. V. Eremeev, C.-R. Hsing, J.-P. Chou, C.-M. Wei, A. V. Zotov, and A.A. Saranin, Sci. Rep. 6, 19446 (2016).
9. A. V. Matetskiy, S. Ichinokura, L. V. Bondarenko, A.Y. Tupchaya, D. V. Gruznev, A. V. Zotov, A.A. Saranin, R. Hobara, A. Takayama, and S. Hasegawa, Phys. Rev. Lett. 115, 147003 (2015).

A. Acun et al. “Atomically Controlled Surfaces Interfaces and Nanostructures”
edited by A. Bianconi, A. Marcelli (Superstripes Press, Rome 2016) isbn: 9788866830597

Th3T session

2D germanene layers

M. E. Dávila[1] and G. Le Lay[2]
[1]*Instituto de Ciencia de Materiales de Madrid-ICMM-CSIC, C/Sor Juana Inés de la Cruz, 3 Cantoblanco, 28049-Madrid, Spain.*
[2]*Aix Marseille Université, CNRS, PIIM UMR 7345, 13397, Marseille, France.*

Email: *M.E.D. (email: mdavila@icmm.csic.es) or G.L.L. (email: guy.lelay@univ-amu.fr)*
Key words: Growth and applications of thin films; Graphene and other 2D materials; Nanoelectronics, molecular electronics

Two-dimensional (2D) materials attract major interest in both basic and applied research due to their unique structural and electronic properties. On special focus are those 2D materials which do not exist in nature[1]. Here, we will show the structural and electronic properties, using synchrotron-radiation-based photoemission, scanning tunneling microscopy imaging and surface electron diffraction techniques, from a single layer to few layer germanene, these layers we create artificially by dry epitaxy on a gold template[2].
In fact, until now germanene have been experimentally successfully synthesized recently on several metal substrates; Pt(111)[3], Au(111)[2] and Al(111)[4]. For germanene are expected many behaviors, such as the tunable band-gap by electric-field and much stronger spin–orbit interaction, displaying great potential in electronic and spintronic applications[5]. However, germanene shares a problem with silicene: one cannot utilize germanene's ultimate properties unless suitable substrates are found for germanene. Currently, ML germanene as mentioned can only be synthesized on metal surfaces, until now only in the case of Au(111) we show that few layer germanene posseses Dirac cones thanks to a reduced interaction, but electronic devices such as FETs require substrates with a large band-gap for this reason we will compare the results using different substrates and hopefully this will end up with the fabrication of the first germanene field-effect transistor (FET) in the near future as already exist on silicene[6].

References

1. J. Wang et al. National Science Review, 2, 22-39 (2015).
2. M.E. Dávila et al. New Journal of Physics 16 (9): 095002 (2014) and M.E. Dávila and G. Le Lay, accepted Nature Scientific Reports.
3. L. Li et al. Advanced Materials 26 (28): 4820–4824 (2014).
4. M. Derivaz et al. Nano Lett. 15, 2510−2516 (2015).
5. A. Acun et al. J. Phys. Condens. Matter. 27, 443002 (2015).
6. L. Tao et al., Nat. Nanotechnol.,10, 227-231 (2015).

A. Acun et al. "Atomically Controlled Surfaces Interfaces and Nanostructures"
edited by A. Bianconi, A. Marcelli (Superstripes Press, Rome 2016) isbn: 9788866830597

Atomic view of metal atom intercalation into black phosphor

Woei Wu Pai[1], Yi Reng Tzeng[2], Horng Tay Jeng[3]
[1]*Center for condensed matter sciences, National Taiwan University, Taipei Taiwan 106*
[2]*Institute of nuclear energy research, Long Tang, TaoYuan Taiwan 325*
[3]*Institute of physics, Academia Sinica, NanKang, Taipei Taiwan 115*

Email: *wpai@ntu.edu.tw*
Key words: Graphene and other 2D materials; Scanning probe and surface microscopy

Black phosphor (BP) is a promising material for electronics due to its non-zero band gap and good ambipolar carrier mobility [1]. One important issue for applications is the property of metal-BP contact and how it modifies the band gap of BP. BP subjected to ambient exposure is often p-doped and a high work function metal, such as platinum, is then a preferred choice of contact material.

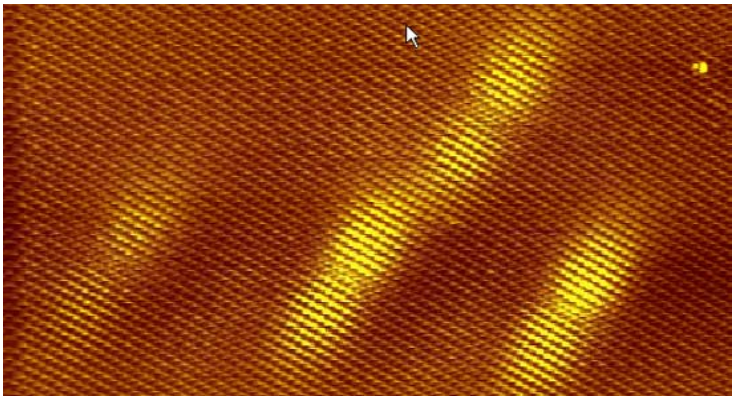

Figure 1: An atomic view of intercalated Pt on black phosphor surface.

We studied the initial stage of Pt deposition on in-situ vacuum-cleaved BP surface at either 300 K or 78 K with scanning tunneling microscopy. In both cases, Pt atoms do not stay atop the BP surface. Instead, peanut-like protrusions with overlayed BP atomic lattice was observed, as shown in figure 1. We interpreted this as Pt atoms intercalating into the van der Waals gap between the first and second BP layers. Ab-initio calculations indicate significant energy gain of intercalated Pt versus non-intercalated Pt, with >1 eV gain per Pt atom. Molecular dynamics simulations also reveal significant BP deformation upon Pt adsorption – which is expected to lead to possible paths of intercalation. For pristine in-situ vacuum-cleaved BP surface, we found a band gap value of ~0.3-0.4 eV close to the band gap value of bulk BP. This is in contrast to a

recent report claming a bulk BP surface has a ~2 eV band gap of a single BP layer [2]. Increased strain applied to BP surface also induces significant reduction of BP’s band gap value and eventually leads to metallic behavior. In contrast to a BP surface cleaved in air showing strongly p-doped character, in-situ vacuum-cleaved BP is nearly intrinsic. The band gap of BP appears to increase by ~0.2 eV near the Pt-intercalation sites and is consistent with theoretical calculations. Our results show that BP-metal interaction can be unexpectedly strong and can have significant effect on BP band gap. Finally, Au adsorption on BP will be compared with the Pt case.

References

1. Likai Li, Yijun Yu, Guo Jun Ye, Qingqin Ge, Xuedong Ou, Hua Wu, Donglai Feng, Xian Hui Chen, and Yuanbo Zhang, Nature Nanotechnology, 9, 372 (2014)
2. Liangbo Liang, Jun Wang, Wenzhi Lin, Bobby G. Sumpter, Vincent Meunier, and MingHu Pan, Nano Letters, 14, 6400 (2014)

Initial stage of growing of Si on Si(111)√3-√3-Pb surface

Agnieszka Stępniak-Dybala[1], Mieczysław Jałochowski[1], Mariusz Krawiec[1]
[1]*Maria Curie-Skłodowska University in Lublin*

Email: *agnieszka.stepniak@poczta.umcs.lublin.pl*
Key words: Silicon, two-dimensional materials, superstructure, silicene, lead, STM/STS.

A single layer of Si atoms ordered in a two-dimensional honeycomb structure has been attracting increasing scientific and technological interest in view of the exploration of its electronic properties. This new material, called silicene, is difficult to realize as a free standing layer. Therefore an appropriate substrate has to be chosen. Studies show that silicen can be obtained on the Ag(110) and Ag(111) surfaces [1-3], on ZrB2 [4], Ir(111) [5]. Since silicene cannot be prepared by exfoliation, interaction between silicene and the substrate has to considered. Consequently, the electronic structure of the silicene can be modified dramatically by changing the substrate. This effect, although inevitable, may be employed to tune the electronic structure of this material [6,7]. We provide first experimental results on one monolayer of Si on the Si(111)√3×√3-Pb surface. We use Low Temperature-Scaning Tunneling Microscopy and Spectroscopy (LT-STM/STS) to characterize structural and electronic properties of the system at liquid helium temperatures. Our STM/STS investigations reveal, that Si deposited onto √3×√3-Pb surface forms small nanoflakes which may be identified as silicene. This work has been supported by the National Science Centre (Poland) under Grant No. DEC-2014/15/B/ST5/04244.

References

1. B. Aufray, A. Kara, S. Vizzini, H. Oughaddou, C. Lenardi, B. Ealet, G. Le Lay, Appl. Phys. Lett. 96, 183102 (2010), http://dx.doi.org/10.1063/1.3419932
2. P. Vogt, P. De Padova, C. Quaresima, J. Avila, E. Frantzeskakis, M.C. Asensio, A. Resta, B. Ealet, G. Le Lay, Phys. Rev. Lett. 108, 155501 (2012), http://dx.doi.org/10.1103/PhysRevLett.108.155501
3. H. Jamgotchian, Y. Colignon, N. Hamzaoui, B. Ealet, J. Y. Hoarau, B. Aufray and J. P. Bibérian, J. Phys.: Condens. Matter , 172001 (2012).
4. A. Fleurence, R. Friedlein, T. Ozaki, H. Kawai, Y. Wang, and Y. Yamada-Takamura, Phys. Rev. Lett. 108, 245501 (2012), http://dx.doi.org/10.1103/PhysRevLett.108.245501
5. L. Meng, Y. Wang, L. Zhang, S. Du, R. Wu, L. Li, Y. Zhang, G. Li, H. Zhou, W.A. Hofer, H. Gao, Nano Lett. 13, 685 (2013), DOI: 10.1021/nl304347w
6. A. Podsiadły-Paszkowska, M. Krawiec, Phys. Chem. Chem. Phys. 17, 2246 (2015).
7. A. Podsiadły-Paszkowska, M. Krawiec, Phys. Rev. B. 92, 165411 (2015) http://dx.doi.org/10.1103/PhysRevB.92.165411

A. Acun et al. “Atomically Controlled Surfaces Interfaces and Nanostructures”
edited by A. Bianconi, A. Marcelli (Superstripes Press, Rome 2016) isbn: 9788866830597

Electronic Properties of Nanoribbons: Graphenen and Silicene

Osamu Kubo[1] , Nobuya Mori[1], Hiroshi Tabata[1], Mitsuhiro Katayama[1]
[1]*Graduate School of Engineering, Osaka University*

Email: *okubo@eei.eng.osaka-u.ac.jp*
Key words: Graphene and other 2D materials, Scanning probe and surface microscopy

Nanoribbons made of graphene and other group IV materials have recently attracted great attention because of their unique properties. In particular, graphene nanoribbons (GNRs) have been studied in many groups, and it has been theoretically predicted that the quantum-confined structure forms a bandgap in armchair GNRs (A-GNRs) while edge state is localized at the zigzag edge. [1,2]

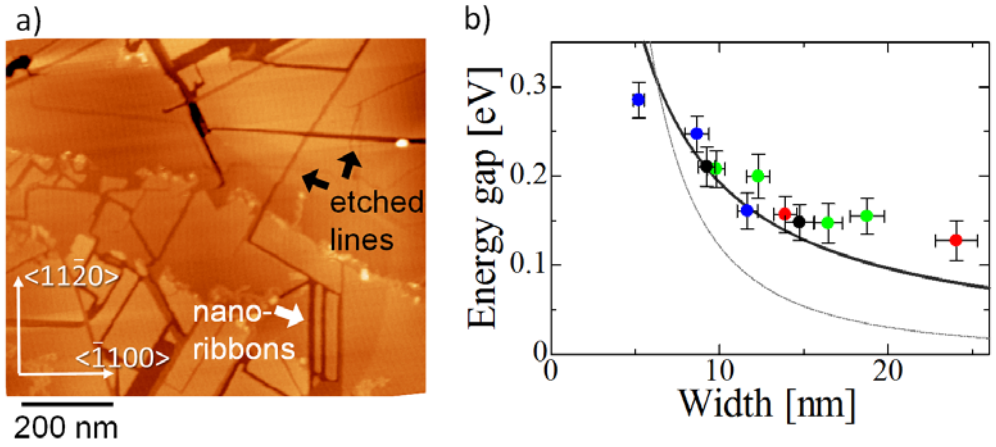

Figure 1:
(a) Three-dimensional STM image of HOPG surface after crystallographic etching (V_s = 1.0 V, I_t = 80 pA). GNRs are unintentionally found as shown by the white arrow. The scale of the image is 1 × 1 μm^2.
(b) Experimentally estimated energy gaps as a function of width of A-GNRs. The blue, green, red, and black plots were obtained on monolayer, bilayer, trilayer, and four-layer GNRs, respectively. The solid line shows the inverse proportional fitting of the data, while the dotted line shows the theoretical result obtained by tight-binding calculation.

Experimental reports on GNRs has recently been increasing. However, there are still few reports on the electronic properties of GNRs systematically examined with changing widths and layer numbers. In this study, GNRs with various widths and layer

numbers are formed on a highly oriented pyrolytic graphite (HOPG) surface by crystallographic etching method,[3] and their local density of states (LDOS) is systematically evaluated by scanning tunneling spectroscopy (STS) in ultrahigh vacuum chamber at 78K.[4] We confirmed that the energy gap of the LDOS depression monotonically decreases with increasing GNR width, whereas there is no apparent dependence on the layer numbers (Fig. 1). From the quantitative scaling of energy gaps of LDOS depression with respect to GNR widths, the relation between the two is obtained as $E_{gap} = 1.9$ [eVnm]/W.

We also examined the LDOS of silicene nanoribbons (SiNRs). Silicene is a two-dimensional (2D) honeycomb structure formed by Si atoms. According to theoretical studies, silicene has cone-like band dispersion at Dirac point, similarly to graphene, and has superior characteristics not found in graphene such as *tunable* band gap by electric fields.[5] Though many studies are recently reported on silicene formation, [6,7] the first silicene experimentally reported is not a 2D silicene but a one dimensional (1D) silicene nanoribbon (SiNR) which is formed on Ag(110).[8,9] It was revealed by angle-resolved photoemission spectroscopy that linear electronic band dispersion were formed in the densely-arranged SiNRs along the direction of their longitudinal axis, which was the first evidence of Dirac fermion in silicene.[8,9] However, it has not been much reported for the local electronic density of states (DOS) of individual SiNRs [10], and the origin of the linear electronic band dispersion in 1D system is still not clear. In this study, we present local distribution of the DOS on the SiNRs array formed on Ag (110) by differential conductance (dI/dV) mapping, and suggest the origin of their linear electronic band dispersion.

This work was supported by JSPS KAKENHI Grant Number 26286052.

References

1. M. Fujita, et al., J. Phys. Soc. Jpn. 65, 1920 (1996).
2. K. Nakada, et al., Phys. Rev. B 54, 17954 (1996).
3. S. S. Datta, et al., Nano Lett. 8, 1912 (2008).
4. Y. Sugiyama, et al., Appl. Phys. Lett. 105, 123116 (2014).
5. M. Ezawa et al., Phys. Rev. Lett. 109, 055502 (2012).
6. P. Vogt et al., Phys. Rev. Lett. 108, 155501 (2012).
7. A. Fleurence et al., Phys. Rev. Lett. 108, 245501 (2012).
8. P. De Padova et al., Appl. Phys. Lett. 96, 261905 (2010).
9. P. De Padova, O. Kubo, et al., Nano Lett. 12, 5500 (2012).
10. F. Ronci, et al., Phys. Status. Solidi C 7, 2716 (2010).

A. Acun et al. “Atomically Controlled Surfaces Interfaces and Nanostructures”
edited by A. Bianconi, A. Marcelli (Superstripes Press, Rome 2016) isbn: 9788866830597

Accessing the electronic structure of armchair graphene nanoribbons by in-situ intercalation

Okan Deniz[1] , Carlos Sanchez-Sanchez[1], Roman Fasel[1], Pascal Ruffieux[1]
[1]*Swiss Federal Laboratories for Materials Science and Technology, Empa, 8600 Dübendorf, Switzerland*

Email: *okan.deniz@empa.ch*
Key words: Graphene nanoribbons, on-surface synthesis, intercalation, scanning tunneling spectroscopy

Graphene nanoribbons (GNRs) attract considerable interest due to their width-tunable electronic band gap. However, precise band gap engineering is only maintained by controlling width and edge topology with atomic precision.
This ultimate structural precision has so far only been achieved using a bottom-up fabrication approach where GNRs are synthesized by surface-assisted colligation and subsequent cyclodehydrogenation of specifically designed precursor monomers [1,2]. The main drawback of this strategy is the need for the metal substrate as a reaction catalyst.

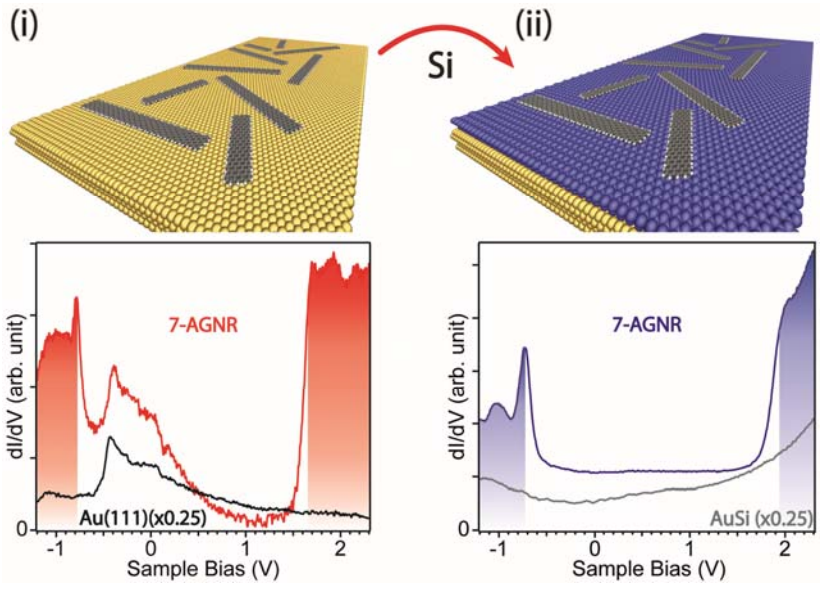

Figure 1: Schematic of in-situ Si intercalation approach with the STS spectra of 7-AGNR on corresponding substrate

Therefore the electronic properties of GNRs are strongly dominated by the screening effect and the surface state, which are intimately linked to preferred metallic growth substrate such as Au(111) [2,3]. One approach to access the GNRs' electronic properties is to intercalate an ultra-thin dielectric layer in-situ which allows for an atomically clean interface.
We have successfully intercalated Si in-situ into the 7, 9, 14, 18 and 21- armchair GNRs (AGNRs)/Au(111) interface and resolved GNRs' frontier states by suppressing the Au(111) surface state, which allows us to unambiguously determine the band gap of armchair GNRs and to test their width-dependent magnitude with available theoretical predictions.
Furthermore, we performed MgO intercalation at the 7-AGNR/Au(111) interface and tracked the band gap by scanning tunneling spectroscopy [4].
In this talk, we will report our experimental findings and point out the importance of the in-situ intercalation for GNRs aimed for a clear understanding of their electronic properties for future electronics.

References

1. J. Cai, P. Ruffieux, R. Jaafar, M. Bieri, T. Braun, S. Blankenburg, M. Muoth, A.P. Seitsonen, M. Saleh, X. Feng, K. Muellen, and R. Fasel, Nature 466, 470 (2010). http://dx.doi.org/10.1038/nature09211.
2. P. Ruffieux, J. Cai, N.C. Plumb, L. Patthey, D. Prezzi, A. Ferretti, E. Molinari, X. Feng, K. Müllen, C.A. Pig-nedoli, and R. Fasel, ACS Nano 6, 6930 (2012). http://dx.doi.org/10.1021/nn3021376.
3. J. Cai, C.A. Pignedoli, L. Talirz, P. Ruffieux, H. Söde, L. Liang, V. Meunier, R. Berger, R. Li, X. Feng, K. Müllen, and R. Fasel, Nat. Nanotechnol. 9, 896 (2014).http://dx.doi.org/10.1038/nnano.2014.184.
4. H. Söde, L. Talirz, O. Gröning, C.A. Pignedoli, R. Berger, X. Feng, K. Müllen, R. Fasel, and P. Ruffieux, Phys. Rev. B 91, 045429 (2015). http://dx.doi.org/10.1103/PhysRevB.91.045429.

A. Acun et al. "Atomically Controlled Surfaces Interfaces and Nanostructures"
edited by A. Bianconi, A. Marcelli (Superstripes Press, Rome 2016) isbn: 9788866830597

Photoluminescence Imaging Spectroscopy of Water Adsorption Layer on a Suspended Single-walled Carbon Nanotube

Shohei Chiashi[1] , Kazuki Yoshino[2], Takashi Kato[2], Yoshikazu Homma[2]
[1]*Department of Mechanical Engineering, The University of Tokyo*
[2]*Department of Physics, Tokyo University of Science*

Email: *chiashi@photon.t.u-tokyo.ac.jp*
Key words: Single-walled carbon nanotube, photoluminescence, photoluminescence, imaging spectroscopy, adsorption and desorption

Single-walled carbon nanotube (SWNT) is a rolled-up graphene. Since the interaction between graphene and water molecule is weak, the outer surface of SWNTs is regarded as hydrophobic surface. However, we have found that stable adsorption layer of water exist on the outer surface of SWNTs using photoluminescence (PL) spectroscopy, Raman scattering spectroscopy and molecular dynamics (MD) simulation [1, 2]. PL spectroscopy elucidates that water exhibits adsorption and desorption phenomena at transition pressure and the transition pressure depends on temperature of SWNT and water vapor. On the other hand, MD simulation shows that the water molecules on the SWNT surface form two-layered structure and most of their hydrogen-bonds are parallel to SWNT surface. It is interesting to understand the collective behavior of water molecules weakly trapped with SWNT surface, which have nano-scale curvature. In this study, we investigated the adsorption phenomena of water molecules by using PL imaging spectroscopy and discussed the dynamics of water adsorption.
PL imaging spectroscopy were performed to SWNTs suspended between a pair of silica pillars. SWNTs were synthesized on the basis of alcohol catalytic chemical vapor deposition (ACCVD) method [3]. Because the SWNTs were grown from metal nano-particles and the metal particles were deposited on only pillar top area, SWNTs grew from the pillar top and suspended SWNTs were effectively obtained. A Ti:sapphire laser was used for excitation and PL images were measured by a 2D allayed detector through a tunable band-pass filter.
Figure 1(A) shows SEM image of suspended SWNT. It shows that SWNTs are grown from only pillar tops and one of them are suspended. When suspended SWNTs have semiconducting property and are isolated, they emit PL signal. PL images were measured from suspended SWNTs in different water vapor pressure at room temperature. Figure 1(B) shows PL image of semiconducting SWNT. While PL emission wavelength was approximately 1290 nm at higher pressure, it was 1250 nm at lower pressure. In the case of higher and lower pressure, the emission wavelength was uniform along the tube axis. On the other hand, at intermediate pressure, the PL emission wavelength showed spatial distribution, as shown in Fig. 1(B). Water molecules did not adsorb at the center part, while they adsorbed at the edges. We will

discuss the adsorption and desorption dynamics on SWNT surface on the basis of the experimental results.

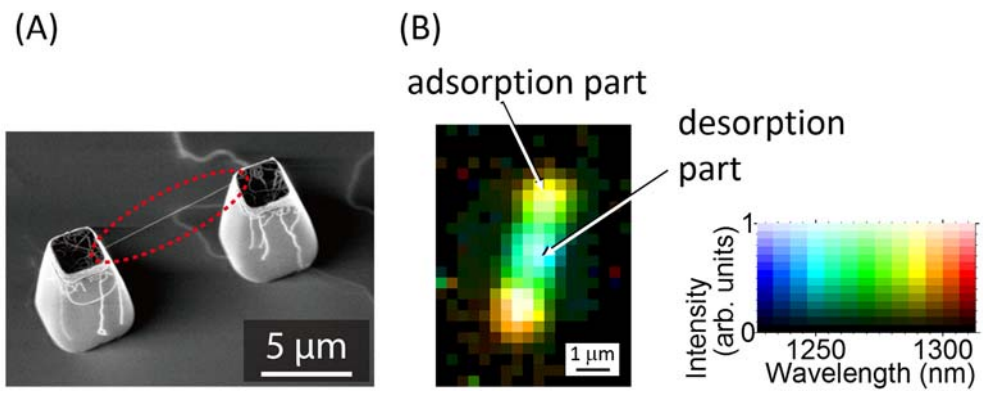

Figure 1: (A) SEM image and (B) PL image of suspended SWNT. The PL image was measured in water vapor (1.5 Torr).

References

1. Y. Homma, S. Chiashi, T. Yamamoto, K. Kono, D. Matsumoto, J. Shitaba, and S. Sato, *Phys. Rev. Lett.*, 110, 157402 (2013). http://dx.doi.org/10.1103/PhysRevLett.110.157402
2. S. Chiashi, K. Kono, D. Matsumoto, J. Shitaba, N. Homma, A. Beniya, T. Yamamoto, and Y. Homma, *Phys. Rev. B*, 91, 155415 (2015). http://dx.doi.org/10.1103/PhysRevB.91.155415
3. S. Maruyama, R. Kojima, Y. Miyauchi, S. Chiashi, and M. Kohno, *Chem. Phys. Lett.*, 360, 229 (2002). http://dx.doi.org/10.1016/S0009-2614(02)00838-2

A. Acun et al. “Atomically Controlled Surfaces Interfaces and Nanostructures”
edited by A. Bianconi, A. Marcelli (Superstripes Press, Rome 2016) isbn: 9788866830597

Th3S session

A. Acun et al. "Atomically Controlled Surfaces Interfaces and Nanostructures"
edited by A. Bianconi, A. Marcelli (Superstripes Press, Rome 2016) isbn: 9788866830597

Non-vortical Rashba spin structure induced by the C_{1h} symmetry of the surface

K. Sakamoto[1], E. Annese[1], T. Kuzumaki[1], B. Müller[1], Y. Yamamoto[1], H. Ishikawa[1], H. Nakano[2], A. Harasawa[3], Y. Takeichi[3], K. Yaji[3], T. Shirasawa[3], K. Miyamoto[4], K.-i. Nittoh[5], K. Miki[5], H.W. Yeom[6], T. Oda[2]
[1]*Dept. of Nanomaterials Science, Chiba Univ., Japan*
[2]*Institute of Science and Engineering, Kanazawa Univ., Japan*
[3]*ISSP, The University of Tokyo, Japan*
[4]*HiSOR, Hiroshima Univ., Japan*
[5]*National Institute for Materials Science, Japan*
[6]*Dept. of Physics, POSTECH, Korea*

Email: *kazuyuki_sakamoto@faculty.chiba-u.jp*
Key words: Rashba effect, Spin-polarized electronic bands, Symmetry, Photoelectron spectroscopy, Low-energy electron diffraction, Scanning tunneling microscopy, First-principles theoretical calculation

In this paper, we report a totally novel spin-structure found on a surface with C_{1h} symmetry by spin- and angle-resolved photoelectron spectroscopy, and first-principles theoretical calculation. The spin-polarized band originates from the Rashba-Bychkov (RB) effect [1] and the constant energy contour of the upper RB split band has a warped elliptical shape centered at a *k* point without time-reversal symmetry. The spin-polarization vector of this state is in-plane, and points almost the same direction along the whole elliptic contour. This novel non-vortical RB spin structure is confirmed as a general phenomenon originating from the C_{1h} symmetry.

RB effect is an exotic low-dimensional solid-state property that produces a spin-polarized two-dimensional electron gas from a combined effect of spin-orbit coupling and structural inversion asymmetry even for nonmagnetic materials. In an ideal two-dimensional system, the constant energy contour shows isotropic vortical spin structures around the Γ point, with the spin orientation locked in-plane and perpendicular to the electron momentum. In real surface, however, the RB effect is known to show variety of spin structures depending on the symmetry of the *k* point of the surface Brillouin zone (SBZ) [2,3], i.e., a *k* point with C_3 symmetry shows spins with polarization vector perpendicular to the surface [3-5]. The focus of this work is to investigate the RB spin of a surface that has a C_{1h} symmetry, which holds the potential to yield a novel spin structure that should be insensitive to back scattering.

The constant energy contour of the upper RB branch of the Si(110)-(1x1) surface, which is formed by the adsorption of one monolayer of Thallium and has a C_{1h} symmetry, is shown in Fig. 1. This constant energy contour is totally different from those of ordinary RB effect that show two concentric circles with their center at the Γ point. This difference comes from the lack of rotational symmetry of this surface. In

this paper, we will also discuss the origin of this peculiar locked-spin structure based on the symmetry of the surface.

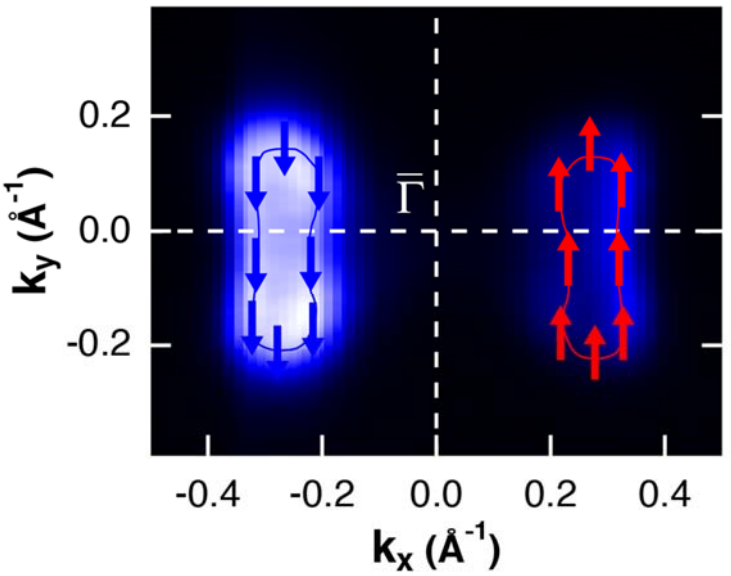

Figure 1: Constant energy contour at E_B=100 meV with superimposed spin orientation obtained by spin-and angle resolved photoelectron spectroscopy.

References

1. Y. A. Bychkov and E. I. Rashba, JETP Lett. 39, 78 (1984).
2. E. Frantzeskakis and M. Grioni, Phys. Rev. B 84, 155453 (2011). http://dx.doi.org/10.1103/PhysRevB.84.155453.
3. T. Oguchi and T. Shishidou, J. Phys.: Condens. Matter 21, 092001 (2009). http://dx.doi.org/10.1088/0953-8984/21/9/092001.
4. S. D. Stolwijk, A. B. Schmidt, M. Donath, K. Sakamoto, and P. Krüger, Phys. Rev. Lett. 111, 176402 (2013). http://dx.doi.org/10.1103/PhysRevLett.111.176402
5. K. Sakamoto *et al.*, Nat. Commun. 4:2073 doi: 10.1038/ncomms3073 (2013).

A. Acun et al. “Atomically Controlled Surfaces Interfaces and Nanostructures”
edited by A. Bianconi, A. Marcelli (Superstripes Press, Rome 2016) isbn: 9788866830597

Theory of localized plasmons for 2D and 3D metal nanostructures in the random phase approximation

Masakazu Ichikawa
University of Tokyo, Department of Applied Physics

Email: *ichikawa@ap.t.u-tokyo.ac.jp*
Key words: Graphene and other 2D materials, Theory of localized plasmons for metal nanostructures, Nanophotonics and plasmonics for 2D and 3D materials

Localized surface plasmons can concentrate optical waves into regions that are much smaller than their wavelengths and can also greatly enhance their local electric fields at surface plasmon excitation energies. These have opened a field called plasmonics [1] and a new field called graphene plasmonics has recently developed, where the plasmon energies can be varied over a wide range by gating graphene sheets [2].
Many theoretical studies of the localized plasmons in metal nanostructures have been reported until now [3]. We have also reported a theory of localized plasmons for metal nanostructures in the random phase approximation (RPA) [4] and have recently developed it to consider the retardation of the electromagnetic potentials [5, 6].
In this presentation, we report theories of localized plasmons for two dimensional (2D) and three dimensional (3D) materials and their applications to the metal nanostructures.
Neglecting the retardation of the scalar potentials, an effective scalar potential $\varphi_{eff}(\mathbf{r},\omega)$ and an external scalar potential $\varphi_{ext}(\mathbf{r},\omega)$ satisfy the following equation in the RPA at high-frequency condition (palsmon frequency region) [5]:

$$\varphi_{eff}(\mathbf{r},\omega)=\varphi_{ext}(\mathbf{r},\omega)+\frac{e^2}{m_e\omega^2}\int \mathrm{d}\mathbf{r}_1\, n(\mathbf{r}_1)\nabla_1\frac{1}{|\mathbf{r}-\mathbf{r}_1|}\cdot\nabla_1\varphi_{eff}(\mathbf{r}_1,\omega), \quad (1)$$

where m_e is the electron mass, $n(\mathbf{r}_1)$ is the local electron density which is expressed by $n(\mathbf{r}_1)=\sum_n n_0(\mathbf{r}_1-\mathbf{R}_n)$ for multiple metal nanostructures and $\mathbf{R}_n$ is the position of the each nanostructure.
Considering a case of periodic metal nanospheres where the electron density is assumed to have a step function shape at the each nanosphere surface ($r=a$), the following determinant is derived to calculate the dispersion relation for the surface plasmon using the Bloch’s theorem:

$$\det\left[\left(\omega^2-\frac{\omega_p^2\, l}{2l+1}\right)\delta_{ll'}\delta_{mm'}-\frac{\omega_p^2\, l'\, a^{l'+1}}{(2l'+1)}B_{lm;l'm'}(\mathbf{k},a)\right]=0, \quad (2)$$

$$\because B_{lm;l'm'}(\mathbf{k},a)=\sum_{\mathbf{R}_n\neq\mathbf{R}_s}\exp\left[i\mathbf{k}\cdot(\mathbf{R}_n-\mathbf{R}_s)\right]\int \mathrm{d}\Omega_{\mathbf{r}}\left.\frac{Y_{lm}^*(\mathbf{r})Y_{l'm'}(\mathbf{r}+\mathbf{R}_s-\mathbf{R}_n)}{|\mathbf{r}+\mathbf{R}_s-\mathbf{R}_n|^{l'+1}}\right|_{|\mathbf{r}|=a}, \quad (3)$$

where ω_p is the bulk plasmon frequency, $\mathbf{k}$ is the wave number vector of the surface plasmon, $Y_{lm}(\mathbf{r})$ is the normalized spherical harmonics and $\Omega_{\mathbf{r}}$ is the solid angle for $\mathbf{r}$. When the nanospheres are aligned on the z axis with equal spacing R, Eq. (2) gives the following dispersion relation of the surface plasmon frequency in the dipole approximation ($l = l' = 1,\ m = m' = 0$):

$$\omega_{sp}(k_z) = \frac{\omega_p}{\sqrt{3}}\sqrt{1-(a/R)^2\left[(k_z R-\pi)^2-\pi^2/3\right]}, \quad (4)$$

where k_z is the z-component of $\mathbf{k}$. Figure 1 shows the dispersion relations calculated by changing the a/R ratio, indicating that the surface plasmon frequency can be widely tuned by changing the ratio.

An equation for the effective scalar potential of 2D materials can be derived by assuming that $n(\mathbf{r}_1) \approx n_{2D}(\mathbf{X}_1)\delta(z_1)$ ($\delta(z_1)$ is the delta function) in Eq. (1):

$$\varphi_{eff}(\mathbf{X},\omega) = \varphi_{ext}(\mathbf{X},\omega) + \frac{e^2}{m_e\omega^2}\int d\mathbf{X}_1\, n_{2D}(\mathbf{X}_1)\nabla_{\mathbf{X}_1}\frac{1}{|\mathbf{X}-\mathbf{X}_1|}\cdot\nabla_{\mathbf{X}_1}\varphi_{eff}(\mathbf{X}_1,\omega). \quad (5)$$

Using Eq. (5), the planar plasmon ($\omega_{pl}(k)$) in a uniform 2D layer and the edge plasmon (ω_{ed}^m) in a nanodisk with radius of a are given by

$$\omega_{pl}(k) = \sqrt{\frac{2\pi e^2 n_{2D}\,k}{m_e}}, \quad \omega_{ed}^m = \sqrt{\frac{\pi e^2 n_{2D}}{m_e a}\int_0^\infty ds\, s\left[J_{m-1}(s)-J_{m+1}(s)\right]J_m(s)}, \quad (6)$$

where n_{2D} is the constant 2D electron density and $J_m(s)$ is the Bessel function.

We also compare the above results with those calculated for the plasmons in a single layer graphene where the electrons satisfy the 2D Weyl equation.

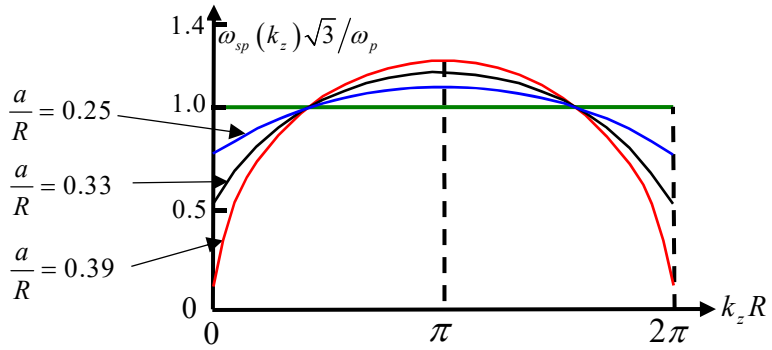

Figure 1: Dispersion relation of the surface plasmon for periodic metal nanospheres

References

1. S. A. Maier, Plasmonics (Springer, New York, 2007) p.1~p.219.
2. F. J. García de Abajo; ACS Photonics 1, 135 (2014).

3. M. I. Stockman, Opt. Express 19, 22029 (2011).
4. M. Ichikawa, J. Phys. Soc. Jpn 80, 044606 (2011).
5. M. Ichikawa, e-J. Surf. Sci. Nanotech. 12, 431 (2014).
6. M. Ichikawa, e-J. Surf. Sci. Nanotech. 13, 391 (2015).

Giant Circular Dichroism in Soft X-ray Photoelectron Diffraction and Valence-Band Photoemission from W(110) and Ir (111)

K. Medjanik[1], O. Fedchenko[1], S. Chernov[1], D. Kutnyakhov[1], M. Ellguth[1], A. Oelsner[2], B. Schönhense[3], T. R. F. Peixoto[4], P. Lutz[4], C.-H. Min[4], F. Reinert[4], S. Däster[5], Y. Acremann[5], J. Viefhaus[6], W. Wurth[6,7], G. Öhrwall[8], J. Braun[9], J. Minár[9,10], S. Borek[9], H. Ebert[9], H. J. Elmers[1] and G. Schönhense[1]
[1] *Institut für Physik, JOGU, Staudinger Weg 7, D-55128 Mainz, Germany*
[2] *Surface Concept GmbH, Mainz, Germany*
[3] *Dept. of Bioengineering, Imperial College London, UK*
[4] *Universität Würzburg, Experimentelle Physik VII, Würzburg, Germany*
[5] *Laboratorium für Festkörperphysik, ETH Zürich, Switzerland*
[6] *DESY Photon Science, 22607 Hamburg, Germany*
[7] *Center for Free-Electron Laser Science, Univ. Hamburg, 22761 Hamburg, Germany*
[8] *Lund University, MAX IV Laboratory, Lund, Sweden*
[9] *Universität München, München, Germany*
[10] *University of West Bohemia, Pilsen, Czech Republic*

Email: *medyanyk@uni-mainz.de*
Key words: momentum microscopy, photoelectron diffraction, circular dichroism in the angular distribution.

We report on first measurements of circular dichroism in photoemission from non-magnetic samples using a *k*-microscope in the soft X-ray range. Starting from pioneering work for magnetic materials by Schütz et al. [1] and others, X-ray magnetic circular dichroism (XMCD) has developed into very versatile tool in the field of magnetism. The generalization for non-magnetic systems and angular-resolved observation was termed circular (or linear) dichroism in the angular distribution CDAD (LDAD) [2,3]. The novel technique of time-of-flight *k*-microscopy [4] is ideal for the study of CDAD and LDAD, since the complete Brillouin zone (BZ) is observed simultaneously.
Circular dichroism in ***photoelectron diffraction*** from W(110) and Ir(111) was studied at beamline I1011 at MAX II, Lund, Sweden. Pronounced dichroism is present in the 4f core-level diffraction patterns. CDAD maps vary strongly with photon energy between hν = 300 and 1000 eV. Using the same technique, dichroism in ***valence-band photoemission*** was performed at beamline P04 of PETRA III, Hamburg, Germany, using circularly-polarized photons in the energy range up to 1300 eV. The CDAD asymmetry of the valence bands shows a rich structure as function of *k*-vector and photon energy and reaches up to 80%. Theoretical calculations using the one-step model in its density matrix representation reproduce the essential CDAD features; deviations occur with respect to relative intensities of surface states and resonances.

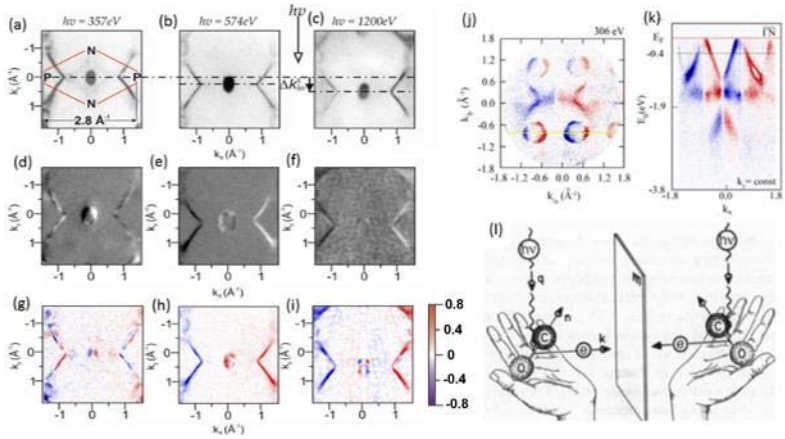

Figure 1: Momentum-distribution patterns (a-c) and CDAD patterns (d-f and g-i, on grey and false-color scale) of W(110) at E_F. *k*-space cuts run through the N-point of the 4th, 5th and 8th repeated BZ of the extended zone scheme (hν given on top). (j) Cut at E_F and k_z midway Γ-N, (k) corresponding E_B vs k_x cut. (l) Chiral setting of helicity vector q, sample orientation n and photoelectron momentum k, being a precondition for CDAD≠0 (scheme from [3]).

Fig. 1 shows intensity (a-c) and circular dichroism patterns (d-i) of the valence bands of tungsten at the Fermi energy for photon energies of 357, 574 and 1200eV, corresponding to k-space cuts through the N-point of different repeated BZs. The transfer of photon momentum $\Delta k_{h\nu}$ is visible as a rigid shift of the momentum slice in the direction of the photon beam. Although the intensity patterns are very similar (except for the rigid shift), the dichroism maps are markedly different. This reflects the fact that CDAD depends on matrix elements and relative phases of partial waves, which are functions of photon energy. The *k*-microscope records the full 4D data array [5], here $A_{CDAD}(E_B,k_x,k_y,k_z)$. Cuts can be made (offline after the experiment) in any plane; Fig.1 (top right) show sections about midway the Γ-N line, where we see the constant k_z-cut (j) and binding-energy dependence (k) of the CDAD for the hole pockets at the N-points (ovals).

A necessary precondition for the occurrence of CDAD is an electronic alignment or orientation and a handedness in the photoemission geometry as sketched in Fig.1 (l) for the simple case of a diatomic molecule. In solid-state photoemission this condition causes characteristic nodes in mirror planes.

Projects funded by BMBF (05K13UM2,05K13GU3).

References

1. G. Schütz et al., *Phys. Rev. Lett*. 58, 737 (1987).
2. N. A. Cherepkov, *Chem. Phys. Lett.* 87, 344 (1982).
3. G. Schönhense, *Phys. Scripta* T31, 255 (1990).
4. G. Schönhense, K. Medjanik and H. J. Elmers, *JESRP* 200, 94 (2015).
5. K. Medjanik et al., *submitted* (2016).

HR-TEM and HR-PES studies of metal nanoparticles in organic molecular thin film

O.V. Molodtsova [1,2], S.V. Babenkov [1], I.M. Aristova [3], A. Hloskovsky [1], and V.Y. Aristov [1,3,4]
[1] *Deutsches Elektronen-Synchrotron DESY, D-22607 Hamburg, Germany,*
[2] *National Research University of Information Technologies, Mechanics and Optics, Saint Petersburg, Russia*
[3] *Institute of Solid State Physics of Russian Academy of Sciences, 142432 Chernogolovka, Russia*
[4] *Institut für Experimentelle Physik, TU Bergakademie Freiberg, Leipziger Straße 23, 09599 Freiberg, Germany*

Email: *olga.molodtsova@desy.de*
Key words: Hybrid systems, phthalocyanines, metal nanoparticles, HR-TEM, HR-PES

Currently information technology is rapidly penetrating all spheres of our life. Extreme downsizing and the simultaneous increase in productivity require the search for new materials with uncommon properties. Since recent years the research activity has tendency to focus on investigation of advanced materials based on low dimensional systems, which includes in particular hybrid organic-inorganic systems composed of inorganic nanoparticles embedded in an organic semiconductor thin film matrix [1].
The aim of this work was to study hybrid systems consisting of metal nanoparticles (gold, silver and aluminum) embedded in the organic semiconductor $CuPcF_x$, i.e. creation of model of nanocomposite materials and study of their fundamental characteristics [2-6]. The relevance of the work is determined by the need to identify key physical parameters (morphology and electronic properties) for each pair of materials.
Evolution of morphology of hybrid nanocomposite films, depending on the nominal coating was studied by high-resolution transmission electron microscopy (HR-TEM). An analysis of electron microscopic photographs showed that after the metal deposition in ultrahigh vacuum on the surface of the organic semiconductor takes place a process of self-organizing of deposited atoms, which are likely due to the surface and bulk diffusion and join together to form nanoparticles. By HR-TEM the images of metal nanoparticles with direct resolving of atomic planes were obtained. For some coatings the coalescence processes of nanoparticles depending on the initial mutual orientation of the nanoparticles was observed.
The electronic structure and alignment of the energy levels at the interfaces formed between the metal nanoparticles and an organic semiconductor, and chemical reaction at these interfaces were studied at room temperature by high-resolution photoelectron spectroscopy (HR-PES) using synchrotron radiation. Part of the research was carried out on a new dynamic X-ray photoemission (Fast-XPS) station, which is intended for research of advanced materials in in-situ mode in real time (data acquisition about 0.1 sec/spectrum), built in the P04 beamline of synchrotron PETRA III (DESY, Hamburg).

This cycle of investigations with observation of some new phenomena may lead to opening up opportunities for a range of new applications.

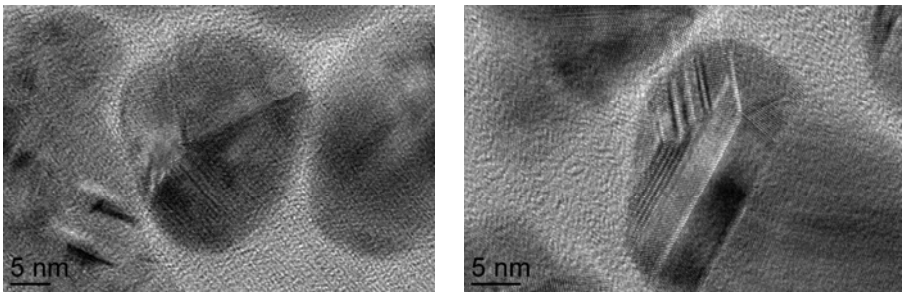

(a) (b)

Figure 1: Microstructure of nanocomposite thin films consisted of silver nano-particles embedded in CuPc matrix (HR-TEM) with nominal Ag deposition 5.7 nm. Magnifications are indicated by insert marks (a,b).

References

1. J.C. Scott and L.D. Bozano, Adv. Mater. 19, 1452, (2007).
1. doi: 10.1002/adma.200602564
2. V.Yu. Aristov, O.V. Molodtsova, C. Laubschat, V.M. Zhilin, I.M. Aristova, V.V. Kveder, and M. Knupfer, Appl. Phys. Lett. 97, 113103, (2010). http://dx.doi.org/10.1063/1.3488809
3. O. Molodtsova, I. Aristova, V. Kveder, M. Knupfer, C. Laubschat and V. Aristov, J. Phys. Sci. App. 2, 166, (2012). jpsa: 7139
4. I.M. Aristova, O.Yu. Vilkov, A. Pietzsch, M. Tchaplyguine, O.V. Molodtsova, and V.Yu. Aristov, Adv. in Materials Phys. and Chem. 2, 60, (2012).
1. doi: 10.4236/ampc.2012.24B017
5. O.V. Molodtsova, I. M. Aristova, S.V. Babenkov, O.V. Vilkov, and V.Yu. Aristov, J. Appl. Phys. 115, 164310, (2014) http://dx.doi.org/10.1063/1.4874161
6. S.V. Babenkov, O.V. Molodtsova, I.M. Aristova, M. Tchaplyguine, S.L. Molodtsov, V.Yu. Aristov, Organic Electronics 32, 228, (2016). http://dx.doi.org/10.1016/j.orgel.2016.02.038

A. Acun et al. "Atomically Controlled Surfaces Interfaces and Nanostructures"
edited by A. Bianconi, A. Marcelli (Superstripes Press, Rome 2016) isbn: 9788866830597

Submolecular AFM Imaging and Spectroscopy on Single Molecules Using KolibriSensor™ and Cantilevers

Tomoko K. Shimizu[1,2] , Oscar Custance[1]
[1]*National Institute for Materials Science, Japan.*
[2]*JST-PRESTO, Japan.*

Email: *SHIMIZU.Tomoko@nims.go.jp*
Key words: Frequency-modulation atomic force microscopy; single molecule; KolibriSensor; Si cantilever.

Submolecular imaging using frequency-modulation (FM) atomic force microscopy (AFM) has recently been established as a stunning technique to reveal the chemical structure of unknown molecules, to characterize intra-molecular charge distributions, and to observe chemical transformations. So far, most of these feats were achieved on planar molecules using the so-called qPlus sensor, a specially designed quartz AFM sensor. The KolibriSensor, another type of quartz AFM sensor, is also expected to be capable of high-resolution imaging, but only very few experimental results have been reported to date.

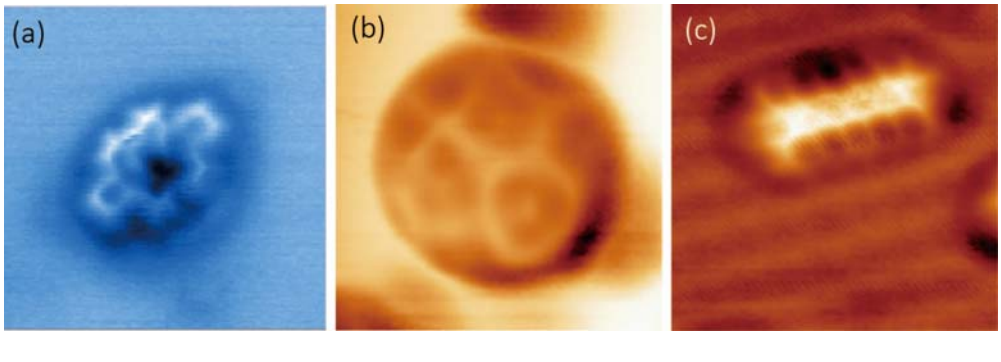

Figure 1: Intramolecular resolution AFM images of (a) *mezo*-Dibenzoporphycene on Cu(100) with a KolibriSensor, (b) C_{60} and (c) pentacene on TiO_2(101) with Si cantilevers.

Here, we present submolecular resolution images and spectroscopic data on single molecules of a porphycene derivative [1] using small oscillation amplitudes with KolibriSensors (Figure 1a). Force volume measurements with CO-functionalized probes [2] revealed features related to the isomers of porphycene molecules.

We also report a novel imaging method to achieve submolecular resolution on three-dimensional molecules (Figure 1b) and structures using a silicon (Si) cantilever-based AFM operated with large oscillation amplitudes. At variance with previous

implementations, this method allowed us to simultaneously image both intra-molecular structures and the atomic arrangement of the substrate (Figure 1c) [3]. Force volume measurements over C_{60} molecules clarified the validity of our method to achieve submolecular resolution [3].

Based on these results, a comparison between AFM operations with above two sensors will be discussed.

References

1. K. Oohora, A. Ogawa, T. Fukuda, A. Onoda, J. Hasegawa, T. Hayashi, Angew. Chem. Int. Ed. 54, 6227 (2015). http://dx.doi.org/10.1002/anie.201501496.
2. L. Gross, F. Mohn, N. Moll, P. Liljeroth, G. Meyer, Science 325, 1110 (2009). http://dx.doi.org/10.1126/science.1176210.
3. C. Moreno, O. Stetsovych, T. K. Shimizu, O. Custance, Nano Lett. 15, 2257 (2015). http:/dx.doi.org/10.1021/nl504182w

A. Acun et al. "Atomically Controlled Surfaces Interfaces and Nanostructures"
edited by A. Bianconi, A. Marcelli (Superstripes Press, Rome 2016) isbn: 9788866830597

Interfacial water layer on doped graphene surfaces

Akira Akaishi[1,2] , Jun Nakamura[1,2]
[1]*The University of Electro-Communications*
[2]*JST-CREST*

Email: *akaishi@natori.ee.uec.ac.jp*
Key words: doped graphene, water layer, wetting property

Water wettability of graphitic surfaces is of great interest for fundamental understanding of graphene surfaces and for practical applications of graphene-based materials. While graphite has been considered as a typical hydrophobic material, recent experiments of contact angle measurement of clean graphene surfaces have called into question the hydrophobicity of pristine graphene [1]. A wetting property of a surface is closely related to adhesion energy of water on the surface. It is known that surface modification or heteroatom doping alters the electronic property of graphene, leading to potential alteration of the adhesion energy [2]. However, wettability and water adsorption of heteroatom-doped graphene have not been discussed so far.

We examined water adsorption of nitrogen-doped or boron-doped graphene surfaces by use of first-principles calculations within the density functional theory. To introduce the van der Waals interactions between a water molecule and doped graphene, we carried out vdW-DF2 calculations [3]. Nitrogen or boron atoms were doped at graphitic sites of a single layer of graphene in such a way that the distance between dopants were large enough so as to make the interactions between the dopants negligible.

In order to evaluate the interaction between water and doped graphene, we have calculated the adhesion energy. Figure 1 shows the adhesion energy for doped graphene as a function of the distance between a water molecule and graphene. The adhesion energy for N-doped (B-doped) graphene is larger (smaller) than that for pristine graphene. These observations can be explained by a simple electrostatic model: The doped nitrogen atom is positively charged and neighboring carbon atoms are negatively charged due to delocalization of an electron of graphitic nitrogen and vice versa for boron doping. The water adhesion energy of the doped graphene can be described by, in addition to the van der Waals forces, the electrostatic interactions between charged dopants and polarized water. The water wettability of the doped graphene is examined by means of molecular dynamics simulations. In the presentation, we will discuss the effect of charged dopants on the double layer structure which is found to play a key role in the wettability of pristine graphene surfaces [4].

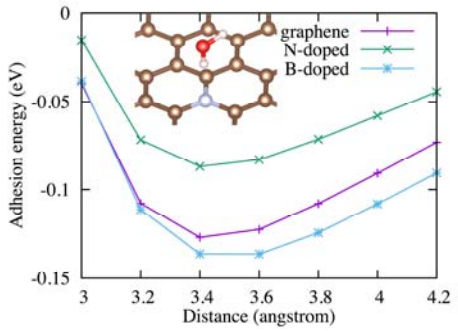

Figure 1 Adhesion energy for pristine, nitrogen-doped, and boron-doped graphene. Inset indicates the adhesion configuration.

References

1. Z. Li, Y. Wang, A. Kozbial, G. Shenoy, F. Zhou, R. McGinley, P. Ireland, B. Morganstein, A. Kunkel, S. P. Surwade, L. Li, and H. Liu, Nat. Mater. 12, 925 (2013).
2. A. Ashraf, Y. Wu, M. C. Wang, N. R. Aluru, S. A. Dastgheib, and S. Nam, Langmuir 30, 12827 (2014)
3. K. Lee, E. D. Murray, L. Kong, B. I. Lundqvist, and D. C. Langreth, Phys. Rev. B 82, 081101(R) (2010).
4. A. Akaishi, T. Yonemaru, and J. Nakamura, submitted.

A. Acun et al. “Atomically Controlled Surfaces Interfaces and Nanostructures”
edited by A. Bianconi, A. Marcelli (Superstripes Press, Rome 2016) isbn: 9788866830597

Th4T session

A. Acun et al. "Atomically Controlled Surfaces Interfaces and Nanostructures"
edited by A. Bianconi, A. Marcelli (Superstripes Press, Rome 2016) isbn: 9788866830597

Density functional calculation Au, Pt and Ru adatom on CeO_2, ZrO_2 and Al_2O_3 surfaces for catalysis

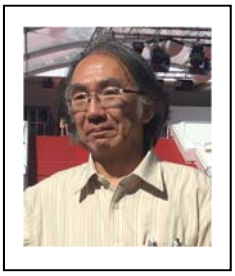

A. Ishii,[1] Y. Matsui[1] and K. Okumura[2]
[1]*Department of mechanical and physical engineering, Tottori University, Koyama, Tottori 680-8552, Japan*
[2]*Department of Applied Chemistry, Kogakuin University, 2665-1 Nakano-machi, Hachioji City, Tokyo 192-0015, Japan*

Email: *ishii@damp.tottori-u.ac.jp*
Key words: gold, platinum, ruthenium, nano particle, catalysis, oxide substrate, DFT

It is well-known that gold nano particle can be used as powerful catalysis. There are some DFT calculations of Au nano particles on CeO_2 (110) surface [1], ZrO_2 (111) surface [2] and alpha-Al_2O_3(0001) surface [3]. For purposes of catalysis, Pt and Ru nano particles are also good candidate for catalyst on these surfaces. Thus, in this study, we calculate adsorption of Au, Pt and Ru on these surfaces in order to check that which pair of adatom and substrate is best for catalysis. The calculation method is the density functional theory using the program code VASP.[4-7] The calculation result shows us that CeO_2 (110) surface is the best surface for all Au, Pt and Ru as catalysis. The binding energies also suggest us for the formation of nano particle of Au, Pt and Ru.

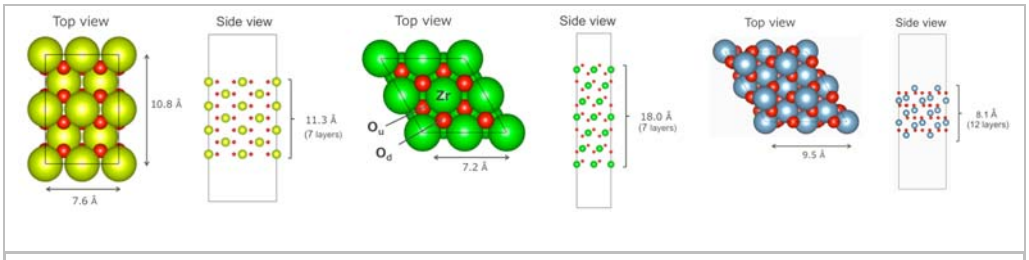

Figure 1: Model of DFT calculation for CeO_2(110), ZrO_2(111) and **α**-Al_2O_3(0001) surfaces.

References

1. Chen, Ying, et al. Surface Science 602.10 (2008): 1736-1741. □
2. Grau-Crespo, Ricardo, et al. The Journal of Physical Chemistry C 111.28 (2007): 10448-10454.
3. Hernández, Norge Cruz, and Javier Fdez Sanz. Applied surface science 238.1 (2004): 228-232.
4. G. Kresse, Thesis, Technische Univesiat Wien (1993)
5. G. Kresse and J. Hafner, Phys. Rev.B47RC558(1993)
6. G. Kresse and J. Furthmuller, Comput.Mot.Sci.6,15-50(1996)
7. G. Kresse and J. Furthmuller, Phys.Rev.B 54,11169(1996)

A. Acun et al. "Atomically Controlled Surfaces Interfaces and Nanostructures"
edited by A. Bianconi, A. Marcelli (Superstripes Press, Rome 2016) isbn: 9788866830597

Helium diffraction and acoustic phonons of graphene grown on copper catalysts

A. Al Taleb[1], H.K. Yu[2,3], G. Anemone[1] , A.M. Wodtke[2,3] and D. Farías[1,4,5]
[1]*Departamento de Física de la Materia Condensada, Universidad Autónoma de Madrid, Spain*
[2]*Institute for Physical Chemistry, University of Göttingen, 37077 Göttingen, Germany*
[3]*Max Planck Institute for Biophysical Chemistry, 37077 Göttingen, Germany*
[4]*Instituto "Nicolás Cabrera", Universidad Autónoma de Madrid, Spain*
[5]*Condensed Matter Physics Center (IFIMAC), Universidad Autónoma de Madrid, Spain*

Email: *daniel.farias@uam.es*
Key words: Growth and applications of thin films; Graphene and other 2D materials.

In this work we use Helium Atom Scattering (HAS) as a sensitive probe of the crystallinity of graphene (Gr) grown by chemical vapor deposition (CVD) on Cu, and as a probe of its interactions with its substrate. The high sensitivity of HAS to surface defects precluded its use with current available Gr/Cu foil samples. Our current results have been obtained using Gr/Cu(111) grown on sapphire samples and Gr grown on a peeled-off epitaxial Cu(111) foil using a recently developed scheme. We have measured the structure and the acoustic phonon modes of CVD graphene grown on these two samples [1]. The observation of high reflectivities and clear diffraction peaks demonstrates the presence of high-quality Gr, with both long-range order and a very low density of defects over a surface area of the order of $1mm^2$. The shape of elastic and quasi-elastic scattering features proves that, surprisingly, Gr grown on a peeled-off epitaxial Cu(111) foil exhibits a much higher crystallinity than the one grown on $Cu(111)/Al_2O_3$ samples. The Gr lattice parameter was found to remain constant in the temperature range between 110-500 K, which proves that Gr is decoupled from the Cu substrate. A parabolic dispersion phonon branch has been measured along ΓM, as expected for the acoustic ZA mode in free-standing graphene (see Fig. 1). This mode allows determining the interlayer bonding strength as well as the bending rigidity of Gr on Cu foil. Finally, the acoustic phonon modes are compared to the ones measured with HAS in our laboratory for Gr/Ru(0001) [2,3] and Gr/Ni(111) [4,5].

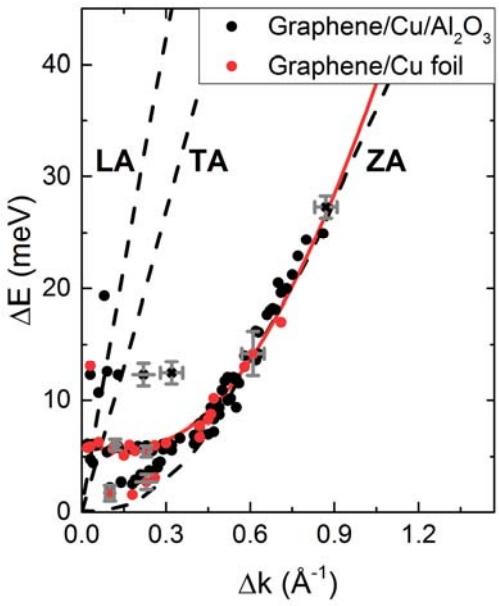

Figure 1: Experimentally derived surface phonons for Gr/Cu(111)/Al_2O_3 (black dots) and Gr on Cu(111) foil (red dots) measured along the ΓM direction, shown with DFT calculations for free standing Gr (dashed curves). From [1].

References

1. A. Al Taleb, H. K. Yu, G. Anemone, D. Farías and A. M. Wodtke, Carbon 95, 731 (2015).
2. D. Maccariello, D. Campi, A. Al Taleb, G. Benedek, D. Farías, D. Bernasconi and R Miranda, Carbon 93, 1 (2015).
3. D. Maccariello, A. Al Taleb, F. Calleja, A.L.Vázquez de Parga, P. Perna, J. Camarero. E. Gnecco, D. Farías and R Miranda, Nano Letters 16, 2 (2015).
4. A. Al Taleb, G. Anemone, D. Farías and R. Miranda, Carbon 99, 416 (2016).
5. A. Al Taleb and D. Farías, J. Phys.: Condens. Matter 28, 103005 (2016).

A. Acun et al. “Atomically Controlled Surfaces Interfaces and Nanostructures”
edited by A. Bianconi, A. Marcelli (Superstripes Press, Rome 2016) isbn: 9788866830597

Neutralization of an epitaxial graphene on the SiC(0001) by means of palladium intercalation

Kazuma YAGYU[1] , Kazutoshi TAKAHASHI[2], Hiroshi TOCHIHARA[1], Hajime TOMOKAGE[1] and Takayuki SUZUKI[1]
[1]*Department of Electronics Engineering and Computer Science, Fukuoka University*
[2]*Synchrotron Light Application Center, Saga University*

Email: *yagyu@fukuoka-u.ac.jp*
Key words: Atomic and nanoscale structure of surfaces and interfaces: advanced methods; Graphene and other 2D materials; Scanning probe and surface microscopy

Graphene made by thermal annealing of the SiC(0001) substrate attracts much attention becuse it is compatible to the conventional manufactural process of electronic devices. In the thermal annealing method, the first formed graphene, which is called “zero layer graphene (ZLG)”, is not an ideal one. Intercalation is an effective technique to change the ZLG to an ideal one. According to the studies so far, because of the charge transfer, Dirac point of the graphene usually shifts to the negative direction with respect to the Fermi energy by the the intercalation of metal atoms. In other words, the intercalated graphenes with metal atoms are all n-type.

For the purpose to produce electronic devices using graphene, p-type or neutralized graphene is also desired. In this study, Palladium (Pd) atoms were intercalated under the ZLG to shift the Dirac point toward positive energy.

A SiC(0001) surface (Si-face) , cut out from an on-axis oriented 4H-SiC(0001) wafer of Cree, Inc., was used as a substrate in the present study. After an appropriate cleaning process, the samples were introduced in an ultra-high-vacuum (UHV) chamber which is equipped with a Low-Energy Electron Diffraction (LEED) and a Scanning Tunneling Microscopy (STM) (JEOL Ltd. model JSTM-4610). Then the samples were annealed at some proper temperatures and finally at 1200°C for 15min to induce the ZLG, which is confirmed by a $(6\sqrt{3}\times6\sqrt{3})R30°$ LEED pattern. The detailed preparation process of the ZLG is described elsewhere[1]. Then Pd atoms were deposited on the surface at room temperature. The surface structure is observed by STM at an each step of experiment. The energy dispersions around the $\bar{K}$ point were obtained by angle-resolved photoemission spectroscopy (ARPES) using synchrotron radiation at beam line BL13 of the SAGA Light Source, which is equipped with a hemispherical electron-energy analyzer (MB Scientific AB, MBS A-1).

Pd atoms were intercalated between the ZLG and the SiC substrate after the annealing at 700 °C. A hexagonal lattice of the surface graphene is confirmed by STM (Fig. 1(a)).

Fig. 1(b) shows a one dimensional structure which is observed in part of Pd-intercalated graphene surface.
Fig. 1(c) shows the energy dispersion at the $\bar{K}$ point of the ZLG. A faint dispersion is due to a small area of the conventional single layer graphene which was formed incidentally by slight overheating. After the Pd intercalation, an additional dispersion appeared as shown in fig. 1(d), which is originated from a single layer intercalated graphene on top of the Pd layer. Its Dirac point is equal to the Fermi energy, i. e. 0 eV. This means no charge transfer between the intercalating Pd atoms and the intercalated graphene on top of them.

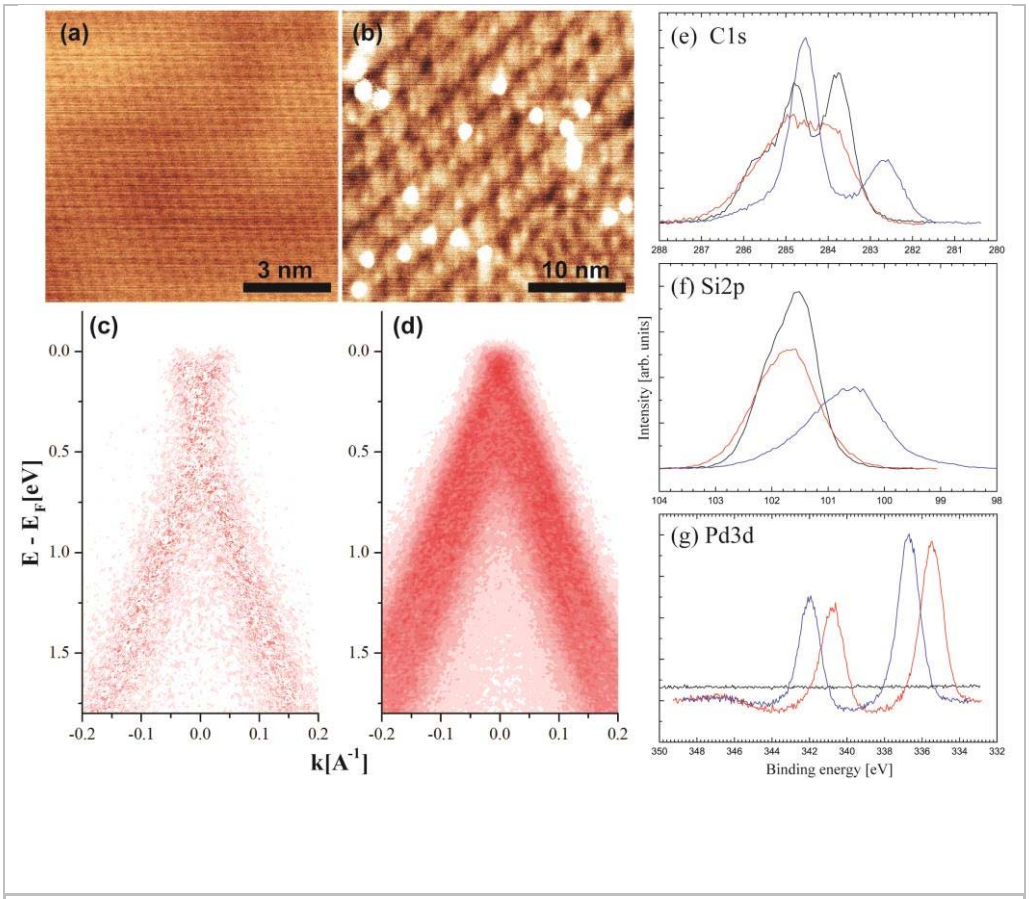

Figure 1: STM images obtained at room temperature of (a) a graphene lattice and (b) a one dimensional structure on the surface of a Pd-intercalated graphene. Energy dispersions around $\bar{K}$ point of (c) the ZLG slightly covered by the conventional single layer and (d) the Pd-intercalated single layer graphene measured by ARPES. XPS spectra of (e) C1s, (f) Si2p, and (g) Pd3d core levels. Black, red, and bule curves of each core level show the spectra of the ZLG, the Pd deposited surface, and the Pd-intercalated sample.

XPS spectra of C1s, Si2p, and Pd3d core level are shown in Fig. 1(e-g). A single layer graphene component at 284.5 eV increased after the Pd intercalation in (e), which

indicates that the ZLG changed to a single layer graphene. A component of the SiC substrate is confirmed at 283.8 eV on the ZLG in (e). It shifted to 282.6 eV after the Pd intercalation. In the Si2p spectra, the similar shift of substrate component from 101.6 eV to 100.5 eV was confirmed. This is due to the band bending caused by the charge transfer from Pd atoms to the SiC substrate. A peak shift of Pd3d spectra was also confirmed, which is consistent to those of C1s and Si2p. The shape of Pd3d spectrum unchanged. Thus the Pd atoms remain metallic between the SiC substrate and the graphene.

References

1. K. Yagyu et al., Appl. Phys. Lett. 104, 053115 (2014).

A. Acun et al. "Atomically Controlled Surfaces Interfaces and Nanostructures"
edited by A. Bianconi, A. Marcelli (Superstripes Press, Rome 2016) isbn: 9788866830597

Giant Rashba-type splitting of surface states in Pb nanoribbons on Si(553)

Ryszard Zdyb, Marek Kopciuszyński, Mariusz Krawiec, Mieczysław Jałochowski
Institute of Physics, Maria Curie-Sklodowska University

Email: *ryszard.zdyb@umcs.pl*
Key words: Rashba effect; nanowires; SARPES; DFT; Si(553); Pb.

Breaking of the inversion symmetry at the crystal surface in the presence of spin-orbit coupling leads to the lifting of spin degeneracy of electronic states. The phenomenon is known as the Rashba effect and it has been predicted in the 80 of the 20th century [1]. The first experimental evidence of the spin-split surface state bands has been reported for the Au(111) surface [2]. According to the original model the spin-split bands reveal 100 % polarization and the polarization vector is perpendicular to the electron wave vector and to the surface normal.
Quite different spin texture is expected for one dimensional metallic structures. Au atomic chains prepared on vicinal silicon surfaces like Si(557)-Au or Si(553)-Au seem to be a perfect choice for observation of such effect [3]. With the spin-resolved photoemission spectroscopy technique it has been shown that the spin-split one dimensional electronic states indeed exist and they have unexpected large out-of-plane component of the polarization vector [4].
In the present contribution we report on a giant Rashba-type splitting of surface states induced by Pb on the Si(553) surface. Although the surface is covered with 1.3 ML Pb the electronic structure reveals one dimensional character. It is due to the unique arrangement of lead atoms in the form of parallel nanoribbons [5]. The quasi one-dimensional character of the surface is manifested by the presence of multiple surface state bands crossing the Fermi level in the direction parallel to the nanoribbons and a small band gap in the perpendicular direction. These parabolic-like bands are spin polarized as shown by the spin and angle resolved photoemission experiments. Beside the in-plane component there is also significant out-of-plane component of the polarization vector. The splitting of more than 0.2 $Å^{-1}$ and 0.6 eV for the wave vector and energy, respectively, at the Fermi level at room temperature has been observed. As revealed by density functional theory calculations the spin-split bands are associated with the Pb nanoribbons and are due to the spin-orbit interaction. The observed giant spin splitting of the surface bands and large out-of-plane component of the polarization vector are associated with the unique arrangement of the Pb atoms in the nanoribbons. They form strongly distorted and strained hexagonal-like lattice. This causes non uniform distribution of charge in the plane of the surface and consequently in-plane component of the potential gradient.

Acknowledgments - This work has been supported by the National Science Center under Grant No. 2013/11/B/ST3/04003.

References

1. Y.A. Bychkov, and E.I. Rashba, JETP Lett. 39, 78 (1984).
2. S. LaShell, B. A. McDougall, and E. Jensen, Phys. Rev. Lett. 77, 3419 (1996).
3. J. N. Crain, J. L. McChesney, Fan Zheng, M. C. Gallagher, P. C. Snijders, M. Bissen, C. Gundelach, S. C. Erwin, and F. J. Himpsel, Phys Rev B 69, 125401, (2004).
4. Taichi Okuda, Koji Miyamaoto, Yasuo Takeichi, Hirokazu Miyahara, Manami Ogawa, Ayumi Harasawa, Akio Kimura, Iwao Matsuda, Akito Kakizaki, Tatsuya Shishidou, and Tamio Oguchi, Phys. Rev. B 82, 161410 (2010).
5. M. Kopciuszyński, P. Dyniec, M. Krawiec, P. Łukasik, M. Jałochowski, and R. Zdyb, Phys. Rev. B 88, 155431 (2013).

A. Acun et al. "Atomically Controlled Surfaces Interfaces and Nanostructures"
edited by A. Bianconi, A. Marcelli (Superstripes Press, Rome 2016) isbn: 9788866830597

IV-VI monolayers with alkaline-earth chalcogenide supports

Katsuyoshi Kobayashi
Department of Physics, Ochanomizu University

Email: *kobayashi.katsuyoshi@ocha.ac.jp*
Key words: Topological crystalline insulator, Monolayer

Topological crystalline insulator (TCI) is a new concept of topologically non-trivial matters defined by point group symmetries of crystals [1]. SnTe and IV-VI compounds are the first materials that have experimentally been identified as TCIs. It was theoretically proposed that SnTe thin films are two-dimensional TCIs [2,3]. But, it seems not experimentally being confirmed. It was also theoretically proposed that IV-VI monolayers including SnTe are also 2D TCIs [4,5]. However, it seems also that IV-VI monolayers have not been materialized. We present a theoretical study on IV-VI monolayers with alkaline-earth chalcogenide supports. In a previous paper we showed a theoretical study of IV-VI monolayers with alkali halide supports [6] and following results are found. First, planar structures of free-standing IV-VI monolayers are not stable. TCI states are lost by buckling. Second, planar structures of monolayers are maintained by sandwiching them between alkali halide surfaces, and TCI states are preserved. One problem in that system is that the interaction between monolayers and alkali halide surfaces is weaker that between monolayers. It is expected that this property prevent monolayers from stably existing on surfaces. Therefore we study the system of IV-VI monolayers on alkaline-earth chalcogenide surfaces in this study. Since alkaline-earth chalcogenides are divalent ionic crystals, it is expected that the interaction between monolayers and alkaline-earth chalcogenide surfaces is stronger than that between monolayers and alkali halide surfaces. We performed density-functional calculations for various combinations of IV-VI monolayers and alkaline-earth chalcogenide surfaces, and found that the interaction between them is stronger that between monolayers and alkali halide surfaces. This result suggests possibility of realization of IV-VI monolayers on surfaces.

References

1. L. Fu, Phys. Rev. Lett. 106, 106802 (2011).
2. J. Liu, T. H. Hsieh, P. Wei, W. Duan, J. Moodera, and L. Fu, Nature Mat. 13, 178 (2014).
3. H. Ozawa, A. Yamakage, M. Sato, and Y. Tanaka, Phys. Rev. B 90, 045309 (2014).
4. E. O. Wrasse and T. M. Schmidt, Nano Lett. 14, 5717 (2014).
5. J. Liu and X. Qian and L. Fu, Nano Lett. 15, 2657 (2015).
6. K. Kobayashi, Surf. Sci. 639, 54 (2015).

Th4S session

A. Acun et al. "Atomically Controlled Surfaces Interfaces and Nanostructures"
edited by A. Bianconi, A. Marcelli (Superstripes Press, Rome 2016) isbn: 9788866830597

Interaction of copper phthalocyanines with metal-passivated Si surfaces – assembly and dynamics.

Peter Matvija[1], Pavel Sobotík[1], Barbara Pieczyrak[2], Leszek Jurczyszyn[2], Karel Majer[1], Filip Rozbořil[1], Petr Zimmermann[1], Ivan Ošťádal[1] and Pavel Kocán[1]
[1]*Charles University in Prague, Czech Republic*
[2]*Institute of Experimental Physics, University of Wrocl'aw, Poland*

Email: *pavel.kocan@mff.cuni.cz*
Key words: Metal-semiconductor and insulator-semiconductor interfaces; Supramolecular structures and functionalization of surfaces and interfaces; Scanning probe and surface microscopy

Ordered layers of organic molecules are usually grown on weakly interacting surfaces, typically those of metal mono-crystals. An interesting alternative, consistent with silicon technologies, is represented by silicon surfaces passivated by metal mono-layers. Such surfaces carry interesting electronic properties, such as Rashba-type spin-split bands in the case of Tl/Si(111)-(1x1) [1] or anisotropic band structure in the case of In/Si(111)-(4x1) [2]. Due to passivation of surface Si dangling bonds, adsorbants are mobile [3] which allows growth of self-assembled monolayers (SAMs) of the deposited molecules.

We use room-temperature scanning tunneling microscopy (STM) to study interaction of copper phthalocyanines (CuPc) and fluorinated CuPc molecules (F_{16}CuPc) with selected metal-passivated surfaces. Different electron affinity of CuPc and F_{16}CuPc molecules results in distinct interactions with substrates. In some cases we are able to influence ordering of molecules locally by the STM tip. Observed dynamics of the molecules allows to describe their interaction with the substrates. Influence of surface defects on the dynamics will be discussed. A detailed information is gained from calculations based on density functional theory.

Two aspects are important for discussion of observed morphologies and dynamic behavior – 1) the charge transfer between the molecules and the substrate and 2) competition between the symmetry of the substrate and the symmetry of the nanometer-sized square-shaped molecules.

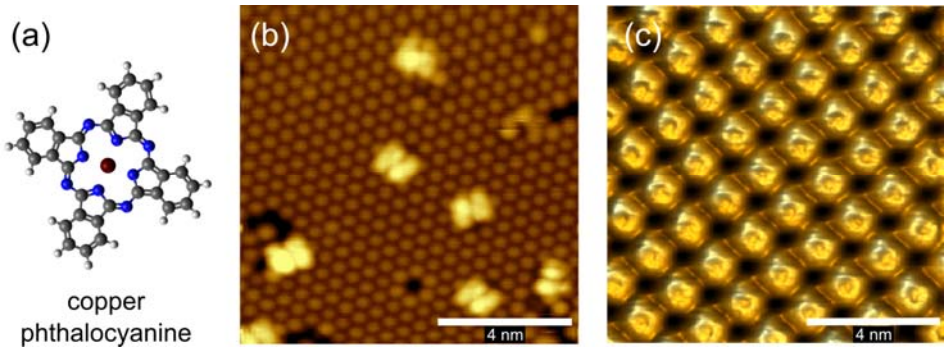

Figure 1: (a) Molecular structure of the copper phthalocyanine molecule. (b,c) STM images of isolated adsorbed CuPc molecules (b) and of self-assembled monolayer

References

1. K. Sakamoto, T. Oda, A. Kimura, Y. Takeichi, J. Fujii, R. I. G. Uhrberg, M. Donath, and H. Woong, J. Electron Spectros. Relat. Phenomena 201, 88 (2015).
2. H. Morikawa, C. C. Hwang, and H. W. Yeom, Phys. Rev. B 81, 075401 (2010).
3. P. Matvija, P. Sobotík, I. Ošťádal, and P. Kocán, Appl. Surf. Sci. 331, 339 (2015).

Magnetic spectra of atomic and molecular adsorbates

Nicolas Lorente[1], Jean-Pierre Gauyacq[2]
[1]*Centro de Física de Materiales (CSIC)*
Paseo de Manuel de Lardizabal 5, E-20018 San Sebastián
[2]*Institut des Sciences Moléculaires d'Orsay (ISMO), CNRS, Univ. Paris-Sud, Université Paris-Saclay, Bât.351, 91405 Orsay Cedex, France*

Email: *nicolas.lorente@ehu.eus*
Key words: Magnetic adsorbates, Kondo physics, IETS, magnetic excitations

A magnetic impurity on a non-magnetic host can undergo spin-flip screening giving rise to Kondo physics. The magnetic structure of the impurity can change the spectra close to zero energy. Instead of the Kondo peak more complex structures can appear. The combination of Kondo correlations and magnetic excitation is thus an interesting field that can give much information on the way electronic and magnetic excitations correlate on the atomic scale.
We will show our results with the modelisation of conductance spectra to compare with scanning tunneling microscope data on atoms and molecules adsorbed on various substrates [1-5].

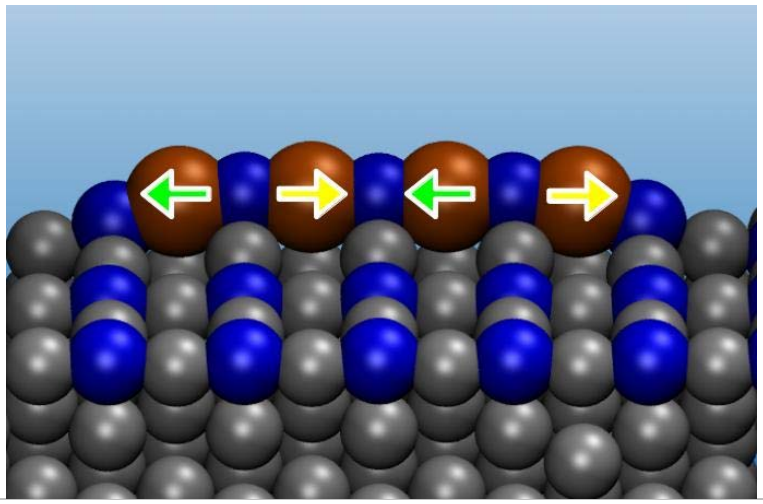

Figure 1: Antiferromagnetic atomic chain of iron atoms glued by N atoms on a $Cu_2N/Cu(100)$ substrate in a Néel state produced by decoherence [5].

References

1. R. Korytar, N. Lorente, J. Phys.: Cond. Matt. 23, 355009 (2011)
2. R. Korytar, N. Lorente and J.-P. Gauyacq, Phys. Rev. B 85, 115420 (2012)
3. J.-P. Gauyacq, S. M. Yaro, X. Cartoixa, N. Lorente, Phys. Rev. Lett. 110, 087201 (2013)
4. J.-P. Gauyacq, N. Lorente, J. Phys.: Cond. Matt. 26, 394005 (2014)
5. J.-P. Gauyacq, N. Lorente, J. Phys.: Cond. Matt. 27, 455301 (2015)

Formation of bimolecular structures on metal-passivated silicon substrates.

Pavel Sobotík , Petr Zimmermann, Peter Matvija, Karel Majer, Pavel Kocán, Ivan Ošťádal
Charles University in Prague, Czech Republic

Email: *pavel.sobotik@mff.cuni.cz*
Key words: Metal-semiconductor and insulator-semiconductor interfaces; Organic nanofilms and devices; Supramolecular structures and functionalization of surfaces and interfaces; Scanning probe and surface microscopy

Metal phthalocyanines are promising candidates for fabrication of organic devices due to their high chemical and thermal stability. Among them, copper phthalocyanine (CuPC) is a well known organic p-type semiconductor, while fluorinated cooper phthalocyanine (FCuPC) has been tested as a promising candidate for n-channel transistor [1,2]. It is highly attractive to study interaction of the two types of molecules on technologically important surfaces. To interconnect current silicon technology with organic devices technology and overcome problems with deposition of ordered molecular layers on a highly reactive silicon surfaces we tested several metal-passivated silicon surfaces.

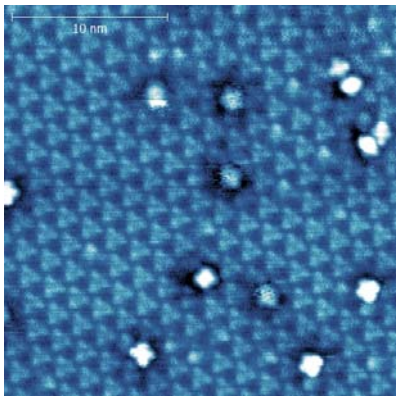

Figure 1: STM image of isolated co-deposited CuPC and FCuPC molecules on In-passivated Si(111) surface.

Molecules were deposited and studied at room temperature, which is much more important from practical point of view. Various ratios of the two components, various orders of deposition, and also co-deposition were tested. Amounts up to one monolayer were deposited. We exploited scanning tunneling microscopy (STM) and tunneling

spectroscopy (STS) to study mutual interactions of different types of molecules, as well as stability and structure of bimolecular assemblies on selected substrates.

References

1. Yasutaka Kuzumoto, Hirotaka Matsuyama, and Masatoshi Kitamura, Japanese Journal of Applied Physics 53, 04ER16 (2014)
2. Seok Min Yoon, Sylvia J. Lou, Stephen Loser, Jeremy Smith, Lin X. Chen, Antonio Facchetti, and Tobin Marks, Nano Lett. 12, 6315 (2012)

A. Acun et al. “Atomically Controlled Surfaces Interfaces and Nanostructures”
edited by A. Bianconi, A. Marcelli (Superstripes Press, Rome 2016) isbn: 9788866830597

Atomic and Electronic Structure of half-Hydrogenated Silicene on Ag(111): A Study by LEED, STM and ARPES

W. Wang, W. Olovsson and R. I. G. Uhrberg
Department of Physics, Chemistry, and Biology, Linköping University, S-581 83 Linköping, Sweden

Email: *weiwa49@ifm.liu.se*
Key words: 2D materials, Silicene, LEED, STM, ARPES

Silicene, a two dimensional network of Si atoms, is predicted to be similar to graphene. The exotic electronic properties theoretically predicted for free standing silicene have initiated a great interest in experimental studies recently. However, the interaction between the silicene layer and the substrate modifies the atomic and electronic structure which deviate from the properties in its free-standing form.
Finding a proper way to reduce the interaction is crucial for future applications of silicene. Chemical functionalization is one of the most promising methods. In the case of graphene, a fully hydrogen terminated graphene sheet, called graphane, has been theoretically and experimentally studied in the literature [1, 2]. The finite gap opening at the Dirac point after hydrogenation has an important application potential for electronic devices. Theoretical calculations also suggest that hydrogenated silicene, so called silicane, has the same hydrogen chemisorption geometry and band gap opening as hydrogenated graphene [3].

We report a detailed and comprehensive study of the atomic and electronic structures of hydrogenated silicene on Ag(111) using low energy electron diffraction (LEED), scanning tunneling microscopy (STM) and angle-resolved photoelectron spectroscopy (ARPES). LEED shows that the hydrogenation removes the buckling of the silicene sheet on Ag(111) which indicates a reduced interaction between Si and Ag atoms. The process of hydrogenation is reversible, i.e., the hydrogen can be desorbed by heating the sample leaving the silicene sheet in its original buckled structure. STM images reveal a hexagonal structure with the periodicity of the silicene (1×1) lattice which is consistent with the chair-like model [3]. The ARPES data show two dispersive bands around normal emission which are in good agreement with the theoretical band structure of our density functional theory (DFT) calculations based on a chair-like model of free-standing half-silicane.

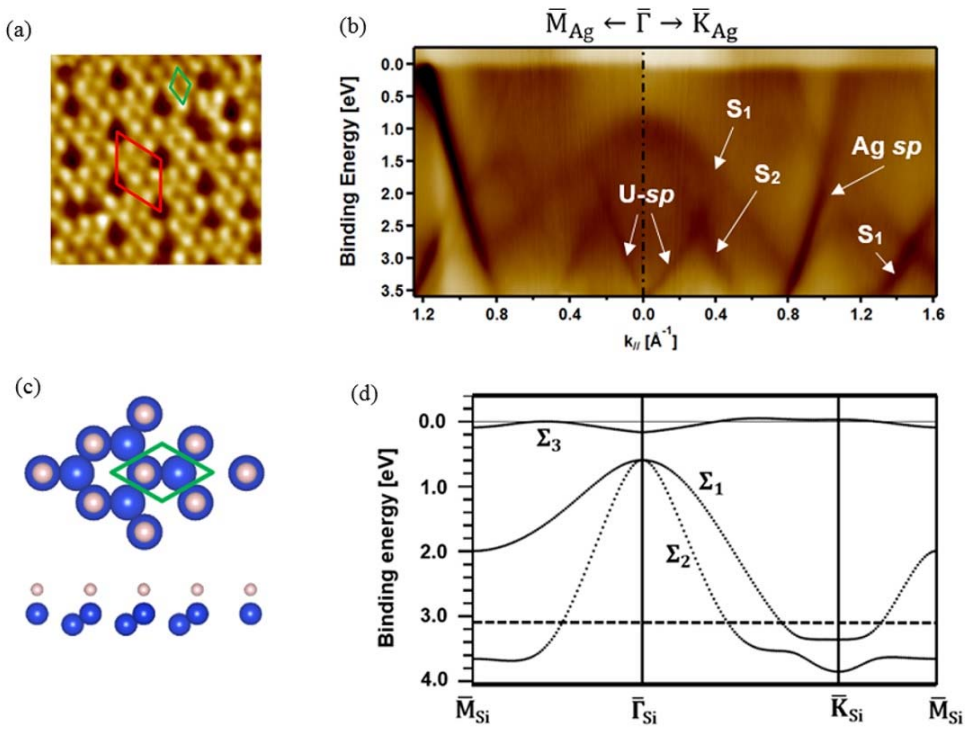

Figure 1 (a) STM image of a 4.3×4.3 nm^2 area of hydrogenated silicene. The (1×1) periodicity is indicated by a green diamond and the red diamond illustrates a (2√3×2√3) cell. The STM image was recorded at room temperature in constant current mode with a tunneling current of 200 pA and a sample bias of +50 mV. (b) ARPES data from half-silicane obtained at a photon energy of 26 eV along $\bar{\Gamma} \rightarrow \bar{M}_{Ag}$ and $\bar{\Gamma} \rightarrow \bar{K}_{Ag}$ of the Ag (1×1) SBZ. S_1 and S_2 are two dispersive bands which originate from half-silicane. The label Ag-*sp* indicates Ag bulk emission and U-*sp* points at dispersive features due to Umklapp scattering of the Ag-*sp* emission by (2√3×2√3) reciprocal lattice vectors. (c) Top and side views of a half-silicane model with hydrogen adsorbed on one of the two hexagonal sub-lattices of free-standing silicene. The green diamond represents the (1×1) silicane unit cell, blue and pink balls represent Si and H atoms, respectively. The bond length between Si and H atoms is 1.52 Å, and the Δz of the two Si sub-lattices is 0.68 Å. (d) Calculated band structure of the half-silicane model in (c). The dashed line indicates the binding energy limit of the ARPES data in (b) relative to the top of the Σ_1 and Σ_2 bands at $\bar{\Gamma}$.

References

1. Jorge O. Sofo, Ajay S. Chaudhari and Greg D. Barber, Phys. Rev. B. 75, 153401 (2007).
2. D. C. Elias *et al.*, Science, 323, 610 (2009).
3. M. Houssa *et al.*, Appl. Phys. Lett. 98, 223107 (2011).

A. Acun et al. "Atomically Controlled Surfaces Interfaces and Nanostructures"
edited by A. Bianconi, A. Marcelli (Superstripes Press, Rome 2016) isbn: 9788866830597

Metastability phenomena and high magnetic field effects in VO_2 thin films

Daniele Di Gioacchino[1], Augusto Marcelli[1,2], Alessandro Puri[3], Chongwen Zou[4], Fan Lele[4], Uli Zeitler[5] and Antonio Bianconi[2]
[1]*INFN-LNF, E. Fermi 40- 00044 Frascati, Italy*
[2]*RICMASS, Via Sabelli 119A.00185 Rome, Italy*
[3]*CNR-IOM-OGG c/o ESRF, 71 Avenue des Martyrs CS 40220 F-38043 Grenoble, France*
[4]*USTC, University of Science and Technology of China, Hefei, 230026, P.R .China.*
[5]*HFML, Radboud University Nijmegen, Toernooiveld 7, 6525 ED Nijmegen, Netherlands*

Email: *daniele.digioacchino@lnf.infn.it*
Key words: Strain in thin layer and interface; Metal-semiconductor interfaces; VO_2 oxide

VO_2 is a transition metal oxide where electron correlation and collective electrons-lattice interactions strongly affect electrical conductivity and optical properties. In particular, this system is characterized by a well-recognized first order metal (high T)-insulator (low T) transition (MIT) around 341 K [1]. This transition shows hysteresis due to coexistent phase separation domains [2] and, in addition, a paramagnetic behavior independent by the temperature [3]. The MIT dynamical behavior is controlled by the characteristic time scale associated to the metallic and insulating phases, to compare the time scale of control parameters such as temperature, stress rates and measurement ranges [4].

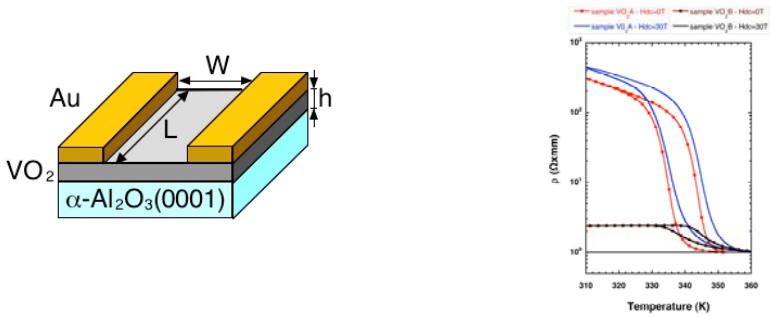

Figure 1: left) Layout of the photolithographic setup for resistive measurements; right) two resistivity hysteresis cycles at H_{DC}=0 T and 30 T for two VO_2 samples.

The origin and the evolution of the different phase domains are also governed by the local defects structure [5], dislocations, inhomogeneities, strains, etc. [1]. In this

research, we show how the sample dimensionality affects the MIT. In fact, the sensitivity to the microstructure of the substrate surface is correlated to the surface area and to the thickness of the film.

In the left panel of Figure 1 we show the photolithographic pattern of two VO_2 samples, in particular, the sample A (W_a=514 μm, L_a= 4541 μm, h_a=40 nm) and B (W_b= 1102 μm, L_b= 3760 μm, h_b=60 nm). In the right panel of Figure 1 we shown the resistive hysteresis cycle during the MIT transition of these samples, with an applied magnetic field of 0 T and 30 T.

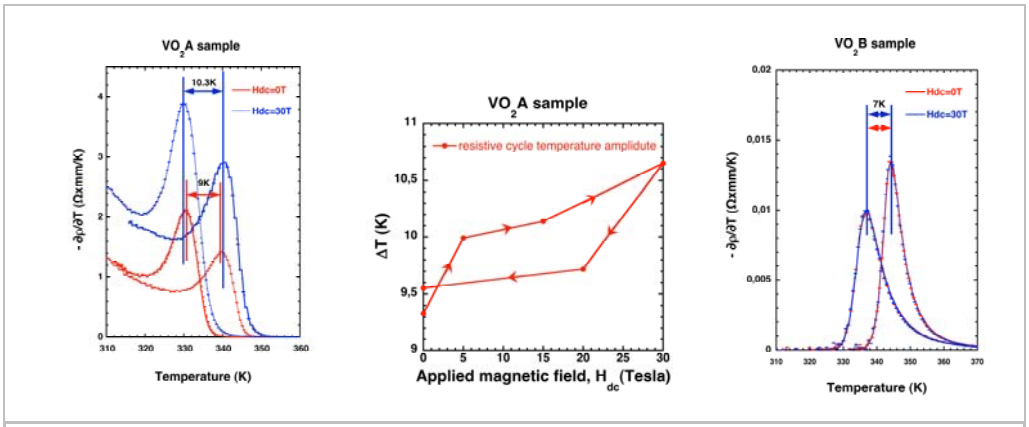

Figure 2: The derivative resistivity vs. temperature at 0 and 30 T for the sample A (left) and B (center) and the width of the hysteretic MIT temperature cycle (right).

The data point out that '*the insulating state sample with a greater area has a higher conductivity. The increase of defect due to the substrate/film area interface, has a clear effect on the resistivity of the insulating state*'. Regarding the high magnetic field, in Figure 2 we show the derivative resistivity vs. T to measure the transition width, ΔT(K), as a function of the magnetic field.

It is evident that ΔT in the A sample (40 nm thick) an applied magnetic field dependence (Figure 2 left) occurs as confirmed by the ΔT vs. H_{dc} (0-30 T) behavior (Figure 2 center). The behavior is different from the B sample (60 nm thick) and confirms the bulk VO_2 data [3] with a MIT independent by the magnetic field also at high magnetic (Figure 2 right). The result points out that '*decreasing the thickness of the VO_2 film amplifies the effect of defects present at the interface substrate/film introducing an unexpected magnetic dependence at high magnetic fields*'.

References

1. J. Cao, J. Junqiao Wu, Mat. Sci. Eng. R71, 35-52 (2011).
2. M. M. Qazilbash, M. Brehm, Byung-Gyu Chae, P.-C. Ho, G. O. Andreev, Bong-Jun Kim, Sun Jin Yun, A. V. Balatsky, M. B. Maple, F. Keilmann, Hyun-Tak Kim, D. N. Basov, Science 318, 1750 (2007)

3. C.N.Berglund and H.J. Guggenheim, Phys. Rev.185, 1022 (1969)
4. M. Nakano, K. Shibuya, D. Okuyama, T. Hatano, S. Ono, M. Kawasaki, Y. Iwasa & Y. Tokura, Nature 487, 459 (2012)
5. N. Poccia, A. Ricci, G. Campi, M. Fratini, A. Puri, D. Di Gioacchino, A. Marcelli, M. Reynolds, M. Burghammer, N. L. Saini, G. Aeppli, A. Bianconi, Proc. Nat. Acad. Sciences 109, 15685 (2012)

A. Acun et al. “Atomically Controlled Surfaces Interfaces and Nanostructures”
edited by A. Bianconi, A. Marcelli (Superstripes Press, Rome 2016) isbn: 9788866830597

Fr1T session

A. Acun et al. “Atomically Controlled Surfaces Interfaces and Nanostructures”
edited by A. Bianconi, A. Marcelli (Superstripes Press, Rome 2016) isbn: 9788866830597

Silicene, germanene, and something in between

Yukiko Yamada-Takamura
School of Materials Sciences, Japan Advanced Institute of Science and Technology (JAIST)

Email: *yukikoyt@jaist.ac.jp*
Key words: 12- Graphene and other 2D materials

“Silicene” and “germanene” are an-atom thick sheets made of silicon (Si) and germanium (Ge), respectively, which are emerging as elemental two-dimensional (2D) materials beyond graphene. They are characterized as buckled honeycomb lattices with extended π-electronic states [1]. In their freestanding form, they are predicted to host massless Dirac electrons [2] just like graphene, and to behave as 2D topological insulators at experimentally accessible temperatures [3] unlike their carbon counterpart. Although the first theoretical study on such materials was published in 1994 [2], it was not until a few years ago that experimental evidence has been reported [4,5]. Since then, the number of publications related to non-graphene elemental 2D materials has dramatically increased, but still, most of them are theoretical studies, and the number of experimental studies are limited due to their inherent difficulties in synthesis and characterization [1].
Since both Si and Ge prefer to crystallize in diamond structure and their graphitic counterparts are lacking as possible parent crystals for silicene and germanene to be formed through simple mechanical exfoliation, they have to be grown in the form of epitaxial sheets on appropriate substrates through techniques such as vapor deposition. While the formation of silicene sheets on Ag(111) single crystals has been reported through vapor deposition of Si atoms on the clean surfaces [4], we had demonstrated that epitaxial silicene sheet spontaneously forms as a surfactant layer on single-crystalline ZrB_2(0001) thin films grown on Si(111) wafers and also on the same film surface after oxidation followed by removal of oxides through heating at 800 ^oC under ultrahigh vacuum [5]. At temperatures higher than 650^oC, silicene looses its structure on ZrB_2 film surface while Si atoms remain on the film surface. Upon cooling down, these Si atoms originating from the Si substrate crystallize into atomically-thin epitaxial sheet with characteristic stripe domain structure [5]. The areal density of Si atoms in this sheet was measured by medium energy ion scattering, and determined to be very close to a monolayer amount of ($\sqrt{3}\times\sqrt{3}$)-reconstructed Si honeycomb lattice with the cell size of that of ZrB_2(0001)-(2×2) surface [6]. Thus, there is no need to add or control the amount of Si atoms for this spontaneously-formed silicene sheet, but interestingly, when we do add Si atoms slightly, we can form a “true monolayer” sheet without domain structures with retained electronic properties [6.. Alternatively, when Ge atoms were added to this spontaneously-formed silicene sheet, a number of 2D Si-Ge heterostructures - lateral, vertical, and alloy - were formed [7.. In this talk, I would

like to introduce our recent effort to synthesize and characterize silicene, germanene, and their heterostructures on ZrB_2 thin film surfaces.

References

1. Y. Yamada-Takamura and R. Friedlein, Science and Technology of Advanced Materials 15, 064404 (2014). http://dx.doi.org/10.1088/1468-6996/15/6/064404
2. K. Takeda and K. Shiraishi, Physical Review B 50, 14916 (1994). http://dx.doi.org/10.1103/PhysRevB.50.14916
3. C.-C. Liu, W. Feng, and Y. Yao, Physical Review Letters 107, 076802 (2011). http://dx.doi.org/10.1103/PhysRevLett.107.076802
4. P. Vogt, P. De Padova, C. Quaresima, J. Avila, E. Frantzeskakis, M. C. Asensio, A. Resta, B. Ealet, and G. Le Lay, Physical Review Letters 108, 155501 (2012). http://dx.doi.org/10.1103/PhysRevLett.108.155501
5. A. Fleurence, R. Friedlein, T. Ozaki, H. Kawai, Y. Wang, and Y. Yamada-Takamura, Physical Review Letters 108, 245501 (2012). http://dx.doi.org/10.1103/PhysRevLett.108.245501
6. A. Fleurence, T. G. Gill, R. Friedlein, J. T. Sadowski, K. Aoyagi, M. Copel, R. M. Tromp, C. F. Hirjibehedin, and Y. Yamada-Takamura, Applied Physics Letters 108, 151902 (2016). http://dx.doi.org/10.1063/1.4945370
7. Y. Awatani, A. Fleurence, and Y. Yamada-Takamura, APS March Meeting 2016. http://meetings.aps.org/link/BAPS.2016.MAR.T1.307

A. Acun et al. “Atomically Controlled Surfaces Interfaces and Nanostructures”
edited by A. Bianconi, A. Marcelli (Superstripes Press, Rome 2016) isbn: 9788866830597

Observation of van Hove singularities in multilayer silicene

Jincheng Zhuang, Zhi Li, Xun Xu, Shi Xue Dou, and Yi Du,
Institute for Superconducting and Electronic Materials (ISEM), Australian Institute for Innovative Materials (AIIM), University of Wollongong, Wollongong, NSW 2525, Australia

Email: *ydu@uow.edu.au*
Key words: silicene, twisted, STM, Moiré pattern, van Hove singularities

Silicene, a new allotropy of silicon in a two-dimensional honeycomb structure, recently attracts a great interest. Due to its graphene-like electronic band structure, charge carriers in silicene behave as massless Dirac fermions. Theoretical studies indicate that silicene has a larger energy gap at the Dirac point and may show a detectable Quantum Spin Hall Effect (QSHE), because it shows even a stronger spin-orbit coupling in contrast to graphene. Moreover, its scalability and compatible with current silicon-based nanotechnology makes silicene a promising candidate for spintronic applications.

Multilayer silicene is quite unique that silicon atoms adopt competing *sp* hybridization states leading to a low-buckled structure and a relative strong interlayer interaction. It is still unclear that whether multilayer silicene retains layered stacking structure and characteristic Dirac fermion with such a strong interlayer interaction. In addition, stacking order provides an important yet rarely explored degree of freedom for tuning multilayer silicene’s electronic structures. In this talk, we report the atomic arrangement of 1×1 structure as the building block in epitaxial $\sqrt{3}\times\sqrt{3}$ multilayer silicene by scanning tunneling microscopy. Underlying silicene layers remain $\sqrt{3}\times\sqrt{3}$ structure after the top silicene layer being mechanically peeled off. We demonstrate that a rotation between stacked silicene layers can create van Hove Singularities even with a large twisting angle. Our study verifies the layered stacking structure of multilayer silicene, and suggests intriguing method for modulating electronic properties by van Hove singularity engineering in this two-dimensional material.

Abstract text here made of about 2500 characters including spaces (times new roman 11pt - normal).

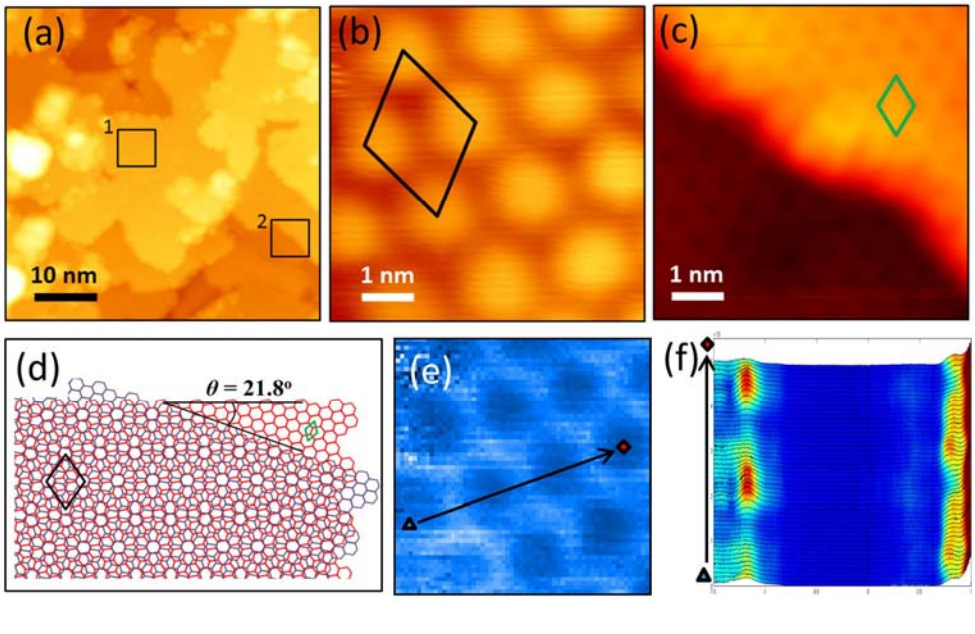

Figure 1: STM and STS on twisted silicene multilayers. (a) STM topographic image of multilayer silicene. (b) and (c) are high-resolution STM images corresponding to twisted silicene multilayers in Area 1 and normal stacking silicene multilayers in Area 2 in (a), respectively. (d) An obvious Moiré pattern demonstrates interlayer rotation angle of 21.8° in twisted silicene layers. (e) and (f) are STS mapping obtained in Area 1 in (a), which demonstrate a set of new Dirac-cone structures created by a Moiré-pattern-modulated honeycomb potential field in twisted silicene.

References

1. Yi Du, Jincheng Zhuang, Hongsheng Liu, Xun Xu, Stefan Eilers, Kehui Wu, Peng Cheng, Jijun Zhao, Xiaodong Pi, Khay Wai See, Germanas Peleckis, Xiaolin Wang, and Shi Xue Dou, *ACS Nano 8*, 10019 (2014)
2. Xun Xu, Jincheng Zhuang, Yi Du, Haifeng Feng, Nian Zhang, Chen Liu, Tao Lei, Jiaou Wang , Michelle Spencer, Tetsuya Morishita, Xiaolin Wang and Shi Xue Dou, *Sci. Rep. 4*, 7543 (2014)
3. J. Zhuang, X. Xu, Y. Du, K. Wu, L. Chen, W. Hao, J. Wang, W. K. Yeoh, X. L. Wang, and S. X. Dou, *Phys. Rev. B 91*, 161409(R) (2015)

Ab initio explorations of elemental 2D materials beyond graphene

Si Zhou[1] , Jijun Zhao[1]
[1] *Key Laboratory of Materials Modification by Laser, Ion and Electron Beams (Dalian University of Technology), Ministry of Education, Dalian 116024, China*

Email: *sizhou@dlut.edu.cn*
Key words: 2D Materials, silicene, phosphorene, graphyne

In recent years, there have been tremendous interests in elemental 2D materials beyond graphene, such as silicene [1], boron monolayer [2], and phosphorene. In this presentation, I will briefly introduce the recent progress on theoretical simulation of post-graphene elemental 2D materials from my group. We explored a variety of point defects in (4×4) and (√13×√13)R13.9º silicene superstructures on Ag(111) surface and compared with experimental STM images [3]. The computed formation energies and diffusion barriers can nicely explain experimental observation of the defect behaviors of these two silicene superstructures. We also systematically compared the interaction strength between silicene (and germanene, stanene) and various metal substrates reported in experiments. We explore the atomic structure, thermodynamic stability, and electronic properties of phosphorene GBs [4]. A total of 19 GBs were predicted and found to be energetically stable with formation energies much lower than those in graphene. These GBs do not severely affect the electronic properties of phosphorene: the band gap of perfect phosphorene is preserved, and the electron mobilities are only moderately reduced in these defective systems. Finally, we predicted growth of graphyne on selected transition metal substrates.

References

1. 1. J. J. Zhao, et al., Progress in Materials Science 83, 24 (2016).
2. 2. H. S. Liu, J. Gao, J. Zhao, Scientific Reports 3, 3238 (2013).
3. 3. H. S. Liu, H. F. Feng, Y. Du, J. Chen, K. H. Wu, J. J. Zhao, arXiv:1512.08860
4. 4. Y. Guo, S. Zhou, J. F. Zhang, Y. Z. Bai, J. J. Zhao, 2D Materials 3, 025008 (2016).

A. Acun et al. “Atomically Controlled Surfaces Interfaces and Nanostructures”
edited by A. Bianconi, A. Marcelli (Superstripes Press, Rome 2016) isbn: 9788866830597

Nanostructures and nanochemistry at graphene and silicon carbide surfaces and interfaces

Patrick Soukiassian
Commissariat à l’Energie Atomique et aux Energies Alternatives, Saclay, & Université Paris-Sud, Orsay, France

Email: patrick.soukiassian@cea.fr
Key words: graphene/SiC, surface, interface, nanowire, nanotunnel, nanochemistry

The Moore’s law has powered the information-technology revolution since the 1960s. However, due to new needs and challenges, it is approaching its end [1]. Thermal transport is becoming a major issue, requiring specific investigations, especially at low dimensional scales [2]. Graphene & silicon carbide (SiC) are advanced semiconductors having figures of merit scaling well above those of well-established ones. SiC, has a wide band-gap, is especially suitable for high-power, high temperatures and high frequencies devices/sensors. In addition, it is biocompatible and resistant to radiation damages, with the same thermal conductivity than copper. Graphene, a 2D material made of a single atomic layer of C atoms in sp2 bonding configuration, has unsurpassed properties with a very large phase coherence lengths > 1 μm at 4 K, unprecedented high mobility at μ=250,000 cm2/V.s (1,360 cm2/V.s for Si). In addition, graphene has unsurpassed spin diffusion lengths exceeding > 100 μm (few μm for Si), a thermal conductivity 10 times higher than Cu, and mechanically, the strongest material ever measured [3-6]. Functionalization remains however challenging since interacting too strongly with a graphene layer may alter its properties. As a 2D single atomic layer material, graphene needs a substrate. In this view, SiC is an excellent choice since “graphene” could be grown epitaxially on its surface. Understanding/mediating SiC and graphene surfaces & interfaces properties are of central importance toward functionalization. In addition, interacting with the SiC surface may offer an alternative approach in successful functionalization. The 1st case of H/D-induced metallization of a semiconductor surface has been shown for Si-rich 3C-SiC(001)-3x2 surface [7]. Combining advanced experimental techniques as STM/STS, vibrational & 3rd generation synchrotron radiation-based photoelectron spectroscopies, and state-of-the-art calculations bring the 1st evidence of H/D-induced nanotunnel opening at a semiconductor sub-surface for SiC – Fig. 1a - [8]. Dangling bonds generated inside a nanotunnel offer a promising template to capture atoms or molecules, opening nano-tailoring capabilities towards advanced applications in electronics, chemistry, storage, sensors or biotechnology. Such a mechanism open routes to selective surface/interface functionalization of epitaxial graphene [8]. Such nanotunnels have also been recently predicted for C-terminated 3C-SiC(001)-c(2x2) surface - Fig. 1b - [9]. Finally, another amazing aspect is H interaction with graphene

on SiC dust grains to polycyclic aromatic hydrocarbons (PAH) formation in the interstellar medium, as possible route toward prebiotic roots of life in the universe [10].

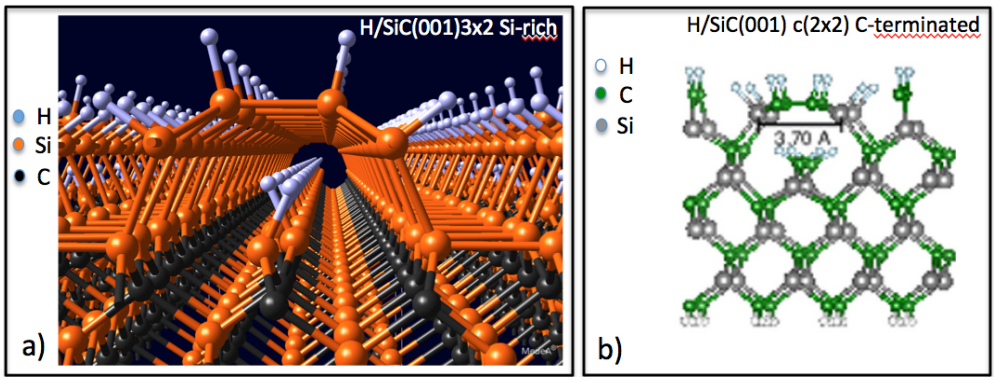

Figure 1: H-induced nanotunnel opening at a) Si-rich 3C-SiC(001)-3x2 [8] and b) C-terminated 3C-SiC(001)-c(2x2) [9] the sub-surfaces.

References

1. M. Mitchell Waldrop, "*The semiconductor industry will soon abandon its pursuit of Moore's Law. Now, things could get a lot more interesting*", Nature 360, 146 (2016)
2. A. France-Lanord, P. Soukiassian, C. Glattli, E. Wimmer "*Ab initio parameterization of a charge optimized many-body forcefield for Si–SiO_2: Validation and thermal transport in nanostructures*" J. Chem. Phys. 144, 104705/1-12 (2016)
3. W. Lu, P. Soukiassian, J. Boeckl "*Graphene: fundamentals and functionalities*", MRS Bull. 37, 1119 (2012)
4. P. Soukiassian "*Will graphene be the material of 21th century?"* MRS Bull. 37, 1321 (2012)
5. J. Baringhaus, M. Ruan, F. Edler, A. Tejeda, M. Sicot, A. Taleb-Ibrahimi, Z. Jiang, E. Conrad, C. Berger, C. Tegenkamp, W.A. de Heer, "*Exceptional ballistic transport in epitaxial graphene nanoribbons*", Nature 506, 349 (2014)
6. B. Dlubak, M.B. Martin, C. Deranlot, B. Servet, S. Xavier, R. Mattana, M. Sprinkle, C. Berger, W.A. De Heer, F. Petroff, A. Anane, P. Seneor, A. Fert, "*Highly efficient spin transport in epitaxial graphene on SiC*", Nature Phys. 8, 557 (2012)
7. V. Derycke, P. Soukiassian, F. Amy, Y.J. Chabal, M. D'angelo, H. Enriquez, M. Silly "*Nanochemistry at the atomic scale revealed in H-induced semiconductor surface metallization*", Nature Mat. 2, 253 (2003)
8. P. Soukiassian, E. Wimmer, E. Celasco, Cl. Giallombardo, S. Bonanni, L. Vattuone, L. Savio, A. Tejeda, M. Silly, M. D'angelo, F. Sirotti, M. Rocca "*Hydrogen-induced nanotunnel opening within semiconductor subsurface*" Nature Com. 4, 2800 (2013)

9. E.F. Rosso, R.J. Baierleb, W. Orellana, R.H. Miwada, “*Hydrogen-induced nanotunnel structure on the C-terminated 3C-SiC(001)-c(2×2) surface investigated by ab-initio calculations*” Appl. Surf. Sci. 357, 1753 (2015)
10. P. Merino, M. Švec, J.I. Martinez, P. Jelinek, P. Lacovig, M. Dalmiglio, S. Lizzit, P. Soukiassian, J. Cernicharo, J.A. Martin-Gago “*Graphene etching on SiC grains as a path to interstellar PAHs’ formation*” Nature Com. 5, 3054 (2014)

A. Acun et al. “Atomically Controlled Surfaces Interfaces and Nanostructures”
edited by A. Bianconi, A. Marcelli (Superstripes Press, Rome 2016) isbn: 9788866830597

Hydrogenated Silicene

Daniel Beato-Medina[1], Eric Salomon[1], Guy Le Lay[1], and Thierry Angot[1]
[1]*Aix Marseille Université, CNRS, PIIM UMR 7345, 13397, Marseille, France*

Email: *thierry.angot@univ-amu.fr*
Key words: Graphene and other 2D materials; Frontiers aspects of semiconductor, surfaces and interfaces

Silicene is a synthetic low-dimensional allotrope of silicon with a honeycomb structure similar to graphene. Silicene is attracting a lot of attention because of its fundamental possibilities as well as its potential compatibility with microelectronics technologies [1]. Synchrotron radiation photoelectron spectroscopy results acquired at the SOLEIL facility have demonstrated that silicene grown on Ag(111) hosts Dirac fermions with a Fermi velocity about one-third of that of free standing graphene [2]. Functionalization by atoms or molecules may be used to modify the electronic properties of silicene. Yet, fundamental knowledge about functionalizing silicene is in its infancy. To contribute to the actual state of the art, we have undertaken experimental works dedicated to studying the reactivity of silicene with respect to hydrogen atoms.
The interaction between silicene and atomic hydrogen has been investigated by Scanning tunneling Microscopy (STM) and High Resolution Electorn Energy Loss Spectroscopy (HREELS). As shown recently [3], the fully hydrogenated silicene monolayer prefers to accomodate seven H atoms in one silicene-(3×3)/(4×4) unit cell. Nevertheless, other configurations, of which the origin will be discussed, were observed in coexistence with the previous one. We will also focus on the vibrationnal properties as measured by HREELS. We demonstrate that depending on the film thickness, the reactivity of the silicene films differs. Atomic H interaction with silicene will be compared with that of the Si(111) surface, as well as with $ErSi_2$,/Si(111) [4], another 2d materials that may be considered as related to silicene.

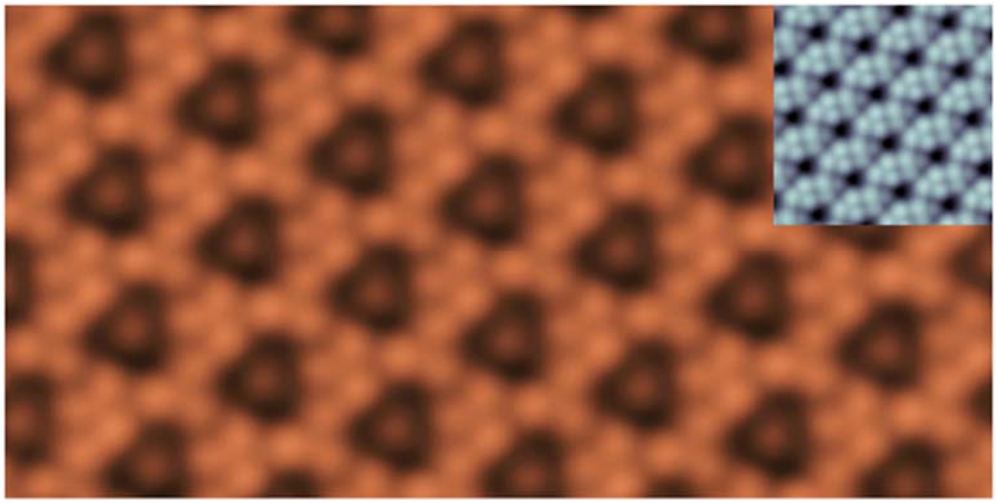

Figure 1: Monolayer of silicene-(3×3)/(4×4) exposed atomic hydrogen. Inset silicene-(3×3)/(4×4) on Ag(111)

References

1. A. Dimoulas, Microelectronic Engineering, 131, 68 (2015).
2. P. De Padova et al., 2D Materials 1, (2014) 021003.
3. J. Qiu et al. Phys. Rev. Lett. 114, 126101 (2015).
4. T. Angot et al. Surf. Sci. 368, 190 (1996)

Fr2T session

From SPM to Transport in Molecules -Theoretical Aspects-

Masaru Tsukada
WPI-AIMR, Tohoku University, 2-1-1 Katahira, Aoba-ku, Sendai, 980-8577

Email: tsukada@wpi-aimr.tohoku.ac.jp

Recently scanning probe microscopy (SPM) including STM, AFM, KPFM and so forth has been remarkably developed to be a major measurement method of surfaces and nanostructures. Interpretation of observed images, however, is often not simple and requires theoretical analyses based on deep consideration of phenomena taking places around tip and surface. Therefore theory and theoretical simulation of SPM became more and more important. In this talk, recent theoretical topics of SPM are introduced in which collaboration with experiments produced fruitful pioneering results. They include AFM images of various protein molecules, a quasi water structure appeared in microscopic 3D force pattern at solid-water interfaces, finding of a new reconstructed structure of $SrTiO_3$(001) surface, as well as theory of KPFM applied to Si surfaces with embedded impurity. Moreover some important issues of electron transport through large molecules between the tip and substrate will be discussed. The problems discussed include loop currents in carbon network molecules, Franck-Condon blockade of a molecule sandwiched between nano-electrodes, and transport in Helical polyacetylene. These systems are more or less related to the issue of wave (coherent) vs particle (dissipative) nature of electrons.

References

1. M. Tsukada, K. Tagami, Q. Gao and N. Watanabe, Current nanoscience 3 (2007) 084005
2. S. Ido, et al, ACS Nano, (2013), 7(2), 1817
3. M. Tsukada, N. Watanabe, M. Harada and K. Tagami, J. Vac. Sci., Techn, B 28, C4C1, (2010)
4. M. Tsukada, A. Masago and M. Shimizu, J. of Phys. Condensed Matter, 24 (2012) 084002
5. M. Araidai and M. Tsukada, Phys. Rev. B 81 235114 (2010)
6. K. Mitsutake, K. Yano and M. Tsukada, J. Phys. Chem. (2015) 119, 10282

A. Acun et al. “Atomically Controlled Surfaces Interfaces and Nanostructures”
edited by A. Bianconi, A. Marcelli (Superstripes Press, Rome 2016) isbn: 9788866830597

Exotic properties of group-IV honeycomb crystals

Friedhelm Bechstedt
Friedrich-Schiller University Jena
Institute of Solid State Theory and Optics

Email: *bechsted@ifto.physik.uni-jena.de*
Key words: atomically thin films; novel 2D crystals; graphene-like materials; chemical functionalization; electronic structure; topological invariants; quantum spin Hall phase; edge states

The rediscovery of graphene and its peculiar physical properties have caused intense research on two-dimensional (2D) sheet crystals. They unify features of bulk, surface and nanostructure in one-and-the-same atomic arrangement. Hexagonal graphene-like 2D crystals of other group-IV elements such as silicene, germanene and stanene are predicted to be ‘wonder’ materials since their honeycomb structure is responsible for Dirac electrons and spin-orbit interaction (SOI) increases along the group IV of the periodic table. Especially, silicene with similar electronic properties as graphene may add further possibilities for novel Si-nanostructure-based electronic devices and integration into current silicon semiconductor technology. Germanene and stanene become interesting because of the SOI-induced gap opening. Chemical functionalization with hydrogen (H) and halogens such as iodine (I) or geometrical modification in nanoribbons increase the variety of possible applications.

The recent realization of silicene on graphene [1] or germanene on MoS2 [2], exfolation of hydrogenated germanene [3], and epitaxial growth of stanene [4] have induced manifold first-principles studies and electronic structure calculations to study their geometries and properties. This talk reports important results of such theoretical activities and discuss them in the light of available experiments. Four complexes are investigated in more detail:
(i) The conical linear bands seem to survive in the case of weak adsorbate-substrate interaction [5] but not in other energetically more favored 2D polymorphs [6].
(ii) The linear bands have enormous consequences for the IR optical properties. Independent of the group-IV element and the degree of hybridization the universal absorbance is ruled by the Sommerfeld finestructure constant [7]. The optical properties in general are significantly influenced despite the fact of having atomically thin layers [8].
(iii) Spin-orbit interaction not only modifies the optical properties by band gap opening [9]. It makes the 2D crystals to topological insulators which exhibit a quantum spin Hall (QSH) conductivity [8]. Their QSH phase can be destroyed within vertical electric fields [10].
(iv) Germanene and stanene nanoribbons give rise to topological edge states independent of zigzag or armchair edge orientation, if the edges are non-magnetic [10].

(a)

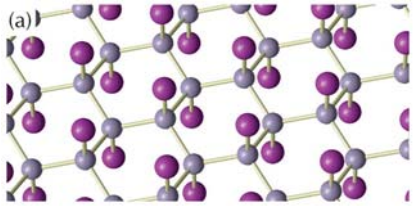

(b)

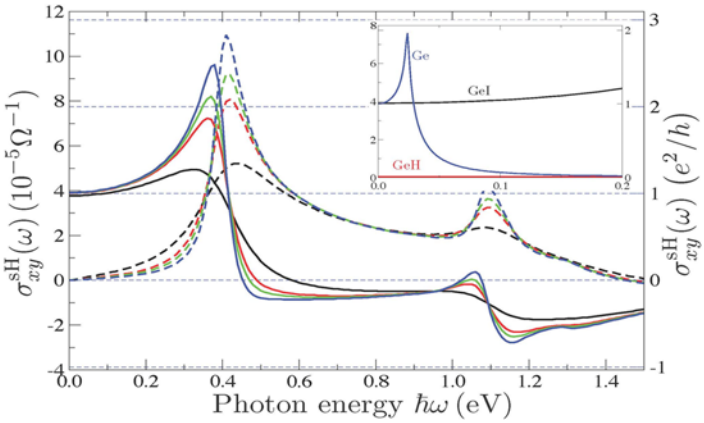

Figure 1: (a) Perspective view on GeI geometry. (b) Spin Hall conductivity of GeI. Its quantization is also visible for germanene but not germanane.

References

1. M. De Crescenzi, I. Berbezier, M. Scarselli et al., Nature Commun. (in print).
2. L. Zhang, P. Bampoulis, A. N. Rudenko et al., private communication.
3. E. Bianco, S. Butler, S. Jiang et al., ACS Nano 7, 4414 (2013).
4. F. Zhu, W. Chen, Y. Xu et al., Nature Mater. 14, 1020 (2015).
6. S. Kokott, F. Bechstedt, pss RRL 7, 538 (2013), J. Phys. CM 26, 185002 (2014).
7. F. Matusalem, M. Marques, and F. Bechstedt, Phys. Rev. B 92, 045436 (2015).
8. L. Matthes, P. Gori, O. Pulci, and F. Bechstedt., Phys. Rev. B 87, 035438 (2013).
9. L. Matthes, O. Pulci, and F. Bechstedt, New J. Phys. 16, 105007 (2014).
10. L. Matthes, S. Kuefner, and F. Bechstedt, Phys. Rev. B 93, 121106(R) (2016).
11. L. Matthes and F. Bechstedt, Phys. Rev. B 90, 165431 (2014).

A. Acun et al. "Atomically Controlled Surfaces Interfaces and Nanostructures"
edited by A. Bianconi, A. Marcelli (Superstripes Press, Rome 2016) isbn: 9788866830597

A complete multiple scattering approach to core-state EELS cross-section

Didier Sébilleau[1], Junqing Xu[2], Rakesh Choubisa[3] and Calogero Natoli[4]
[1]*Groupe Théorie, Institut de Physique de Rennes, Université de Rennes-1, 35042 Rennes cedex, France*
[2]*National Synchrotron Radiation Laboratory, University of Science and Technology of China, Hefei, China*
[3]*Physics Department, Birla Institute of Technology and Science, BITS-Pilani, Pilani, Rajasthan, India*
[4]*Theory Group, INFN-Laboratori Nazionali di Frascati, 00044 Frascati, Italy*

Email: *didier.sebilleau@univ-rennes1.fr*
Key words: 1-Atomic and nanoscale structure of surfaces and interfaces: advanced methods; 14-State-of-the-art theoretical approaches on surfaces and interfaces

Electron-energy-loss spectroscopy (EELS) is a very versatile tool that can probe quite different physical phenomena (phonons, intraband/interband transitions, electronic structure). We focus here on the excitation of core states with incoming electron energy in the range [50-1000] eV so that the sensitivity to the surface is maximized. Indeed, in this range of energy, it has been demonstrated experimentally that EELS can be used to study the local atomic structure around the absorbing atom [1,2]. In this range, the standard approach to EELS which makes use of the Kincaid *et al* [3] XAS-like approach where multiple scattering in the incoming and scattered beams is neglected, cannot be used anylonger. In contrast to previous attempts to go beyond the XAS-like model and that were relying either on a crystal field approach [4] or on the periodicity of the sample [5,6], we derive a complete multiple scattering approach of core-level EELS in the real space that treat all electrons on an equal footing and does not require any periodicity of the sample. By complete, we mean that we take fully into account into our formulation that fact that the interaction between the incoming electron and the core state on the absorbing atom is long-ranged. The direct consequence is that the cross-section of EELS depends not only on the absorbing atom, but it contains also contributions from neighbouring atoms. We discuss the relative importance of these contributions on an example (see figure 1). We find in particular that the matrix elements of the Coulomb field which we take as screened as we are in a solid, should vanish after a few shells of neighbours. Finally, we show which approximations have to be made in the multiple scattering EELS theory in order to recover the XAS model [3] which is generally used to describe core-level EELS.

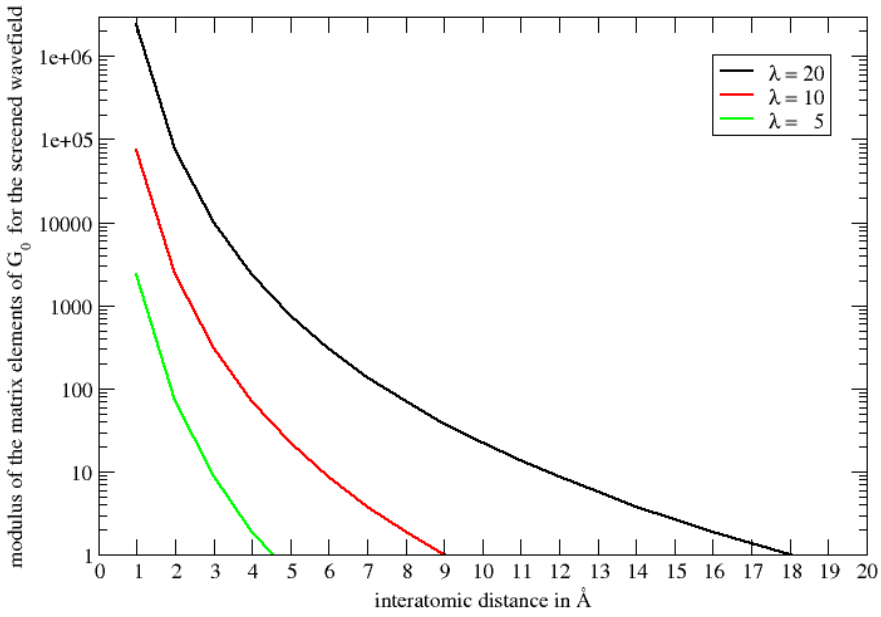

Figure 1: Modulus of the screened Coulomb field propagator as a function of the distance and the screening constant λ.

References

1. M. De Crescenzi, F. Antonangeli, C. Bellini and R. Rosei, Phys. Rev. Lett. 50, 1949 (1983).
2. L. S. Caputi, O. Comite, A. Amoddeo, G. Chiarello, S. Scalese, E. Colavita and L. Papagno, Phys. Rev. Lett. 77, 1059 (1996).
3. B. M. Kincaid, A. E. Meixner and P. M. Platzman, Phys. Rev. Lett. 40, 1296 (1978).
4. J. J. M. Michiels, J. E. Inglesfield, C. J. Noble, V. M. Burke and P. G. Burke, Phys. Rev. Lett. 78, 2851 (1997).
5. D. K. Saldin, Phys. Rev. Lett. 60, 1197 (1988).
6. M. De Crescenzi, L. Lozzi, P. Picozzi, S. Santucci, M. Benfatto and C. R. Natoli, Phys. Rev. B 39, 8409 (1989).

A. Acun et al. "Atomically Controlled Surfaces Interfaces and Nanostructures"
edited by A. Bianconi, A. Marcelli (Superstripes Press, Rome 2016) isbn: 9788866830597

Rapid Fermi-Surface, Fermi-Velocity and Spin Mapping Using ToF *k*-Microscopy: Application to Topological Systems.

Gerd Schönhense
Johannes Gutenberg-University of Mainz, Institute of Physics, Staudingerweg 7, D-55099 Mainz, Germany

Email: *schoenhe@uni-mainz.de*
Key words: momentum microscopy, imaging spin filter, spin texture

The Fermi surface, Fermi velocity v_F and spin texture are of high importance for the design of materials with tailored electronic properties. Moreover, the topology of the Fermi surface plays a crucial role in the existence of topologically non-trivial electronic states like the metallic states in the surface region of topological insulators. A novel experimental technique, termed time-of-flight (ToF) momentum microscopy, allows mapping of the full surface electronic structure in a single measurement on a time scale of 20 min [1,2]. In combination with high-brilliance soft X-rays ($h\nu$ = 300 to 1300eV) the novel method was extended towards 3D mapping of the topology of the full Fermi surface, the *k*-dependence of v_F, and quantitative analysis of electron and hole pockets for tungsten [3]. Implementation of an imaging spin filter allows an as-yet-unachievably rapid access to the complete spin-dependent electronic band structure of solid state materials. The full-field momentum microscope is based on a cathode lens optimized for imaging large (k_x,k_y)-fields up to 5 Å^{-1} diameter at high resolution (down to 0.01 Å^{-1}). Measured 3D data arrays I(k_x,k_y,t) consist of many *k*-slices with 512x512 pixels (in this experiment 18,000 *k*-points are resolved in slices close to E_F). The time-of-flight t of each electron (recorded by a delay-line detector @ > 5 Mcps) is converted into kinetic energy, calibrated at the Fermi edge. Several hundred energy slices (bin-size 9 meV) are acquired in parallel.
The Fermi surface and *k*-dependence of the Fermi velocity have been studied at beamline P04 at PETRA III (DESY, Hamburg). At a sample temperature of 30 K the band features stay sharp up to $h\nu$ =1300 eV. Momentum components k_x and k_y are resolved by the cathode lens, the binding energy is recorded via ToF and k_z is varied between the 3rd and 4th repeated Brillouin zone by varying the photon energy in many steps between 306 and 574 eV, exploiting the concept of direct transitions [4]. The resulting 4D data array $I(k_x,k_y,k_z,E_B)$ contains the complete information on all bands in the full 3D Brillouin zone. The Fermi surface is obtained when all (k_x,k_y)-slices at E=E_F are concatenated along the k_z-axis. Finally, v_F is determined from the *k*-distance of adjacent energy isosurfaces (E_F, E_F-ΔE) or, in high-symmetry directions, from the slope of the bands at E_F (being the classical way). Three different 3D views of the Fermi surface with a false-color scale of the Fermi velocity are shown in Fig.1a, together with a selection of energy isosurfaces at the Fermi energy (b-f, as denoted by white dotted lines) and at higher binding energy (g-i). The Fermi surface of W is a fragmented object with isolated electron and hole pockets, labelled A-D. v_F varies from 10^5 to 10^6 m/s in the hole pockets and from 10^5 to 2.5 x10^5 m/s for electron pockets.

The maximum is a factor of 2 smaller than the expectation for a free electron gas with the parameters of tungsten.
The first studies of spin textures with the new instrument (taken at BESSY), focused on anomalous surface states with Dirac-like signature on W(110) [5] and the bulk and surface Rashba bands of GeTe(111) [6]. Fig.1j shows a view of the measured spin texture for the W(110) surface (red-blue-grey denote degree of spin polarization and intensity). The 3D array $P(k_x,k_y,E_B)$ reveals a tilted Dirac cone with circularly shaped cross section and a Dirac crossing within the projected bulk band gap of tungsten, 0.84eV below E_F. Dispersion and spin texture show eye-catching similarities to the spin-locked surface states of topological insulators.
Experiments are supported by one-step photoemission calculations (H. Ebert et al.).
Projects funded by BMBF (05K13UM2,05K13GU3).

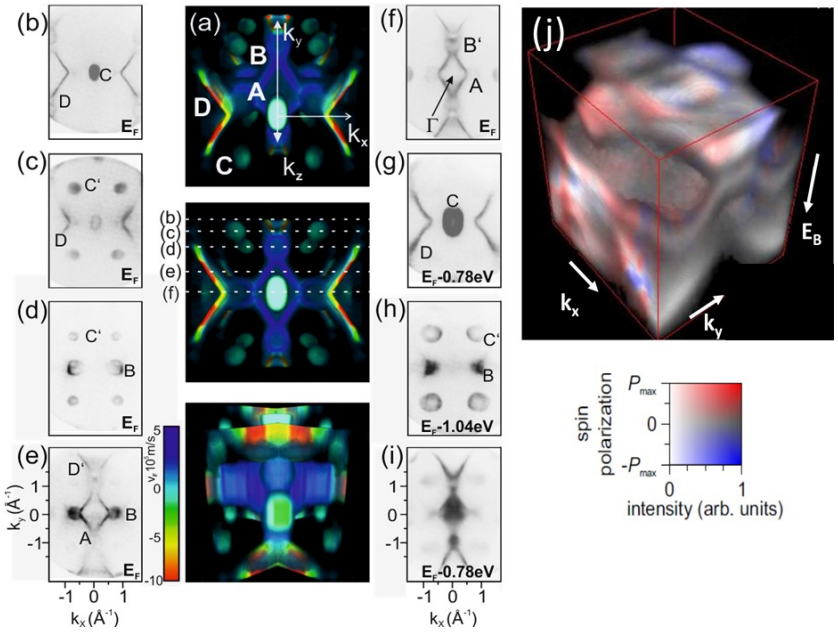

Figure 1: (a) Experimentally-determined ***Fermi surface*** of tungsten in different views. The color scale denotes the ***Fermi velocity*** v_F (see color bar, in units of 10^5 m/s). Blue and red correspond to electron and hole conductivity, respectively. (b-f) selected $E=E_F$ isosurfaces (momentum slices); (g-i) isosurfaces for larger binding energy (from [3]); (j) ***spin texture*** of anomalous surface states on W(110) (from [5]).

References

1. G. Schönhense, K. Medjanik and H. J. Elmers, *JESRP* 200, 94 (2015).
2. S.V. Chernov et al., *Ultramicroscopy* 159, 463 (2015).
3. K. Medjanik et al., *submitted*.
4. A. X. Gray et al., *Nature Mat.* 10, 759 (2011).
5. D. Kutnyakhov et al., *submitted*.
6. H.-J. Elmers et al., *arXiv* 1512.01363 (2015)

A. Acun et al. “Atomically Controlled Surfaces Interfaces and Nanostructures”
edited by A. Bianconi, A. Marcelli (Superstripes Press, Rome 2016) isbn: 9788866830597

A reinvestigation of the high pressure structural phase diagram of black phosphorous

Boby Joseph[1] , Paolo Lotti[1], Andrea Lausi[1], Paolo Dore[2]
[1]*Elettra Sincrotrone, Strada Statale 14 – km 163,5 in Area Science Park, 34149 Basovizza, Trieste, Italy*
[2]*Department of Physics, Sapienza University of Rome, Piazzale Aldo Moro 2, 00185 Rome, Italy*

Email: *boby.joseph@elettra.eu*
Key words: Graphene and other 2D materials

Two dimensional crystals are important class of materials with several potential applications [1]. Black phosphorus (BP) with its tunable direct bandgap, 1.51 eV for the a monolayer to 0.59 eV for a five-layer, is recently demonstrated as a useful candidate for applications like field effect transistor, [2,3]. Application of hydrostatic pressure on the structure and electronic properties is important to understand the fundamental properties and to indicate newer routes to further material manipulation. Considering these aspects in mind, we have recently carried out a systematic high pressure x-ray powder diffraction (HP-XRPD) study on black phosphorus. These studies were carried out at the newly commissioned dedicated high pressure x-ray powder diffraction facility, Xpress beamline [4], at Elettra Synchrotron, Trieste. Measurements were carried out in the pressure range 0- 12.2 GPa using a screw-driven plate diamond anvil cell (DAC) with large x-ray opening. Silicone oil was used as the pressure transmitting medium (PTM). Considering the possibility of degradation of BP due to prolonged air exposure, sample grinding and transfer to the PTM were carried out inside a N_2 filled glove box before being used for the high pressure DAC loading.

Earlier high pressure studies [5-7] on black phosphorus indicated occurrence of two structural phase transitions in BP in the studied pressure range. However, these previous results were not sufficient to fully explain the recent Raman results [8] thus motivating further studies. X-ray powder diffraction results (Fig. 1 (a)) at ambient conditions obtained from a capillary sample could readily be refined with existing structural model. Unlike the capillary data, XRD pattern from the DAC was somewhat different, a comparison of the lowest pressure data is shown in Fig. 1(b). Such a difference was due to the occurrence of preferred orientation which could not be avoided due to the stationary experimental geometry in the HP-XRPD case unlike the capillary measurement, which in the present case permitted the sample oscillations, thus avoiding the preferred orientation effects.

Analysis of the HP-XRPD permitted to follow the structural evolution of the BP with pressure. We observed two transitions in agreement with the earlier studies [5,6]. The ambient condition orthorhombic structure start to convert to rhombohedral around 5 GPa, however with a large co-existence pressure regime. The rhombohedral phase converts further to cubic phase by increasing pressure, however the transition is not yet

complete even at 12.2 GPa. The large co-existence regimes between different phase can qualitatively explain the high pressure Raman results. Further HP-XRPD and high pressure single crystal studies are in program to have ulterior information.

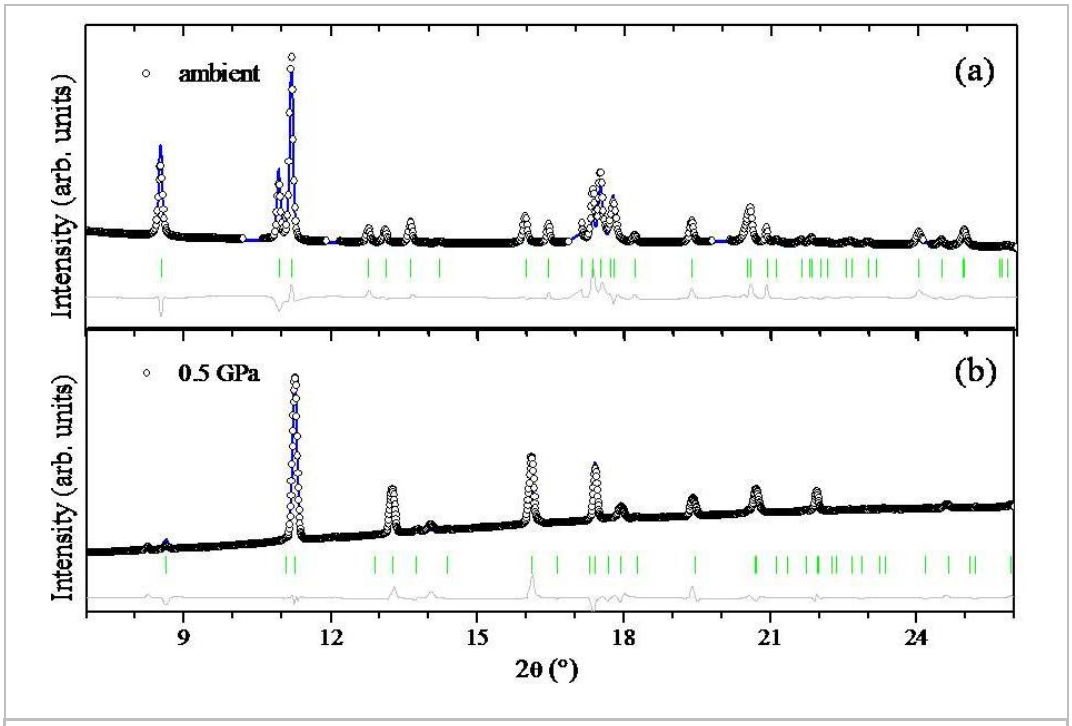

Fig. 1: (a) ambient pressure XRD spectrum of black phosphorus taken with a capillary set-up (with oscillations). (b) A typical low pressure XRD spectrum BP. In both panels symbols are the experimental data, blue line is the results of the refinement and green vertical bars are the Bragg peak positions.

References

1. A. C. Ferrari, et al., “Science and technology roadmap for grahene, related two-dimensional crystals and hybrid systems”, Nanoscale 11, (2015)
2. J. Qiao et al., “High-mobility transport anisotropy and linear dichroism in few-layer black phosphorus” Natur. Comm. 5, 4475 (2014)
3. Z. P. Ling et al., “Black phosphorus transistors with near band edge contact schottky barrier” Scientific Reports 5, 1800 (2015)
4. www.elettra.trieste.it/elettra-beamlines/xpress.html
5. T. Kikegawa et al., “An x-ray diffraction study of lattice compression and phase transition of crystalline phosphorus” Acta Cryst. B 39, 158 (1983)
6. A. Morita “Semiconducting black phosphorus” Appl. Phys. A 39, 227 (1986)
7. Z. J. Xing et al., “Pressure-induced electronic transition in black phosphorus” Phys. Rev. Lett. 115, 186403 (2015)
8. P. Dore et al., (unpublished)

A. Acun et al. “Atomically Controlled Surfaces Interfaces and Nanostructures”
edited by A. Bianconi, A. Marcelli (Superstripes Press, Rome 2016) isbn: 9788866830597

In situ diagnostic of stress generation and evolution in oxide heterostructures

Daniele Pergolesi[1], Aline Fluri[1], Thomas Lippert[1,2]
[1] *Department for Energy and Environment, Paul Scherrer Institut, CH-5232 Villigen-PSI, Switzerland.*
[2] *Department of Chemistry and Applied Biosciences, Laboratory of Inorganic Chemistry, Vladimir-Prelog-Weg 1-5/10, ETH Zürich, CH-8093 Zürich, Switzerland.*

Email: *daniele.pergolesi@psi.ch*
Key words: Pulsed laser deposition, oxigen ion conductors, epitaxial strain, multi-beam optical stress sensor

Stress-induced lattice distortions (strain) can significantly affect physicochemical characteristics of materials modifying electronic, optical, catalytic or charge transport properties. In some cases specific properties of the bulk, or fully relaxed structure, can be enhanced or inhibited by the effect of strain. In other cases, new functionalities, not present in the unperturbed structure, appear in strained lattices.[1-7]

Thin heteroepitaxial films where the strain can be induced by the lattice misfit with the substrate are ideal model systems to investigate the effect of strain on the material properties. With this respect, a comprehensive understanding of the mechanisms of the stress generation at the initial film nucleation and of its evolution during the film growth is of fundamental importance.

When a thin film grows on a substrate under in-plane (i.e. along the direction of the substrate surface) tensile or compressive stress a force applies parallel to the substrate surface arising from the elastic energy accumulated in the system. To release the elastic energy the substrate bends up or downward depending on whether the in-plane stress is compressive or tensile respectively. By measuring during the film growth the curvature of the substrate and knowing its elastic properties, it is possible to monitor *in situ* the stress-thickness product of the growing film by applying the Stoney equation.[9]

This study describes an *in situ* simultaneous diagnostic of the stress by multi-beam optical stress sensor and of the growth mode by reflection high energy electron diffraction during pulsed laser deposition of the oxide films.[10] The simultaneous application of these two techniques has been never attempted so far during the growth of oxide thin film heterostructures.

The stress state and evolution up to the relaxation onset are monitored during the growth of $Ce_{0.85}Sm_{0.15}O_{2-\delta}$ thin films. This material is an oxygen ion conductor mainly used as electrolyte for solid oxide fuel and electrolyzer cells and has been selected for this investigation since a strain effect on its conducting properties is expected.[8] In

particular, a tensile strain along the direction of the migration of the charge carriers should lower the activation energy for charge transport.[7] However, literature reports controversial data and the extent of the effect spreads over several orders of magnitudes.[8] This investigation confirms the expected effect of strain on the ionic conductivity and a thorough characterization of stress and morphology allows quantifying this effect using samples with the conductive properties of single crystals.

The combined *in situ* application of optical deflectometry and electron diffraction provides an invaluable tool for strain engineering in Materials Science to fabricate novel devices with intriguing functionalities.

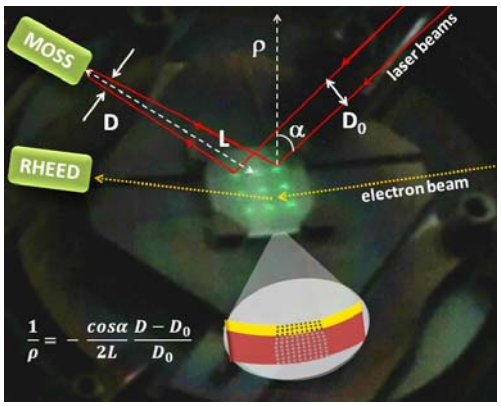

Figure 1: Simultaneous *in situ* monitoring of growth mode by reflection high energy electron diffraction and stress evolution by optical wafer curvature measurement during the growth of oxide heterostructures.

References

1. N. Healy, et al. Nat. Mater. 13, 1122 (2014). http://dx.doi.org/10.1038/nmat4098
2. R. Ramesh, N. A. Spaldin, Nat. Mater. 6, 21 (2007). http://dx.doi.org/10.1038/nmat1805
3. P. Strasser, et al. Nat. Chem. 2, 454 (2010). http://dx.doi.org/10.1038/nchem.623
4. S. Li, et al. Sci. Rep. 4, 6375 (2014). http://dx.doi.org/10.1038/srep06375
5. A. Llordés, et al. Nat. Mater. 11, 329 (2012). http://dx.doi.org/10.1038/nmat3247
6. G. Giri, et al. Nature 480, 504 (2011). http://dx.doi.org/10.1038/nature10683
7. J. A. Kilner, Nat. Mater. 7, 838 (2008). http://dx.doi.org/10.1038/nmat2314
8. B. Yildiz, MRS Bull. 39, 147 (2014). http://dx.doi.org/10.1557/mrs.2014.8
9. S. Suresh, L. B. Freund, Thin Film Materials: Stress, Defect Formation and Surface Evolution (Cambridge Univ., 2006).
10. A. Fluri et al., Nat. Comm. 7, 10692 (2016). http://dx.doi.org/10.1038/ncomms10692

Fr3T session

Optimization of experimental conditions for characterization of thin films in the infrared region of electromagnetic spectrum

K. Banas[1] , A. Banas[1], N. Ali[2], A. Toh[2], P. Saravanan[2], Ch. A. Nijhuis[3], J. Li[3] and M. Breese[1]
[1]Singapore Synchrotron Light Source, National University of Singapore, 5 Research Link, Singapore 117603
[2]School of Applied Science, Temasek Polytechnic, 1 Tampines Avenue 1, Singapore 529757
[3]Department of Chemistry, National University of Singapore, 3 Science Drive 3, Singapore 117543

Email: *slskb@nus.edu.sg*
Key words: Organic nanofilms and devices; Atomic biomaterials interfaces

Very thin and ultrathin films deposited on various substrates have found many applications in different industries. For example, polymeric films used in the biomedical field are gaining considerable interest because they offer great versatility in the chemical groups that can be incorporated at the surface. The constraints imposed by the surface additionally allow for unique physical properties not usually observed for the bulk polymer. Also self-assembled monolayers (SAMs) [1] used in a number of technical areas show applications in material science, biology and biochemistry, sensors, electrochemistry, and nanotechnology.

Analysis of thin and ultrathin layers has been unachievable task for Fourier Transform Infrared (FTIR) spectroscopy for many years. However, with the development of dedicated devices it seems that probing layers of even few nanometers in thickness can be now fulfilled reliably and reproducibly.

Specular reflection mode at grazing incidence angle is a very important technique for analysis of thin layers deposited on reflective substrates. However, in the case where silicon is the substrate, the reflection spectrum contains the signature of the base material in addition to the monolayer and resolving the distinctive features of the surface film becomes difficult. Monolayers and ultrathin films deposited on silicone or gold are easily analyzed by using Attenuated Total Reflection (ATR) mode [2] - an increase in sensitivity up to 1-2 orders of magnitude can be observed comparing to specular reflection mode.

In this contribution two of the most popular IR sampling techniques to investigate the chemistry of monolayers and ultrathin films (of various thickness) deposited on various substrates will be discussed. Special attention will be paid to optimize ATR experimental settings by selection of crystal with proper refractive index and adequate angle of incidence.

Application of FTIR spectroscopy and microscopy for analysis of graphene, self-assembled monolayers, layers of oxides and biofilms allows for characterization of their response in the infrared range of electromagnetic spectrum. Proper spectral pre-processing and statistical analysis [3, 4] is required to extract information from the spectral datasets.

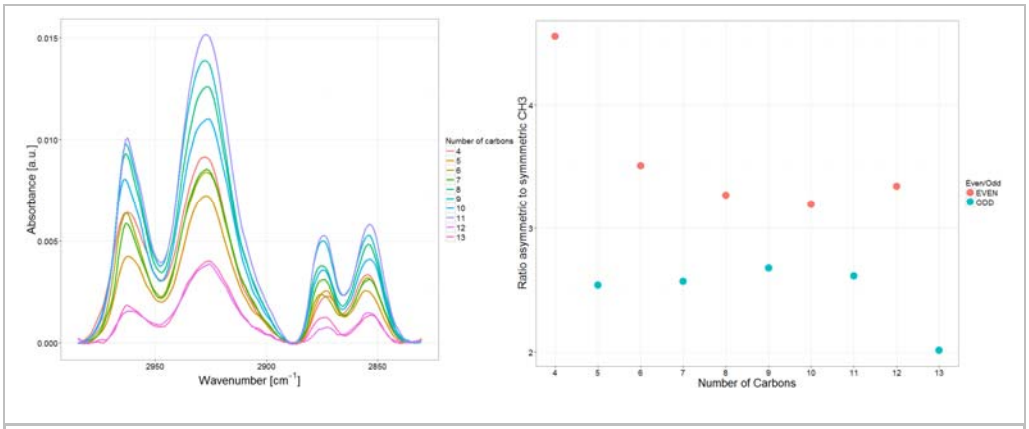

Figure 1: ATR-FTIR spectra of SAMs in the region 2980-2840 cm^{-1} (left) and calculated ratios of asymmetric to symmetric CH_3 stretch showing even/odd effect (right)

References

1. V. J. Angelico, S. A. Mitchell, V. H. Wysocki, Analytical Chemistry, 72, 2603 (2000) http://pubs.acs.org/doi/abs/10.1021/ac0001028
2. G. Laroche, J. Fitremann, N. Gherardi, Applied Surface Science 273, 632 (2013) http://dx.doi.org/10.1016/j.apsusc.2013.02.095
3. R Core Team, R: A Language and Environment for Statistical Computing. R Foundation for Statistical Computing: Vienna, Austria, (2016)
4. RStudio: Integrated development environment for R. (2016) http://www. rstudio.com

A. Acun et al. "Atomically Controlled Surfaces Interfaces and Nanostructures"
edited by A. Bianconi, A. Marcelli (Superstripes Press, Rome 2016) isbn: 9788866830597

The Initial Stages of ZnO Thin Film Growth by Atomic Layer Deposition

Dillon D. Fong[1] , E. Skopin[2], A. Claudel[2], R. Boichot[3], L. Tian[2], M.-I. Richard[4,5], A. Crisci[3], A. Chaker[2], V. Cantelli[2,5], S. Coindeau[3], S. Lay[3], T. Ouled[4], C. Guichet[4], M. H. Chu[6], N. Aubert[6], G. Ciatto[6], E. Blanquet[3], O. Thomas[4], J.-L. Deschanvres[2], and H. Renevier[2] [2,3]
[1]*Materials Science Division Argonne National Laboratory*
[2]*LMGP, Univ. Grenoble Alpes*
[3]*SIMAP, Univ. Grenoble Alpes*
[4]*Aix-Marseille Université*
[5]*European Synchrotron Radiation Facility*
[6]*Synchrotron SOLEIL*

Email: *fong@anl.gov*
Key words: Atomic and nanoscale structure of surfaces and interfaces: advanced methods; Nanoscale structure, growth processes and strain in thin layers and interfaces; Oxides, nitrides and high-k dielectrics

Atomic layer deposition (ALD) is a technique that permits monolayer-by-monolayer synthesis, but this often not the case at the earliest stages of growth [1]. Using *in situ* synchrotron X-ray techniques, we investigate the nucleation and growth of nanoscale ZnO islands, examining how the crystal structure, strain, texture, and composition, evolve as the islands merge during deposition to form continuous layers [2]. The results naturally depend strongly on the type of substrate, which were varied from SiO_2/Si to Al_2O_3 (001) to InGaAs (001). For the SiO_2 and Al_2O_3 substrates, we observed the development of tensile strains during coalescence and found that the ZnO microstructure developed at this stage determines the overall structure of the resulting film (Figure 1, left). The different symmetries of the substrate surfaces led to distinct preferred orientations, with ZnO / SiO_2 exhibiting self-texture with a preference for (001) surfaces and ZnO / Al_2O_3 exhibiting three dominant textures with in-plane rotational domains (Figure 1, right). In the latter case, the relative texture populations depend on temperature but appear to be set during the coalescence stage.

For ZnO on InGaAs (001), the results depended sensitively on growth temperature. At the lowest ALD temperatures, the films remained amorphous, but at slightly higher temperatures, the films underwent amorphous-to-crystalline transitions after reaching a critical thickness. We will discuss these results with those from additional *in situ* stress measurements and *ex situ* studies to provide a general description of initial growth behavior.

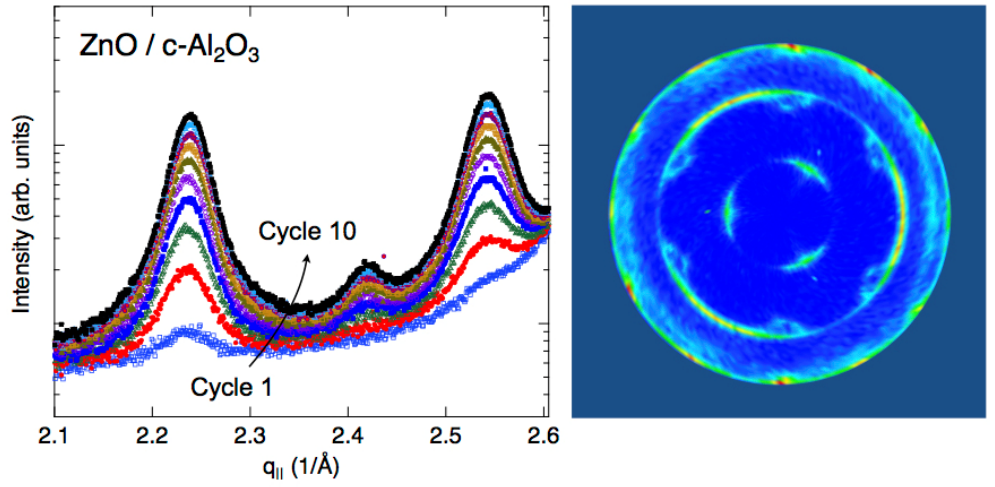

Figure 1: Left: *In situ* grazing incidence X-ray diffraction (GIXRD) radial scans run after the completion of each ZnO layer for cycles 1−10 on Al_2O_3. Right: (100) pole figure of ZnO layers grown by ALD at 250 °C on Al_2O_3. (001).

References

1. D. D. Fong, et al., Appl. Phys. Lett. 97, 191904 (2010).
2. R. Boichot, et al., Chem. Mater. 28, 592 (2016).

A. Acun et al. "Atomically Controlled Surfaces Interfaces and Nanostructures"
edited by A. Bianconi, A. Marcelli (Superstripes Press, Rome 2016) isbn: 9788866830597

Atomic Layer Deposition of ZnO onto GaN and SiC (000.) surfaces: is this True Epitaxy?

Catherine Marichy[1], Sebastien Linas[1],
Jonathan Faugier-Tovar[1], Florica Lazar[2], François Cauwet[1],
Christian Brylinski[1]
[1]*University of Lyon, LYON 1, CNRS, UMR 5615*
Laboratoire des Multimatériaux et Interfaces
[2]*Université de Reims Laboratoire LISM*

Email: *christian.brylinski@univ-lyon1.fr*
Key words: 5 Compound, Wide Bandgap; Organic and Magnetic Semiconductors; Heterojunctions and nanomagnetism; Oxides, nitrides and high-k dielectrics

Devices for electronics and opto-electronics make use of a widening range of hetero-structures such as quantum wells and superlattices. The main wide bandgap hetero-structures currently available are endogenic ones (inside the same compounds family) based on III-N and II-VI compounds, and mostly fabricated using MBE or MOCVD epitaxy. However, there are still functional needs that are not fulfilled today.

In order to extend the range of available hetero-structures, it is interesting to explore exogenic hetero-structures such as II-VI / III-V or III-V / IV material systems. Only few exogenic material couples are predicted to be compatible, i.e. offering sufficiently close crystal and surface structures. In the present work, we have chosen to explore a synthesis route to demonstrate highly ordered ZnO/GaN and ZnO/SiC epitaxial stacks made of very thin layers for both undoped and Al-doped ZnO.

For this kind of exogenic hetero-structures, there is a special interest in performing low temperature process, since any diffusion of the matrix element of one layer into the adjacent one may lead to undesired high doping level in this adjacent layer.

Atomic Layer Deposition (ALD) appears to be the technique of choice as it allows the deposition of highly ordered crystalline materials even at low deposition temperature (< 350 °C) [1]. Moreover, ALD easily provides excellent uniformity and conformality, as well as precise control of the deposition thickness [2-4] and doping, at the atomic scale, for very thin layers over large depositions areas [3]. This is why we have chosen to use an ALD deposition process, in which the growth surface, maintained at controlled temperature in the range of 180 - 350°C, is exposed alternatively to Di-Ethyl-Zinc (DEZn) and H_2O vapors, with purge periods inserted between the two types of chemical adsorption periods.[3]

Preliminary growth trials on different surfaces (Si, SiO_2, GaAs, InP) have shown that the ZnO nucleation process is very surface - sensitive. For both GaN and SiC (000.+) surfaces, efficient nucleation has been obtained.

Moreover, we have confirmed that ZnO with a high level of atomic ordering can be successfully grown this way on both types of surfaces.

TEM images show very abrupt transitions in both cases, with a low-density of defects for ZnO/GaN and a higher density of extended defects for ZnO/SiC (fig. 1 a and b). On ZnO/GaN, epitaxial stacking has been confirmed by asymmetric X-ray diffraction, leading to high coherence pole figures.

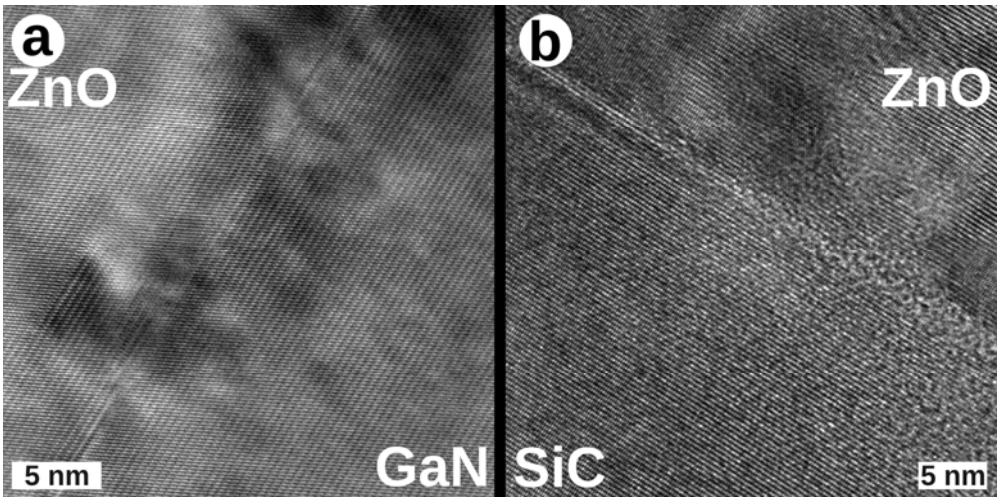

Figure 1: High resolution TEM images recorded at the interfaces between the substrate and the ZnO thin film grown: (a) at 180 °C on GaN MOCVD epilayer, and (b) at 250 °C on SiC substrate.

References

1. V. Miikkulainen, M. Leskela, M. Ritala and R. L. Puurunen, J. Appl. Phys., 113, 021301, (2013). http://dx.doi.org/10.1063/1.4757907
2. S.M. George, Chem Rev., 110, 111 (2010). DOI: 10.1021/cr900056b
3. M. Knez, K. Nielsch and L. Niinistö, Adv. Mater., 19, 3425 (2007). 10.1002/adma.200700079
4. C. Marichy, M. Bechelany and N. Pinna, Adv. Mater, 24, 1017 (2012). 10.1002/adma.201104129
5. A. Yangas-Gils, K. E. Peterson and J. W. Elam, Chem. Mater., 23, 4295 (2011). http://dx.doi.org/10.1021/cm2014576 |
6. T. Tynell and M. Karppinen, Semicond. Sci. Technol. 29, 043001(2014). http://dx.doi.org/10.1088/0268-1242/29/4/043001

A. Acun et al. “Atomically Controlled Surfaces Interfaces and Nanostructures”
edited by A. Bianconi, A. Marcelli (Superstripes Press, Rome 2016) isbn: 9788866830597

Application of the AFM tip for local modification of the electrical potential and topography profile of atomically flat semiconductor surfaces

P. N. Brunkov[1,2,3], N.D. Prasolov[1,2], A.E. Fedorovskiy[1,2], A.V.Baklanov[3], A. A. Gutkin[1]
[1] *Ioffe institute, 194021, Saint Petersburg, Russia*
[2] *ITMO University, 197101, Saint Petersburg, Russia*
[2] *Polytechnic University,195251, Saint Petersburg, Russia*

Email: *brunkov@mail.ioffe.ru*
Key words: atomic force microscopy, semiconductor surface, defects

It was found that the scanning of the semiconductor surface both in contact and in tapping AFM mode results in local change of the topography and the surface potential which was measured with Scanning Kelvin Probe Microscopy (SKPM). The value of those changes depends on both the force applied to the AFM tip and its velocity during scanning.

It supposed that mechanical interaction of the AFM tip with semiconductor surface results in the generation of the point defects, which forms deep levels. The observed change in the surface potential could be due the formation of point defects located very close to the surface, which change of the energy of the Fermi level pinning.

The model developed to describe the experimental data revealed that small value of the contact area between the tip of the scanning probe microscope and surface under study (with diameter below 100 nm) allows realizing in the surface layer the very high pressure (up to a few GPa). The value is very close to the plastic limit of the semiconductor material and may cause the generation of defect in crystal lattice, which results in the destruction of the surface [1,2].

It was demonstrated that with the forces below 100 nN applied to the AFM tip it is possible to remove just single monolayer from GaAs surface (Fig.1).

The presented technology could be used to form the shape of solid state surfaces with subnanometer resolution without wet etching processes.

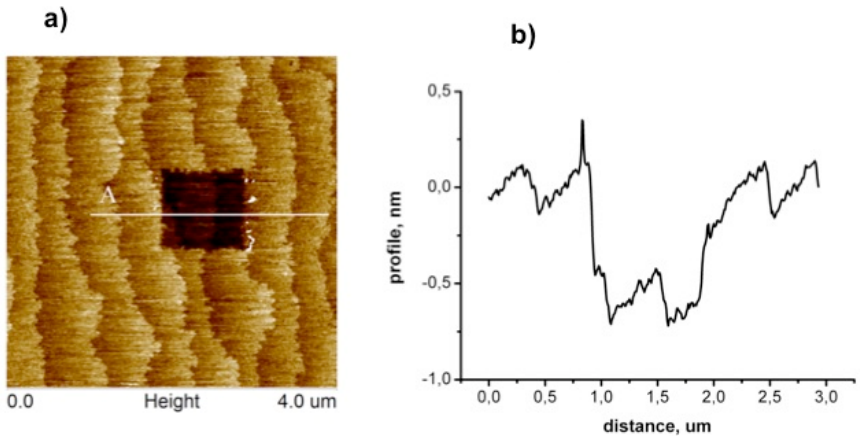

Figure 1: Topography (a) and profile (b) of the modified surface of the GaAs epitaxial layer.

References

1. P.N. Brunkov, V.V. Goncharov, M.E. Rudinsky, A.A. Gutkin, N.Y. Gordeev, V.M. Lantratov, N.A. Kalyuzhnyy, S.A. Mintairov, R.V. Sokolov, S.G. Konnikov, Semiconductors, 47, 1170 (2013). doi: 10.1134/S1063782613090054
2. A.V. Baklanov, A.A. Gutkin, N.A. Kalyuzhnyy, P.N. Brunkov, Semiconductors, 49, 1057 (2015). doi: 10.1134/S1063782615080060.

A. Acun et al. "Atomically Controlled Surfaces Interfaces and Nanostructures"
edited by A. Bianconi, A. Marcelli (Superstripes Press, Rome 2016) isbn: 9788866830597

The simultaneous detection of the near-surface and bulk coordination environments of a trivalent metal cation (europium) in an aqueous solution by use of X-ray absorption spectroscopy

Mrinal K. Bera[1] , Mark R. Antonio[2]
[1]*DUBBLE-CRG, ESRF, Grenoble, France*
[2]*Chemical Sciences and Engineering Division, Argonne National Laboratory, Lemont, USA*

Email: *mrinal.bera@esrf.fr*
Keywords: Atomic and nanoscale structure of surfaces and interfaces: advanced methods

Bulk coordination environments of ions in their aqueous solutions can be easily probed by techniques like X-ray absorption spectroscopy (XAS) and high-energy X-ray scattering measurements. But obtaining similar information near the surfaces of solutions is very challenging. In this regard, grazing-incidence X-ray absorption [1, 2] was developed to detect interfacial ion coordination environments. Nonetheless, the requirement of large solution volumes (> 20 mL) and very specialized interface-sensitive instrumentation have limited the application of this technique to a very small community of researchers. In the pursuit of a simple and easy-to-use method, we have developed a new setup [3] that can measure total-electron yield (TEY) and fluorescence-yield (FY) XAS data simultaneously from a pendant drop of an aqueous electrolyte solution, as shown in Figure 1; the system requires only 0.5-1 mL of electrolyte solution. The TEY signal provides the coordination environment within first few nanometers of the solution surface, whereas the FY response provides metrical details about the coordination in the bulk. The difference in probing depths stems from the shallow escape depth (few nanometers) of electrons compared to the large (several hundred micrometers) escape depth of the fluorescence (X-ray) photons, as depicted in Figure 1. We measured the coordination behavior of one of the lanthanide elements, europium, in an acidic aqueous electrolyte of its chloride salt. The analyses of EXAFS data extracted from TEY and FY responses showed contrasting differences between the bulk and interfacial coordination behaviors of Eu^{3+} ions. Within the first few nanometers of the surface of the aqueous electrolyte solution, the Eu^{3+} exhibit oxygen coordination typical of inner-sphere hydration of an aquated Eu^{3+} cation. Beyond that, outer-sphere cation-anion (Eu-Cl) and cation-cation (Eu-Eu) correlations are observed (upper-left cartoon in Figure 1) that are otherwise not present in the bulk electrolyte (lower-left cartoon in Figure 1). Hence the measurements using our newly developed setup show that simple air-water interfaces can drive the formation of correlated structures that can be very different from bulk structures. These differences between interfacial and bulk structures can have immense implications in understanding interfacial ion-transfer phenomena in physics, chemistry, biology and atmospheric sciences. This work is supported by the U.S. DOE, Office of Science, Office of Basic Energy Science, Division of Chemical Sciences, Biosciences and Geosciences, under Contract No DE-AC02- 06CH11357.

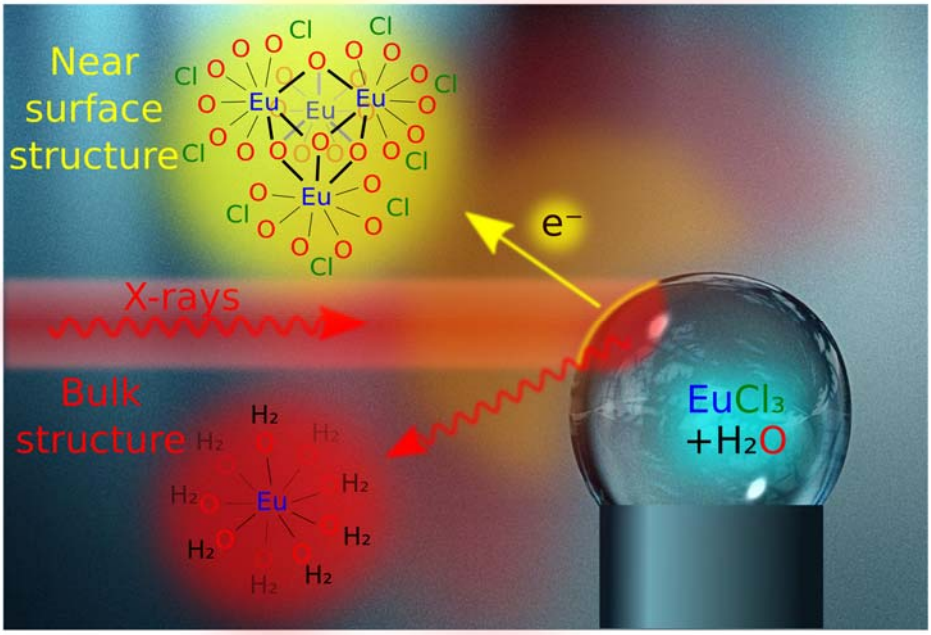

Figure 1: A newly developed inverted pendant drop setup for simultaneous detection of bulk and near-surface coordination environments of ions in aqueous solutions.

References

1. I. Watanabe et al, Rev. Sci. Instrum, 68 , 3307 (1997)
2. M. K. Bera et al, J. Phys. Chem. B, 119, 8734 (2015)
3. M. K. Bera and M. Antonio, Langmuir, 31, 5432 (2015)

A. Acun et al. “Atomically Controlled Surfaces Interfaces and Nanostructures”
edited by A. Bianconi, A. Marcelli (Superstripes Press, Rome 2016) isbn: 9788866830597

Fr4T session

Motor molecules

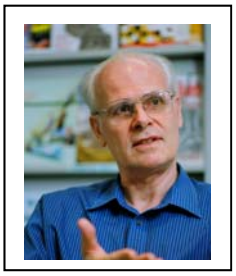

M.A. Van Hove
Hong Kong Baptist University, Hong Kong, China
Department of Physics, and Institute of Computational and Theoretical Studies

Email: *vanhove@hkbu.edu.hk*
Key words: State-of-the-art theoretical approaches on surfaces and interfaces; Supramolecular structures and functionalization of surfaces and interfaces; Frontiers aspects of semiconductor, surfaces and interfaces; Scanning probe and surface microscopy

Molecular machines are gaining increasing interest from biological to energetic perspectives. They promise to convert energy and control mechanical motion at length scales down to the nanometer. Some molecular machines cause reciprocal motion, as in muscles and switches, while others cause rotational motion, as in flagellae: we discuss theoretical models of both. Nature developed a variety of molecular machines to convert energy and control motion. These natural machines tend to be complex and robust. In the last few decades, scientists have synthesized a wide range of new, relatively simpler molecular machines and learned to control and observe some of their important motions, mostly in solution. Increasingly, molecular motors have also been investigated at solid surfaces, allowing the use of surface science techniques for studying monolayers of well-oriented molecules. Nanoscience techniques have added further possibilities. We shall discuss basic issues of the operation of molecular motors, including energy conversion steps, continuous energy supply, the role of thermal energy, intentional start and stop of motion, and unidirectionality of motion. Without intentional control of these aspects, motors create random motion and are largely useless.

This work was supported by grants from the Hong Kong Baptist University Strategic Development Fund, the Hong Kong RGC, and by HKBU’s High Performance Cluster Computing Centre, which receives funding from the Hong Kong RGC, UGC and HKBU.

A. Acun et al. "Atomically Controlled Surfaces Interfaces and Nanostructures"
edited by A. Bianconi, A. Marcelli (Superstripes Press, Rome 2016) isbn: 9788866830597

Nanoparticle mobility in organic media - a model of motion at the cellular level

Katarzyna Dziedzic-Kocurek[1] , Piotr Fornal[2] ,Jan Stanek[1]
[1]*M. Smoluchowski Institute of Physics, Jagiellonian University in Cracow*
[2]*Institute of Physics, Technical University of Cracow*

Email: *k.dziedzic-kocurek@uj.edu.pl*
Key words: hematite nanoparticles, Brownian motion, cellular level, mobility, Mössbauer spectroscopy

Taking into account biochemical processes that take place in the living cells, the mobility of proteins and different organelles is one of the main factors that regulates that processes. While analyzing the speed of life processes, it turns out that it exceeds by few order of magnitude the speed derived from theoretical calculation, where classically evaluated efficiency of diffusion transport of the macromolecules in cytoplasm is applied. This problem has been already partly analyzed, by introducing a concept of the macro- vs. local viscosity (η), that becomes a function of a radius of migrating objects [1].

In proposed approach, we attempt to elucidate that problem by studying a simple model system: 110 nm Fe2O3 particles in a sucrose water solution (60% wt.). The size of these nanoparticles is typical for a cellular organelle and the viscosity of the solution at 20°C, η = 58 mPa·s, is close to the average viscosity of the mammal cell cytoplasm.

The Brownian motion of nanoparticles, determined from the Mössabuer line broadening (σv) is in a good agreement with Einstein – Smoluchowski theory if one assumes for the nanoparticles the hydrodynamic radius, Rh = 130 nm, as estimated from DLS (Dynamic Light Scattering) measurements [2,3]. We have shown recently that the mobility of nanoparticles abruptly decreases with their concentration when the average particle-particle distance approachesa value of 2Rh [Fig. 1], [4].

According to the Einstein-Smoluchowski theory, within 141 ns, the charactristic observation time of the 57Fe Mössbauer spectroscopy, nanoparicles should exibit tausends of junps, which should lead to the Gaussian distribution of the observed velocities and, consequently, the Gaussian broadening of the Mössbauer absorption lines.

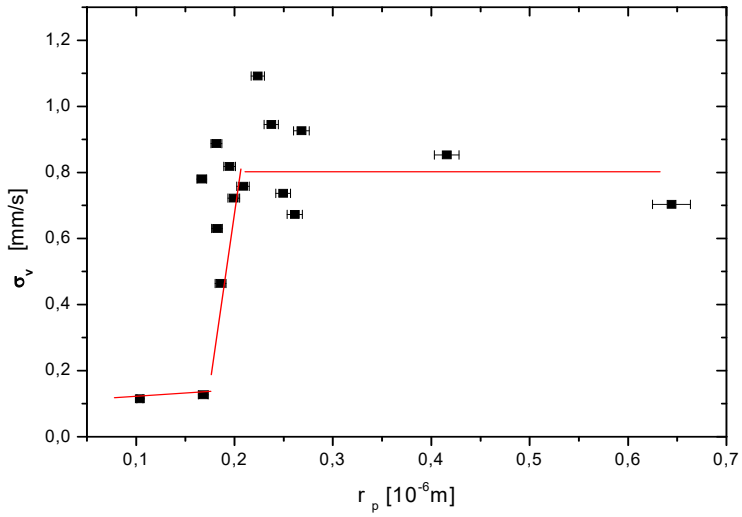

Figure 1: The nanoparticle mobility measured by a Mössabuer line broadening σ_v vs. interparticle distance r_p.

However, the shape of the experimental Mössbauer lines of the nanoparticles suspended in vicious media, is definitelly non-Gaussian. It might imply a new approach for understanding the nature of the processes that happens within the interior of the living cells.

References

1. J. Szymanski, A. Patkowski, J. Gapinski, A. Wilk, R. Holyst, J. Phys.Chem B 110, 7367 (2006). doi: 10.1021/jp0666784
2. A. Einstein, Annalen der Physik 17, 549 (1905).
3. M. Smoluchowski, Annalen der Physik 21, 756 (1906). Doi: 10.1002/andp.19063261405
4. K. Dziedzic-Kocurek, P. Fornal, J. Stanek, Nukleonika 60, 19 (2015).doi: 10.1515/nuka-2015-0006

A. Acun et al. "Atomically Controlled Surfaces Interfaces and Nanostructures"
edited by A. Bianconi, A. Marcelli (Superstripes Press, Rome 2016) isbn: 9788866830597

SNOM spectroscopy for tissue imaging and cancer diagnostics

A. Cricenti[a] , M. Luce[a], M. Ortenzi[a], M.R.F. Siggel-King[b], T. Craig[b], J. Ingham[b], D. Martin[b], P. Weightman[b],
[a]*Istituto di Struttura della Materia (ISM-CNR), via del Fosso del Cavaliere 100, 00133 Rome, Italy*
[b]*Department of Physics, University of Liverpool, Liverpool L69 7ZE, United Kingdom*

Email: *antonio.cricenti@ism.cnr.it*
Key words: Nanophonics, cancer diagnostics

We present a fully implemented Infrared (IR) Scanning Near-field Optical Microscopy (SNOM) in spectroscopic mode for tissue imaging and early cancer diagnostics. The SNOM has been coupled with an infrared light source, based on Free Electron Laser at the ALICE facility in Daresbury. The potential of IR spectroscopy to characterise cancerous tissues has long been recognised and studies of various cancers by many groups have established that regions of malignant tissue can be easily identified on the basis of its IR spectrum. The oesophageal adenocarcinoma, the cancer with the fastest rise in incidence in the Western world, requires an instrument providing specific chemical images at sub-cellular level of oesophagus tissue. This approach demonstrates the potential of the IR-SNOM spectroscopy for yielding an accurate diagnostic test for oesophageal and other types of cancers.

The SNOM employed in this work was developed on the IR FEL at Vanderbilt and established on the IR FEL on the ALICE energy recovery linear accelerator at Daresbury [1]. Preliminary results of IR-SNOM on oesophageal adenocarcinoma have shown that the system can operate at nanometer resolution and has been able to distinguish between healthy and malignant tissues [2]. The optical fibre has been driven in particular areas of the oesophageal tissue and topographical and optical images have been collected simultaneously at different wavelengths. In particular, SNOM images were collected at wavelengths of 7.0 μm (no strong biomarker), 7.3 μm (protein/glycoprotein), and 8.05 μm (DNA).

Figure 1 shows 40 μm x 40 μm optical SNOM images for two samples, labelled Cancer and Benign: the colour maps show the location of intense DNA (red), intense protein/glycoprotein (blue) and of strong overlap of DNA and protein/glycoprotein (orange). As clearly visible, Cancer sample shows a large spread of intense signal from DNA whereas Benign sample shows a lower overall density of DNA, which is more dispersed and exhibits more localised centres.

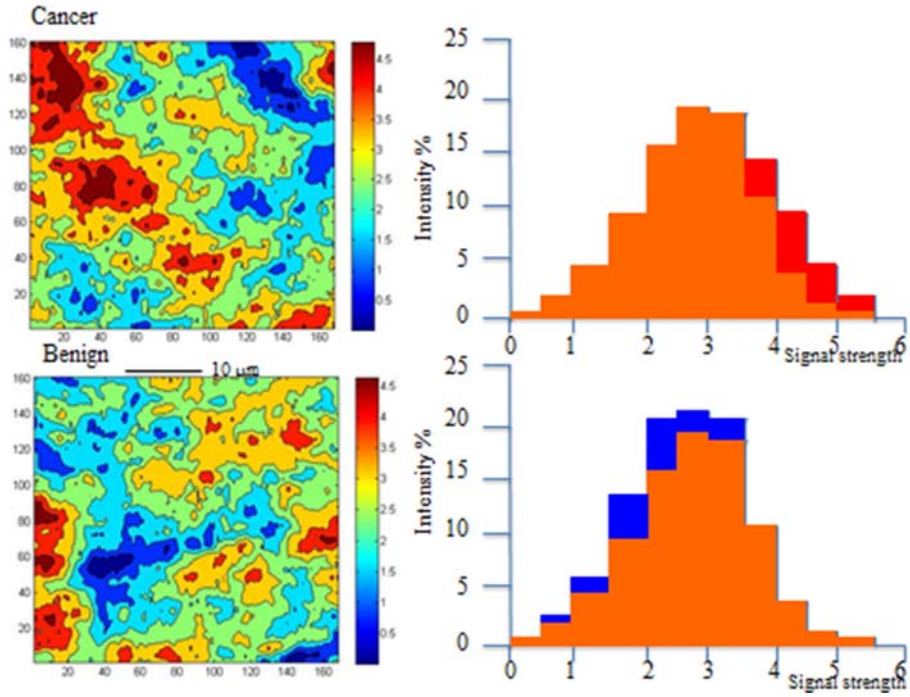

Figure 1: IR-SNOM image maps showing the location of intense DNA (red), intense protein/glycoprotein (blue) and of strong overlap of DNA and protein/glycoprotein (orange).

This combination of InfraRed radiation and Scanning Near-field Optical Microscopy, in its spectroscopic mode, can be an important tool for tissue imaging and early cancer diagnostics. It is expected to produce a major advance in imaging of malignant tissues, leading to the development of portable diagnostic devices for hospital use for various types of cancer. It is also planned to utilise the powerful combination of high spatial resolution and chemical specificity of the mentioned methodologies to study the key components, responsible for cancer formation.

References

1. Cricenti A, Luce M, Tolk NH, Margaritondo G; Nanosci. Nanotechnol. Lett.; 3 (2011) 913;
2. Smith AD, Siggel-King MRF, Holder GM, Cricenti A, Luce M, Harrison P, Martin DS, Surman M, Craig T, Barrett SD, Wolski A, Dunning DJ, Thompson NR, Saveliev Y, Pritchard DM, Varro A, Chattopadhyay S, Weightman P; Near-field optical microscopy with an infra-red free electron laser applied to cancer diagnosis; Applied Physics Letters; 102 (2013) 053701.

A. Acun et al. “Atomically Controlled Surfaces Interfaces and Nanostructures”
edited by A. Bianconi, A. Marcelli (Superstripes Press, Rome 2016) isbn: 9788866830597

Near-Field identification of gold nanoshells inside cells

Mario D’Acunto[1,2], Andrea Cintio, Antonio Cricenti[1], Davide Moroni[2], Marco Luce[1], Ovidio Salvetti[2]
[1]CNR, Istituto di Struttura della Materia, Rome, [2]CNR, Istituto di Scienza e Tecnologie dell’Informazione, Pisa.

Email: *mario.dacunto@ism.cnr.it*
Key words: Scanning Near-Optical Microscope, Near-Infrared biological transparency window, gold nanoshells.

Because of their strongly resonant light-absorbing and light-scattering properties that depend on shape, noble metal nanoparticles (NPs) provide a new and powerful tool for innovative light-based approaches both in nanophotonics and nanomedicine. In particular in medicine, gold NPs nanoshells (AuNPs) met large interest and have found application for cancer treatments. The use of plasmonic nanoparticles as highly enhanced photoabsorbing agents has thus introduced a much more selective and efficient cancer therapy strategy. This is because at wavelengths just beyond the visible spectrum in the near-infrared, blood and tissue are maximally transmissive. As a consequence, by manipulating AuNPs shape and dimension, it is possible tune the optical resonance of such NPs to this region of the spectrum so that they become useful contrast agents in the diagnostics imaging of tumors. In addition, when illuminated by an external near-infrared (NIR) source, NPs can serve as nanoscale heat sources, phototermally inducing cell death and tumor remission, the so-called plasmonic photothermal therapy (PPTT).
In addition, in biological applications, the AuNPs must be coniugated with biomolecules in order to recognize cancer cells. A satisfactory study of the interaction between single cell-single AuNP should define and delineate the basic key-mechanisms induced by the conjugated biomolecules for selective cellular uptake for cancer cells. In fact, the best conjugating biomolecules with AuNP able to recognize and bind target cells. In turn, their response to illuminating NIR light when internalized in the cancer cells requires useful strategies to be studied.
The possibility to study the interaction between single cells-sigle AuNPs is based on the ability to identify the AuNs inside the cells. An innovative contribution for such identification has been recently made by D’Acunto and co-workers demonstrating the possibility to identify single AuNPs with dimensions 100-150nm, inside a single h9c2 mouse cell, figure 1, using an illumination wavelength of 780nm [1-3]. This demonstration opens the possibility to study the single NP uptake and the inside cell thermal induced effect before the cells being eventually destroyed as in standard PPTT.
Such progress and the correspondent ability to study the interaction between single AuNP-single cell has been made possible by the usage of Scanning Probe Microscopy (SPM) techniques. SPM denotes a versatile family of scanning microscopies with spatial resolution of nanometers. In our experimental setup, we used a home-made aperture Scanning Near-Optical Microscope (SNOM) operating in air. In turn, a near-

field Green based Mie theory for the quantification of near-field optical properties of the AuNPs has been developed to calculate the *z*-localization of the AuNP inside the cells [4].

Figure 1: (Left), 20μm×20μm topography of h9c2 mouse cell recorded with a home-made aperture SNOM; (middle) an overlapping of the topography image with the correspondent optical map, the arrows denote the (120nm diameter) nanoparticles identified within the cell; (right), strong-absorption points marked by arrows in the overlapping image and denoting the dimensions of the nanoshells.

References

1. M. D'Acunto, A. Cricenti, S. Dinarelli, M. Luce, NanoSpectroscopy, 1, 97, (2015). DOI:10.1515/nansp-2015-0007
2. A. Cricenti, M. Luce, D. Moroni, O. Salvetti, M. D'Acunto, Optoelectronics Review 39, 23 (2015). DOI:10.1515/oere-2015-0010
3. M. D'Acunto, A. Cricenti, M. Luce, S. Dinarelli, Computer Modelling & New Technologies, 29, 19, (2015). http://www.cmnt.lv/upload-files/ns_39art06.pdf.
4. M. D'Acunto et al. submitted to Applied Optics

A. Acun et al. "Atomically Controlled Surfaces Interfaces and Nanostructures"
edited by A. Bianconi, A. Marcelli (Superstripes Press, Rome 2016) isbn: 9788866830597

Developments of the nano-carbon bio sensors using glycan for influenza virus

Toshio Kawahara[1], Hiroaki Hiramatsu[2], Yasuo Suzuki[2], Shinichi Nakakita[3], Yasuhide Ohno[4], Kenzo Maehashi[5], Kazuhiko Matsumoto[6], Kazumasa Okamoto[7], Teruaki Matsuba[8], Risa Utsunomiya[8]
[1]*College of Engineering, Chubu University*
[2]*College of Life and Health Sciences, Chubu University*
[3]*Life Science Research Center, Kagawa University*
[4] *Graduate School of Science and Technology, Tokushima University*
[5] *Department of Applied physics, Tokyo University of Agriculture and Technology*
[6]*The Institute of Scientific and Industrial Research, Osaka University*
[7]*Faculty of Engineering, Hokkaido University*
[8]*Nissin Electric.Co. Ltd.*

Email: *toshi@isc.chubu.ac.jp*
Key words: Self-aligned growth process for carbon nanowalls, Nano-carbon biosensors, Sugar chains for Influenza virus detection

Nano-carbon materials have highly potential for advanced devices because of the many superior properties such as high mobility, high strength and so forth [1]. For nano devices, we can use field effect transistors using nano-carbon channels, and high performance sensors, noise enhanced nonlinear devices has been developed [2].
On the other hand, Influenza is a major issue in public health [3], and we should continuously check the spreading of influenza A virus variants because of a high mutation rate of this RNA virus. Many infections to human have been reported and it might be the potential to mutate the host from bird to human. The surveillance of such mutation is highly required, and we need high sensitive sensor systems. We have developed the bio-sensor using nano-carbon materials, which can detect the preferable host by the virus. The host change can be observed as the change of the bonding between the virus protein and the host sugar chain.

We have developed several processes to fabricate the field effect transistors for the bio-sensor. One is the self-alignment process using grapho-epitaxy for the nano-carbon channels [4]. Second is the deposition process for the binding molecules for the specific molecules such as avian influenza viruses and human-type ones [5].

In this paper, we will discuss about the self alignment process and then the fabricated nano-carbon channels can recognize the ionic density in the water as the pH sensor (Fig. 1). On the other hand, influenza virus can detect the structure of the ganglioside

to infect the specific host. Therefore, we will use the glycan as the detection molecules in the bio-sensor. However, for the electronic detection, the size of molecules should be small because of the Debye screening. We have tried to estimate the size of sialyllactose as shown in Fig. 2, which seems to be the one of the candidates of the detection parts in the bio-sensor for influenza virus.

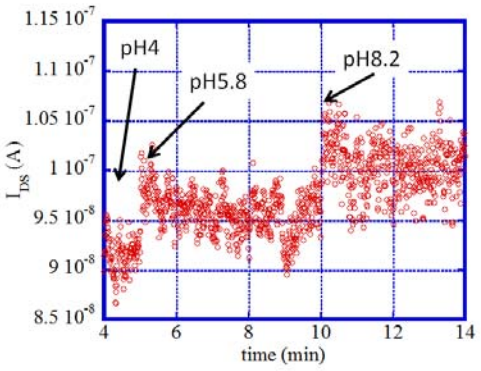

Figure 1: Drain-source current change depending on pH.

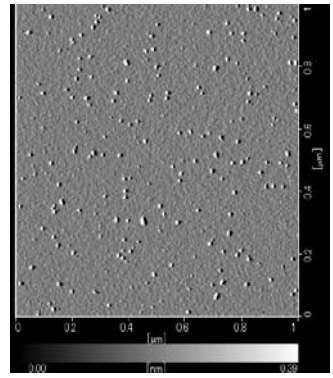

Figure 2: AFM image for sialyllactose (10 ng/ml).

References

1. K. S. Novoselov, V. I. Fal'ko, L. Colombo, P. R. Gellert, M. G. Schwab, K. Kim, Nature 490, 192 (2012).
2. T. Kawahara, S. Yamaguchi, K. Maehashi,Y. Ohno, K. Matsumoto, S. Mizutani, IEEE Conf. Proc.: 2011 21st ICNF, 364 (2011).
3. H. Heesterbeek, R. M. Anderson, V. Andreasen, S. Bansal, D. De Angelis, C. Dye, K. T. D. Eames, W. John Edmunds, S. D. W. Frost, S. Funk, T. D. Hollingsworth, T. House, V. Isham, P. Klepac, J. Lessler, J. O. Lloyd-Smith, C. J. E. Metcalf, D. Mollison, L. Pellis, J. R. C. Pulliam, M. G. Roberts, C. Viboud, Isaac Newton Institute IDD Collaboration, Science 347, aaa4339 (2015).
4. T. Kawahara, S. Yamaguchi, Y. Ohno, K. Maehashi, K. Matsumoto, K. Okamoto, R. Utsunomiya, T. Matsuba, e-J. Surf. Sci. Nanotch. 12, 225 (2014).
5. S. Yamada, Y. Suzuki, T. Suzuki, M. Q. Le, C. A. Nidom, Y. Sakai-Tagawa, Y. Muramoto, M. Ito, M. Kiso, T. Horimoto, K. Shinya, T. Sawada, M. Kiso, T. Usui, T. Murata, Y. Lin, A. Hay, L. F. Haire, D. J. Stevens, R. J. Russell, S. J. Gamblin, J. J. Skehel, Y. Kawaoka, Nature 444, 378 (2006).

A. Acun et al. “Atomically Controlled Surfaces Interfaces and Nanostructures”
edited by A. Bianconi, A. Marcelli (Superstripes Press, Rome 2016) isbn: 9788866830597

Poster Session

Electronic States of two-dimensional crystals of group IV element on α-Al_2O_3(0001) surfaces

Masaaki Araidai[1,2,3,4], Masashi Kurosawa[1,2,3], Akio Ohta[2,3], Kenji Shiraishi[1,2]

[1] *Institute of Materials and Systems for Sustainability (IMaSS), Nagoya University*
[2] *Graduate School of Engineering, Nagoya University*
[3] *Institute for Advanced Research (IAR), Nagoya University*
[4] *CREST-JST*

Email: *araidai@nagoya-u.jp*

Key words: Silicene; Germanene; Stanene; Metal-insulator interfaces; Electronic states; First-principles study

Two dimensional crystals consisting of group IV element heavier than carbon (silicene, germanene, and stanene) are supreme thin-film materials. They have been theoretically predicted to possess high carrier mobility and some intriguing functions such as band-gap control and topological insulator.[1,2] Among them, silicene and germanene have been recently synthesized on metallic substrate and novel synthesis technique has been also developed intensively.[3,4,5,6] However, it has been reported that the electronic state of silicene on metallic substrates is dramatically modified by the strong interactions with the surface atoms.[7,8] This indicates that one cannot utilize successfully the intriguing electronic states inherent in silicene when silicene is placed on a metallic substrate. Therefore, toward the device fabrication utilizing the electronic states inherent in the two-dimensional crystals, it is prerequisite for understanding the electronic properties on insulating substrates.

In this work, we have investigated optimized structures and electronic states of two-dimensional crystals of group IV element on insulating films by the first-principles calculations based on the density-functional theory.[9] The two dimensional crystals on the insulating film were simulated by the slab models. Figure 1 shows the optimized structure and electron-density distribution of 5×5 silicene on α-Al_2O_3(0001)-3×3 surface. We clearly see from Fig. 1(a) that the silicene sheet is disordered due to the strong interactions between Si and O atoms. The corresponding electronic band structure drawn by vasp_unfold code[10] is given in Fig. 1(b). The band structure is basically preserved upon the presence of the surface, as in Ref.11. In addition to the detail analyses of the electronic states, we will show the results of germanene and stanene on α-Al_2O_3(0001) surfaces in presentation, and also discuss the results of the two-dimensional crystals with hydrogen terminations.

This work was partly supported by Grants-in-Aid for Scientific Research (Grant Nos. 15K13943, 15H03564 and 16K17551) from MEXT of Japan. The computation in this work has been done in part using the facilities at the Supercomputer Center, the

Institute for Solid State Physics, the University of Tokyo and at the Infomation Technology Center, Nagoya University.

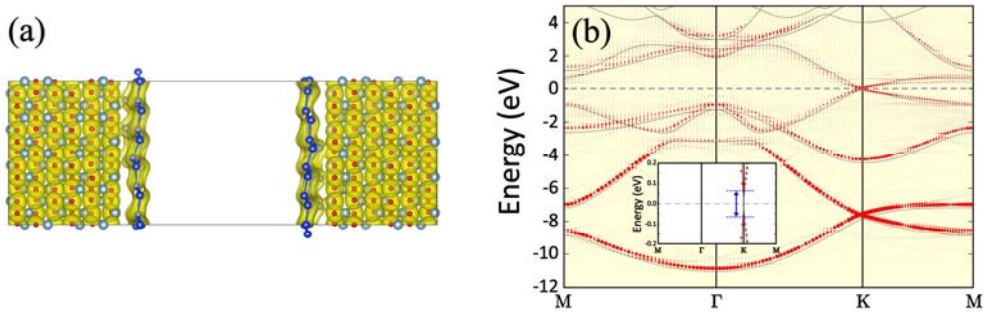

Figure 1: (a) Optimized atomic configuration and electron density distribution of 5×5 silicene on α-Al_2O_3(0001)-3×3 surface. VESTA was used to draw atomic configurations and electronic states.[12] (b) Unfolded electronic band structure of the silicene.

References

1. K. Takeda and K. Shiraishi, Phys. Rev. B 50, 14916 (1994).
2. M. Ezawa, New J. Phys. 14, 033003 (2013).
3. A. Fleurence, R. Friedlein, T. Ozaki, H. Kawai, Y. Wang, and Y. Yamada-Takamura, Phys. Rev. Lett. 108, 245501 (2012).
4. P. Vogt, P. De Padova, C. Quaresima, J. Avila, E. Frantzeskakis, M. C. Asensio, A. Resta, B. Ealet, and G. Le Lay, Phys. Rev. Lett. 108, 155501 (2012).
5. L. Li, S. Lu, J. Pan, Z. Qin, Y. Wang, Y. Wang, G. Cao, S. Du, and H.-J. Gao, Adv. Mat. 26, 4820 (2014).
6. M. Kurosawa, A. Ohta, M. Araidai, and S. Zaima, Jpn. J. Appl. Phys. (to be published).
7. Z.-X. Guo, S. Furuya, J. Iwata, and A. Oshiyama, J. Phys. Soc. Jpn. 82, 063714 (2013).
8. M. X. Chen and M. Weinert, Nano Lett. 14, 5189 (2014).
9. G. Kresse and J. Hafner, Phys. Rev. B 47, 558 (1993).
10. M. Tomić, H. O. Jeschke and R. Valentí, Phys. Rev. B 90, 195121 (2014).
11. M. X. Chen and M. Weinert, arXiv:1509.04641 (2015).
12. K. Momma and F. Izumi, J. Appl. Crystallogr. 44, 1272 (2011).

ISMI beamline at Singapore Synchrotron Light Source in service of nanometers-thick films analysis

A. Banas[1], K. Banas[1], N. Ali[2], A. Toh[2], P. Saravanan[2], Ch. A. Nijhuis[3], J. Li[3] and M.B.H. Breese[1]
[1]*Singapore Synchrotron Light Source, National University of Singapore, 5 Research Link, Singapore 117603, Singapore*
[2]*School of Applied Science, Temasek Polytechnic, 1 Tampines Avenue 1, Singapore 529757*
[3]*Department of Chemistry, National University of Singapore, 3 Science Drive 3, Singapore 117543*

Email: *slsba@nus.edu.sg*
Key words: Organic nanofilms and devices; Atomic biomaterials interfaces, synchrotron radiation, FTIR spectroscopy

Fourier Transform Infrared (FTIR) spectroscopy and microscopy are excellent tools for investigation the number of phenomena within thin films. Due to sample thickness special sampling techniques must be applied in order to record FTIR spectra of this type of materials [1,2].

In this contribution various sampling techniques to analyse ultrathin films (with the special attention to grazing incidence angle reflection and attenuated total reflection – ATR) will be discussed. Experiments performed with both classic blackbody IR and synchrotron radiation (SR) at ISMI (Infrared Spectro/Microscopy) beamline at Singapore Synchrotron Light Source will be presented.
The infrared light at ISMI is extracted from the edge region of one of the bending magnets of the compact superconducting electron storage ring Helios 2. The nominal source point is located at half the maximum magnetic field, i.e., at 2.25 T.

Monolayers and nanometers-thick films placed on various substrates may be easily sampled using the VeeMAX II accessory - available at ISMI beamline. VeeMAX II offers continuous variable angle of incidence (between 30 and 80 degrees) and a variety of crystal plates to selectively control the depth of penetration of the IR beam; its high throughput provides excellent sensitivity and reduced sampling time. Utilization of grazing incidence angle objective attached to IR microscope can be helpful in analysis of monolayers, but in this case they must be placed on reflective (typically metallic) substrates.

Application of FTIR spectroscopy and microscopy for analysis of graphene, self-assembled monolayers, layers of oxides and biofilms allows for characterisation of their response in broad infrared range from 10 to 10000 cm^{-1} (that correspond to photon energy from 1.24 to 1240 meV).

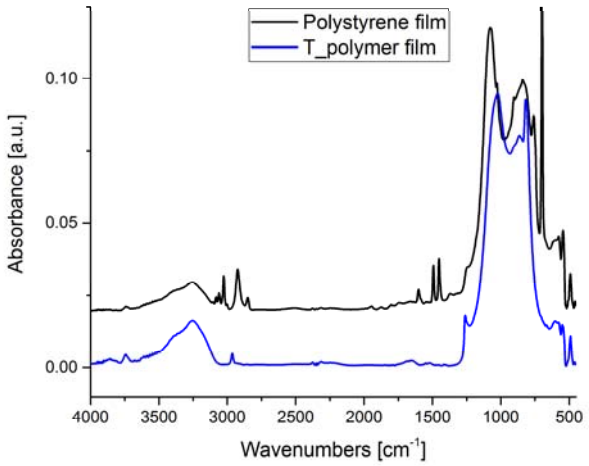

Figure 1: ATR-FTIR spectra collected for 20 nm films (Polystyrene and T_polymer) deposited on silicone substrate.

References

1. T. Lummerstorfer, J. Kattner and H. Hoffmann, Anal Bioanal Chem 388, 55 (2007). doi 10.1007/s00216-006-1010-4.
2. M. E. Mulcahy, S. L. Berets, M. Milosevic and J. Michl, J. Phys. Chem. B, 108 (5), 1519 (2004), doi: 10.1021/jp036035d

A. Acun et al. "Atomically Controlled Surfaces Interfaces and Nanostructures"
edited by A. Bianconi, A. Marcelli (Superstripes Press, Rome 2016) isbn: 9788866830597

Molecular-dynamics simulation of water absorbed on nanocarbon surface: structure and its influence on tribology

Atsushi Beniya[1] , Naoki Homma[1] , Shohei Chiashi[2] , Yoshikazu Homma[1] , Takahiro Yamamoto[3]
[1]*Department of Physics, Tokyo University of Science*
[2]*Department of Mechanical Engineering, The University of Tokyo*
[3]*Department of Liberal Arts, Tokyo University of Science*

Email: *1215637@ed.tus.ac.jp*
Key words: Graphene and other 2D materials; Nanotubes and other 1D materials

The nature of hydrophobicity in atomic scale is one of the important questions to understand water properties. In our previous work, we studied adsorption on the "hydrophobic" carbon nanotube surface at room temperature in water vapor by optical measurement of individual single-walled carbon nanotubes (SWNTs) suspended between micropillars and classical molecular dynamics (MD) simulation in the NVT ensemble. We found that water molecules condense on the "hydrophobic" SWNT surface and that the water molecules form double-layered structure in atomic scale [1].

Here, we have investigated the diameter (d_t) dependence of RBM frequency in vacuum and in water vapor for a wider range of d_t from 1.0 nm to 2.5 nm using MD simulation and a dynamical matrix (DM) calculation. We studied effects of water vapor on the frequency ω_{RBM} of radial breathing mode (RBM) of SWNTs within a narrow range of tube diameter around $d_t \approx 1$ nm, and we clarified that the d_t dependence of ω_{RBM} follows a phenomenological expression $\omega_{RBM} = A/d_t + B$, where A=227.9 cm^{-1} nm and B=7.5±1.5 cm^{-1}. This behavior of ω_{RBM} is in good agreement with our experimental result: $\omega_{RBM} = A/d_t + B$, where A = 232.4 cm^{-1} and B = 7.5±2.5 cm^{-1}. On the other hand, we investigated the d_t dependence of RBM frequency for a wider range of d_t up to ≈ 2.5 nm. Figure 1 shows the DM calculation results of ω_{RBM}^{vacuum} (red curve) and ω_{RBM}^{vapor} (blue curve). The d_t-dependence of ω_{RBM}^{vapor} (blue curve) deviates from the $1/d_t$ behavior (dashed curve) with increasing d_t, i.e., influence of water vapor surrounding an SWNT on the RBM frequency becomes larger than the conventional $1/d_t$ behavior as d_t increases [2].

In addition to SWNT surface, we have performed MD simulation on the water on graphene surface, and we found a similar double-layered water structure on "hydrophobic" graphene surface at room temperature in water vapor. One of the interesting phenomena related to double-layered water on graphene surface is tribology. To understand the effect of the double-layered water on tribology of graphene surface, we calculate the friction force acting on graphene nanoflake put on the graphene surface in vacuum and water vapor. In the presentation, we show simulation results of friction force under various conditions of the loading force acted on the graphene nanoflake.

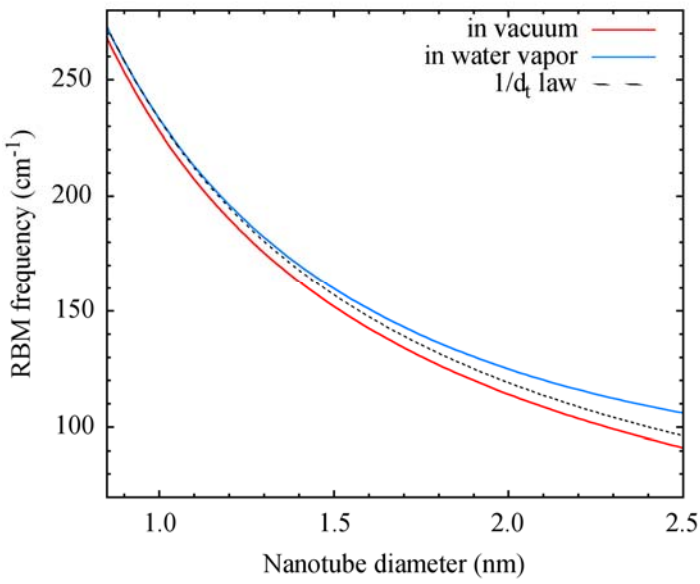

Figure 1: $\omega_{\mathrm{RBM}}^{\mathrm{vapor}}$ and $\omega_{\mathrm{RBM}}^{\mathrm{vacuum}}$ calculated by the dynamical matrix method.

References

1. Y. Homma, S. Chiashi, T. Yamamoto, K. Kono, D. Matsumoto, J. Shitaba, and S. Sat., Phys. Rev. Lett. 110, 157402 (2013).
2. S. Chiashi, K. Kono, D. Matsumoto, J. Shibata, N. Homma, A. Beniya, T. Yamamoto and Y. Homma, Phys. Rev B 91, 155415 (2015).

A. Acun et al. “Atomically Controlled Surfaces Interfaces and Nanostructures”
edited by A. Bianconi, A. Marcelli (Superstripes Press, Rome 2016) isbn: 9788866830597

Investigation of silver growth and surface diffusion on polycrystalline tungsten surface

A. Bukaluk, K. Okulewicz, M. Trzcinski,
A. Dittmar-Wituski
University of Science and Technology in Bydgoszcz, Institute of Mathematics and Physics,
al. S. Kaliskiego 7, PL-85-796 Bydgoszcz

Email: *bukaluk@utp.edu.pl*
Key words: silver; tungsten; mechanisms of growth; surface diffusion; Auger electron spectroscopy; ESCA

Silver layers of 0.1 to 6.0 ML thickness were deposited at room temperature on the surface of tungsten substrate of 10 mm diameter. Analysis of silver growth on tungsten was studied by thermodesorption (TDS) and Auger electron spectroscopy (AES). TDS measurements indicated that the first layer grew in a layer-by-layer manner, whereas further layers formed islands on the first monolayer. The recognition of the mechanism of growth by AES was performed in two ways – by observation of the slope changes of the Ag(351, 356 eV) Auger line versus time dependence and the change of the shape of the Ag(351,356 eV) line during silver layer growth [1]. Auger investigations confirmed TDS results that the first Ag layer grew in a Frank-van der Merwe mode of growth, and the successive silver layers formed island structures according to the Stranski-Krastanov model. Surface diffusion of Ag on W surface was studied by using ESCA imaging property of SCIENTA SES200 instrument [2]. During surface diffusion studies half of tungsten surface was deposited by Ag layer. Next the sample was annealed to a temperature of 400-550 K, involving surface movement of silver on the substrate. Measuring the photoelectron intensity as a function of position and energy surface diffusion coefficient of Ag on W was determined [3]. Results of investigation of Ag growth and diffusion on the polycrystalline tungsten surface was compared with other studies.

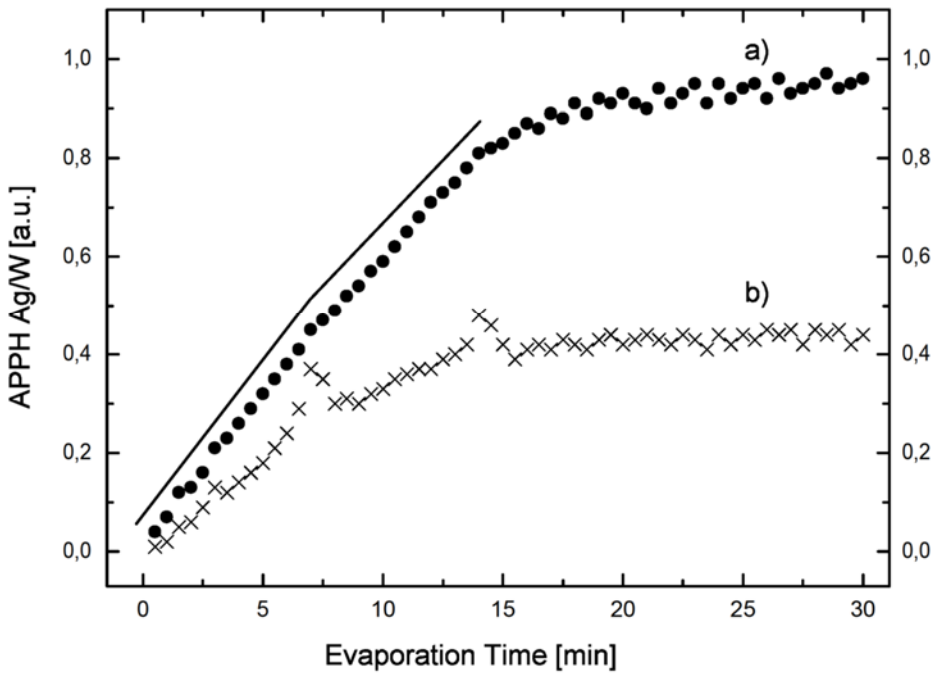

Figure 1: ***a)*** Ag (351; 356 eV) line intensity changes as a function of silver evaporation time, **b)** changes of shape factor as a function of silver evaporation time.

References

1. A. Bukaluk, Application of Surface Sensitive Methods to Materials Science,UTP Edition, Bydgoszcz, 2014.
2. M. Bürgener, A. Bukaluk, M. Cyrankiewicz, A. Goldmann, R. Siuda, M. Trzcinski, Surf. Sci. 529, 490 (2003).
3. M. Trzcinski, A. Bukaluk, M. Bürgener, A. Goldmann, Surf. Sci. 589, 192 (2005).

An analytical model for evaluating the effective skin depth in multilayer structures

Giovanni Castorina[1,2], Augusto Marcelli[1,3], Stefano Sarti[4] and Bruno Spataro[1].
[1]*INFN - Laboratori Nazionali di Frascati, Via E. Fermi 40, 00044 Frascati, Italy*
[2]*University of Catania, Dipartimento di Ingegneria Elettrica, Elettronica e Informatica, 95126 Catania, Italy*
[3]*RICMASS, Rome International Center for Materials Science Superstripes, Via dei Sabelli 119A, 00185 Rome, Italy*
[4]*University of Rome Sapienza, Dipartimento di Fisica, 00185 Rome, Italy*

Email: *giovanni.castorina@lnf.infn.it*
Key words: analytical model, TM coating, accelerating structures.

Coatings are used in several technological applications. Their functional properties strongly depend on the coating material, the coating microstructure and process parameters. Many experimental tests can be can be carried out with different materials, different thickness and process parameters to investigate this dependency. However, modeling and simulation represent an effective alternative to experiments [1] and have become more and more important in the last years. This contribution focuses on metallic coatings suitable for accelerator technologies and a simple analytical model is presented and discussed.
The model uses the well-known equations of propagation matrices theory [2] applied for an infinite metallic bulk with no reflection and a dielectric or metallic coating. The electromagnetic fields and the effective skin depth, in bulk-coating multilayer structure, are evaluated in order to estimate the quality factor and the surface resistance of metallic-coated devices such as RF cavities.

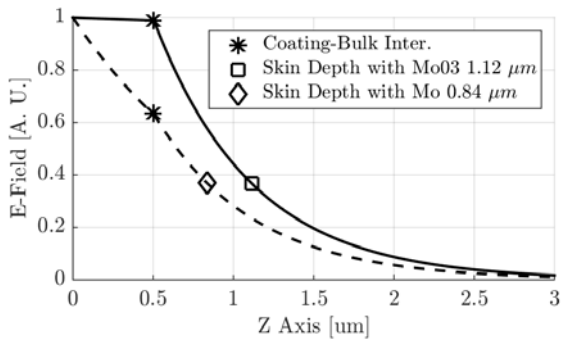

Figure 1: Comparison of the real part of the electric field at 10 GHz inside a bulk of copper coated with a 500 nm coating made by Mo or MoO_3. The square and diamond markers show the estimated effective skin depth of these multilayer structures.

The analytical model has been also extended to high frequency (THz) structures adopting the Drude model of transition metal (TM) oxides for the coating region [3].
The research is established in the framework of an international collaboration among INFN-LNF, SLAC, KEK and UCLA working to design novel X-band accelerating structures. This activity is particularly devoted to the research and development of key components of existing accelerators to fulfill the demands of new compact accelerators for scientific and industrial applications. [4]
As an example, to determine the maximum sustainable gradients in normal conducting RF powered particle beam accelerators operating in the X-band with extremely low probability of RF breakdown, we are investigating the possibility to growth coatings on copper based RF cavities. We will present calculations of TM or TM oxides to minimize the breakdown events while preserving the conductivity of the copper surface.

References

1. A. Marcelli, B. Spataro, S. Sarti, V.A. Dolgashev, S. Tantawi, D.A. Yeremian, Y. Higashi, R. Parodi, A. Notargiacomo, Junqing Xu, G. Cappuccio, G. Gatti, G. Cibin, *Characterization of thick conducting molybdenum films: enhanced conductivity via thermal annealing*, Surf. Coat. Tech. **261**, 391 (2015)
2. Sophocles J. Orfanidis, *Electromagnetic Waves and Antennas*, July 2, 2014.
3. A. D. Rakic, A.B. Djurisic, J.M. Elazar, and M.L. Majewski, *Optical properties of metallic films for vertical-cavity optoelectronic devices*, Appl. Opt. **37**, 5271 (1998)
4. G. Gatti, A. Marcelli, B. Spataro, V. Dolgashev, J. Lewandowski, S.G. Tantawi, A.D. Yeremian, Y. Higashi, J. Rosenzweig, S. Sarti, C. Caliendo, G. Castorina, G. Cibin, L. Carfora, O. Leonardi, V. Rigato and M. Campostrini, *X-band accelerator structures: on going R&D at the INFN*, Nucl. Instr. Meth. A (2016) doi:10.1016/j.nima.2016.02.061

A. Acun et al. "Atomically Controlled Surfaces Interfaces and Nanostructures"
edited by A. Bianconi, A. Marcelli (Superstripes Press, Rome 2016) isbn: 9788866830597

Inspection of ALD cobalt thin film incubation by using Magnetic Force Microscopy

Chien-Wei Chen[1],
Chi-Chung Kei[1], Bo-Heng Liu[1], Chien-Ying Su[1], Nien-Nan Chu[1]
[1]*Instrument Technology Research Center*

Email: danielchen@narlabs.org.tw
Key words: MFM; ALD; Cobalt; thin film

Nowadays, copper has become the mainstream material as back-end interconnect due to its good electric conductivity. However, it is easy for copper to induce electromigration (EM), then voids form and cause electrical functions failure. Using cobalt as a cover of copper is one solution for this issue.

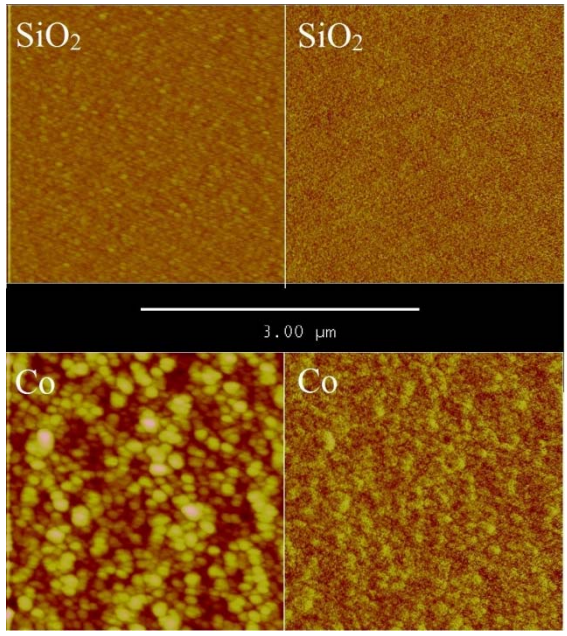

Figure 1: Topography(left) / MFM(right) image of SiO_2 & Co surface

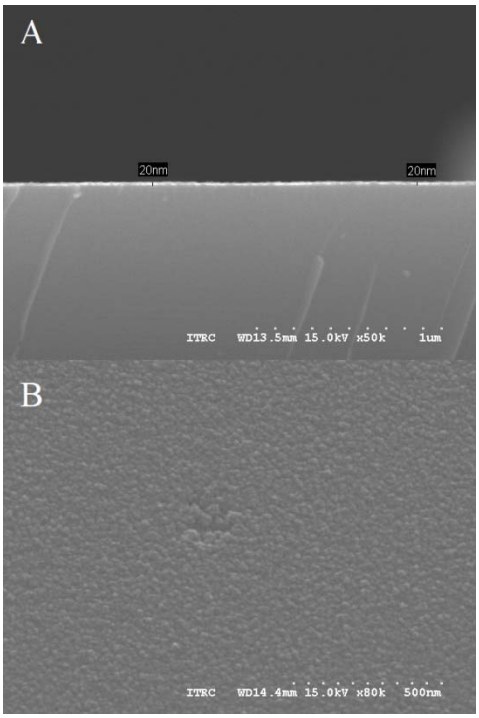

Figure 2: SEM image of ALD Co film (A) cross section (B) plane-view

Atomic layer deposition (ALD) could deposit conformal ultrathin cobalt film; on the other hand, magnetic force microscopy (MFM) could be a method to analyze the cobalt film incubation mechanism of ALD, especially with the low cycle number film.
Thermally grown SiO_2 are applied as substrates for cobalt films to demonstrate the feasibility of the experiment. We prepare a ALD cobalt film which AFM shows the thickness is about 16 nm and use MFM to scan the surface. From the MFM results in Figure 1, the surface morphology of cobalt film is much different from that of bared SiO_2 substrate. It’s because only the magnetic of cobalt could be detected by MFM, but SiO_2 substrate don’t. According to the theory of thin film growth, the film normally forms island shape before it merges into continuous film. The SEM images in Figure 2 also show the similar topography corresponding to MFM results.
It has shown that MFM technique is quite suitable to inspect the magnetic film morphology for the study of ALD cobalt thin film on copper base in the future, with the low cycle number film in particular.

A. Acun et al. "Atomically Controlled Surfaces Interfaces and Nanostructures"
edited by A. Bianconi, A. Marcelli (Superstripes Press, Rome 2016) isbn: 9788866830597

Local refractive index variation of FIB milled CVD diamond areas via Raman and IR micro-reflectivity

G. Cinque[1], A. Marcelli[2,3], S. Macis[4], M. Pea[5], A. Notargiacomo[5]
[1]*Diamond House, Harwell Science and Innovation Campus, Didcot, Oxfordshire, OX11 0DE, United Kingdom*
[2]*Istituto Nazionale di Fisica Nucleare - Laboratori Nazionali di Frascati, 00044, Frascati, Italy*
[3]*RICMASS, Rome International Center for Materials Science Superstripes, Via dei Sabelli 119A, 00185 Rome, Italy*
[4]*Department of Mathematics and Physics, Università di Roma Tor Vergata, Via della Ricerca Scientifica 1, 00133, Rome, Italy*
[5]*Institute for Photonics and Nanotechnologies - CNR, Rome, 00156, Italy*

Email: *gianfelice.cinque@diamond.ac.uk*
Key words: CVD diamond, IR reflectivity, Raman, FIB milling, nanoindentation

The unique physical properties of diamond make this material suitable for fabrication of devices in a variety of fields from electronics, to high-energy physics, detectors, sensors, etc. Some of these devices are based on conductive patterns integrated on diamond. Different technologies based on the hydrogenation process and the laser annealing or the focused ion beam (FIB) allow to obtain patterned conductive areas. We already investigated the electrical properties of shallow (few tens of nm thick) diamond conductive layers obtained with a FIB working with Ga^+ ions at 30 keV. We demonstrated the possibility to control the resistivity over two orders of magnitude changing the doses [1] and characterized the morphology of the irradiated regions upon annealing in oxygen at T=400° C. [2]

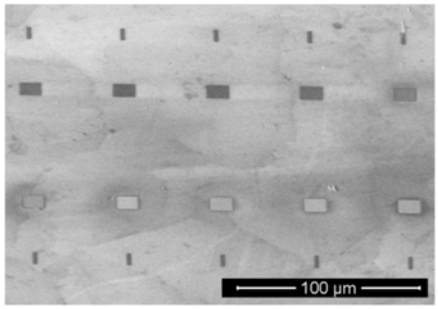

Figure 1: SEM image of a set of 10x10 μm^2 square regions treated by FIB at different ion doses (dose range 2.55 ÷ 650 μm^2).

The effect of ion-beam induced structural damage in diamond, and in particular the change of the refractive index, has been observed since the '60. Within this framework, we used both a synchrotron radiation IR microbeam and a Raman microscope to investigate a set of micro-conductive amorphous carbon squared pads patterned by FIB

on a CVD diamond polished surface. Ion currents in the range 28 pA to 280 pA and doses from 2.5 pC/μm^2 to 650 pC/μm^2 were used to pattern the areas on the CVD diamond plate showed in Fig. 1. These small areas were investigated in reflectivity using SR FTIR at the beamline B22 of the Diamond Light source. To complement the IR reflectivity data, micro-Raman spectroscopy was performed on the same regions.

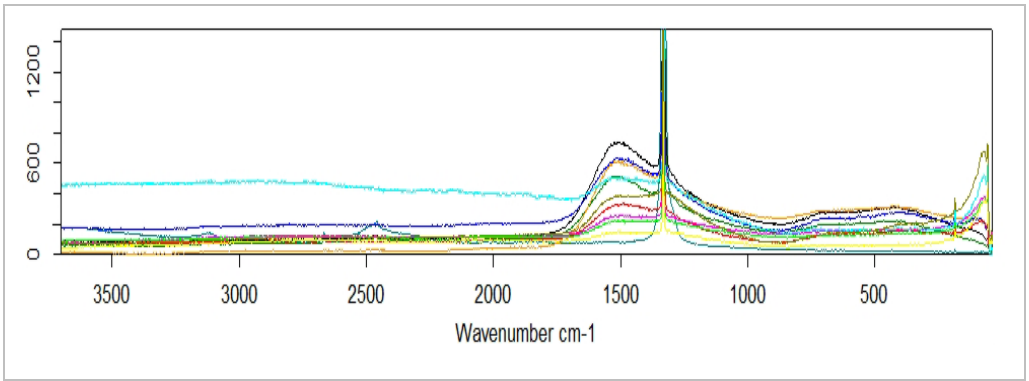

Figure 2: Comparison of Raman spectra of the irradiated areas showed in Figure 1. Spectra have been measured using the BRUKER-Senterra micro-Raman microscope available at the B22 beamline with a 633 nm laser.

A powerful and direct method to obtain the refractive index of a material is to measure the reflectivity and obtain both the real and the imaginary part via the *Kramers-Kronig* transformation. We investigated patterns at high and low doses measuring changes in the refractive index of the CVD diamond plate. Work is in progress but preliminary estimations point out an increase up to 10-15 % with the material still remaining in a highly ordered phase. To characterize the ordering of these irradiated area vs. dose we collected also micro-Raman spectra. Some data showed in Fig. 2 point out for these values of dose, no changes in shape and in position of the intense and narrow peak characteristic of the diamond structure. However, a large sideband at higher wavelengths and other larger structures due to the strong amorphization of the surface of these irradiated regions appear. No clear signature of graphitic carbon has been detected by Raman spectroscopy.
These experiments may allow estimating the associated changes of the refractive index of synthetic CVD diamond, which could be used to design specific optical devices based on synthetic diamond.

References

1. G. Di Gioacchino et al., ACS Appl. Mater. Interfaces 7, 10896-10904 (2015)
2. M. Pea, et al., Microelectron. Eng., 141, 27-31 (2015)
3. P. Dore, *et al.*, Appl. Opt. 37, 5731 (1998)

A. Acun et al. “Atomically Controlled Surfaces Interfaces and Nanostructures”
edited by A. Bianconi, A. Marcelli (Superstripes Press, Rome 2016) isbn: 9788866830597

Isotropic thin PTCDA films on GaN(0001)

Jens Falta[1,2], Christian Ahrens[1], Jan Ingo Flege[1], Cherno Jaye[3], Daniel.A. Fischer[3], Thomas Schmidt[1]
[1] *Institute of Solid State Physics, University of Bremen, Otto-Hahn-Allee 1, 28359 Bremen, Germany*
[2] *MAPEX Center for Materials and Processes, University of Bremen, Bibliothekstr. 1, 28359 Bremen, Germany*
[3] *Ceramics Division, National Institute of Standards and Technology, Gaithersburg, MD 20899*

Email: * *falta@ifp.uni-bremen.de*
Key words: Atomic and nanoscale structure of surfaces and interfaces: advanced methods; Compound, wide band gap, organic and magnetic semiconductors; Organic nanofilms and devices; Scanning probe and surface microscopy

The growth of 3,4,9,10-perylene tetracarboxylic dianhydride (PTCDA) on the Ga-polar GaN(0001) surface has been studied in detail by X-ray photoelectron spectroscopy (XPS), spot profile analysis low-energy electron diffraction (SPA-LEED), near edge x-ray absorption fine structure (NEXAFS), as well as scanning tunneling microscopy (STM). The stoichiometric ratios as obtained from XPS show that the molecules remain intact upon adsorption on the surface. In addition, no chemical shifts can be observed in the C*1s* and O*1s* core levels with progressing deposition of PTCDA, suggesting none or only very weak interaction between the molecules and the substrate. NEXAFS measurements show that the PTCDA molecules are oriented with their molecular plane parallel to the surface. High-resolution STM shows PTCDA islands of irregular shape on the sub-micron scale (fig. 1), and together with corresponding SPA-LEED data reveals a lateral ordering of the molecules that is compatible with the presence (102) oriented PTCDA nano-crystals. High resolution SPA-LEED clearly shows the presence of homogeneously distributed rotational domains of two-dimensionally isotropic PTCDA.

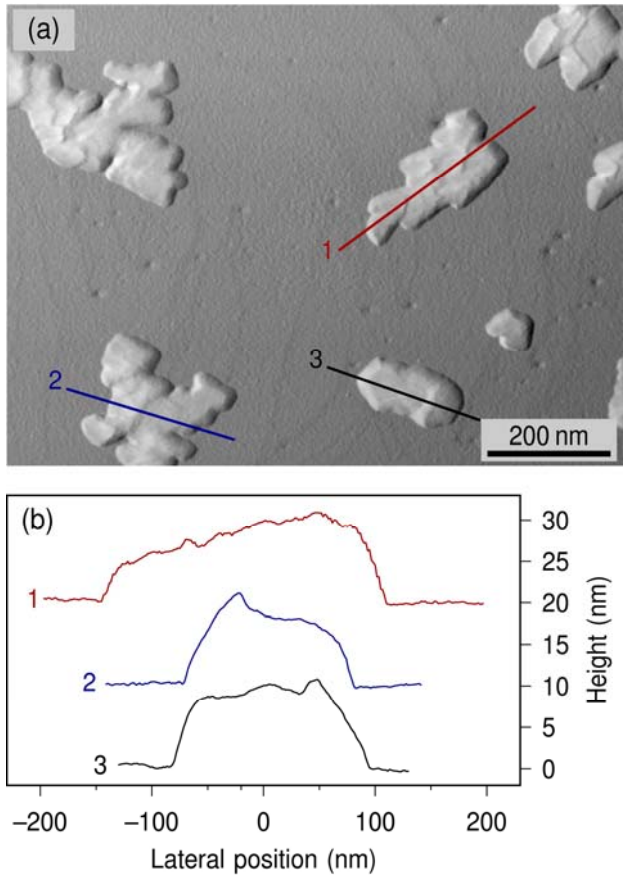

Figure 1: (a) STM image of PTCDA islands on GaN(0001); tip bias -3V, tunneling current 0.3nA; (b) heiht profiles of the islands as indicated by the lines in (a).

A. Acun et al. “Atomically Controlled Surfaces Interfaces and Nanostructures”
edited by A. Bianconi, A. Marcelli (Superstripes Press, Rome 2016) isbn: 9788866830597

EUSpec - Modern tools for spectroscopy on advanced materials: a European modelling platform

Keisuke Hatada[1], H. Herper[2], H. Ebert[3], D. Sébilleau[1]
[1]*Département Matériaux-Nanosciences, Institut de Physique de Rennes, UMR UR1-CNRS 6251, Université de Rennes1, 35042 Rennes cedex – France*
[2]*Division of Materials Theory, Department of Physics and Astronomy, Uppsala University, Box 516, SE-75120, Uppsala, Sweden,*
[3]*Universität München, Department Chemie, Physikalische Chemie, Haus E2.033, Butenandtstr. 5-13, D-81377 München*

Email: *keisuke.hatada@univ-rennes1.fr*
Key words: Atomic and nanoscale structure of surfaces and interfaces: advanced methods, State-of-the-art theoretical approaches on surfaces and interfaces

The study of materials is of central significance for progress in science and technology. At present the focus is on materials with reduced dimensions such as nano-structures or molecule based systems. These materials offer new tunable properties. In order use them in devices a deep understanding of the properties of the materials on the atomic scale is a prerequisite.

Non-destructive spectroscopies are a fundamental tool of analysis at the nanoscopic level, allowing to probe matter and its constituents with an atomic resolution, and to monitor their time evolution down to the femtosecond range, transforming them into unique methods to trace chemical reactions. However, in order to make use of the continuously increasing resolution in space, energy, momentum, spin and time, complementary theoretical support is indispensable. This is where new EU-funded COST action *EUSpec*[1] gets in.

This COST action brings together the expertise of experts working in the science of advanced materials in order to build a coherent theory and computing platform with a new common data format to model sophisticated spectroscopy experiments performed at advanced radiation sources as well as at academic and industrial research laboratories.

The goal is to strengthen the communication between between theoreticians and experimentalists because on the one hand new types of experiments are important benchmarks for the status of theory and often require or trigger new formal theoretical and corresponding code developments. On the other hand, experimental groups are not always aware of the available tools and program packages provided to them by the colleagues from theory to analyze and interpret the experimental findings. *EUSpec* will lead to a large-scale network in order to give a strong impetus to the spectroscopy research and to give Europe a decisive lead. It will establish a platform that goes far beyond the applicability of the actual individual computational codes in order to address the relevant questions and problems for many more materials and

spectroscopies. In line with these ambitious goals, *EUSpec* will be presented to initiate strong interactions between theory and experiment in the future.

References

1. http://www.euspec.eu/

A. Acun et al. “Atomically Controlled Surfaces Interfaces and Nanostructures”
edited by A. Bianconi, A. Marcelli (Superstripes Press, Rome 2016) isbn: 9788866830597

Edge states and electron transport of silicene, germanene and stanene nanoribbons with edge hydrogen terminations

Ayami Hattori[1] , Masahiro Araidai[1,2,3,4], Keiji Yada[1], Yukio Tanaka[1,4]
[5] *Department of Applied Physics, Nagoya University*
[6] *Institute of Materials and Systems for Sustainability (IMaSS), Nagoya University*
[7] *Institute for Advanced Research, Nagoya University*
[8] *CREST-JST*

Email: *hattori@rover.nuap.nagoya-u.ac.jp*
Key words: silicene, germanene, stanene, nanoribbons, edge states, conductance

Silicene, germanene, and stanene are quasi-two dimensional graphene like materials composed of silicon, germanium and tin atoms, respectively. Graphene has a massless Dirac cones at the *K* and *K'* points in the Brillouin zone where π and π bands linearly cross the Fermi level. The electronic properties of silicene, germanene and stanene are akin to those of graphene. However, Dirac cones become massive due to the spin-orbit coupling.

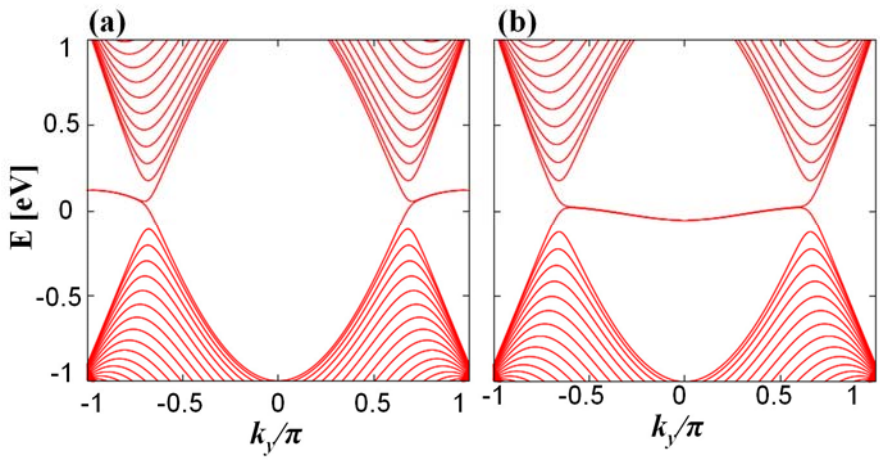

Figure 1: Energy spectra of ZSiNRs with (a) mono- and (b) di hydrogen terminations at both edge sites.

These three materials prefer to construct sp^3-like hybridized orbitals rather than sp^2 ones and have low buckled structures different from grapheme.[1,2] Owing to this low buckled structure, the magnitude of the energy gap is tunable by electric field.[3,4]

Since the low buckled structures are crucial for these materials, not only π but also σ orbitals influence seriously on the energy spectra of edge states, in contrast to graphene nanoribbons.[5] This orbital degree of freedom is also important for describing the hydrogen termination effects.

We study electronic states of zigzag silicene, germanene and stanene nanoribbons (ZSiNRs, ZGeNRs, ZSnNRs) with and without hydrogen terminations based on a multi-orbital tight-binding model. Similar to zigzag graphene nanoribbons (ZGrNRs), various intriguing in-gap edge states appear depending on the types of edge hydrogen terminations. Mono-hydrogen termination effects at edge sites can realize zigzag-like edge states (Fig. 1(a)). On the other hand, di-hydrogen ones at edge sites can realize Klein-like edge states (Fig. 1(b)). The obtained edge states with the hydrogen terminations show helical edge states in quantum spin Hall system. In presentation, we will discuss electron transport properties and band-gap tuning by vertical electric fields, together with the results of germanene and stanene.

References

1. K. Takeda and K. Shiraishi, Phys. Rev. B, 50, 14916 (1994).
2. S. Cahangirov, M. Topsakal, E. Aktürk, H. Sahin, and S. Ciraci, Phys. Rev. Lett. 102, 236804 (2009).
3. N. D. Drummond, V. Zólyomi, and V. I. Fal’ko, Phys. Rev. B 85, 075423 (2012).
4. M. Ezawa, Phys. Rev. Lett. 109, 055502 (2012).
5. A. Hattori, S. Tanaya, K. Yada, M. Araidai, M. Sato, Y. Hatsugai, K. Shiraishi, and Y. Tanaka, arXiv: 1604.04717 (2016).

A. Acun et al. "Atomically Controlled Surfaces Interfaces and Nanostructures"
edited by A. Bianconi, A. Marcelli (Superstripes Press, Rome 2016) isbn: 9788866830597

Crossover of 2D and 3D growth during chemical vapor deposition of graphene on Cu-In alloy observed by in-situ scanning electron microscopy

Yudai Hoshi[1] , Tomohiro Koyama[1], Junro Takahashi[1], Hiroki Kato[1,2], Yoshikazu Homma[1]
[1] *Tokyo University of Science*
[2] *JEOL Ltd.*

Email: *1215638@ed.tus.ac.jp*
Key words: Growth and applications of thin films; Graphene and other 2D materials.

Monolayer graphene is usually synthesized on the copper surface at high temperature by chemical vapor deposition (CVD). To improve the quality of graphene, understanding of growth mechanism is essential and thus further fundamental studies are necessary [1-2]. In this work, we explored lower temperature CVD growth of graphene by using in situ scanning electron microscopy (SEM). We used Cu-In alloy as the substrate because a clear contrast of graphene was easily obtained at elevated temperature.

A copper (99.96 %) substrate was soldered with indium (99.99 %) on an SiO_2 (100 nm)/Si substrate (17 × 4 mm). The weight fraction of indium to copper was 4-6 %. Then DC current though the sample was applied during SEM observation to alloy copper with indium at around 800 °C (±50 °C). For growth, carbon source gas composed of C_2H_5OH and H_2 was flowed into the SEM chamber at 8.5×10^{-2} Torr. When the alloy surface was observed by SEM, gas flow was temporarily stopped. The growth process of graphene was tracked by repeating the observation and gas supply at around 800°C.

Figure 1 shows SEM images of the Cu-In surface after (a) first one-hour growth and (b) successive one-hour growth at the same position. Initially dendritic islands appeared in (a). While the dendritic islands grew slightly larger, new circular islands appeared and almost covered the remaining area in (b). AFM measurements revealed that the dendritic islands were 3D-like while the circular islands were 2D-like, and Raman spectroscopy confirmed that the circular islands were graphene. Therefore, transformation from 3D island (amorphous-like carbon) growth to 2D island (graphene) growth occurred during CVD at around 800°C.

The initial dendritic island growth in (a) occurred at surface impurities that acted as nucleation sites. Thus, the density of the islands was low and the island distance might be larger than the carbon adatom diffusion length. In such a case, the adatom flux to the islands are high, inducing dendritic growth. On the other hand, the circular islands uniformly nucleated on the terrace area between dendritic islands. Because the growth rate of 3D islands is low, the adatom concentration on the terrace increases, resulting in the homogeneous nucleation of graphene on the terrace. The relatively low temperature, around 800°C, should responsible to the crossover of 2D and 3D growth.

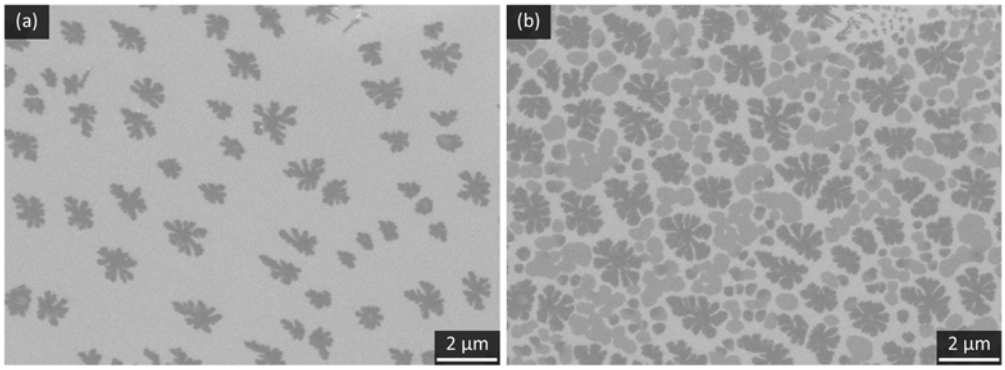

Figure 1: Graphene growth process observed at the same place on copper-indium alloy. Growth was performed for (a) 1 hour and (b) additional 1 hour before SEM observations.

References

1. Y. Ogawa, et al., Nanoscale, 6, 7288 (2014)
2. X. Li, et al., Science, 324, 1312 (2009)

A. Acun et al. "Atomically Controlled Surfaces Interfaces and Nanostructures"
edited by A. Bianconi, A. Marcelli (Superstripes Press, Rome 2016) isbn: 9788866830597

Analysis of Surface Structure with Total-Reflection High-Energy Positron Diffraction (TRHEPD)

T. Hyodo[1] , Y. Fukaya[2], I. Mochizuki[1], H. Ariga[3], K. Wada[4], M. Maekawa[4], A. Kawasuso[4], T. Shidara[5], K. Asakura[3], A. Ichimiya[1]
[1]*IMSS, KEK, Tsukuba, Japan.*
[2]*Advanced Science Research Center, JAEA, Tokai, Japan.*
[3]*Institute for Catalysis, Hokkaido University, Sapporo, Japan.*
[4]*Takasaki Advanced Radiation Research Institute, QST, Takasaki, Japan.*
[5]*Accelerator Laboratory, KEK, Tsukuba, Japan.*

Email: *toshio.hyodo@kek.jp*
Key words: Oxides, Graphene and other 2D materials

Materials research consists of the analysis of the structure of materials and that of their characteristics and functions. X-ray diffraction is the standard technique to determine the bulk structure. For the determination of the topmost- and near-surface atomic geometries, an equivalent single method is yet to be established. A recently developed technique, *i.e.*, total-reflection high-energy positron diffraction (TRHEPD) may serve for the purpose because it can observe exclusively the topmost surface atomic arrangement as well as observe the sub-surface atomic arrangements.

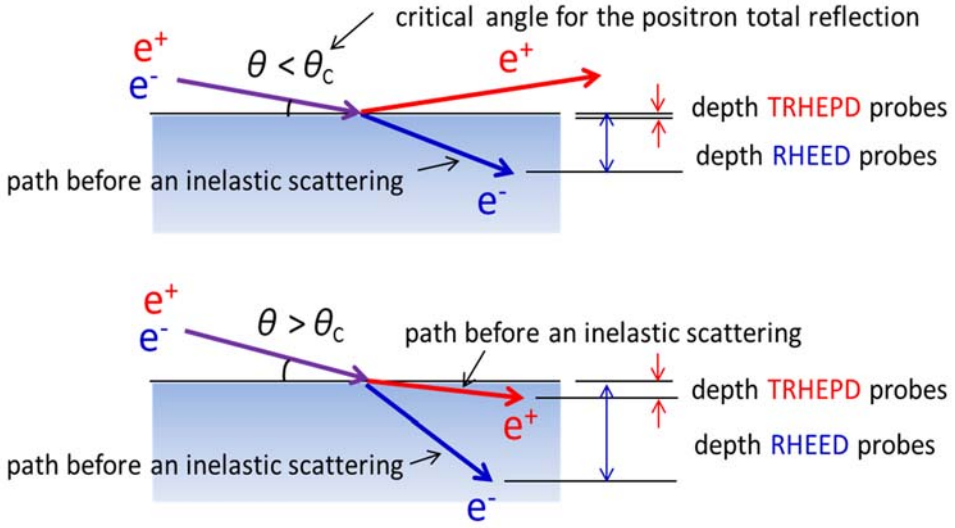

Figure 2 Total reflection of the positron and the refraction of the positron and the electron.

TRHEPD is the positron counterpart of the RHEED (reflection high-energy electron diffraction). It was proposed in 1992 (then called reflection high-energy positron diffraction, RHEPD)[1], and the first data were obtained with a radioisotope-based positron beam [2], followed by investigations of various surface structures and phase transitions [3]. Then an electron linac-based TRHEPD apparatus was developed that made it possible to observe clearer patterns within a much shorter time [4, 5].

The key of the unique characteristics of TRHEPD is the universally positive electrostatic potential in every material. It leads to the total reflection of the positron and the refraction toward the surface of the penetrating positron.

Such refraction makes it possible to continuously increase the observation depth form the topmost surface. (We call the whole technique as TRHEPD regardless of the possible inclusion of the data out of the total-reflection condition.) Figure 1 shows schematically the comparison with the case of the electron that refracts off the surface. It is worth mentioning that TRHEPD is the only diffraction method where the conditions for the total reflection and the Bragg diffraction are satisfied simultaneously in the same angular region.

It has been demonstrated [6] that the observed THREPD and RHEED patterns from the Si(111)-(7×7) for the glancing angle 1.3° are certainly different from each other, reflecting the difference in the probed depth. The degree of the agreement between the observed and calculated TRHEPD patterns is much better than that for the RHEED case. This suggests that unrevealed relaxation may exist in the region that RHEED probes. The good agreement of the TRHEPD patterns confirms that the uncertainly in the deeper region does not affect the analysis of the data for a small glancing angle.

Following the first determination of the structure of silicene on Ag(111) [7], we recently determined the structure of graphene on Cu(111) and Co(0001) [8]. On both metals graphene does not have appreciable magnitude of buckling but the distance between the graphene and the substrate metal surface is different.

We also determined a complex structure of rutile-TiO_2(110)-(1×2) surface. During the long debates lasting for more than 30 years since its discovery, many models were proposed for this surface. The structure finally determined by TRHEPD [9] is an asymmetric Ti_2O_3 structure, where the two Ti atoms with the surrounding O atoms added on the top have different height. This conclusion agrees well with a recent theoretical result by Wang et al. [10] who optimized the atomic composition and the atomic arrangement concurrently using the USPEX code.

This study was performed under the PF Proposal No. 2014S2-004 and 2013U002, and the auspices of the JAEA-KEK Joint Development Research at the High Energy Accelerator Research Organization (KEK). It was partly supported by a Grant-in-Aid for Scientific Research (S) 24221007 and those for Young Scientists (B) 25800182 and 26800170 from JSPS, and by Toray Science and Technology Grant from Toray Science Foundation.

References

1. A. Ichimiya, Solid State Phenom. 28/29, 143 (1992).
2. A. Kawasuso and S. Okada, Phys. Rev. Lett. 81, 2695 (1998).
3. Y. Fukaya, et al, J. Phys.: Conf. Series 443, 012068 (2013).
4. K. Wada, et al., ”,Eur. Phys. J. D 66, 37 (2012).
5. M. Maekawa, et al., Eur. Phys. J. D 68, 165 (2014).
6. Y. Fukaya, et al., Appl. Phys. Express 7, 056601 (2014)
7. Y. Fukaya, et al., Phys. Rev. B 88, 205413 (2013)
8. Y. Fukaya, et al., Carbon 103, 1 (2016)
9. I. Mochizuki et al., Phys. Chem. Chem. Phys., 18, 7085 (2016).
10. Q. Wang et al., Phys. Rev. Lett., 113, 266101 (2014).

A. Acun et al. “Atomically Controlled Surfaces Interfaces and Nanostructures”
edited by A. Bianconi, A. Marcelli (Superstripes Press, Rome 2016) isbn: 9788866830597

Unoccupied Electronic structure of BiAg surface alloy studied with angle-resolved two-photon photoemission spectroscopy

Masaki Imamura, Koutaro Matsuishi, Kazutoshi Takahashi, Isamu Yamamoto, and Junpei Azuma
Synchrotron Light Application Center, Saga University

Email:*mimamura@cc.saga-u.ac.jp*
Key words: Graphene and other 2D materials

Spin-splitted surface state at metal surface attracts much attention from the viewpoints of the fundamental physics and the applications. It is inevitable to investigate the unoccupied electronic dispersions which play an important role for electron transport phenomena. In contrast to an understanding of the electronic states in the occupied state in BiAg surface alloy, the experimental investigations for the electronic state in the unoccupied state are very few to date. In this study, we have carried out the angle-resolved photoemission (ARPES) and two-photon photoemission spectroscopy (AR2PPE) for a BiAg surface alloy grown on Ag thin film. From the detailed analysis of ARPES and AR2PPE spectra, occupied and unoccupied electronic dispersions in the vicinity of Fermi-level were specified.

All measurements in this study were conducted at BL13 (Saga University beamline) at SAGA-LS. BiAg surface alloy grown on Ag thin film were prepared by the 1/3 ML of Bi deposition onto 15 ML Ag thin film. ARPES measurement was carried out with synchrotron radiation. AR2PPE measurements to observe the unoccupied states were performed with the *p*-polarized third harmonics of a Ti:Sapphire laser. The excitation energies were varied between 3.96 and 4.28 eV.

Figure 1 shows the AR2PPE intensity map for the BiAg surface alloy grown on 15 ML Ag thin film measured along □- □ direction in SBZ. The excitation energies were 4.00, 4.18, and 4.38 eV. As shown in Fig. 1, the excitation-energy-dependent AR2PPE spectra were observed. From the detailed analysis of excitation energy dependance in ARPES spectra, the occupied electronic dispersions, unoccupied electronic dispersions, and photoexcitation process were specified. The complex electronic dispersions observed at higher-final-energy were assigned as the occupied Rashba-surface state, quantum-well states of Ag thin film, and image potential state. The occupied electronic dispersions were consistent with those obtained from ARPES measurements. [1, 2] The band dispersions located at 6 - 7 eV in final energy were the unoccupied electronic dispersions. From the comparison with the theoretical study for BiAg surface alloy on Ag thin film, the unoccupied electronic dispersions can be attributed to the spin-splitted surface states.[3]

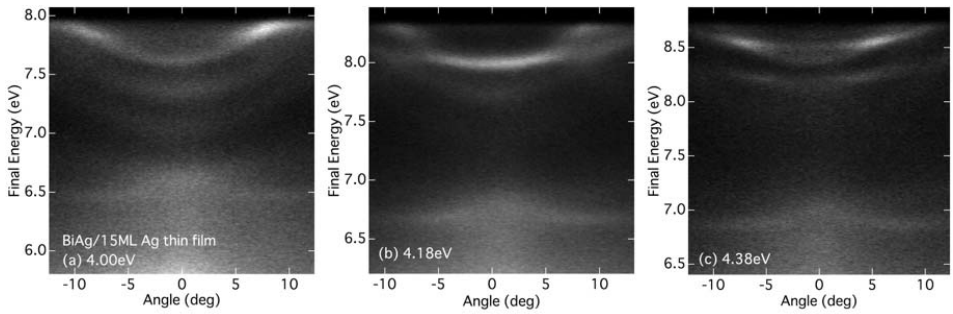

Figure 1: Excitation-energy-dependent AR2PPE images for BiAg surface alloy grown on 15 ML Ag thin film.

References

1. G. Bihlmayer, S. Blügel, and E. V. Chulkov, *Phys. Rev*. B, 75, 195414 (2007).
2. G. Bian, X. Wang, T. Miller, and T.-C. Chiang, Phys. Rev. Lett., 108, 186403 (2012).
3. G. Bian, X. Wang, T. Miller, and T.-C. Chiang, *Phys. Rev*. B, 88, 085427 (2013).

A. Acun et al. “Atomically Controlled Surfaces Interfaces and Nanostructures”
edited by A. Bianconi, A. Marcelli (Superstripes Press, Rome 2016) isbn: 9788866830597

Electronic structure of surface conduction band of Ge(001)-c(4x2) and Ge(111)-c(2x8) surfaces studied by two-photon photoelectron spectroscopy

Isamu Yamamoto[1], Junpei Azuma[1], Jun’ichi Kanasaki[2]
[1]*Synchrotron Light Application Center, Saga University*
[2]*The Institute of Scientific and Industrial Research, Osaka University*

Email: *kanasaki@sanken.osaka-u.ac.jp*
Keywords: Surfaces and interfaces for electronic devices, Frontier aspects of semiconductor, surface and interfaces

Surface band structure is one of the most important concepts in the fields of surface physics and applied surface science. Here we determine the surface conduction band structure of the clean Ge(001)-c(4x2) and Ge(111)-c(2x8) with high energy and momentum resolution by means of time-resolved two-photon photoelectron spectroscopy. Electrons with the high excess energy are injected into the bulk conduction band with 824 nm pump laser pulses (0.4 ps) and the subsequent electron dynamics is probed with the third-or fourth-harmonic pulses with changing the delay time between the pump and probe pulses. Photoinjected bulk electrons are then transferred to the unoccupied surface band (SB) and relaxed within the band. In this study, the electrons transiently populated and relaxed in the unoccupied SB are directly imaged as functions of energy and momenta parallel to the surface to determine the surface conduction band structure.

On Ge(001)-c(4x2), the structure of unoccupied (π) SB is asymmetric: the dispersion is little in the direction ($\bar{\Gamma}\bar{J}$) perpendicular to the surface dimer row, while large in the direction ($\bar{\Gamma}\bar{J}'$) parallel to the dimer row [1]. The photoexcitation generates highly¬excited electrons in the $\bar{\Gamma}$-valley of bulk conduction band. On this surface, some bulk electrons are transferred fast into the dispersive branch of the π -SB, followed by the relaxation toward the bottom at the $\bar{\Gamma}$-point in the surface Brilluoin zone. In figure 1(a), the relaxation pathway of photo-excited electrons along the $\bar{\Gamma}$-$\bar{J}'$ direction is superimposed as broken curve on the angle-resolved photoelectron image acquired at 4.0 ps. The flat band shows the branch along the $\bar{\Gamma}\bar{J}$ direction. The surface band gap is determined to be 0.3 eV above the valence band maximum, consistent with previous ARUPS study [1].

Figure 1(b) shows the photoelectron image acquired at 1.5 ps after the photoexcitation of Ge(111)-c(2x8). In contrast to the case of Ge(001) surface, photo-injected electrons are transferred to the adatom-related SB after relaxation to the bottom of bulk conduction band, because of small overlapping of bulk and surface energy bands. The surface electrons are then relaxed towards the bottom at $\bar{\Gamma}$ point along the apparently symmetric band. The bottom of the unoccupied SB is located 0.3 eV below that of bulk

conduction band. The directly-observed band structure is consistent with the calculated surface structure [2] and the DOS measured by scanning tunneling spectroscopy [3].

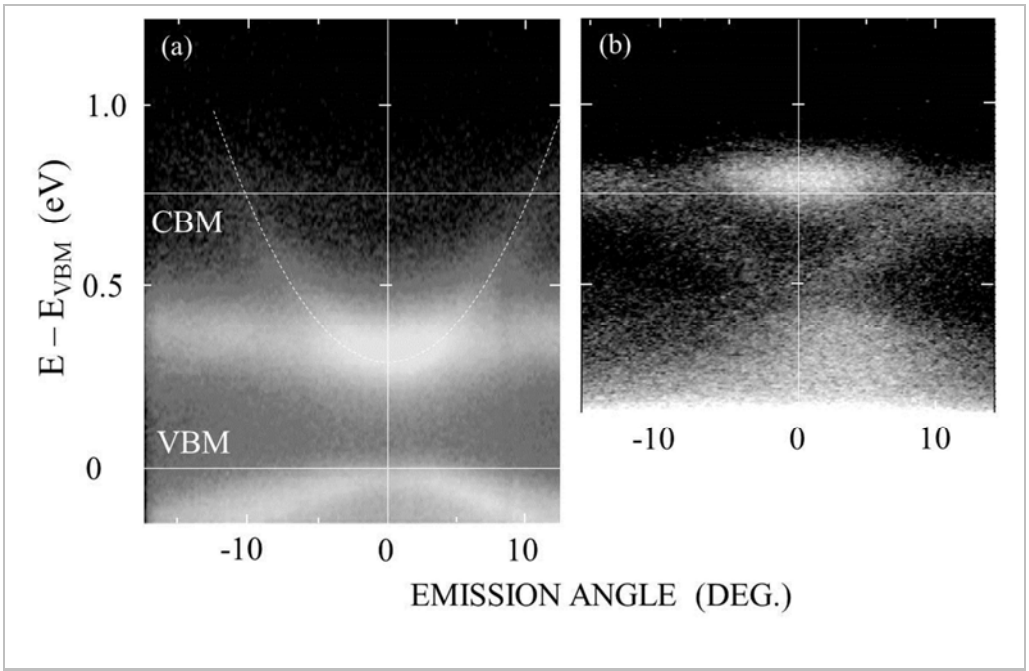

Figure 1: (a) The angle-resolved photoelectron image acquired at 4psec after photoexcitation of Ge(001)-c(4x2). Also shown by dotted line is the relaxation pathway of photo-excited electrons. (b) The photoelectron image at 1.5 ps after the excitation of Ge(111)-c(2x8).

References

1. K. Nakatsuji, Y. Takagi, F. Komori, H. Kusuhara, A. Ishii, Phys. Rev. B72, 241308(R) (2005).
2. P. V. Smith, M. W. Radny, G. A. Shah, RSC Adv. 4, 48245 (2014).
3. R. M. Feenstra, J. Y. Lee, M. H. Kang, G. Meyer, K. H. Rieder, Phys. Rev. B73, 035310 (2006)

A. Acun et al. “Atomically Controlled Surfaces Interfaces and Nanostructures”
edited by A. Bianconi, A. Marcelli (Superstripes Press, Rome 2016) isbn: 9788866830597

Electrical conductivity of the biaxially-strained GaSb (111) and GaSb (001)

H. Kishimoto , T. Hatayama, A. Akaishi, and J. Nakamura
The University of Electro-Communications (UEC-Tokyo), Tokyo, Japan

Email: *kishimoto@natori.ee.uec.ac.jp*
Key words: electrical conductivity, biaxial strain

GaSb is an attractive material for the p-channel of next-generation metal-oxide-semiconductor field-effect-transistor on Si because of its high hole mobility. Recently, it has been reported that high-quality GaSb films can be epitaxially grown on the Si (111) substrate using the InAs buffer layer[1]. The lattice constant in the plane of growth for the thin GaSb epilayer inherits that of InAs, causing inherent biaxial strain in the GaSb film. As a result, the electronic structure of the GaSb film can be modified. Nainani *et al.* have reported that tensile strain enhances the hole mobility of GaSb as well as compressive strain[2]. However, the mechanism of such mobility enhancement under the strain has not been revealed. In this study, we evaluate the electrical conductivity of the biaxially-strained GaSb bulk and thin films using first-principles calculations within the density fuctional theory and the semi-classical Boltzmann transport theory. We assume the biaxial strain parallel to the (111) and (001) plane.

Figure 1 shows the in-plane electrical conductivity, $\sigma_{\text{in-plane}}$, of the biaxially-strained GaSb (111) and GaSb (001) as a function of the biaxial strain. For GaSb (111), $\sigma_{\text{in-plane}}$ varies monotonically as a function of the biaxial strain for a high hole consentration, while $\sigma_{\text{in-plane}}$ for a low hole concentration has a singular point at ε=0. Such peculiar behavior of $\sigma_{\text{in-plane}}$ results from the change in the band structure under the biaxial strain. The biaxial strain breaks the cubic symmetry of GaSb, which lifts the degeneracy of the heavy hole (HH) and light hole (LH) states at the valence band maximum (VBM). For a low hole concentration, only a vicinity of the VBM contributes to the electron transport. The density of states at the VBM is reduced by the lifting of degeneracy, thus, $\sigma_{\text{in-plane}}$ decreases under both the compressive and the tensile biaxial strain. For GaSb (001), $\sigma_{\text{in-plane}}$ for a low hole concentration has the maximum value at ε=0 as well as that for GaSb (111). On the other hand, $\sigma_{\text{in-plane}}$ for a high hole concentration varies non-monotonically as a function of the biaxial strain as shown in Fig. 1(c). $\sigma_{\text{in-plane}}$ increases not only under the compressive strain but also under the tensile strain unlike in the case of GaSb (111). The mechanism of the enhancement of $\sigma_{\text{in-plane}}$ under the strain will be discussed and the results for the GaSb thin films will also be shown.

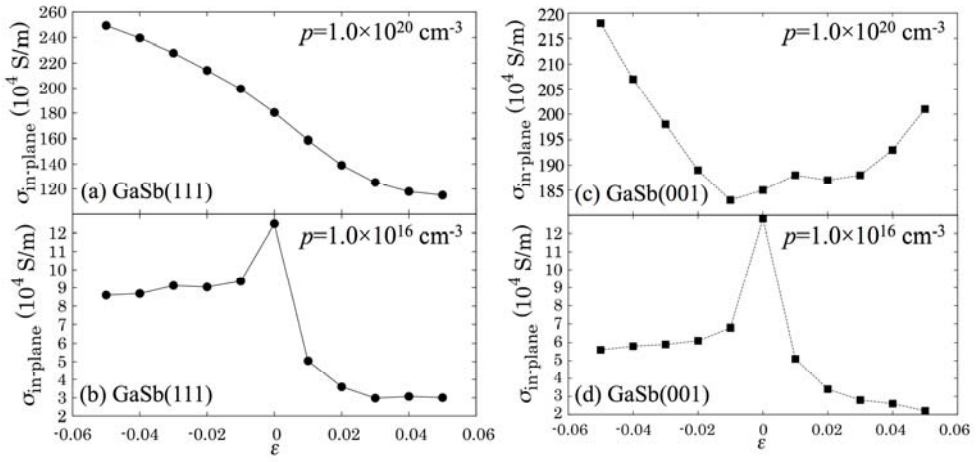

Figure 1: In-plane electrical conductivity $\sigma_{\text{in-plane}}$ of (a), (b) the GaSb (111) and (c), (d) GaSb (001) as a function of the biaxial strain at 300K for the hole concentrations of 1×10^{20} cm^{-3} and 1×10^{16} cm^{-3}.

References

1. A. Ohtake, T. Mano, N. Miyata, T. Mori, and T. Yasuda, Appl. Phys. Lett. 104, 032101 (2014).
2. A. Nainani, B. R. Bennet, J. B. Boos, M. G. Ancona, and K. C. Saraswat, J. Appl. Phys. 111, 103706 (2012).

A. Acun et al. “Atomically Controlled Surfaces Interfaces and Nanostructures”
edited by A. Bianconi, A. Marcelli (Superstripes Press, Rome 2016) isbn: 9788866830597

Thermal property modulation of graphene by strain-induced phonon engineering

Satoru Konabe[1] , Kento Tada[2], Takashi Funatani[3], Kenji Sasaoka[3], Matsuto Ogawa[3], Satofumi Souma[3], Takahiro Yamamoto[1,2]
[1]*Research Institute for Science and Technology, Tokyo University of Science*
[2]*Department of Electrical Engineering, Tokyo University of Science*
[3]*Department of Electrical and Electronic Engineering, Kobe University*

Email: *konabe@rs.tus.ac.jp*
Key words: graphene, phonon, thermal property, strain effects

Atomically thin materials such as graphene [1], silicene [2,3], transition metal dichalcogenides [4], and phosphorene [5] have greatly attracted attention due to rich physical properties. One of the important aspects of those materials is their extraordinal flexibility owing to their single atomic layered structure. There have been studied of the strain effect on electronic properties in atomically thin materials. These include, for instance, the modification of electronic properties in various materials [6,7], the enhancement of a chemical reactivity [8], and the improve of the thermoelectric performance in phosphorene [9,10]. However, phonon properties of atomically thin layered materials associated with the strain have not extensively been investigated.
In the present paper, we examine the strain dependence on phonon dispersions and a specific heat by performing the first principles calculation based on the density functional theory. For the phonon dispersion, we focus on the high-energy and lowenergy region of the phonon modes. We found that the high-energy phonon modes show the softening due to the strain. In particular, the G-modes exhibit the red-shift with the energy splitting as a function of the strain. Furthermore, it has been shown that the split of these are different for the strain of the zigzag direction and armchair direction. On the other hand, the low-energy acoustic modes exhibit the hardening; the dispersion relation of the out-of-plane mode essentially changes from the quadratic to the linear associated with the strain. The comparison between the first principles result and the analytical result explains this modification in terms of the ratio of the nearestneighbor and the next-nearest-neighbor force constants. To see the effect of the straininduced phonon modification on thermal properties, we calculated a specific heat. We show that the classical limit of a specific heat achieves faster for the larger strain (Fig.1(a)). This originates with the softening of the phonon mode due to the strain. We also elucidate that the temperature dependence of the low-temperature specific heat also changes from the linear to the quadratic (Fig.1 (b)). We ascribe this to the different wavenumber dependence of the phonon dispersion in the presence of the strain.

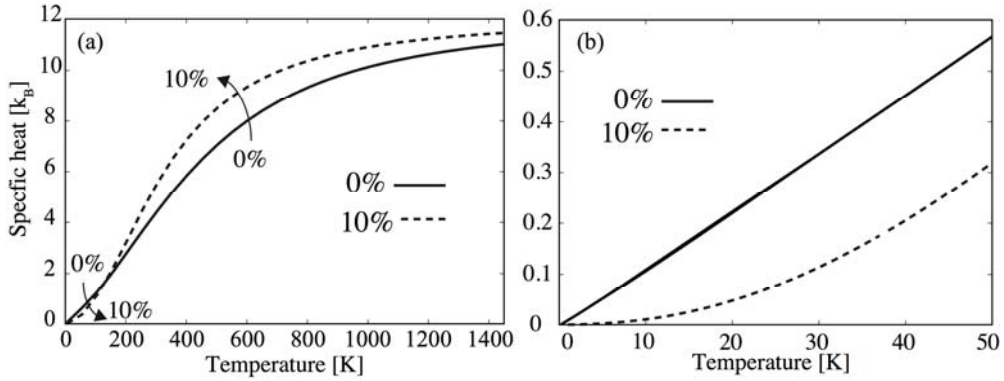

Figure 1: The strain dependence of the specific heats of uniformly strained graphene as a function of temperature. The panel (a) shows the specific heat over wide temperature range from 0 to 1400K. The panel (b) shows the lower temperature region. The amount of strain is zero to 10% by 2%.

References

1. A. H. Castro Neto, F. Guinea, N. M. R. Peres, K. S. Novoselov and A. K. Geim: Reviews of Modern Physics 81, 109 (2009).
2. A. Kara, H. Enriquez, A. P. Seitsonen, L. C. L. Y. Voon, S. Vizzini, B. Aufray and H. Oughaddou: Surface Science Reports 67, 1 (2012).
3. P. Vogt, P. De Padova, C. Quaresima, J. Avila, E. Frantzeskakis, M. C. Asensio, A. Resta, B. Ealet and G. Le Lay: Physical Review Letters 108, 155501 (2012).
4. Q. H. Wang, K. Kalantar-Zadeh, A. Kis, J. N. Coleman and M. S. Strano: Nature Publishing Group 7, 699 (2012).
5. H. Liu, A. T. Neal, Z. Zhu, Z. Luo, X. Xu and D. Tomanek: ACS Nano 8, 4033 (2014).
6. V. M. Pereira and A. H. Castro Neto: Physical Review Letters 103, 046801 (2009).
7. S. Souma, M. Ueyama and M. Ogawa: Applied Physics Letters 104, 213505 (2014).
8. M. A. Bissett, S. Konabe, S. Okada, M. Tsuji and H. Ago: ACS Nano 7, 10335 (2013).
9. H. Y. Lv, W. J. Lu, D. F. Shao and Y. P. Sun: Physical Review B 90, 085433 (2014).
10. S. Konabe and T. Yamamoto: Applied Physics Express 8, 015202 (2015).

A. Acun et al. "Atomically Controlled Surfaces Interfaces and Nanostructures"
edited by A. Bianconi, A. Marcelli (Superstripes Press, Rome 2016) isbn: 9788866830597

Characterization of interfacial water layer between single-layer graphene and substrate by Raman spectroscopy

Tomohiro Koyama[1] , Takumi Inaba[1], Katsuyoshi Komatsu[2,3], Satoshi Moriyama[3], Maki Shimizu[1], Yoshikazu Homma[1]
[1]*Tokyo University of Science*
[2]*Institute of Innovative Research, Tokyo Institute of Technology*
[3]*National Institute for Materials Science*

Email: *1215624@ed.tus.ac.jp*
Key words: Electronic and optical properties of surfaces and interfaces; Graphene and other 2D materials

An interfacial water layer is always formed between the graphene and substrate when graphene is transferred onto a hydrophilic substrate by mechanical exfoliation. It can induce charge doping in graphene on an SiO_2/Si substrate [1] or inhibit charge transfer between graphene and a mica substrate [2]. Therefore, understanding the behavior and effects of it is essential for controlling the properties of devices made from graphene.
The hydrophilic nature of the SiO_2 surface is due to the hydrogen bonding between silanol group (Si-OH) and water molecule. The increase in silanol group density by removing hydrocarbon contaminants on SiO_2 by O_2-plasma treatment enhances the hydrophilicity [3]. The water is desorbed from two silanol groups at high temperature, which causes formation of siloxane group (Si-O-Si) that forms almost no hydrogen bonding with water molecules [4].

In this study, graphene was transferred on a SiO_2(285 nm)/Si produced by O_2-plasma treatment and reoxidization. We focused on the interfacial water layer between single-layer graphene and the substrate and evaluated change in the amount of water depending on the environment through the change in graphene vibration mades by Raman spectroscopy. We controlled temperature and pressure around the graphene during Raman measurements with an environmental chamber by heating and pumping. First, the Raman spectrum of the single-layer graphene was measured in the chamber in air. Second, it was measured after annealing (at ~200 ˚C for 2 h, ~2 Pa) in Ar atmosphere. Finally, it was measured in water vapor atmosphere.

Figure 1 shows shifts and change of intensity ratio for G- and 2D-peaks. After annealing, G- and 2D-peaks down-shifted and intensity ratio (I_{2D}/I_G) increased. In water vapor, G- and 2D-peaks up-shifted and I_{2D}/I_G decreased from those after annealing.
Up-shifts of G- and 2D-peaks can be caused by either compressive strain [5] or hole-doping in graphene [6,7]. The 2D-peak intensity decreases with an increase in charge density [6]. The result indicates that the interfacial water layer induces hole-doping in the graphene. In additon, the amount of the interfacial water layer decreased to form

the siloxane groups by annealing and increased by intercalation of water molecule in water vapor.

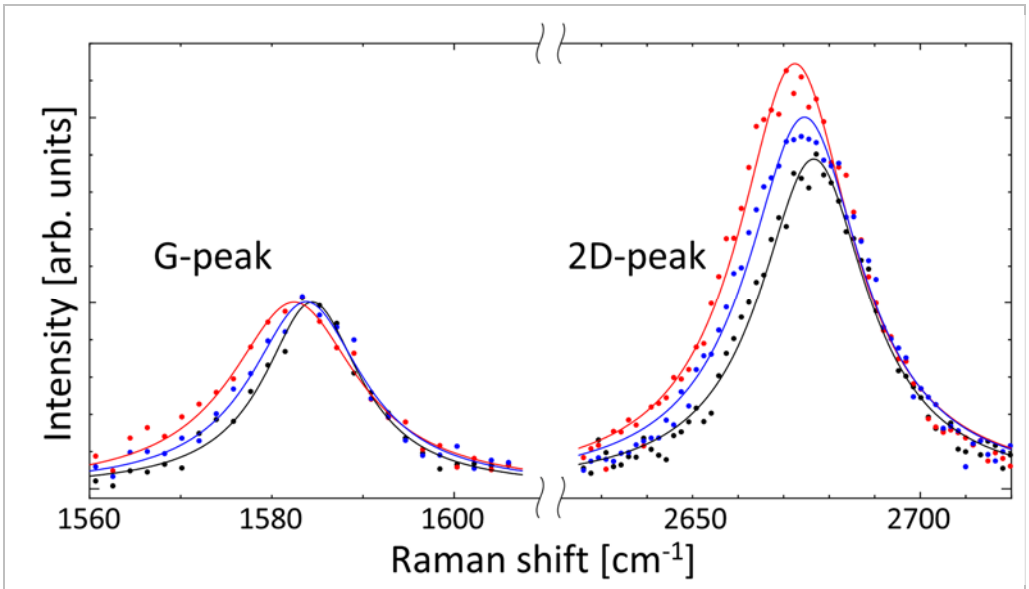

Figure 1: The Raman spectra of the single-layer graphene after transfer (black), after annealing (red) and in water vapor (blue).

References

1. T. O. Wehling, A. I. Lichetenstein, M. I. Katsnelson: Appl. Phys. Lett. 93, 202110 (2008)
2. J. Shim, C. H. Lui, T. Y. Ko, Y. J. Yu, P. Kim, T. F. Heinz, S. Ryu: Nano Lett. 12, 648 (2012)
3. K. Nagashio, T. Yamashita, T. Nishimura, K. Kita, A. Toriumi: Appl. Phys. Lett. 110, 024513 (2011)
4. R. K. Iler, *The Chemistry of Silica* (Wilcy-Interscience, New York, 1979), p. 622.
5. Z. H. Ni, T. Yu, Y. H. Lu, Y. Y. Wang, Y. P. Feng, Z. X. Shen: ACS Nano 3, 483 (2009)
6. A. Das, S. Pisana, B. Chakraborty, S. Piscanec, S. K. Saha, U. V. Waghmare, K. S. Novoselov, H. R. Krishnamurthy, A. K. Geim, C. A. Ferrari, A. K. Sood: Nano. Lett. 3, 210 (2008)
7. S. Ryu, L. Liu, S. Berciaud, Y.-J. Yu, H. Liu, P. Kim, G. W. Flynn, L. E. Brus: Nano. Lett. 10, 4944 (2010)

A. Acun et al. “Atomically Controlled Surfaces Interfaces and Nanostructures”
edited by A. Bianconi, A. Marcelli (Superstripes Press, Rome 2016) isbn: 9788866830597

Experimental identification of Indium single layer and double layer formed on Si(111)- √7×√3 surface

Jeongseok Woo, Dongchul Shin, Sangsoo Lee, Geunseop Lee
Inha University, Republic of Korea
Department of Physic

Email: *glee@inha.ac.kr*
Key words: In/Si(111), √7 × √3 superstructures, Scanning tunneling microscopy (STM)

When indium (In) atoms were deposited on a In/Si(111)-√3×√3 surface various superstructure phases were observed to form depending on the In coverage. Among them are the √7×√3 surfaces, which appear with hexagonal (√7×√3-hex) and rectagular (√7×√3-rec) geometries in scanning tunneling microscopy (STM) images, and were recently shown to become superconducting at low temperature. The atomic structures as well as the In coverages of the √7×√3 surfaces are not well established as yet. Recently, the structural models and In coverages of the two √7×√3 phases were proposed in theoretical studies [2,3,4]. While a double-layer structure is agreed for the √7×√3-rec phase, the structure and In coverage (a single layer vs double layers) remain debated.

By using STM, we investigated the √7×√3 superstructure phases prepared by two different procedures, room-temperature deposition of In on a In/Si(111)-√3×√3 surface and high-temperature deposition of In on a Si(111)-7×7 surface. We found that the superstructures labeled as √7×√3-hex and √7×√3-rec phases in a previous room-temperature-deposition study [1] were indeed identical to the ‘striped’ and the √7×√3-hex phase formed by high-temperature In deposition. An additional phase, truly identical to the √7×√3-rec phase formed by high-temperature In deposition, was also found. The ‘striped’ phase is also found to have √7×√3 structure (√7×√3-‘striped’) and concluded to have a single-layer In coverage in that it typically coexists with a 4×1 phase, a well-established structure with one monolayer of In coverage. The √7×√3-hex phase is observed to form on top of the √7×√3-‘striped’ phase, indicating that the √7×√3-hex phase, like the √7×√3-rec phase, is made up of double layers of In. This contrasts to the expectations of single-layer In [2,3], but agrees with a recent theoretical calculation proposing the double-layer structure of the √7×√3-hex phase [4].

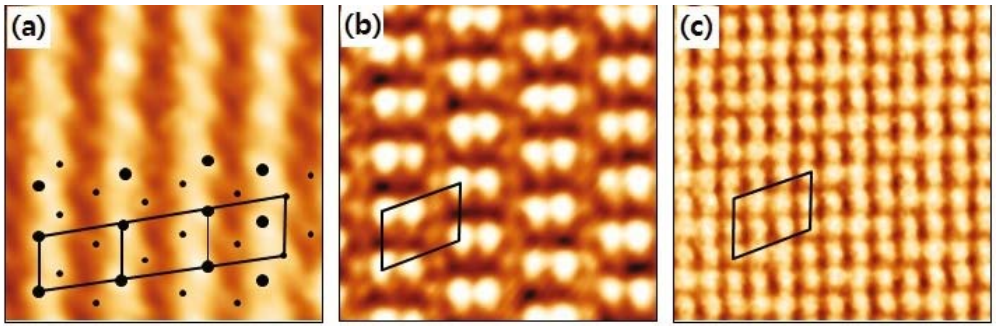

Figure 1: High-resolution STM images of (a) √7×√3-‘striped’, (b) √7×√3-hex, and (c) √7×√3-rec phases.

References

1. A. A. Saranin et al., Phys. Rev. B 74, 035436 (2006).
2. B. Shang, L-F. Yuan, and J-L. Yang, Chin. J. Chem. Phys. 25, 403 (2012).
3. K. Uchida and A. Oshiyama, Phys. Rev. B 87, 165433 (2013).
4. J. W. Park and M. H. Kang, Phys. Rev. B 92, 042306 (2015).

A. Acun et al. "Atomically Controlled Surfaces Interfaces and Nanostructures"
edited by A. Bianconi, A. Marcelli (Superstripes Press, Rome 2016) isbn: 9788866830597

Nanolaminate Copper Barriers of Ruthenium and Tantalum Nitride Thin Films by Inductively Coupled Plasma Enhanced Atomic Layer Deposition

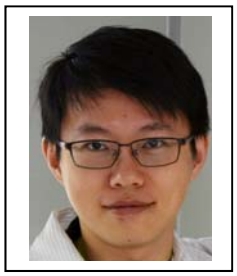

Bo-Heng Liu,[1,*], Sheng-Hsin Huang,[2] Chien-Wei Chen,[1] and Chi-Chung Kei[1]
[1]*Instrument Technology Research Center, National Applied Research Laboratories, Hsinchu 300, Taiwan, R.O.C.*
[2]*Department of Materials Science and Engineering, Hsinchu 300, Taiwan, R.O.C.*

Email: * *jazerox@itrc.narl.org.tw*
Key words: Ru/TaN nanolaminate barriers, Cu interconnect and inductively coupled plasma enhanced atomic layer deposition (PEALD)

Ru/TaN nanolaminate barriers and Cu interconnect were sequential directly grown on dual damascene nano-porous dielectrics by inductively coupled plasma enhanced atomic layer deposition (PEALD). Ru/TaN thin films were successfully deposited by home-built PEALD using $[Ru(EtCp]_2]$ [1] and $Ta(NC_2H_6)_5$ [2] as precursor with high energy reductive Ar/H_2 and Ar/O_2 plasma. Fig. 1 shows the chamber design of the PEALD system. The substrate temperature of Ru/TaN thin films were 300 and 250 ℃ with 500 cycles to PEALD process. The N_2 purge time and plasma power were held on 5 s and 400 W. Ru/TaN thin films were analyzed by X-ray photoelectron spectroscopy (XPS: Perkin Elmer PHI 670) and HRTEM (JEOL JEM-2100F). The resistivity was measured by using Hall effect measurement system (Accent/HL 5500PC). Fig. 2 shows the XPS of Ru 3d spectra deposited by PEALD. The energy states of $3d_{5/2}$ (at 280.2 eV) and $3d_{3/2}$ (at 284.3 eV) indicated metallic Ru. However, the lower intensity peaks at 281.2 eV and 285.9 eV are from RuO_2. Growth rate of Ru the films was increased significant from 0.01 to 0.1 nm/cycle by using dc biased PEALD. The resistivity of Ru thin films prepared by PEALD was 40 μΩ cm. The growth rate of TaN thin films was 0.05 nm/cycle as s the PDMAT pulse time is more than 2 s. Cross-section HRTEM image in Fig. 3 shows that the Ru/TaN nanolaminate barriers were formed. In summary, Ru/TaN nanolaminate barriers were prepared by using $Ru(EtCp]_2]$ and $Ta(NC_2H_6)_5$ precursor with the aid of the high energy reductive Ar/O_2 and Ar/H_2 plasma in ITRC PEALD system.

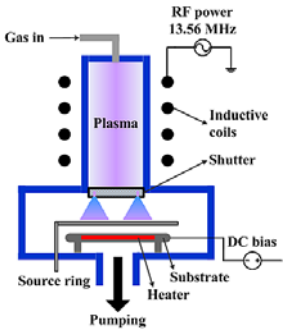

Figure 1: DC biased PEALD system.

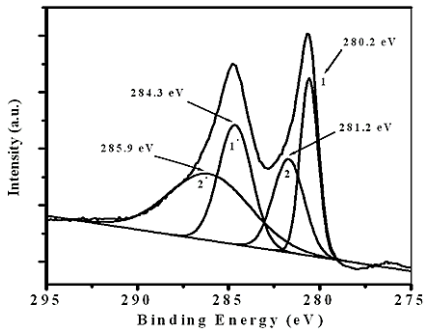

Figure 2: Ru 3d XPS spectra for a 4.8 nm Ru thin film deposited by PEALD.

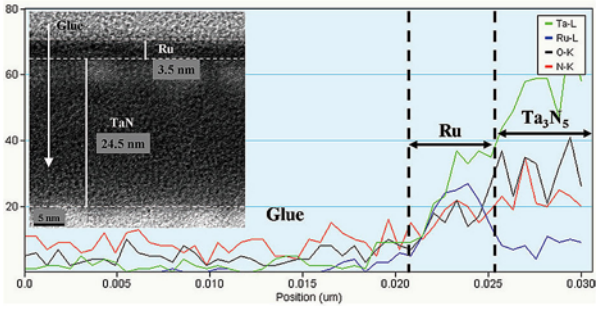

Figure 3: HRTEM image and EDS of Ru/TaN nanolaminate by PEALD.

References

1. Se-Hun Kwon, Oh-Kyum Kwon, Jin-Hyock Kim, Heung-Ryong Oh, Kwang-Ho Kim, and Sang-Won Kang, J. Electrochem. Soc., 155 (5), H296 (1999).
2. E. Langereis, E. Langereis, A. J. M. Mackus, F. Roozeboom, M. C. M. van de Sanden, and W. M. M. Kessels, J. Appl. Phys. 102, 083517 (2007).

Microdrop deposition technique: preparation and characterization of ultradiluted samples.

S. Macis[1], G. Cibin[2], V. Maggi[3], D. Hampai[4] and A. Marcelli[4,5]
[1]*Department of Mathematics and Physics, Università di Roma Tor Vergata, via della Ricerca Scientifica 1, 00133, Rome, Italy*
[2]*Diamond Light Source, Harwell Science and Innovation Campus, OX11 0DE, Didcot, Oxfordshire, UK*
[3]*Dipartimento di scienze dell'ambiente e del territorio e di scienze della terra, Università degli Studi di Milano Bicocca Piazza dell'Ateneo Nuovo, 1 - 20126, Milano*
[4]*Istituto Nazionale di Fisica Nucleare - Laboratori Nazionali di Frascati, 00044, Frascati, Italy*
[5]*RICMASS, Rome International Center for Materials Science Superstripes, Via dei Sabelli 119A, 00185 Rome, Italy*

Email: *salvatore.macis@roma2.infn.it*
Key words: ultra-dilution, droplets, water, evaporation, XRF

The analysis of particulate matter (PM) present in ultra-trace in solutions is an important target for many researches, but difficult to achieve just because of the extremely low concentration. The microdrop technique allows, through the evaporation of small droplets [1,2] to control the deposition of materials dissolved in a solution and to generate a controlled pattern of deposition on a well-defined area. With such technique we may depose onto a substrate, drops with diameters in a range from 70 to 200 μm. Consequently the evaporation process allows depositing the non-volatile materials present in the solution in a relatively short time. This technique allows to evaporate a density of 5ml/cm^2 per hour on a flat substrate and heating up to 80°C the amount evaporated is roughly 30 times higher.
The technique may control also the density of the deposited materials on relatively small areas in order to optimize the density, achieving the deposit of the smallest amount of materials with the highest possible density, a result extremely difficult to achieve with other methods, and in particular when high homogeneity is required. As a matter of fact, using the microdrop deposition it is possible to obtain samples with density comparable to ones prepared with the filtering technique, but with a total amount of the solution ~25 times lower. [3]
A second advantage of the technique is that it significantly minimizes and eventually rules out unwanted effects associated with the evaporation of large drops, such as coffee stains or cluster formations, a requisite mandatory to achieve the highest sample uniformity [4,5]. In addition, unlike filtering techniques, the microdrop method can be applied and optimized for almost any liquid system, as the head of the microdrop is made by highly inert materials. Also the deposition may occur on any surface. It is then possible to select the most suitable substrate for the material to deposit and for the analysis to perform. The technique we will describe may produce samples that could

be used in many applications. Among the many, the deposition and the characterization of aerosols particulate matter for pollution monitoring, studies of polluted water or the investigation of biological diluted materials contained in ultratrace working with concentration values that goes from hundreds to tens of ppm.

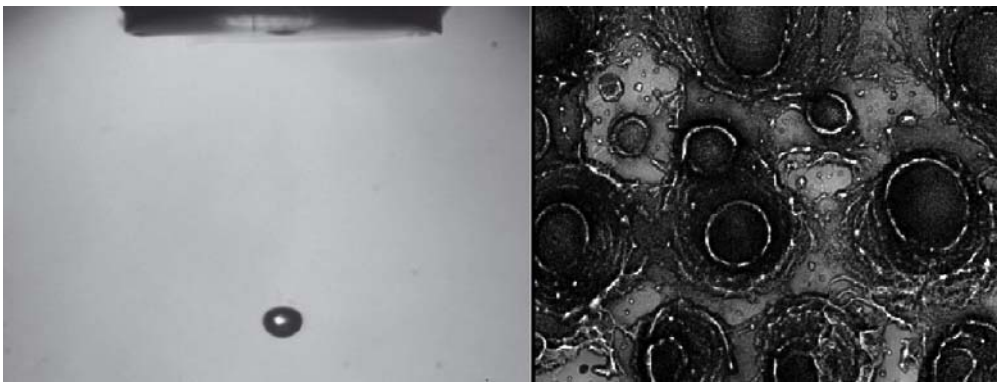

Figure 1: A typical droplet ejected by the microdrop head while approaching the substrate (left) and a magnified view of the deposition pattern (right) obtained using droplets with a diameter of 100 μm and a distance between centres of droplets of ~170 μm.

As an example we will show results related to a project performed in collaboration with the synchrotron radiation facility of the Diamond Light Source, the University of Milano Bicocca and the Laboratori Nazionali di Frascati of the INFN and Tor Vergata University. This project aims to characterize for palaeoclimatology studies the inorganic insoluble amount of particulate trapped in Antarctic deep ice cores through the X-rays absorption and the X-ray Fluorescence techniques. The ultra-pure solutions prepared contain extremely low concentration (about 10-100 ppm) of dust contained in deep ice cores so that the microdrop technique may increase considerably the density and uniformity of the samples. The deposited patterns allow to control the size of the samples to optimize the experimental layout and to reduce the exposition time [6].

References

1. R. G. Picknett, R. Bexon, The evaporation of sessile or pendant drops in still air, Journal of Colloid and Interface Science 61, 336–350 (1977).
2. H. Hu, R.G. Larson, Evaporation of a sessile droplet on a substrate, The Journal of Physical Chemistry B 106, 1334–1344 (2002)
3. S. Macis, *Preparation and characterization of ultra-diluted samples via micro-deposition of droplets*, Thesis Roma Tre University AA 2014-15
4. F. Girard, M. Antoni, S. Faure, A. Steinchen, Evaporation and Marangoni Driven Convection in Small Heated Water Droplets, Langmuir 22, 11085-11091 (2006)
5. P. Innocenzi, L. Malfatti, M. Piccinini, D. Grosso, A- Marcelli, Stain Effects Studied by Time-Resolved Infrared Imaging, Anal. Chem. 81 (2), 551-556 (2009)
6. A. Marcelli, G. Cibin, D. Hampai, F. Giannone, M. Sala, S. Pignotti, V. Maggi, F. Marino, XANES characterization of deep ice core insoluble dust in the ppb range, J. Anal. At. Spectrom. 27, 33-37 (2012)

A. Acun et al. “Atomically Controlled Surfaces Interfaces and Nanostructures”
edited by A. Bianconi, A. Marcelli (Superstripes Press, Rome 2016) isbn: 9788866830597

New theory of Raman peak redshift in thin films

A.P. Meilakhs[1] , S.V. Koniakhin[1,2]
[1] *Ioffe Physical Technical Institute, St. Petersburg, Russia*
[2] *St. Petersburg Academic University, St. Petersburg, Russia*

Email: *mejlaxs@mail.ioffe.ru*
Key words: State-of-the-art theoretical approaches on surfaces and interfaces; Electronic and optical properties of surfaces and interfaces

In thin films, the Raman peak position is redshifted and asymmetrically broadened with respect to bulk materials. The dependence of Raman peak position on film thickness gives possibility to employ Raman spectroscopy for thickness measurements.

The phonon confinement model [1] provided quite good agreement between predicted and measured Raman peak position and shape. However, the theory introduces a parameter α, which has an arbitrary and motiveless value [2]. In phonon confinement model formula, the film thickness, L is a part of the combination α/L^2 and consequently, its value inherently depends on the value of the α parameter. The uncertainty of the value of the parameter α makes application of PCM for independent nanoparticle size determination impossible.

Precise solution, which gives the film vibration modes and their coupling with light, is extremely comprehensive. However, it is possible to qualitatively describe the discretization of nanoparticle vibrations and how the discretization affects the Raman spectra of nanoparticles.

Minimal possible wave vector differs from zero by

$$\Delta q = \frac{\pi}{L+a}, \quad (1)$$

where L is the thickness of the film. The shift of wave vector leads to the downshift of maximal frequency (Fig.1) of vibrations by

$$\Delta\omega = \frac{\pi^2 a^2 B}{2(L+a)^2}. \quad (2)$$

In the equation above, constant B characterizes the dispersion of phonons at Γ point of Brilluin zone.

Due to small thickness of nano films, this shift is not negligible. Hence maximal frequencies of vibrations in thin films are less than those in bulk material. This effect completely explains the red shift of the Raman peak position in nanoparticles.

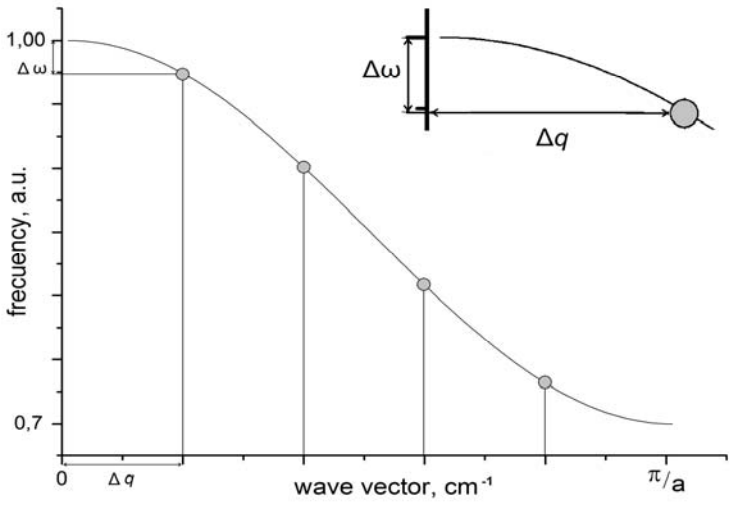

Figure 1: Schematic vibrational spectrum of nano film. Solid line stands for dispersion relation for the optical phonons in bulk material. Actual frequencies of vibrations of film are shown by circles.

Equation (2) straightly relates the frequency shift and the film thickness and contains no arbitrary parameters. The proposed approach will find various applications in nano films thickness measurements.

Acknowledgments. Authors are gratefully indebted to E.D. Eidelman and A.Ya. Vul' for their attention to this study. The work was supported by Russian Science Foundation (grant \# 16-19-00075).

References

1. A.H. Richter, Z.P. Wang, L. Ley, Sol. St. Comm. 39, 625 (1981).
2. J. Zi, K. Zhang, and X. Xie, Phys. Rev. B 55, 9263 (1997)
3. A.P. Meilakhs, S.V. Koniakhin, arXiv:1505.00979

A. Acun et al. “Atomically Controlled Surfaces Interfaces and Nanostructures”
edited by A. Bianconi, A. Marcelli (Superstripes Press, Rome 2016) isbn: 9788866830597

Electron Interference in Ballistic Graphene Nanoconstrictions

Ilio Miccoli[1] , Johannes Aprojanz [1], Jens Baringhaus [1], Mikkel Settnes [2], Stephen Power [2], Antti-Pekka Jauho[2] and Christoph Tegenkamp[1]
[1] *Leibniz Universität Hannover, Institut für Festkörperphysik, 30167 Hannover, Germany*
[2] *Technical University of Denmark, DTU Nanotech, Center for Nanostructured Graphene (CNG), 2800 Kgs. Lyngby, Denmark*

Email: *miccoli@fkp.uni-hannover.de*
Key words: Ballistic Transport, Graphene Nanoconstrinctions, Electron interference

Graphene nanoribbons (GNRs) are an ideal system to study electronic transport phenomena in the coherent regime due to the extremely long mean free path and coherence length of charge carriers [1]. In analogy with subwavelength optics, the coherent transmission of electrons through narrow constrictions within such ballistic ribbons gives rise to interference phenomena [2]. Graphene nanoconstrictions (GNCs) are a central building block of future carbon electronic devices. However, the synthesis of constrictions with well-defined edges is challenging.
Here, we use the tip of a scanning tunneling microscope (STM) for the local etching of graphene, which allows to define GNCs with variable dimensions of down to 1 nm (see Fig. 1 (a)). The GNCs are etched into fully ballistic graphene nanoribbons hosted on the sidewalls of SiC mesa structures [1]. Due to the highly precise etching technique as well as the exceptional electronic quality of the graphene (e.g. mean free path > 10 μm), this system is ideal to study coherent transport phenomena. Therefore, the transport characteristics of constrictions with various dimensions are recorded by means of a variable temperature 4-tip-STM.
Electron interference at the abrupt graphene interfaces gives rise to characteristic conductance peaks and transport gaps which are shown in Fig. 1 (b). Their appearance is described by a tight-binding and recursive Green’s function approach which especially highlights the robustness of the resonances features against temperature as well as disorder [3].

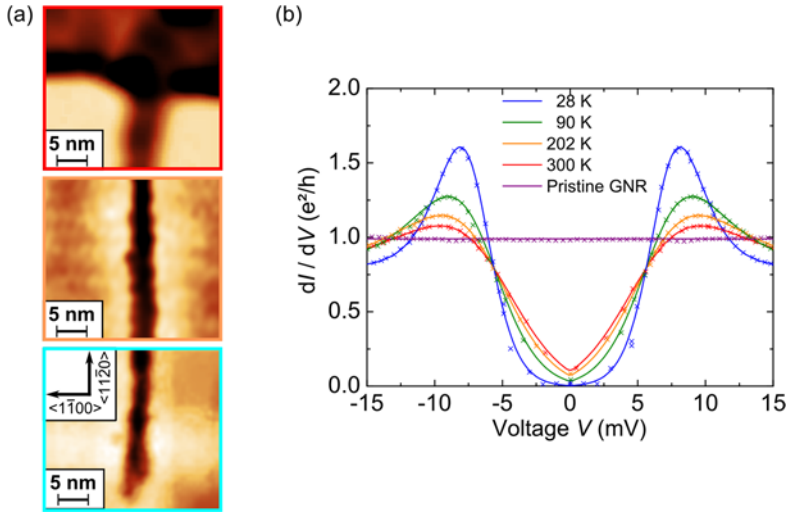

Fig. 1. a) STM images of the top, center and bottom part of the cut etched into a sidewall graphene nanoribbon. b) Differential conductance across a GNC with length L = 6 nm and width W = 2 nm for temperatures between T = 28 K and 300 K.

References

1. J. Baringhaus, M. Ruan, F. Edler, A. Tejeda, M. Sicot, A. Taleb-Ibrahimi, A.-P. Li, Z. Jiang, E.H. Conrad, C. Berger, C. Tegenkamp & W.A. de Heer, Nature 506, 349 (2014). http://dx.doi.org/10.1038/nature12952
2. P. Darancet, V. Olevano, and D. Mayou, Phys. Rev. Lett. 102, 136803 (2009). http://dx.doi.org/10.1103/PhysRevLett.102.136803
3. J. Baringhaus, M. Settness, J. Aprojanz, S.R. Power, A.-P. Jauho, C. Tegenkamp, Phys. Rev. Lett. 116, 186602 (2016). http://dx.doi.org/10.1103/PhysRevLett.116.186602

A. Acun et al. “Atomically Controlled Surfaces Interfaces and Nanostructures”
edited by A. Bianconi, A. Marcelli (Superstripes Press, Rome 2016) isbn: 9788866830597

Interaction of gold with a pinwheel $TiO_{\sim 1.2}$ film formed on Rh(111) facet: STM and DFT studies

Pingo Mutombo[1], Richárd Gubó[2], András Berkó[3]
[1]*Institute of Physics of The Academy of Sciences of the Czech republic, Praha, Czech republic*
[2]*Department of Applied and Environmental Chemistry, University of Szeged, Hungary*
[3]*MTA-SZTE Reaction Kinetics and Surface Chemistry Research Group, Szeged Hungary*

Email: *mutombo@fzu.cz*
Key words: Growth and applications of thin films; Metal-semiconductor and insulator-semiconductor interfaces; State-of-the-art theoretical approaches on surfaces and interfaces; Scanning probe and surface microscopy

Long range ordered ultrathin oxide (UTO) films formed in a completely oxidized or a partially reduced form with determined stoichiometry are recently the subject of intensive experimental and theoretical work because of their technological importance in the fabrication of different supported or self-supporting 2D materials like oxides, graphene, di-chalcogenides or polymers[1].

We have studied the atomic structure of “pinwheel” $TiO_{\sim 1.2}$ ultrathin oxide (w-TiO-UTO) layer and its reaction with gold by STM imaging and Density Functional Theory (DFT) calculations. The UTO film was formed as an encapsulation layer on the top facet (111) of stripe-like Rh nanoparticles supported on a TiO_2(110) substrate. For proposing a structural model, the previous photoelectron (XPS) and ion scattering spectroscopy (LEIS) results were taken into account.

DFT calculations were carried out within the generalized gradient approximation (GGA-PBE) in the frame of the Quantum Espresso code [2]. A Rh(111) slab of 4 layers with a $TiO_{1.14}$ overlayer and a Rh-Ti-O stacking sequence were used. In the starting model, the ratio between hcp and fcc sites filled with Ti atoms was 1.54 (the same value for O atoms was 2.2) on the top of Rh layers. The simulation of the STM images of the relaxed structure was done following the Tersoff-Hamann approximation.

The main structural characteristics obtained experimentally were successfully reproduced in the simulation results: (i) the chemical contrast appeared as a pinwheel structure; (ii) compared to an ideal hexagonal lattice, characteristic local distortions were found in the UTO film. In harmony with the experimental results, the DFT calculations of the adsorption of a single Au atom on a w-TiO-UTO layer indicated that there is a characteristic site-preference within the unit cell of the UTO film. This feature was also experimentally demonstrated for the early stage of the deposition of

Au at room temperature suggesting a moderate template effect adjusted by the pinwheel structure.

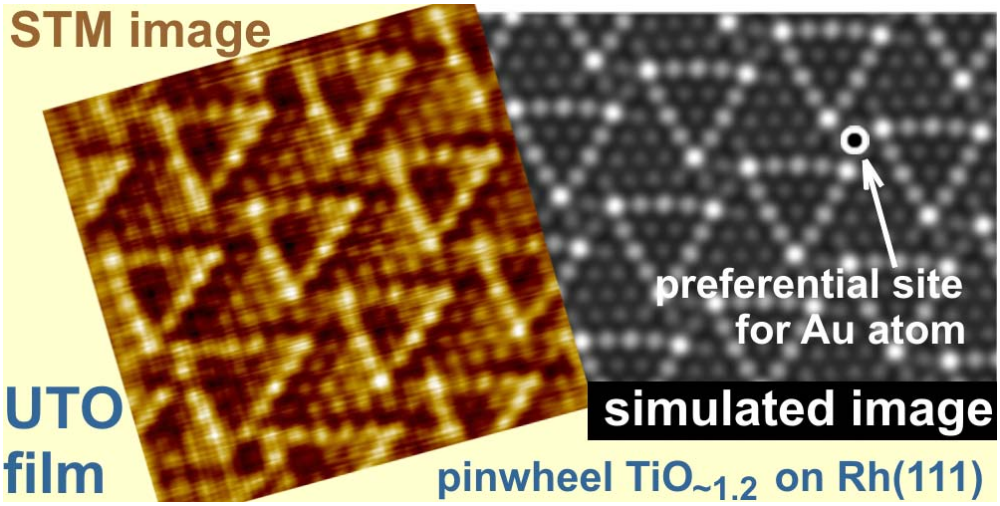

Figure 1: Graphical content

References

1. H.-J.Freunde and G. Pacchioni. Chem. Soc. Review *37*, 2224 (2008).
2. P. Giannozzi et al., J. Phys.: Condens. Matter 21, 395502. (2009).

A. Acun et al. “Atomically Controlled Surfaces Interfaces and Nanostructures”
edited by A. Bianconi, A. Marcelli (Superstripes Press, Rome 2016) isbn: 9788866830597

Effects of Surface Substituents on Electronic Structures of a Cerasome Model

Masato Oda
Department of Materials Science and Chemistry, Wakayama University, Japan

Email: *moda@sys.wakayama-u.ac.jp*
Key words: Cerasomes; First-plinciples calculation; Drug derivery system; Electronic structures

Drug therapy is always accompanied by undesirable side effects, because the drug spread out and affect to healthy tissues and organs as well. One of the ways to reduce the side effects is to develop a system that deliver a desired amount of the drug to a diseased part directly. The system is known as a drug delivery system (DDS). The construction of the DDS requires the technology to encapsulate the drug and release it around the diseased part. Lipid bilayer vesicles, so-called liposomes, are typical DDS materials. However, liposomes are not very stable because all the lipids are connected via van der Waals interactions. As a result of this low stability, sometimes liposomes cannot reach the diseased part intact. There is a pressing need to develop more stable liposomes capable of encapsulating the drug. Recently, cerasomes, i.e., liposomes featuring surfaces reinforced with a siloxane bond network, is developed[1]. Figure 1 shows a chemical structure of a cerasome lipid. It is shown that a cerasome can encapsulate the drug and is much more stable than liposomes. Thus, cerasomes are promising materials for DDS. However, the improvement in stability is accompanied by a difficulty in opening the capsule. Breaking the chemical bonds of a cerasome surface requires information about its microstructure and electronic states, although the microscopic properties of cerasomes remain unclear.

In the previous work, we construct a simple cerasome model as shown in Fig. 2 to investigate the electronic structures of its surface. Comparing the electronic structures of the membrane model with that of the molecule, we reveal that there are mid-gap states in the membrane model that are not in the molecule. These mid-gap states consist of antibonding states of Si-C bonds that connect the siloxane network and organic parts of the lipid[2]. The existence of the antibonding states in the gap indicates that there is a possibility to break cerasomes with some electronic excitations in the system. However, the previous model is extremely simple, we assume perfect siloxane network, although there are many O^- and OH groups on the surface of actual cerasomes. The purpose of this study is to investigate effects of surface substituent groups on the electronic structures of the cerasome model.

We introduce some O^- and OH groups on the surface of the model and calculate the electronic strucutres. All calculations are carried out using the first-principles method based on density functional theory. It is revealed that the energy of the mid-gap states

is modulated around 0.2 eV, but still in the HOMO-LUMO gap of the lipids. This result indicates that we can expect that the mid-gap states valid for the realistic cerasomes.

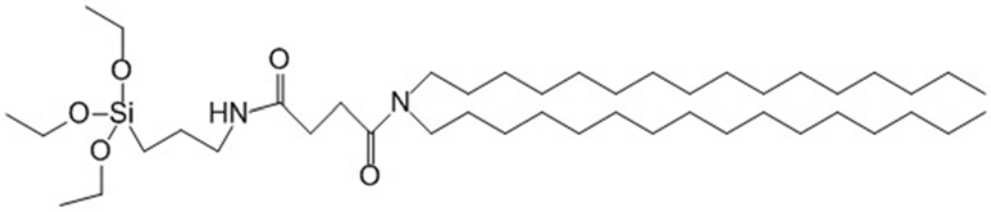

Figure 1: Chemical structure of a cerasome lipid.

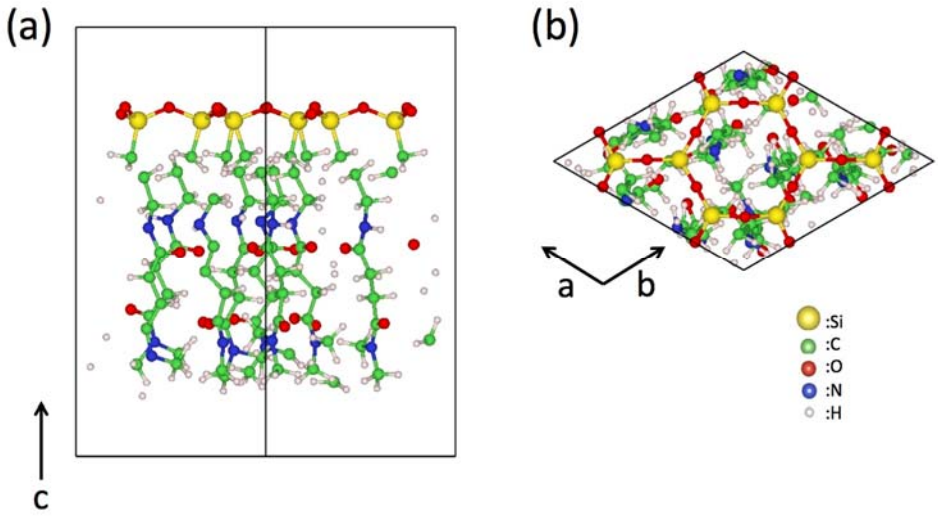

Figure 2: Schematic picture of a cerasome model, (a): side view and (b): top view.

References

1. K. Katagiri, K. Ariga, and J. Kikuchi, Chem. Lett. 28, 661 (1999).
2. S. Yabushita and M. Oda, e-J. Surf. Sci. Nanotech. 12, 112 (2014).

A. Acun et al. “Atomically Controlled Surfaces Interfaces and Nanostructures”
edited by A. Bianconi, A. Marcelli (Superstripes Press, Rome 2016) isbn: 9788866830597

Interface oxidation enhancement at SiO_2/Si(001) by raising O_2 pressure

Shuichi Ogawa , Jiayi Tang, Ryo Taga, and Yuji Takakuwa
Institute of Multidisciplinary Research for Advanced Materials (IMRAM), Tohoku University, Sendai JAPAN

Email: *ogasyu@tagen.tohoku.ac.jp*
Key words: Thermal oxidation, Silicon dioxide, gate dielectric layer, Interface oxidation kinetics, real-time Auger spectroscopy

Thermal oxidation of Si surfaces under the non-equilibrium conditions were used to form a high-quality Si oxide films and/or enlarge the oxidation rate. For example, rapid thermal oxidation (RTO) is performed under the raising the temperature, and then thick oxide can be formed without preventing the dopant diffusions [1]. In addition, oxidation rate of RTO process is faster than that of constant temperature oxidation though the highest temperature of RTO is as same as that of constant temperature oxidation [2]. Based on the these knowledges, it is predicted that the oxidation rate can be quickened even by increase of the O_2 pressure. In this study, the increased O_2 pressure dependence of the interface oxidation rate which proceeds contentiously after the surface oxidation was investigated using real-tile Auger electron spectroscopy.

The oxidation experiments were performed using real-time RHEED-AES apparatus placed at Tohoku University. The time evolution of O KLL Auger electron intensity (I_{OKLL}) was used for estimation of oxidation rate. The clean Boron doped p-type Si(001) surfaces were oxidized and covered with oxide at 400°C under the O_2 pressure of 1.5×10^{-6} Pa. When the clean surfaces were completely covered by the oxide, the O_2 pressure was elevated from 1.5×10^{-6} Pa to P_{O2}(int). The P_{O2}(int) was changed between 3×10^{-5} Pa to 3×10^{-3} Pa.

Figure 1 shows the time evolution of I_{OKLL} during oxidation. The completion of surface oxidation is estimated from the saturation of I_{OKLL}, and it is 3000 s. Then, O_2 pressure is increased up to P_{O2}(int) = 1.5×10^{-3} Pa and it is found that the interface oxidation is enhanced. Here, the oxidation rate at the initial stage of O_2 pressure increase is obtained from the differential of I_{OKLL}. P_{O2}(int) dependence of the oxidation rate is summarized in Fig. 2 by closed circles. The open circle indicates the oxidation rate at the constant O_2 pressure at 1.5×10^{-6} Pa. It is found that the O_2 pressure increase makes the oxidation rate fast. In addition, the interface oxidation rate is proportional to the square root of P_{O2}(int).

This results cannot be explained using traditional oxidation models, because the result the oxidation rate is proportional to the square root of P_{O2}(int) indicates interface oxidation rate is limited by O_2 diffusion through oxide, but oxide is much thinner than 1 nm. To explain these results, we propose the new interface oxidation model named “Unified Si oxidation model mediated by point defects” [3].

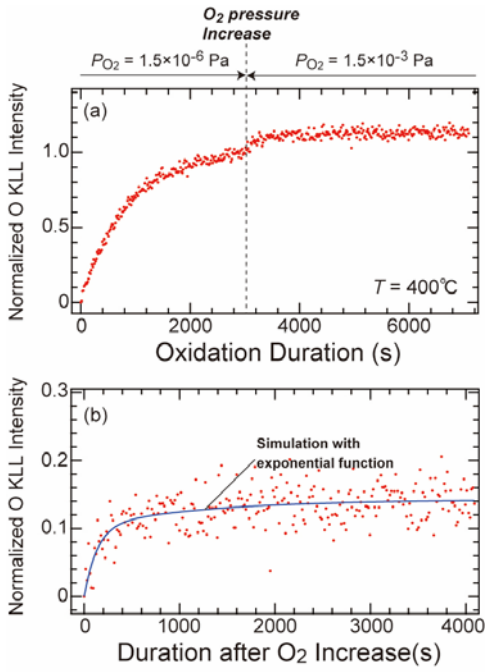

Figure 1: (a) Time evolution of O KLL intensity during oxidation on Si(001) surfaces. The O_2 pressure is increased at end of surface oxidation (t = ~3000 s). (b) Time evolution of O KLL intensity after increasing O2 pressure. The oxidation rate is obtained by differential of simulation shown by solid line.

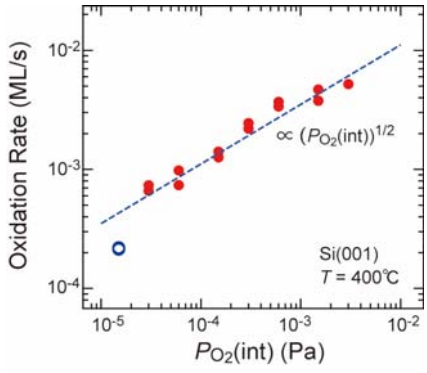

Figure 2: P_{O2}(int) dependence of interface oxidation rate obtained from Fig. 1(b). The open circle indicates the oxidation rate at the constant O_2 pressure at 1.5×10^{-6} Pa.

References

1. H.Y.A. Chung, et al., Mater. Sci. Eng. B 118, 55 (2005).
2. S. Ogawa, et al, in preparation.
3. S. Ogawa, et al., Jpn. J. Appl. Phys. 46, 7063 (2006).

A. Acun et al. “Atomically Controlled Surfaces Interfaces and Nanostructures”
edited by A. Bianconi, A. Marcelli (Superstripes Press, Rome 2016) isbn: 9788866830597

Cerium tungstate as model catalyst support

Tomáš Skála, Nataliya Tsud, Vitaliy Stetsovych, Josef Mysliveček, Vladimír Matolín
Charles University in Prague, Faculty of Mathematics and Physics, Department of Surface and Plasma Science

Email: *tomas.skala@elettra.eu*
Key words: Cerium oxide, Tungsten oxide, Palladium, Platinum, Photoelectron spectroscopy, Scanning Tunneling Microscopy, Thin film growth

Two model catalytic metal/oxide systems were investigated by photoelectron spectroscopy and scanning tunneling microscopy, at the Materials Science Beamline at Elettra synchrotron light source in Trieste and in the Surface Physics Laboratory in Prague, respectively.

The mixed-oxide support was a cerium tungstate epitaxial thin layer $Ce_6WO_{12}(100)$ grown in situ on the W(110) single crystal as recently reported in [1] and references therein. Active particles consisted of high-purity palladium and platinum deposited in situ by physical vapor deposition on the tungstate surface at 300 K. Step-wise growth in the range approximately 0.1 to 1 monolayer was studied by photoemission on core level and valence band spectra utilizing monochromatized synchrotron radiation and conventional laboratory X-ray source.

Both metals were found to interact weakly with the oxide support and the original chemical state of both support and metals was mostly preserved, i.e. stoichiometric mixed oxide Ce_6WO_{12} and metallic Pd or Pt. The evolution of the photoemission spectra acquired after each deposition step suggested the Volmer–Weber growth mode (i.e. 3D islands) of the transition metals on the cerium tungstate surface.

Early stages of the metal growth were then studied by scanning tunneling microscopy in order to directly reveal the surface morphology at submonolayer coverage (1 and 5% of monolayer). Although the oriented growth of the islands was not observed, the micrographs clearly confirmed the growth mode suggested by the photoemission in real space.

The last step of the performed experiments was the step-wise in situ annealing of the prepared samples up to 700 K, giving two important results: (i) a fair thermal stability of the metal/cerium tungstate model thin films was observed, as only a partial coalescence of the metallic particles (deposited at 300 K) was detected; and (ii) self-cleaning of the surfaces from impurities occurred. These impurities were represented mainly by CO molecules adsorbed from the residual gas during the course of the experiments, as both Pd and Pt are known to be extremely reactive towards CO.

Already at 300 K these CO molecules partially dissociated into C and O. Molecularly adsorbed CO left the surface after the annealing at 500 K while the residual graphitic carbon from the dissociated CO disappeared at 700 K, leaving the surface completely free of impurities.

The described results are currently being thoroughly analyzed and prepared for publication [2].

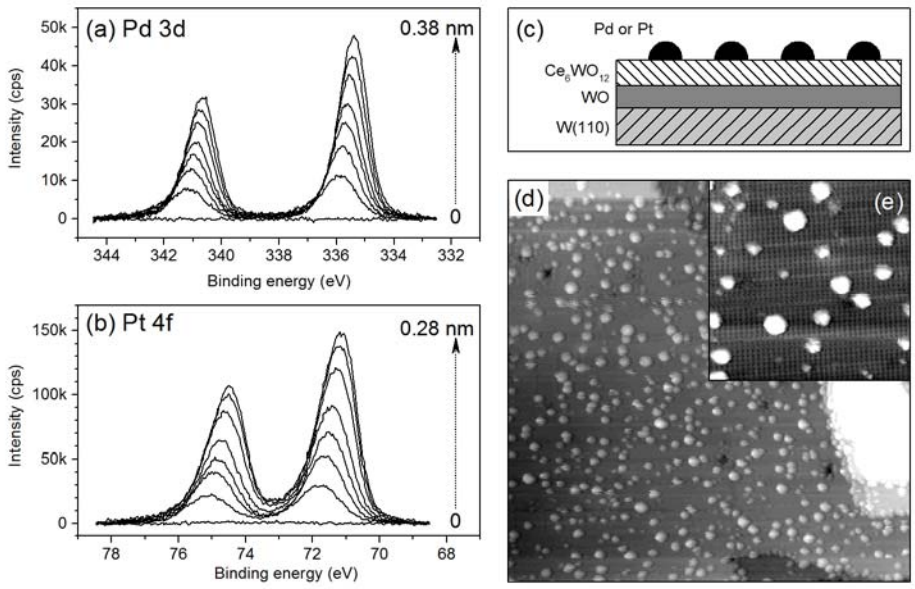

Figure: Palladium or platinum growth on Ce_6WO_{12}(100). (a) Pd 3d photoemission spectra, (b) Pt 4f photoemission spectra, (c) growth model, (d) scanning tunneling micrograph of the Pt islands, overview 120×120 nm^2, (e) detail 30×30 nm^2; square-like structure of the substrate can be seen.

References

1. V. Stetsovych, T. Skála, J. Beran, F. Dvořák, D. Mazur, N. Tsud, K. Mašek, V. Matolín, J. Mysliveček, Applied Surface Science 372, 152 (2016). http://dx.doi.org/10.1016/j.apsusc.2016.03.050.
2. T. Skála, N. Tsud, V. Stetsovych, J. Mysliveček, V. Matolín, in preparation (2016).

A. Acun et al. “Atomically Controlled Surfaces Interfaces and Nanostructures”
edited by A. Bianconi, A. Marcelli (Superstripes Press, Rome 2016) isbn: 9788866830597

Electronic structure of ultrathin Bi(110) films on epitaxial graphene studied by SR and laser photoemission spectroscopy

Kazutoshi Takahashi, Masaki Imamura, Isamu Yamamoto, and Junpei Azuma
Synchrotron Light Application Center, Saga University

Email:*ktaka@cc.saga-u.ac.jp*
Key words: Graphene and other 2D materials

Physical properties of semimetal bismuth (Bi) have been attracting much interest due to a strong spin-orbit coupling, a large Fermi wave length, and a small overlap between valence and conduction bands. Especially, the metallic surface states with spin polarization [1] on Bi have been extensively studied as an promising candidate for energy-efficient electronic and spintronic applications [2]. One-bilayer (BL) of Bi(111) film is predicted to be an elemental two-dimensional topological insulator (TI) and possesses well-localized topological edge states [3]. The Edge states have been confirmed experimentally despite of the complicated features due to the hybridization with the surface state of Bi_2Te_3 and Bi(111) substrate [4]. It has been also reported that the one- and two-BL Bi(110) films become two-dimensional TIs if the buckling is removed [5]. The buckling is suggested to be controllable via substrate induced strain and charge doping. In order to elucidate the topological property of ultrathin Bi films, it is indispensable to identify their atomic arrangement and the two-dimensional band-dispersion over the whole Brillouin zone. In addition, it is also important to elucidate the electron dymnamic in the unoccupied energy region. In this work, angle-resolved photoemission study with synchrotron radiation and time-resolved two-photon photoemission study have been conducted on ultrathin Bi(110) films grown on epitaxial graphene to identify the electronic band dispersion and excited electron dynamics.

Experiments were performed at Saga University beamline BL13 in Saga Light Source. Bi was deposited onto an tri-layer graphene epitaxially grown on a 4H-SiC(0001) at 100 K. To enhance the film quality, the two- and three-BL films were briefly annealed at 300K and 380K, respectively. We have used photon energies of 70 and 15 eV, for core-level and valence band photoemission measurements, respectively. The fundamental and frequency-tripled light of Ti:Sapphire laser have been used as pump and probe light on the time-resolved two-photon photoemission measurement. All photoemission measurements were performed at 40 K.

Figs. 1(a) and (b) show the observed LEED patterns at graphene substrate and Bi film with the coverage of 0.38 ML, respectively. In addition to the spots corresponding to graphene, SiC, and buffer layer with $6\sqrt{3}$ super structure, pairs of spots are located on a circle with a radius of about 1.9 $Å^{-1}$ after the deposition of Bi. These pairs correspond to the alignment of Bi[-110] along the armchair of graphene with small tilting to form

six domains with respect to three armchair direction of graphene. This assignment is also supported by two-dimensional mapping of photoemission spectra.

The intensity map of angle-resolved photoemission spectra along ΓX_1 direction of one-BL Bi(110) film is shown in Fig. 1(c). The overall features fit well with the calculated band-structure of corresponding Bi(110) BL films and resemble those on Bi(110) films grown on HOPG [6]. The bilayer growth of Bi(110) films can also be confirmed by absence of Dirac-cone like feature at M point, which is commonly predicted by band structure calculation for odd number of Bi(110) layers. The transient 2PPE profile of one-BL film is in Fig. 1(d). It has been found that the time constant of 2PPE profile depends on the energy and the film thickness.

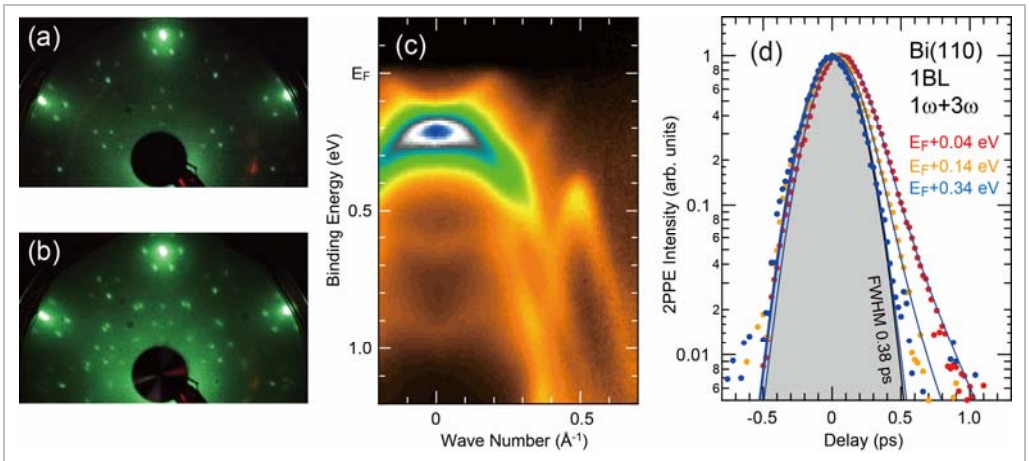

Figure 1: LEED patterns of tri-layer graphene substrate (a) and Bi coverage of 0.38 ML (b) at $E_i = 45.1$ eV. (c) The intensity map of angle-resolved photoemission spectra along ΓX_1 direction of one-BL Bi(110) film. (d) Transient 2PPE profile of one-BL Bi(110) film.

References

1. Ph. Hofmann, Prog. Surf. Sci. 81, 191 (2006).
2. S. A. Wolf *et al*., Science 294, 1488 (2001).
3. M. Wada *et al*., Phys. Rev. B 83, 121310 (2011).
4. T. Hirahara *et al*., Phys. Rev. Lett. 107, 166801 (2011); F. Yang *et al*., Phys. Rev. Lett. 109, 016801 (2012); I. K. Drozdov *et al*., Nat. Phys. 10, 664 (2014).
5. Y. Lu *et al*., Nano Lett. 15, 80 (2015).
6. G. Bian *et al*., Phys. Rev. B 90, 195409 (2014).

A. Acun et al. "Atomically Controlled Surfaces Interfaces and Nanostructures"
edited by A. Bianconi, A. Marcelli (Superstripes Press, Rome 2016) isbn: 9788866830597

Structural stability of graphene nanoflakes

M. Ushirozako[1,2] , A. Akaishi[1,2], and J. Nakamura[1,2]
[1]*The University of Electro-Communications (UEC-Tokyo), Japan*
[2]*JST-CREST, Japan*

Email: *ushirozako@natori.ee.uec.ac.jp*
Key words: graphene nanoflakes, structural stability, formation energy, aromaticity

Recently, nano-scale graphene nanoflakes (GNFs) have attracted great attention as one of the promising materials for electronics and spintronics. Kim *et al*. have successfully fabricated GNFs with various sizes up to 40 nm and have reported that the photoluminescence property of GNFs depends on their size and edge shape [1]. From the theoretical points of views, the structural stability and the electronic properties have been theoretically studied for GNFs with zigzag or armchair edges [2]. However, we have not yet acquired the systematic comprehension with regard to effects of the size and the edge shape of GNFs on the stability. In the present study, we have examined how the stability of GNFs is determined by the size and the type of edges using first-principles calculations within the density functional theory.
In order to evaluate the stability of GNFs, we calculated the edge formation energy using the following equation:

$$E_{\mathrm{edge}} = \frac{1}{T}(E_{\mathrm{cluster}} - n_{\mathrm{C}}E_{\mathrm{C}} - n_{\mathrm{H}}\mu_{\mathrm{H}})$$

$$\mu_{\mathrm{H}} = \frac{1}{6}(E_{\mathrm{benzene}} - 6E_{\mathrm{C}})$$

where T is the number of C atoms at the edge, E_{cluster}, E_{C}, and E_{benzene} are the total energies for GNFs, for graphene per atom, and for benzene, n_{C} and n_{H} are the numbers of C and H atoms in GNFs, μ_{C} and μ_{H} are the chemical potentials of C and H atoms, respectively. We consider GNFs with the six-fold symmetry (D_{6h}) and classify them into zigzag GNFs (ZZGNFs) and armchair GNFs (ACGNFs). ACGNFs have two subtypes, AC(1) and AC(2), depending on whether carbon atoms are just at the corner of the outermost envelope hexagon of GNFs (see Figs.1(b) and 1(c)). We define the edge purity as the ratio of the number of carbon atoms at the edge unambiguously regarded as the armchair to the total number of edge atoms. The purity of AC(1) is higher than that of AC(2). The chemical formulae associated with ZZ, AC(1), and AC(2) are $C_{6n^2}H_{6n}$, $C_{18n^2-18n+6}H_{12n-6}$ and $C_{18n^2-30n+12}H_{12n-12}$, respectively.
Figure 1(d) shows the edge formation energy of the GNFs having up to 1200 carbon atoms as a function of the number of edge carbon atoms. The formation energy of ZZGNFs is higher than that of ACGNFs irrespective of the size of GNFs. This instability of ZZGNFs is attributed to the presence of the so-called edge state. Indeed, it has also been shown that the formation energy of the zigzag graphene nanoribbon is higher than that of the armchair one [3]. It is noted that AC(2) is slightly more stable than AC(1), whereas the purity of AC(2) is lower than that of AC(1). Such peculiar

stabilization can be reasonably explained in terms of the aromaticity of GNFs. Figure 1(e) shows the Nucleus Independent Chemical Shifts (NICS) averaged for the six-membered rings in GNFs. The NICS value of AC(2) is lower than that of AC(1). This means AC(2) is more aromatic than AC(1). We concluded that the structural stability of GNFs depends on whether the edge state is present or absent, and is also dominated by the aromaticity of GNFs.

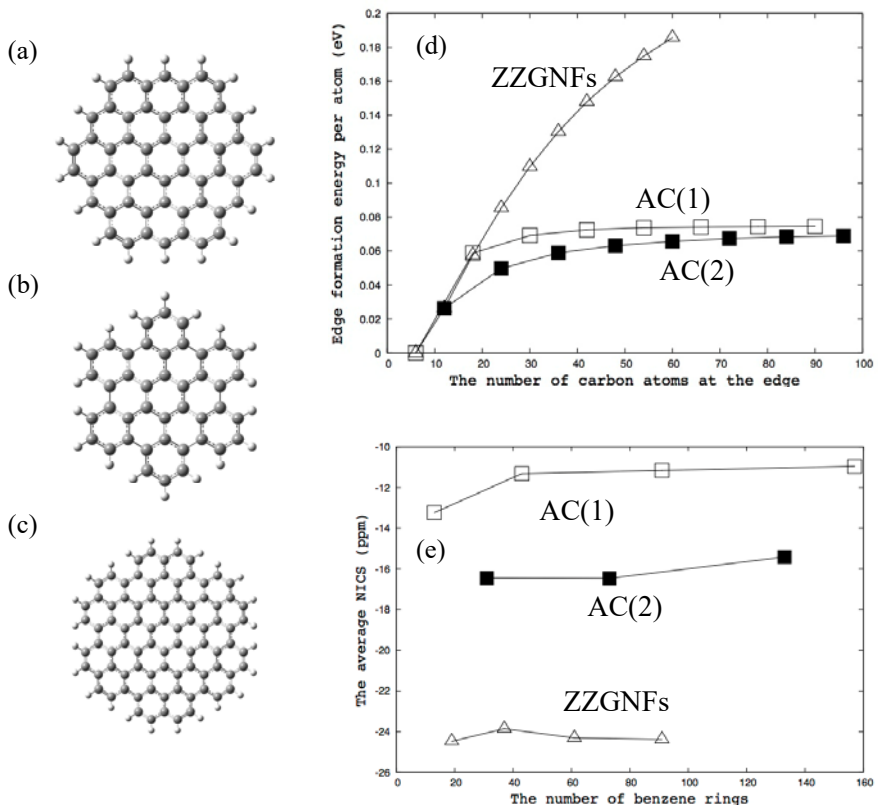

Fig. 1 Structure of GNFs, (a)$C_{54}H_{18}$(ZZ), (b) $C_{42}H_{18}$ (AC(1)), (c) $C_{84}H_{24}$ (AC(2)), (d)The edge formation energy of GNFs as a function of the number of edge carbon atoms. (e) NICS averaged for the six-membered rings in GNFs as a function of the number of benzene rings.

References

1. S. Kim et al., ACS Nano, 6, 9, 8203 (2012)
2. W. Hu *et al*., J. Chem. Phys. 141, 214704 (2014)
3. S. Okada. Phys. Rev. B, 77, 041408 (2008)

A. Acun et al. "Atomically Controlled Surfaces Interfaces and Nanostructures"
edited by A. Bianconi, A. Marcelli (Superstripes Press, Rome 2016) isbn: 9788866830597

Optimization of ZnO:Al layers for applications in thin film solar cells

Agata Zdyb[1], Ewelina Krawczak[1], Piotr Lichograj[2]
[1]*Lublin University of Technology, Faculty of Environmental Engineering*
[2] *Pope John Paul II State School of Higher Education in Biała Podlaska, Faculty of Economics and Technic Sciences*

Email: *a.zdyb@pollub.pl*
Key words: thin film solar cells, photovoltaics, transparent conductive oxides, magnetron sputtering

Transparent conductive oxide (TCO) layers are an important component of a number of electronic devices including light emitting diodes, thin film solar cells and touch screens [1]. Thin film solar cells became more popular in recent years because of low materials usage, decreasing prices and very effective recycling. In applications of TCO in solar cells structures, films with good transparency (>80%) and low resistivity (~10^{-4} Ω·cm) are required.

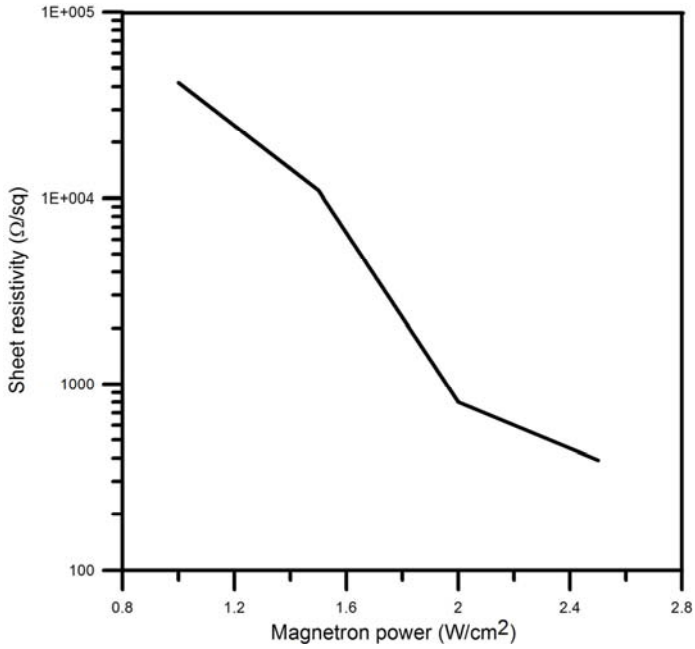

Figure 1: The dependency of sheet resistivity on magnetron power

One of the thin film technologies used to prepare TCO films is magnetron sputtering, a physical deposition method known for high deposition rate, lack of impurities, good control of composition and thickness as well as homogeneity of the obtained structures [2, 3].
In this work ZnO:Al layers were deposited on clean soda lime glass by using RF

magnetron sputtering system Aliance Concept AC 450 from ZnO target (99.9 % purity) doped with Al_2O_3 (2.5 wt.%). We studied the influence of deposition parameters such as substrate temperature, pressure in the deposition chamber and power on the thickness and quality of the obtained layers. Good quality, homogenous layers of more than 80% transparency were obtained by magnetron sputtering in room temperature. The increase of magnetron power results in the conductivity improvement (Fig. 1), growing size of agglomerates and higher thickness of the layers.

References

1. M. Dhankhar, et al., Renewable and Sustainable Energy Reviews 40, 214 (2014).
2. A.M.K. Dagamseh, et al., Thin Solid Films 516, 7844 (2008).
3. W. Li, et al., Surface & Coatings Technology 258, 991 (2014).

Author Index